
Electronic Thesis and Dissertation Repository

10-26-2018 11:00 AM

Immunization With Recombinant Myelin Oligodendrocyte Glycoprotein Identifies Autoreactive T Cells As A Limiting Factor In Autoreactive Germinal Center Maintenance

Rajiv William Jain, *The University of Western Ontario*

Supervisor: Kerfoot, Steven M., *The University of Western Ontario*

A thesis submitted in partial fulfillment of the requirements for the Doctor of Philosophy degree in Microbiology and Immunology

© Rajiv William Jain 2018

Follow this and additional works at: <https://ir.lib.uwo.ca/etd>



Part of the [Immunity Commons](#)

Recommended Citation

Jain, Rajiv William, "Immunization With Recombinant Myelin Oligodendrocyte Glycoprotein Identifies Autoreactive T Cells As A Limiting Factor In Autoreactive Germinal Center Maintenance" (2018). *Electronic Thesis and Dissertation Repository*. 5809.
<https://ir.lib.uwo.ca/etd/5809>

This Dissertation/Thesis is brought to you for free and open access by Scholarship@Western. It has been accepted for inclusion in Electronic Thesis and Dissertation Repository by an authorized administrator of Scholarship@Western. For more information, please contact wlsadmin@uwo.ca.

Abstract

Germinal center (GC) responses are responsible for the protection provided by immunizations but can also drive autoimmunity. B and T cells collaborate in the GC to target the same antigen (Ag) to inform B cell differentiation; however, the properties of Ags differ substantially in autoimmunity and foreign-Ag driven immunity. Currently, it is not well understood how properties of the Ag itself influence the initiation or progression of GC responses, limiting our ability to develop effective vaccinations and predict the progression of autoimmune responses. *The purpose of this thesis is to assess how GC responses initiate and progress when immunizing with an autoAg relative to a model foreign-Ag. It was hypothesized that autoreactive GCs would be relatively short-lived and less productive than foreign-Ag driven GCs due to limiting properties of the autoAg.* To address this hypothesis, we developed a modular protein expression system to purify large amounts of myelin oligodendrocyte glycoprotein (MOG), a commonly targeted autoAg in Multiple Sclerosis (MS), and streamlined the modification of the MOG protein's properties. Relative to immunization with a model foreign-Ag, immunization with MOG induces a short-lived GC that collapses early forming a large numbers of memory B cells. Memory B cells generated from the MOG-induced GC are capable of participating in secondary GCs, however, these memory cells are short-lived resulting in a short window in which MOG-specific memory B cells can be engaged. The progression of the MOG-induced GC is then shown to be limited by low T cell Ag-affinity. A possible explanation for how Ag-properties affect GC progression, is that Ag-properties influence how B and T cells communicate with each other. To address this hypothesis, reporters capable of monitoring the activation status of B and T cells were generated although, attempts to generate mice carrying these reporters were unsuccessful. Overall, these results confirm that properties of Ags affect the progression of GC responses and that the MOG-induced GC is limited by properties of the MOG autoAg. These results have important implications for future vaccine design but also gives insight into how autoreactive B cells may expand in MS.

Keywords

B cell, T cell, NFAT, NF κ B, germinal center, differentiation, protein production, EAE, autoimmunity, Multiple Sclerosis, MS, flow cytometry

Dedication

This thesis is dedicated to my parents Beth Jain and Lalit Jain for their unconditional support throughout my academic studies. None of this would have been possible without their constant kind and caring efforts on my behalf.

Co-Authorship Statement

Chapter 2 is based partially on the adapted manuscript: Jain WR, Dang AK, and Kerfoot SM (2016) Simple and Efficient Production and Purification of Mouse Myelin Oligodendrocyte Glycoprotein for Experimental Autoimmune Encephalomyelitis Studies. *J. Vis. Exp.* The purification of the mMOG_{tag} protein was adapted from the original protocol designed by A Dang. Otherwise the experiments shown were performed by R Jain with additional help from Y Tesfagiorgis and Y El-Sakka for the EAE experiment and *in vivo* T cell proliferation experiments in the lab of S Kerfoot. The publication was written by R Jain with suggestions from S Kerfoot.

Chapter 3 is adapted from Jain RW, Parham KA, Tesfagiorgis Y, Craig HC, Emiliano R, and Kerfoot SM (2018) Autoreactive T cells preferentially drive differentiation of non-responsive memory B cells at the expense of germinal center maintenance. *bioRxiv*. H Craig generated the tissues for histology and R Emiliano and Y Tesfagiorgis conducted analysis on the histological tissues. K Parham conducted many of the ELISA and ELISpots. H Craig, Y Tesfagiorgis, and K Parham also helped generally with FACS experiments. All other experiments were conducted by R Jain in the laboratory of S Kerfoot. This publication was written by R Jain with suggestions from S Kerfoot.

Chapter 4 is based upon unpublished results. L Drysdale performed the nuclear injections of single mouse zygotes, cultured zygotes into blastocysts, and transferred injected zygotes into pseudopregnant female mice in the lab of C Pin. Otherwise, all other experiments were performed by R Jain in the lab of S Kerfoot.

Acknowledgments

None of this would have been possible without the support of my supervisor Steven Kerfoot. Steven is responsible for training me to be the scientist that I am today. Over the years you have taught me to conduct quality science but also how to effectively write and communicate it. Your tireless efforts will not be forgotten and I am incredibly fortunate to have had such an excellent supervisor throughout my academic studies.

Science is conducted in teams, and indeed, conducting the experiments required for this thesis would have been possible without the efforts of my lab mates. I will cherish the friendships I have made within the lab: Amy Dang, Heather Craig, Yodit Tesfagiorgis, Kate Parham, and everyone else who has passed through the lab through the years. I would also like to thank Kate Parham for her efforts in reading and editing my thesis.

The experiments conducted in this thesis would not have been possible without the support of Kristen Chadwick for my work using the LSRII as well as her expertise in cell sorting. To conduct this research I also needed the support of the West Valley Barrier Facility and all of their staff, as we could not have possibly maintained our mouse colony alone.

I would like to thank the members of my advisory committee: Bryan Heit and Gregory Dekaban. They have provided me support throughout my PhD and helped guide my thesis project into what it is today. I would further like to thank Gregory Dekaban for reading and editing this thesis, your comments were immensely helpful and insightful.

Table of Contents

Abstract	I
Keywords	II
Dedication	III
Co-Authorship Statement.....	IV
Acknowledgments.....	V
Table of Contents	VI
List of Tables	XII
List of Figures	XIII
List of Abbreviations	XV
Chapter 1	1
1 Introduction	1
1.1 B and T cells in immunity and autoimmunity	1
1.1.1 The generation and function of Ag-specific receptors on B and T cells	2
1.1.2 The influence of tolerance on autoreactive B and T cell receptors.....	3
1.2 B cell responses in Multiple Sclerosis	5
1.2.1 Multiple Sclerosis and experimental autoimmune encephalomyelitis.....	5
1.2.2 Role of the B cell in Multiple Sclerosis	5
1.3 Germinal center responses	8
1.3.1 The initiation of B and T cell responses	11
1.3.2 The pre-germinal center time point.....	12
1.3.3 The germinal center	13
1.4 Germinal center B cells.....	14
1.4.1 The light and dark zones of the germinal center.....	14
1.4.2 Germinal center B cell differentiation	19

1.5	Memory B cells.....	19
1.5.1	Memory B cell subsets.....	19
1.5.2	Memory B cell differentiation	22
1.6	Plasmablasts and plasma cells	22
1.6.1	Differentiation of plasmablasts and plasma cells.....	23
1.6.2	Subsets of plasmablasts and plasma cells	23
1.7	T follicular helper cells	24
1.7.1	Pre-T follicular helper cells	24
1.7.2	T follicular helper cells and their associated subsets	25
1.8	B and T cell interactions	26
1.8.1	Cellular identity and signal integration.....	26
1.8.2	Receptors and cytokines influencing B cell differentiation.....	27
1.9	Thesis overview	30
1.9.1	<i>Chapter 2: Simple and Efficient Production and Purification of Mouse Myelin Oligodendrocyte Glycoprotein for Experimental Autoimmune Encephalomyelitis Studies</i>	30
1.9.2	<i>Chapter 3: Autoreactive T cells preferentially drive differentiation of short-lived memory B cells at the expense of germinal center maintenance.</i>	30
1.9.3	<i>Chapter 4: Reporters for in vivo and in vitro monitoring of NFκB and NFAT signaling</i>	31
	Chapter 2.....	32
2	Simple and Efficient Production and Purification of Mouse Myelin Oligodendrocyte Glycoprotein for Experimental Autoimmune Encephalomyelitis Studies	32
2.1	Introduction.....	33
2.2	Results.....	35
2.2.1	A protocol for expressing mMOG _{tag} protein	35

2.2.2	TEV protease can remove the tag sequence to generate enriched MOG ₁₋₁₂₅ that can be purified	41
2.2.3	Generation of haMOG _{tag} , a variation of mMOG _{tag} that alters T cell antigen affinity	44
2.2.4	haMOG _{tag} induces greater MOG-specific T cell responses relative to mMOG _{tag} <i>in vitro</i> and <i>in vivo</i>	48
2.2.5	mMOG _{tag} and haMOG _{tag} can both induce EAE incorporating anti-myelin B and T cells	51
2.3	Discussion	54
2.4	Materials and Methods	57
2.4.1	Mice	57
2.4.2	Antibodies used for flow cytometry or histology	57
2.4.3	Recombinant mMOG _{tag} and haMOG _{tag} vector design and purification ...	57
2.4.4	TEV protease cleavage of mMOG _{tag} protein	59
2.4.5	Adoptive transfer of B and T cells and immunization	59
2.4.6	Flow cytometry	60
2.4.7	Induction of EAE	60
2.4.8	Immunofluorescence histology	61
2.4.9	<i>In vitro</i> and <i>in vivo</i> T cell proliferation assays	61
2.4.10	ELISpots and ELISA	62
2.4.11	Statistical analyses	62
Chapter 3	63
3	Autoreactive T cells preferentially drive differentiation of short-lived memory B cells at the expense of germinal center maintenance.	63
3.1	Introduction	64
3.2	Results	66
3.2.1	Immunization with MOG autoAg results in an atypical, unsustained GC response	66

3.2.2	Preferential differentiation of B cells with a memory phenotype in response to MOG autoAg	70
3.2.3	Ag-specific GFP ⁺ CD95 ^{lo} CD38 ^{hi} B cells are Ag experienced.....	76
3.2.4	T cells partially control the outcome of the germinal center response to MOG	80
3.2.5	Low T cell Ag-affinity limits the MOG GC response	83
3.2.6	Levels of T cell activation do not explain the differential B cell response between the different model systems	87
3.2.7	The MOG-induced GC does not generate effective B cell memory.....	91
3.2.8	Memory B cell responsiveness is not programmed by the MOG-specific T cell.....	100
3.3	Discussion	103
3.4	Materials and Methods.....	106
3.4.1	Mice	106
3.4.2	Antibodies for histology/flow cytometry.....	107
3.4.3	MOG production and purification	107
3.4.4	Adoptive transfer of B and T cells and immunization.....	107
3.4.5	Flow cytometry	108
3.4.6	Immunofluorescent histology	109
3.4.7	Digital Droplet PCR (ddPCR)	109
3.4.8	ELISpots and ELISA	110
3.4.9	Image and statistical analyses	110
Chapter 4	111
4	Reporters for <i>in vivo</i> and <i>in vitro</i> monitoring of NFκB and NFAT signaling.....	111
4.1	Introduction.....	112
4.2	Results.....	115

4.2.1	Fusion of p65 or NFAT1 to fluorescent proteins generates functional reporters capable of monitoring their nuclear and cytoplasmic localization.....	115
4.2.2	Using the CRISPR/Cas9 system to generate a reporter knock-in at the <i>p65</i> locus <i>in vitro</i>	119
4.2.3	The CRISPR/Cas9 system can be used to generate a reporter knock-in at the <i>NFAT1</i> locus <i>in vitro</i>	123
4.2.4	Generating knock-in mice using the CRISPR/Cas9 system	126
4.2.5	An overexpression-based NFAT1 reporter.....	129
4.3	Discussion.....	133
4.4	Materials and Methods.....	136
4.4.1	Cloning.....	136
4.4.2	Cell culture and transfections.....	144
4.4.3	Fixed and live cell microscopy	144
4.4.4	Genotyping of CRISPR transfected cells and mouse pups.....	145
4.4.5	Guide RNA design.....	145
4.4.6	Nuclear injections	145
4.4.7	Blastocyst genotyping.....	146
4.4.8	Image analysis.....	146
4.4.9	Statistical analysis.....	147
Chapter 5	148
5	Overall discussion and future directions	148
5.1	Summary of the major findings of this thesis	148
5.2	A model of the autoreactive germinal center.....	149
5.3	Future directions	155
5.3.1	Somatic hypermutation in the MOG-induced germinal center.....	155
5.3.2	T cell antigen-affinity and the germinal center.....	156

5.3.3	Signal exchange and interaction duration of B and T cell conjugates	157
5.4	B cells in MS and EAE	161
5.5	Concluding remarks	162
	Curriculum Vitae	198

List of Tables

Table 1.1. Summary of memory B cell subsets and their functions.	21
Table 1.2. Summary of the expression and functions of key signaling molecules affecting the germinal center response.....	28
Table 4.1. Forward and reverse primers used for cloning	139

List of Figures

Figure 1.1. Summary of developing germinal center responses.	9
Figure 1.2. B cell differentiation and selection in the light and dark zones of the germinal center.	17
Figure 2.1. mMOG _{tag} protein.	37
Figure 2.2. Purification of mMOG _{tag}	39
Figure 2.3. Generation of MOG ₁₋₁₂₅	42
Figure 2.4. Structure and purification of the haMOG _{tag} protein.	46
Figure 2.5. haMOG _{tag} induces greater MOG-specific T cell proliferation than mMOG _{tag}	49
Figure 2.6. mMOG _{tag} and haMOG _{tag} both induce EAE incorporating myelin-specific B and T cells.	52
Figure 3.1. Differential GC development in the NPOVA and MOG model Ag systems.	68
Figure 3.2. Early collapse of the MOG GC to a memory B cell phenotype.	72
Figure 3.3. Administration of pertussis toxin does not save the MOG-induced GC from collapse	74
Figure 3.4. Memory-phenotype B cells generated in response to MOG are Ag-experienced	78
Figure 3.5. MOG-specific T cells induce early GC collapse to a memory B cell phenotype.	81
Figure 3.6. Increasing T cell Ag-affinity partly rescues the MOG GC from early collapse.	85

Figure 3.7. T _{FH} cell phenotype is not altered by Ag.	89
Figure 3.8. Memory B cells produced by the MOG-induced GC response are unresponsive during secondary immune responses.	94
Figure 3.9. MOG-specific memory B cells are responsive but they are short-lived.	96
Figure 3.10. Characterization of MOG-specific memory B cells and their functionality.	98
Figure 3.11. Autoimmune T cells do not induce short-lived memory in MOG-specific B cells during the GC response.	101
Figure 4.1. Reporters capable of monitoring the cytoplasmic and nuclear localization of the p65 and NFAT1 proteins.....	117
Figure 4.2. CRISPR/Cas9-mediated editing of the <i>p65</i> locus.	121
Figure 4.3. CRISPR/Cas9 mediated editing of the <i>NFAT1</i> locus.....	124
Figure 4.4. Insertion of the NFAT1 reporter into C57Bl/6 blastocysts.	127
Figure 4.5. Construction of an NFAT1 reporter that can be overexpressed.	131
Figure 5.1. A model of how T cell antigen-affinity affects germinal center progression	153
Figure 5.2. Pre-GC B and T cell interactions are influenced by properties of immunizing Ags.....	159

List of Abbreviations

3-D - Three dimensional

ABC - Atypical/age/ exhausted/autoimmune associated B cell

Ag - Antigen

APC - Antigen presenting cell

AP-1 - Activator protein 1

ASC - Antibody secreting cell

BCR - B cell receptor

bMOG_{tag} - B cell dependent myelin oligodendrocyte glycoprotein tag

bp - Base pair

BrdU - Bromodeoxyuridine

Breg - Regulatory B cell

CTY - Cell Tracker Yellow

CFA - Complete freund's adjuvant

CFSE - Carboxyfluorescein succinimidyl ester

CNS - Central nervous system

CRISPR - Clustered regularly interspaced short palindromic repeats

CSR - Class switch recombination

DC - Dendritic cell

DZ - Dark zone

DNA - Deoxyribonucleic acids

EAE - Experimental autoimmune encephalomyelitis

ELISA - Enzyme-linked immunosorbent assay

ELISpot - Enzyme linked immune-spot

FDC - Follicular dendritic cell

FMO - Fluorescence minus one

GC - Germinal center

GFP - Green fluorescent protein

haMOG_{tag} - High affinity myelin oligodendrocyte glycoprotein tag

i.p. - Intraperitoneal

IPTG - Isopropyl β -D-1-thiogalactopyranoside

kDa - Kilodalton

LN - Lymph Node

LPS - Lipopolysaccharide

LZ - Light zone

MFI - Mean fluorescence intensity

MHC - Major histocompatibility complex

MOG - Myelin Oligodendrocyte Glycoprotein

mMOG_{tag} - Mouse myelin oligodendrocyte glycoprotein tag

MS - Multiple sclerosis

NP - Nitrophenyl

NFAT - Nuclear factor of activated T cells

NF-M - Neurofilament M

NF κ B - Nuclear factor kappa B

OVA - Chicken ovalbumin protein

PCR - Polymerase chain reaction

PMA - Phorbol 12-myristate 13-acetate

Pre-T_{FH} - Pre-T follicular helper

RFP - Red fluorescent protein

PTX - Pertussis toxin

rMOG_{tag} – Rat myelin oligodendrocyte glycoprotein tag

RNA - Ribonucleic acids

SEM - Standard error of the mean

SDS-PAGE - Sodium dodecyl sulfate-polyacrylamide gel electrophoresis

SHM - Somatic hypermutation

STAT - Signal transducer and activator of transcription

TCR - T cell receptor

TEV - Tobacco etch virus

T_{FH} - T follicular helper

T_{FR} - T follicular regulatory

Treg – Regulatory T

Chapter 1

1 Introduction

Our bodies are exposed to pathogens every day of our lives requiring the combined efforts of the innate and adaptive immune systems to control infections. In the modern world, the control of infectious diseases such as smallpox and polio has been greatly facilitated through the use of vaccinations that induce protective antibody responses by stimulating B cells from the adaptive immune system. Vaccinations are invaluable in modern healthcare (1) yet there are still many diseases, such as human immunodeficiency virus and malaria, that we have difficulty generating effective B cell responses against due to insufficient understanding of how the immune system adapts itself to properties of the immunizing antigen(s) (Ag) (2, 3).

Nonetheless, while the promotion of B cell responses may be beneficial in the context of immunity against pathogens, it is problematic in the context of autoimmunity. Indeed, the induction of B cell responses needs to be regulated heavily as B cells can target Ags within our own bodies, known as autoAgs, resulting in the development and progression of autoimmune diseases (4). Typically, the B cell's contribution to disease has been attributed to the production of autoantibodies that facilitate the destruction of host tissue. However, evidence of B cells playing additional roles beyond antibody production have created a great deal of interest in understanding how new subsets of B cells are generated and how they influence ongoing autoimmune responses (5). Thus, not only is there a need to better understand how B cell responses develop towards pathogens, but a better understanding of factors that limit B cell responses directed against our own bodies is required. In this thesis, I will address both of these needs by investigating the basic rules that inform B cell differentiation in immune responses directed towards a model autoAg and a model foreign-Ag.

1.1 B and T cells in immunity and autoimmunity

I will start by discussing the essential properties of B cells that define how these cells participate in immune responses and how this may change in autoimmunity. In

addition, I will similarly discuss another cell of the immune system, called a T cell, as the B cell responses I will be studying in the thesis involve a necessary collaboration of these two cells types (this will be discussed in more detail later).

1.1.1 The generation and function of Ag-specific receptors on B and T cells

As B and T cells develop in the bone marrow and thymus, respectively, they rearrange genomic DNA through a random process to generate unique receptors specific to each of these cells (6, 7). For B cells, they recombine DNA to generate a B cell receptor (BCR) that is unique to each B cell clone. The BCR can be used to capture or target a specific Ag, which can consist of any unique 3-dimensional (3-D) surface that can be recognized by a BCR (8, 9). The recognition of Ags using the BCR is essential for B cells to act as antigen presenting cells (APCs) and antibody secreting cells (ASCs) and it is through these functions that the B cell contributes to immunity.

T cells similarly generate T cell receptors (TCRs) that are again unique to particular T cell clones and recognize a specific Ag (8). However, unlike B cells, they do not recognize Ag directly, instead they require APCs to collect and process full-length proteins into smaller fragments, often referred to as peptides or peptide fragments. These small peptide fragments are then loaded onto a specialized protein complex called the major histocompatibility complex (MHC). The peptide is loaded into a binding cleft on the MHC where molecular interaction between the MHC and peptide determine the efficiency of peptide loading (10). Once loaded, the peptide can be recognized in the binding cleft by TCR molecules. Classically, $\alpha\beta$ -T cells (that rearrange α and β TCR chains) have been divided in $CD4^+$ and $CD8^+$ T cells that recognize Ag presented on MHC class II and MHC class I molecules, respectively (11). The ability of T cells to recognize Ags through their TCR is essential for T cells to participate in the immune response by either coordinating the activity of other cells (12, 13) or by acting as cytotoxic cells to kill their targets (14). Although there are additional subsets of T cells beyond $\alpha\beta CD4^+$ T cells, for the purposes of this thesis, I focus on these T cells as they are the primary drivers of B cell responses (15).

Collectively, the B and T cell repertoires of Ag-specificity can recognize an almost unlimited number of Ags (16). Although this is highly beneficial for the immune system's ability to recognize pathogens, this is also problematic as many of the BCRs and TCRs generated also recognize autoAgs and can participate in autoimmunity. To limit autoimmunity, the immune system has several systems that act on B and T cells during development (central tolerance) that shape the peripheral B and T cell repertoires. One important mechanism for controlling autoreactive B and T cell responses is to limit the production of B and T cells that recognize autoAgs with high Ag-affinity, a key property of BCRs and TCRs that influences several aspects of B and T cell biology. Antigen-affinity is a measure of how strongly a BCR or TCR forms a physical contact with its target Ag. Antigen-receptor affinity affects not only the capacity of B and T cells to execute their effector functions (17, 18), but of key interest to this thesis, it also affects B and T cell activation and differentiation (17, 19). Thus, it is likely that the cumulative Ag-affinities of the B and T cell receptors available in the periphery of the body can in large part influence how an immune response initiates and progresses. Indeed, the idea that Ag-receptor affinity affects the progression of B cell responses will be addressed in this thesis. In this next section, I will discuss how tolerance mechanisms bias the peripheral autoreactive B and T cell repertoires towards lower Ag-affinities and why this would not occur for foreign-Ag specific B and T cell repertoires.

1.1.2 The influence of tolerance on autoreactive B and T cell receptors

As B and T cells progress through their development, they undergo a process known as negative selection that is responsible for purging autoreactive B and T cells (6, 20). Upon presentation of autoAgs during negative selection, developing B and T cells respond by triggering tolerance pathways that affect B and T cells differently. The fate of B cells upon recognizing an autoAg is to undergo receptor editing, wherein the BCR locus undergoes additional recombination events in an attempt to generate a new BCR that no longer recognizes autoAgs (21). In the event that a B cell cannot recombine and generate a non-autoreactive BCR, the B cell is induced to undergo apoptosis (22). Central tolerance of B cells successfully eliminates the vast majority of autoreactive B cells (6, 23, 24), however, approximately 20-40% of the peripheral B cell repertoire remains

autoreactive (25) although they typically recognize autoAgs with a low Ag-affinity (25, 26). Additionally, many of the leftover autoreactive B cells are anergic (a state of reduced responsiveness to Ag-receptor signaling) (27). Anergic B cells typically have a shorter life-span than non-anergic B cells leading to increased bias against the persistence of autoreactive cells (28-30). Altogether, central tolerance eliminates high-affinity autoreactive B cells thereby biasing the peripheral autoreactive B cell repertoire to B cells of low enough Ag-affinity to pass through central tolerance.

Similarly, autoreactive T cells undergo negative selection by exposure to autoAg in the thymus. In turn, the fate of an autoreactive T cell is determined by its Ag-affinity (31). T cells that recognize autoAgs with high-affinity are induced to undergo apoptosis, T cells that have low-affinity for autoAgs are unaffected, and T cells recognizing autoAgs with intermediate-affinity are induced to become regulatory T (Tregs) cells (32). Regulatory T cells are important as these intermediate-affinity cells would normally potentially induce autoimmune disease but are instead, functionally programmed to become a subset of T cells that potentially inhibits autoimmune responses (33, 34). Overall, central tolerance of T cells effectively removes higher-affinity autoreactive T cells that would otherwise potentially induce autoimmune disease by either deleting or converting them into regulatory cells, leaving a relatively smaller pool of low-affinity autoreactive T cells.

As foreign-Ags are not expressed in organs where B and T cells are developing, tolerance mechanisms do not appreciably affect the Ag-affinities of foreign-Ag specific B and T cell repertoires. Thus, a major difference between foreign-Ag specific and autoAg-specific B and T cells, is the abundance of high-affinity B and T cells in the foreign Ag-specific repertoire (35). Based upon the bias of autoreactive B and T cells towards low Ag-affinities, and given that Ag-affinity affects B and T cell activation, it is likely that the low Ag-affinities of autoreactive B and T cells will limit any immune response directed against protein autoAgs. Thus, I hypothesize that B cell responses, in the form of germinal center (GC) responses that are dependent on collaboration between B and T cells, will be short-lived and generally less productive than foreign-Ag induced GC responses as a result of the low Ag-receptor affinities of autoreactive B and T cells.

1.2 B cell responses in Multiple Sclerosis

Despite tolerance mechanisms limiting the capacity of autoreactive B and T cells to participate in autoimmune responses, it is still possible to engage these cells to do so. In this section, I will describe the autoimmune disease MS that incorporates autoreactive B and T cells into its pathology.

1.2.1 Multiple Sclerosis and experimental autoimmune encephalomyelitis

Multiple Sclerosis is an autoimmune disease where the myelin sheath surrounding neurons in the central nervous system (CNS) is targeted for destruction by the immune system. Damage to the CNS results in cognitive and physical disabilities that vary depending on the region of the brain or spinal cord that has been damaged (36). Studies looking for genetic signatures associated with MS have identified predominantly genes that are associated with the immune system suggesting the immune system plays a key role in the initiation of MS (37). Historically, MS has been thought of as a CD4⁺ T cell mediated autoimmune disease as the induction of a myelin-specific CD4⁺ T cell response is the minimum requirement to induce CNS autoimmunity in animals (38). Collectively, animal models of CNS autoimmunity are known as experimental autoimmune encephalomyelitis (EAE) (39). Typically, EAE is induced by immunizing animals with short peptide fragments corresponding to immunodominant CD4⁺ T cell epitopes derived from one of three major components of the myelin sheath: MOG, proteolipid protein, and myelin basic protein. The disease course of EAE follows a predictable course of ascending paralysis in mice and is characterized by the infiltration of T cells, B cells, and various myeloid cells near regions of demyelination in the spinal cord and brain (40). As MS research has evolved additional cells beyond CD4⁺ T cells have emerged as important mediators of disease including cells of the myeloid lineage, CD8⁺ T cells and, of key interest to this thesis, B cells.

1.2.2 Role of the B cell in Multiple Sclerosis

B cells had originally been thought to be of limited importance to disease progression because the induction of a CD4⁺ T cell response was the minimum requirement to induce EAE and B cell-deficient mice develop worse EAE than wild type

mice (41). These results were misleading however, as B cell deficient mice develop worse EAE as a result of lacking IL-10/IL-35 expressing regulatory B (Breg) cells that potently inhibit T cell responses (42-44). Interest in B cells in MS was reignited when the depletion of B cells in MS patients using an anti-CD20 antibody was shown to be one of the most effective treatments for MS currently available (45, 46). Indeed, although Bregs can be found in MS patients (47), it is now clear that the B cell compartment is overall pro-inflammatory in MS and animal models (48, 49). Interestingly, CD20 is expressed on all human B cell subsets except antibody-secreting plasma cells and the therapeutic benefit of the anti-CD20 monoclonal antibodies occurs before any decrease in serum antibody levels suggesting that non-plasma cell B cells may be the primary contributor to MS (50, 51).

Engaging B cells to participate in immune responses directed against protein Ags, such as those that are targeted in MS, typically occurs by inducing a GC, a structure that normally forms in secondary lymphoid organs such as the spleen, peyers patches, or lymph node (LN) (52). Within the GC, B cells can acquire high-affinity BCRs by mutating their genomes, in particular the BCR locus, using enzymes such as activation-induced cytidine deaminase and uracil-DNA glycosylase in combination with DNA repair pathways to mutate nucleotides in the BCR locus, a process known as somatic hypermutation (SHM) (53). Nucleotide changes within the BCR then translate into amino acid changes in the BCR that can affect the BCRs ability to bind Ag. Activation-induced cytidine deaminase is also involved in another process where B cells undergo immunoglobulin class-switch recombination (CSR) where IgM and IgD BCR isotypes are switched for IgG, IgE, and IgA BCR isotypes (54). Class-switching is important as BCR isotype affects the effector functions of secreted antibodies and also affects Ag-induced signaling through the BCR (55-57). Overall, the GC supports these two processes leading to the production of high-affinity and class-switched B cell subsets that contribute to potent long-term immunity (58). Thus, if B cells are being engaged in an Ag-specific manner in MS, we would expect that there should be evidence of myelin-specific B cells that have undergone CSR and SHM.

In support of the idea that myelin-specific B cells are stimulated in MS, high-affinity MOG-specific IgG antibodies can be found in the serum of 67% of early onset pediatric MS patients (59) and 20-42% of MS patients later in disease (60-62). Furthermore, at the later stages of disease, IgG-antibodies directed against other myelin-Ags are commonly seen (63, 64). As these antibodies are class-switched and of high-affinity, this is highly suggestive that the plasma cells that generated these antibodies were derived from GCs. Myelin-specific B cells have also been seen to contribute to EAE in several different models. The contribution of myelin-specific B cells to EAE is partially through antibodies (65), however, it is clear that myelin-specific B cells also contribute to the initiation and progression of EAE independently of antibody secretion (49, 66, 67). Thus, there is evidence of myelin-specific GCs occurring in MS and there is evidence of myelin-specific B cells contributing to the pathology of EAE suggesting myelin-specific B cells in MS may also contribute to MS pathology.

Germinal centers directed against myelin-Ags could potentially occur within the deep cervical LNs as they are connected to the lymphatic drainage of the brain and thus, make autoAgs available to autoreactive B and T cells (68-70). Consistent with the idea that B cell responses in the deep cervical LNs are contributing to MS pathology, there is evidence that clonally expanded B cells in the deep cervical LNs are clonally related to B cells found within the CNS of MS patients (71, 72). In particular, analysis of SHM in B cells derived from the deep cervical LNs, peripheral blood, and cerebral spinal fluid of MS patients identified B cell clones that were derived from the same GC. Thus, beyond there being evidence of myelin-specific GCs in MS, there is also evidence of GCs occurring outside of the CNS that are generating Ag-experienced B cells that are entering the CNS.

A key assumption in the literature is that the B cell clonal relationships found between the periphery and the CNS are due to myelin-specific B cells proliferating in the periphery and entering the CNS. However, despite the evidence suggesting that GC-derived myelin-specific B cells contribute to the pathology of MS, no study to date has characterized how a GC response directed against a myelin autoAg would initiate or progress. Furthermore, as no one has studied myelin-specific GC responses, we also do

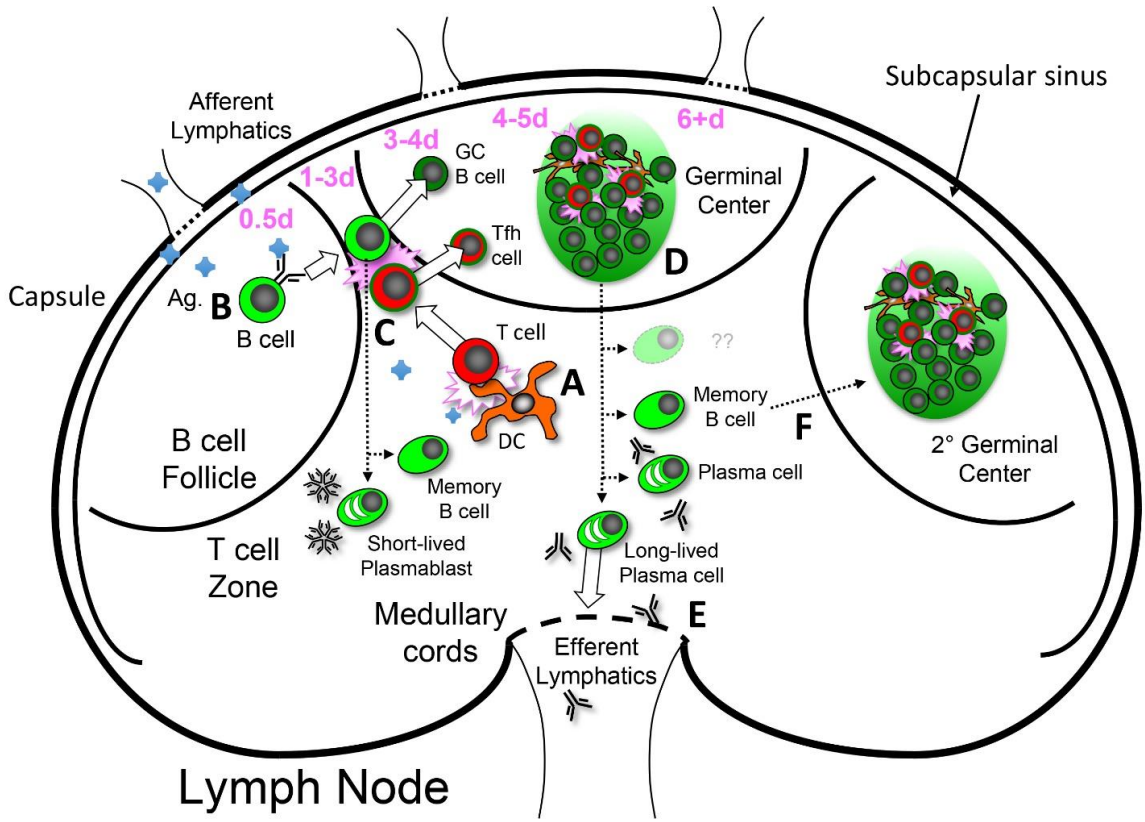
not have a good understanding of what immune cells are generated from myelin-specific GCs or the properties of those cells. Indeed, based upon what is known about B and T cell activation and the properties of autoreactive B and T cells (section 1.1), it is likely that a GC directed against a myelin-autoAg will not progress in the same fashion as foreign-Ag induced GCs. In this thesis, I address this need by studying GC responses directed against the myelin protein, MOG, which is commonly used to induce EAE. In the next sections, I will describe what is currently known about GCs and how Ag-properties affect GCs.

1.3 Germinal center responses

The initiation and progression of GC responses has been classically defined in context of GCs in LNs or the spleen. Germinal center responses proceed similarly in LNs and the spleen despite being structurally different (73, 74). However, the experiments in this thesis focus exclusively on LNs and thus, I will only describe the GC response in the LN. Lymph nodes are found throughout the body where they collect excess lymph from surrounding tissues and process pathogens/debris/Ags that filter through the LN to activate Ag-specific B and T cells (75) (Figure 1.1). Lymph nodes have a thick outer capsule that forms a conduit for incoming lymph in conjunction with the subcapsular sinus. Lymph filters through the subcapsular sinus into the B cell follicle that is located just below the subcapsular sinus (73). B cells reside in the B cell follicle where they can interact with Ags draining through the B cell follicle through a variety of mechanisms that will be described in more detail in section 1.3.1. Below the B cell follicles, CD8⁺ and CD4⁺ T cells reside in the T cell zone that serves as the site of initial T cell activation. Then, at the absolute center of the LN, are the medullary cords where macrophage and plasma cells/plasmablasts reside. After lymph has passed through these sites, it is collected in the efferent lymphatic duct and flows through the lymphatic system until it connects back to circulating blood through the thoracic duct (75). These microstructures are essential in directing B and T cells during immune responses and these structures will be discussed in detail in the following sections.

Figure 1.1. Summary of developing germinal center responses.

Immune responses in LNs start when mature Ag-presenting dendritic cells and soluble Ags flow into the LN. (A) The Ag-specific T cell response is initiated through interactions with mature Ag-presenting dendritic cells (76). (B) The B cell response is initiated when B cells engage their Ag with their BCR, resulting in their activation (77). (C) When these two events occur, approximately 1 day post-immunization, activated B cells and pre-T follicular helper (pre-T_{FH}) cells will migrate to the periphery of the B cell follicle and form cognate interactions (78). These cognate interactions are responsible for driving B cell differentiation into memory B cells, antibody-secreting plasmablasts, and differentiation into GC B cells as well as finishing T_{FH} cell differentiation. (D) Approximately 4 days post-immunization, T_{FH} cells and GC B cells then migrate into the B cell follicle and seed a new GC where they again form cognate interactions. These interactions are responsible for GC maintenance and differentiation of GC B cells into antibody-secreting plasma cell subsets (E) and memory B cells which can participate in secondary GC responses if induced to do so (F) (79).



1.3.1 The initiation of B and T cell responses

At the initiation of immune responses, Ags flow into LNs through lymphatic vessels which permeate surrounding tissues. Once Ag has arrived at the LN, it can diffuse across the subcapsular sinus through small pores that allow small Ags to cross this layer. Alternatively, B cells can actively collect Ag by extending membrane projections into small channels carrying lymph through the B cell follicle (80). Larger Ags can be actively collected in LNs by subcapsular sinus macrophage that shuttle complement associated Ag from the subcapsular sinus into the B cell follicle (81). Moreover, dendritic cells (DCs) that have collected Ag from the periphery of the body can exocytose whole Ag into the B cell follicle (82). Through the BCR, B cells can recognize soluble Ags directly in extracellular fluid (Figure 1.1B) or can recognize Ag deposited on specialized follicular dendritic cells (FDCs), which collect Ags and are found at the center of the B cell follicle (83). The FDC is important at this early stage of the immune response as they retain Ags for long periods of time and can also collect insoluble or low affinity Ags that B cells may have more difficulty responding to (84).

B cell receptor recognition of Ags results in the activation of B cells, culminating in gene expression changes and altered surface expression of co-stimulatory molecules that are important for the next stage of the B cell response, the pre-GC time point (see section 1.3.2). This next stage of the B cell response is initiated when B cells upregulate CCR7, a chemokine receptor, which directs cells to migrate towards the T cell zone as a result of the expression of the CCL19 and CCL21 ligands by follicular reticular cells in the T cell zone (85, 86). Additionally, B cells upregulate EBI2, a chemotactic receptor that directs cells towards the periphery of the B cell follicle (87, 88) due to the expression of oxysterols at the periphery of the B cell follicle (89). This change in chemotactic receptor expression ultimately directs B cells to move towards the border of the B cell follicle and T cell zone where B cells await a cognate T cell partner to continue their differentiation (77).

The T cell response occurs simultaneously with the B cell response. However T cells are activated through an entirely different process. T cell responses are initiated by resident DCs that collect Ags in the periphery of the body. Upon encountering a pathogen

and/or a signal indicating danger/tissue damage, DCs will begin to differentiate into mature DCs. These DCs continue to mature and their activation commences as they migrate from the periphery of the body into draining LNs and localize to the T cell zone where they present Ags on MHC molecules to T cells (76). If a CD4⁺ T cell recognizes one of the Ag peptides being presented on the DC, the T cell and the DC will form a stable and long-lived interaction that is responsible for inducing T cell proliferation and instructing T cell differentiation (Figure 1.1A) (90). The differentiation of CD4⁺ T cells is instructed by a combination of cytokines and T cell Ag affinity that influence the choice to become the various T helper subsets such as T helper 1, T helper 2, T helper 17 cells and other T cell subsets (91-93). One of these other subsets, the pre-T_{FH} cell, is essential for the initiation and maintenance of the GC response and thus, is of the greatest importance to this thesis (15). Pre-T_{FH} cells undergo a transcriptional reprogramming as part of their differentiation involving the expression of the transcription factor, Bcl6, a key regulator directing T_{FH} cell differentiation. The expression of Bcl6 is essential for expressing the co-stimulatory receptors and ligands that are of critical importance to the next stage of the immune response, the pre-GC time point (94). Similar to B cells, pre-T_{FH} cells also modify their expression of chemokine receptors by upregulating CXCR5, a chemokine receptor that directs cells towards the B cell follicle (88) as a result of CXCL13 expression by follicular stromal cells and FDCs in the center of the B cell follicle (95). Ultimately, this results in their localization to the border of the B cell follicle and the T cell zone (78, 96). Once activated B cells and pre-T_{FH} cells meet at the B cell follicle-T cell zone border, the pre-GC time point begins.

1.3.2 The pre-germinal center time point

The pre-GC time point occurs approximately 1-1.5 days post-immunization and begins once activated B cells begin to form physical interactions with pre-T_{FH} cells. During this time point, cognate B and T cells interact via their MHC class II and TCR molecules, co-stimulatory/co-inhibitory receptors, and a variety of integrins whose signaling is incorporated into decisions that result in cell differentiation, proliferation, or initiation of cell death. For a more detailed description of these receptors and the timing of their expression, see section 1.8. Interactions between B and T cells occur along the

border between the B cell follicle and the T cell zone up to a region between B cell follicles known as the interfollicular zone (78) (Figure 1.1C). Pre-GC interactions between B and T cells are typically long-lived in nature, potentially lasting hours in length (78, 97). During these interactions signals are exchanged between cognate B and T cells that are essential for the pre-T_{FH} cells to fully differentiate into T follicular helper (T_{FH}) cells, which are responsible for GC maintenance once they form (98). In addition to T_{FH} cell differentiation, pre-GC B-T interactions have a profound effect on the way that the B cell response will progress.

At the pre-GC stage, B cells can differentiate into several different B cell subsets: low-affinity short-lived plasmablasts, GC-independent memory B cells, and GC B cells. Short-lived plasmablasts are a type of ASC that are responsible for generating low-affinity IgM antibodies early in the immune response to help with infections, before high-affinity antibodies are generated later in the GC. Whereas short-lived plasmablasts contribute to the early immune response, memory B cells contribute to long-term immunity. Memory B cells cease proliferation and become quiescent once differentiated and instead acquire a naïve-like phenotype and rejoin the circulating B cell pool (99, 100). If there is a second challenge with the same Ag, memory B cells can be stimulated to participate in secondary responses by quickly differentiating into plasma cells or GC B cells, accelerating the development of secondary GCs and quickly reinforcing antibody titers (100) (Figure 1.1F). The differentiation of GC B cells marks the end of the pre-GC phase as upon differentiation they migrate into the B cell follicle, along with T_{FH} cells, and are responsible for seeding the GC (78, 101, 102). (Figure 1.1D).

1.3.3 The germinal center

The GC is an organized collection of cells, predominantly GC B cells, T_{FH} cells, FDCs, and other minor populations of cells which form at the center of B cell follicles. From the GC, several B cell subsets are generated: GC-derived memory B cell subsets, plasma cells, and long-lived plasma cells (58). The GC is an environment optimized for inducing SHM and CSR within GC B cells for the purposes of driving GC B cells to acquire high-affinity class-switched BCRs (53, 103). Thus, a GC B cell's affinity for Ag and their BCR isotype is not fixed in a GC.

However, inducing CSR and SHM can generate non-functional BCRs or BCRs that recognize their Ag with a lower-affinity (104, 105). Thus, CSR and SHM in GC B cells needs to be complemented by selective pressure to expand functional high-affinity B cell clones and eliminate low-affinity or non-functional B cell clones. This is the role played by the T_{FH} cell. Much like the pre-GC time point, it is physical interactions between GC B cells and T_{FH} cells within the GC that are responsible for selecting GC B cells to continue in the GC and for directing B cell fate choices. Unlike pre-GC B and T cell interactions however, GC interactions are much shorter in nature but are nonetheless essential for GC maintenance (78, 106). These interactions are ultimately what controls the GC response as a whole and in the following sections I will describe how T cells influence the fate choices B cells make during GC responses. Furthermore, I will discuss the properties of GC B cells, ASCs, memory B cells, and T_{FH} cells in more detail.

1.4 Germinal center B cells

GC B cells are distinguished from naive B cells or memory B cells based upon their expression of the following markers in mice: GC B cells are Bcl6⁺, CD38^{low}, CD95^{high}, GL-7⁺, and IgD⁻ (107). Properties associated with GC B cells include relatively high levels of apoptosis, high levels of proliferation, and active SHM. Below, I will describe in more detail how GC B cells are maintained in immune responses and factors influencing their differentiation.

1.4.1 The light and dark zones of the germinal center

GC B cells exist in two major phases, a light zone (LZ) phase and a dark zone (DZ) phase (Figure 1.2A). These structures are essential and unique as the disruption of either of these structures impacts GC maintenance, SHM, and the production of B cell subsets (108). The LZ of the GC is where FDCs are found and T_{FH} cells concentrate (109). In this zone, GC B cells are referred to as centrocytes and compete with each other for the limiting resource in the GC, Ag, which is concentrated on FDCs (110). The ability of a particular centrocyte to obtain Ag is determined by their affinity for Ag. The acquisition of Ag leads to centrocytes internalizing and processing Ag for presentation on MHC class II molecules (17). The amount of Ag presented by centrocytes is directly

proportional to the interaction time they secure with T_{FH} cells and by extension the amount of costimulatory signaling they receive from T_{FH} cells (111-113). Receiving T_{FH} cell signals are important for influencing the differentiation of GC B cells (this will be further discussed in subsequent sections), but also because T_{FH} cell signals are responsible for selecting centrocytes to enter the DZ of the GC. To enter the DZ, GC B cells upregulate the chemokine receptor CXCR4 that binds the chemokine CXCL12 secreted by follicular reticular cells in the DZ (108, 114). The presence of CXCL12 in the DZ attracts CXCR4⁺ GC B cells, which are now referred to as centroblasts. Once in the DZ, centroblasts downregulate surface BCRs and costimulatory molecules before undergoing SHM and CSR (58).

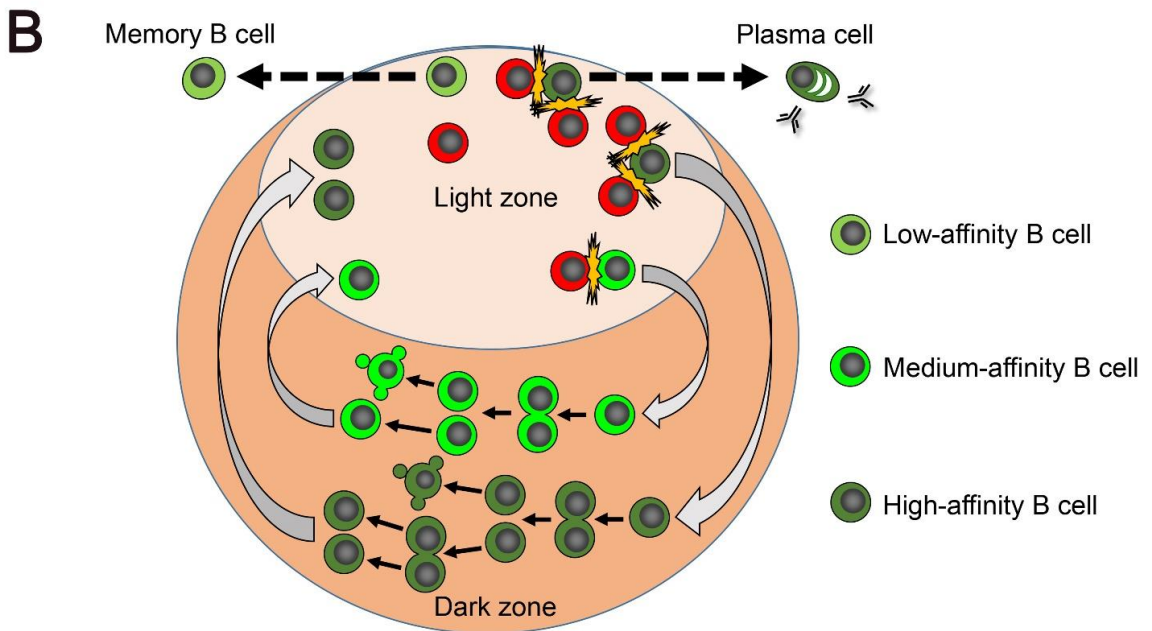
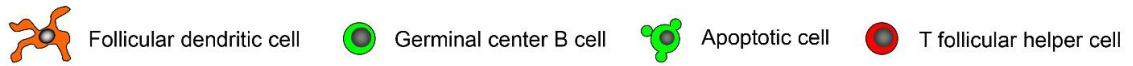
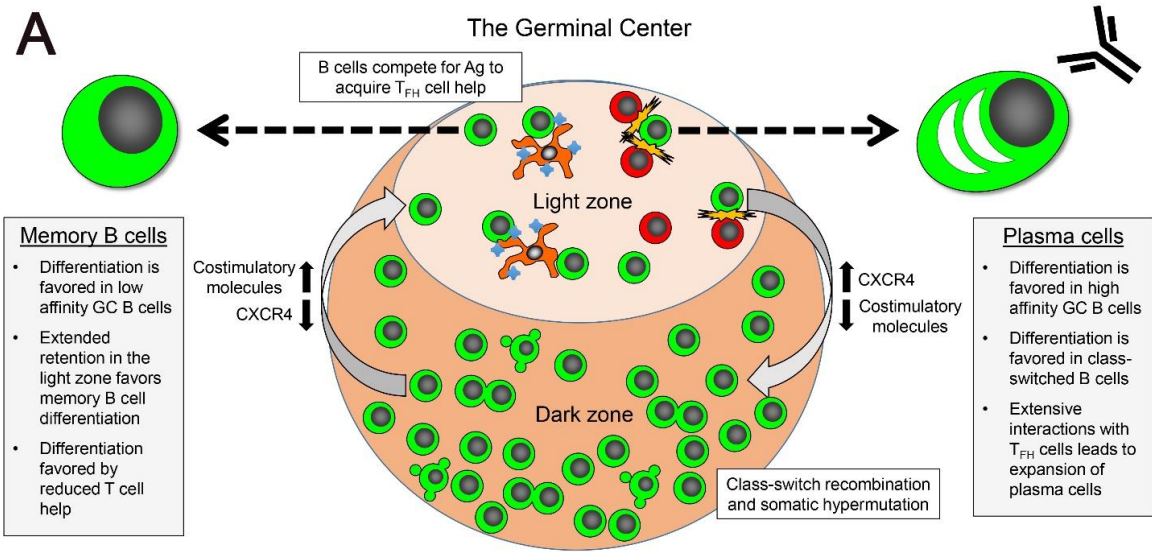
As centroblasts are mutating their BCRs, they are also undergoing extensive proliferation (115, 116). The number of rounds of proliferation and the length of time that a centroblast stays in the DZ are thought to be influenced by their interactions with T_{FH} cells that occurred in the LZ (115, 117). As the length of time in the DZ is directly proportional to the amount of SHM a centroblast will undergo (115), the retention in the DZ of the GC is advantageous for acquiring a high-affinity BCR. Additionally, as centroblasts proliferate, they are also under pressure to undergo apoptosis (118), a process that is thought to be inhibited through signals acquired from the T_{FH} cell (111). Class-switch recombination also occurs in the DZ of the GC and, although CSR does not affect the Ag-affinity of a BCR, switching to other BCR isotypes can modify intracellular signaling in B cells and can affect the fate choices and competitiveness of B cells in the GC (56, 119, 120). Thus, a combination of SHM and CSR can influence the competitiveness of individual B cell clones.

After a period of time, the centroblast will complete its proliferation and will begin expressing its newly mutated BCR and costimulatory molecules, while downregulating CXCR4 allowing it to enter the LZ of the GC where it will again compete for Ag. This process of continuously cycling between the LZ and DZ of the GC is generally known as the cyclic re-entry model of the GC. Overall, the combination of selection pressures to enter the DZ, apoptosis, and proliferation serve to expand the population of high-affinity B cell clones over continuous rounds of LZ-DZ transitions

ultimately resulting in a slow progression in the GC towards higher-affinity B cells (79) (Figure 1.2B). Indeed, the starting affinity of B cells entering the GC can increase by a million fold by the end of the GC (121, 122) where these high-affinity B cell clones typically become the primary B cell clone in the GC when they emerge (123). As GC B cells are the precursor to all other GC-derived B cell subsets, and GCs can potentially continue for months (124, 125), retention and expansion of a particular B cell clone within the GC will lead to that particular B cell clones progeny dominating the products of a GC as it continues. This is further complicated as certain subsets of B cells emerge from the GC at different times. Memory B cells emerge from the GC first, with optimal memory B cell production typically lasting ~22 days post-immunization; thereafter plasma cell differentiation tends to be favored (126). Consequently, retention in the GC not only affects the continued production of a particular B cell clone, but also the differentiation of that clone into particular B cell subsets that are favored in the later portions of the GC response.

Figure 1.2. B cell differentiation and selection in the light and dark zones of the germinal center.

(A) GC B cells in the LZ of the GC are in constant competition with one another to acquire Ag sequestered on FDCs (110). Germinal center B cells that do not acquire Ag do not secure interactions with T_{FH} cells and persist in the LZ promoting memory differentiation (127). B cells that successfully compete for Ag and interact with T_{FH} cells will be selected to transition into the DZ of the GC (111) or alternatively may begin plasmablast/plasma cell differentiation if they receive strong BCR signaling (128). GC B cells that transition into the DZ upregulate CXCR4 and downregulate surface receptors associated with B and T cell interactions (58, 108). Once in the DZ, B cells begin to proliferate at an increased rate (115) and may also undergo apoptosis depending on their resistance to apoptosis determined by T cell help acquired in the LZ (118). As this is occurring, GC B cells that survive mutate their BCR through SHM and CSR in an attempt to generate a new higher-affinity and class-switched BCR before transitioning back to the LZ (58). The transition back to the LZ is associated with the downregulation of CXCR4, upregulation of costimulatory molecules and their newly mutated BCR. (B) The fates of low, medium, and high-affinity GC B cells in the GC are summarized based upon the model provided above.



1.4.2 Germinal center B cell differentiation

The GC status of B cells is a temporary and unstable state that is maintained by the expression of the master transcription factor, Bcl6 (129). As GC B cells are an intermediate, the eventual fate of a GC B cell is death or differentiation that is determined by the expression of transcription factors. The expression of Bcl6 suppresses Blimp-1 expression, where Blimp-1 is the master transcription factor directing plasma cell differentiation, and thus secures the GC B cell identity (130, 131). GC B cell differentiation is not thought to be directly antagonistic with memory B cell differentiation as the expression of Bach2, a transcription factor that has recently emerged as an important driver in memory differentiation, is not directly antagonistic with Bcl6 (127).

1.5 Memory B cells

The study of memory B cells in mice is complicated by the lack of a universal marker to differentiate memory B cells from naïve B cells (132). This is further complicated by a paucity of knowledge on B cell subsets as all non-plasma cell, non-GC B cell, and non-naïve B cells are grouped together as memory B cells. This is in part due to the definition of memory B cells typically used in studies: a B cell that has participated in a B cell response that has since acquired a quiescent, naïve-like phenotype. True memory B cells, however, should also show evidence of: (1st), persistence over time; (2nd), attaining a quiescent state; (3rd), specificity for a known Ag; and lastly, the ability to respond in secondary immune responses (100). Thus, without a universal marker to identify all memory B cells in mice, demonstration of memory requires satisfying the above criteria.

1.5.1 Memory B cell subsets

Historically, memory B cells have been defined as class-switched naïve-like B cells as class-switching only occurs after B cells have participated in an immune response, but also because it was easy to identify class-switched B cells. More recently it was discovered that many memory B cells are IgM⁺ (133) and indeed not all memory B cells require the GC as many differentiate before GC formation (126, 134). Studies

looking at the functionality of IgM⁺ vs IgG⁺ memory B cell subsets identified several differences between the two subsets (Table 1.1) and lead to the idea that memory B cell responses were controlled by their BCR isotype. However, recent studies grouping memory B cells based upon the expression of CD80 and PD-L2, have provided better predictive power than the usage of class-switching alone (135) (Table 1.1). Thus, although class-switching can be useful for predicting how conventional memory B cells will differentiate in secondary immune responses, new markers are providing a more refined view.

Relatively recently a subset of CD27^{+/-} CD21⁻ B cells, also known as Atypical/age/exhausted/autoimmune associated B cell (ABCs), have been identified in a variety of different chronic diseases such as rheumatoid arthritis (136), malaria (137), human immunodeficiency virus (138), cytomegalovirus (139), hepatitis C virus infections (140), and MS (141). Based on these papers, ABCs appear to be Ag experienced as they class-switched and are clonally related to standard memory B cells produced in GCs (137). Furthermore, ABCs tend to be polyreactive often recognizing self-Ags or are specific for Ags associated with the infectious agent or autoimmune disease (136, 138, 140, 142). This subset is only beginning to be defined (Table 1.1) but appears to be a GC-derived subset that can contribute to immune responses.

Table 1.1. Summary of memory B cell subsets and their functions.

Subset	Function and properties
Naïve-like IgM⁺	Primarily enter the GC in secondary immune responses (143) unless their activation is suppressed by circulating IgG (102). Typically these cells are low affinity for Ag and have not undergone extensive SHM (129). A large portion of these cells are generated prior to GC formation (126).
Class-switched, IgD⁻ IgM⁻ IgG⁺	Primarily contribute to the GC and secondary plasma cell responses (143). Recruited into secondary immune responses preferentially over IgM ⁺ memory B cells (144, 145). Typically these cells are higher affinity for their Ag have some SHM (129). Primarily GC derived (126).
CD80⁻ PD-L2⁻	These cells primarily enter the GC in secondary immune responses regardless of isotype (135). These cells are mostly low-affinity and not class-switched. They are typically made early in the GC response (126).
CD80⁺ PD-L2⁺	These cells primarily differentiate into plasma cells in secondary immune responses regardless of isotype (135). Most of these cells are higher affinity and class-switched memory B cells. They are typically generated late in the GC response (126).
CD80^{+/-} PD-L2^{+/-}	These cells express either CD80 or PD-L2, but not both. They have a phenotype intermediate between double positive and double negative memory B cells (135).
ABC	Commonly express Tbet, CD11b, CD11c, and downregulate CD21 and CD23 (146, 147). Some cells with this phenotype can act as potent Ag-specific APCs and are poorly responsive in secondary responses (136-138, 148). Nonetheless, others have found that they can be serial transferred to give rise to new GCs and have stem like properties (149).

1.5.2 Memory B cell differentiation

Although the transcription factors responsible for programming the memory B cell identity are not well characterized, there is one notable transcription factor associated with memory B cells. Memory B cell differentiation tends to be favored by high expression of Bach2 in the GC (127, 150) where Bach2 is antagonistic to the expression of the master regulator of plasma cell differentiation, Blimp-1 (127). Nonetheless, both naïve B cells and memory B cells express Bach2. Thus Bach2 alone cannot be responsible for the memory B cell identity. Another possibility is that memory B cell differentiation may not be controlled entirely by transcription factors but also through epigenetics, an aspect still being characterized (151). B cells destined to differentiate into memory B cells in the GC tend to accumulate in the LZ of the GC as these B cells typically are not selected by T_{FH} cells to transition into the DZ (108, 152). Indeed, low BCR Ag-affinity and, thus, a low capacity to compete for T_{FH} cell help, favors memory B cell differentiation (127). Consistent with this, expression of Bach2 in GC B cells is inversely proportional to BCR Ag-affinity (127). Thus, a relative lack of T cell help tends to favor memory B cell differentiation.

1.6 Plasmablasts and plasma cells

Classically, the primary function of plasmablasts/plasma cells, collectively referred to as ASCs, is to produce antibodies that neutralize, opsonize, or lyse their targets. Antibodies can differ in isotype where particular isotypes are specialized to interface with different immune effector mechanisms. Through the production of antibodies, ASCs can be responsible for completely abolishing infections, the prevention of infectious diseases, and autoimmunity (153, 154). Thus, ASCs represent an important subset of effector cells produced from the B cell response.

ASCs are identified using the CD138 marker (155) and can be broadly split into plasmablasts and plasma cells. Plasmablasts are an actively proliferating precursor to terminally differentiated plasma cells (156). While both plasmablasts and plasma cells make antibodies, plasma cells are more polarized towards effector functions as a result of expanding their endoplasmic reticulum to accommodate increased protein expression

(157). Unlike plasma cells, plasmablasts maintain expression of MHC class II, the BCR, and co-stimulatory molecules and retain the capacity to interact with T cells for proliferative and anti-apoptotic signals (156, 158, 159). Altogether, B cells initially differentiate into highly proliferative plasmablasts that can eventually terminally differentiate into non-proliferative plasma cells that are highly specialized toward their effector functions.

1.6.1 Differentiation of plasmablasts and plasma cells

The fate decision to become a plasma cell originates in the B cell, decided by its BCR affinity, and is completed by the T cell, by influencing the proliferation vs cell death of plasmablasts (128, 160). In particular, differentiation of B cells into ASCs is favored by having a relatively high-affinity for Ag as this primes B cells to begin ASC differentiation but also leads to B cells securing additional T cell help through the presentation of additional Ag on MHC class II (112, 128). Indeed, when two populations of equal-affinity B cells are in competition, targeting Ag to one of the populations will cause the targeted population to secure more T cell help and increased representation in the ASC population as result of increased proliferation (128, 160, 161). B cells destined to become ASCs typically leave the LZ of the GC to undergo a brief period of proliferation in the DZ before these cells leave the GC altogether to become a part of the plasma cell pool (128). Differentiation into ASCs is induced by Blimp-1 (162-164) and by suppressing Bcl6 expression (165). Overall, the size of the plasma cell response is influenced by a combination of B cells choosing to differentiate into plasma cells based upon BCR-affinity, but also expansion based upon T cell signals.

1.6.2 Subsets of plasmablasts and plasma cells

ASCs are generated from two major sources in the GC response: an initial burst prior to GC formation and throughout the ongoing GC (78, 156). Pre-GC ASC differentiation typically consists of low-affinity, primarily IgM plasmablasts that localize to the medullary cords of the LN via CXCR4 expression where they continue to produce antibodies until they apoptose or leave the tissue (99, 159, 166, 167). This population has typically been described as short-lived. However, a portion of these Pre-GC ASC give

rise to long-lived IgM⁺ plasma cells that localize to the spleen and bone marrow (101). From these locations, long-lived plasma cells can produce antibodies continuously over a long period of time and contribute to long-term immunity.

ASCs produced from the GC can be separated into plasma cells and long-lived plasma cells. Plasma cells derived from the GC localize to the medullary cords of the LN similarly to pre-GC-derived ASCs (167). Germinal center-derived long-lived plasma cells localize to the bone marrow where they are maintained as a niche (101). Long-lived plasma cells do not live indefinitely. Their niche in the bone marrow has a maximum capacity and as a result, some vaccinations require booster immunization to maintain long-lived plasma cell numbers (168). Germinal center-derived ASCs are important as both short and long-lived ASCs are more likely to be class-switched, have undergone substantial SHM, and recognize their Ag with high-affinity relative to pre-GC plasma cells (101). Overall, pre-GC and GC-derived ASCs have similar but not necessarily overlapping functions in the immune response.

1.7 T follicular helper cells

T follicular helper cells were originally identified as a cell that accumulates in B cell follicles in autoimmune mice and was associated with excessive GC formation (169). Indeed, it is now clear that the maintenance of the GC response is critically dependent on T_{FH} cells (170). T_{FH} cells localize to the B cell follicle and concentrate in the LZ of the GC where they interact with GC B cells and direct their selection (171). T_{FH} cells are typically identified through the expression of several different markers on CD4⁺ T cells: CXCR5⁺, PD-1⁺, ICOS⁺, GL-7⁺, Bcl6⁺ and low CD62L expression (172).

1.7.1 Pre-T follicular helper cells

The differentiation of T_{FH} cells is initiated through interactions between DCs and CD4⁺ T cells at the initiation of the immune response. T cells that begin to express Bcl6 based on these interactions are known as pre-T_{FH} cells. These cells have acquired most of the features of a T_{FH} cell but they do not localize to the GC. Instead pre-T_{FH} cells go towards the B cell follicle-T cell zone boundary where they form interactions with B cells (78, 172). These interactions are essential for GC formation, but, they are also required

for pre-T_{FH} cells to finish their differentiation into mature T_{FH} cells (78, 173). In addition to pre-T_{FH} cell differentiation, memory T_{FH} cells are also generated from early DC-T cell interactions. Memory T_{FH} cell differentiation does not require B cell interactions as they enter the circulation shortly after interacting with DCs (94). As memory T_{FH} cells circulate through secondary lymphoid organs, they can participate in secondary immune responses if their Ag is present (174).

1.7.2 T follicular helper cells and their associated subsets

T follicular helper cells promote the GC response using cytokines such as IL-4, IL-9, IL-10, IL-21, and surface receptors to modify B cell differentiation (106, 150, 175-177) (discussed in more detail in section 1.8). However, expression of these molecules can differ between individual T_{FH} cells and thus, can differ in their capacity to provide T cell help. In particular, T_{FH} cells found in the B cell follicle have a less polarized phenotype characterized by: lower expression of Bcl6, co-stimulatory molecules, and cytokine expression but normal PD-1 expression (178, 179). Indeed, if T_{FH} cells are forced to localize to the B cell follicle, using mice deficient in CXCR5 and S1PR2, they are less capable of maintaining GC's (178). Both follicular and GC T_{FH} cells require interactions with B cells to maintain their phenotype as inadequate interaction with B cells causes T cells to lose their PD-1 high phenotype required for them to persist in the immune response (78, 170, 180).

Recently another population of T cells called T follicular regulatory (T_{FR}) cells has also been defined. These cells express many of the same receptors and transcription factors as conventional T_{FH} cells do. However, they also express FoxP3, the transcription factor driving regulatory cell identity (181). T follicular regulatory cells can originate from Tregs generated during T cell development (182) or naïve T cells can be induced to differentiate into T_{FR} cells through immunization (183, 184). The differentiation of these cells is thought to be similar to T_{FH} cell generation including the requirement for B-T interactions for their maintenance (94). T follicular regulatory cells have been described to inhibit GC responses by inhibiting both T_{FH} cells (185) and GC B cells (186). Indeed, the ratio of T_{FH} cells to T_{FR} cells can affect GC progression where the maintenance of the T_{FH} cell population is of critical importance (187). Of note, both the T_{FH} cell and T_{FR} cell

populations are dynamic and thus, the ratio of these cells can change over the course of the GC response (182, 183). Nonetheless, the role of the T_{FR} cell in the GC is complicated as these cells are also responsible for producing IL-10 (175), a cytokine that promotes GC B cell survival (188), and thus may in some scenarios promote GCs (189). Overall, the T_{FR} cell population plays an important role in suppressing autoimmunity (190) while in some scenarios, T_{FR} cells can promote GC responses.

1.8 B and T cell interactions

Throughout the GC the physical interaction between B and T cells is essential for the maintenance of the GC and the differentiation of B cells into the various B cell subsets. In these interactions, B and T cells exchange signals via secreted cytokines and ligation of surface receptors. The sum of these signals induce intracellular signaling cascades that ultimately influence B and T cell biology and will be discussed in detail here.

1.8.1 Cellular identity and signal integration

The identity of cells, such as B or T cells, is determined by a set of core transcription factors that program their identity (191). Typically, these transcription factors are constitutively expressed in the nucleus and are responsible for continuously inducing the production of proteins associated with a cell's particular identity. The identity of a cell can change if the expression of the core set of transcription factors changes. Changes in the expression of these transcription factors can occur by several mechanisms: (1st), signaling can drive the inactivation or degradation of core transcription factors (192); (2nd), induced expression of another core transcription factor may repress the expression of others (193); (3rd), and signaling may drive transcription factors normally based in the cytoplasm to enter and accumulate in the nucleus thereby changing the nuclear content of core transcription factors (130). Amongst these mechanisms, the controlled activation of cytoplasmic-based transcription factors to translocate in the nucleus is particularly important as they can act as hubs of signal integration. Indeed, by controlling their nuclear localization, positive and negative signaling from multiple different pathways can be summed together into one decision

(194, 195). Altogether, core transcription factors are responsible for programming cellular identity where the expression of core transcription factors can be modified through cellular signaling.

Two commonly used pathways in the immune system are the nuclear factor kappa B (NF κ B) and nuclear factor of activated T cells (NFAT) pathways. The NF κ B pathway is activated through either a canonical pathway or a non-canonical pathway that converges upon the activation of the I κ B kinase complex. The I κ B complex is responsible for directing the degradation of I κ B proteins which normally retain NF κ B proteins in the cytoplasm preventing them from being active (195). The NFAT pathway is activated by anything that raises intracellular Ca²⁺ levels to a sufficiently high level to activate calmodulin (196, 197). Upon binding Ca²⁺, calmodulin interacts with calcineurin, a phosphatase that removes phosphate groups from the regulatory domain of NFAT proteins, thereby exposing their nuclear localization sequence resulting in their localization to the nucleus. As these activating events are quite common across several immune signaling pathways (see Table 1.2), the activation of these transcription factors commonly coincides with B and T cell interactions. In addition to these pathways, the immune system uses other transcription factors such as the AP-1 complex, STAT proteins, or other factors to contribute to immune cell decisions; however, these will not be discussed in detail in this thesis.

1.8.2 Receptors and cytokines influencing B cell differentiation

B and T cells use a number of surface receptors and cytokines to communicate with one another to influence the others differentiation and survival. These receptors and cytokines have been studied in great detail including the study of: the regulation of their expression over the course of the immune response, how signaling through these receptors and cytokines is transduced and integrated into common signaling pathways, and how they influence the GC response and the production of B cell subsets. Below, I have outlined the expression patterns and effects of receptors and cytokines known to affect the GC response (Table 1.2).

Table 1.2. Summary of the expression and functions of key signaling molecules affecting the germinal center response.

T cell	B cell	Major Pathway(s)	Effect on the GC
FasL (activated T cells (198))	CD95 (activated and GC B cells (198, 199))	Caspase-3, 7 and 8 (200))	Mediates the selection of high-affinity GC B cells and suppresses autoimmunity through the induction of apoptosis (201-203).
CD40L (activated T cells (204))	CD40 (all B cells (204))	NFκB (205)	Required for GC maintenance. Promotes B cell proliferation and resistance to cell death (111, 206, 207).
CD28 (all T cells (208))	CD80 CD86 (activated and GC B cells (209))	NFAT, NFκB, PI3K, AP-1 (210)	CD86 is required to initiate GC responses and CD80/CD86 maintain the GC and promote plasma cell differentiation (198, 211, 212).
CTLA4 (T _{FH} and T _{FR} cells (186, 213))	CD80 CD86	Inhibits NFAT, NFκB, AP-1 (214)	Suppresses the expansion of T _{FH} cells and GC B cells (186, 215, 216).
ICOS (activated T cells (190, 208))	ICOSL (all B cells (217))	NFAT, NFκB, PI3K, AP-1 (208)	ICOS is required for T _{FH} cell maintenance and contributes to the selection of high affinity B cells in the GC (218, 219).
PD-1 (T _{FH} and T _{FR} cells (220, 221))	PD-L1 (Naïve and GC B cells (180))	Inhibits NFAT,	Inhibits T _{FR} cells (222), promotes plasma cell differentiation and GC B cell maintenance (223), and prevents

	PD-L2 (GC B cells (222))	NFκB, PI3K, AP-1 (220)	excessive accumulation of T _{FH} cells in the GC (180).
IL-4 (pre-T _{FH} and T _{FH} cells (224))	IL-4R (activated and GC B cells (224))	STAT6 (225)	Promotes memory B cell differentiation, GC B cell survival, and SHM and CSR (224, 226-228).
IL-9 (T _{FH} cells (150))	IL-9R (GC B cells (150))	STAT1/3/5 (229)	Promotes memory B cell differentiation (150).
IL-10 (T _{FH} and T _{FR} cells (175))	IL-10R (GC B cells (175))	STAT3 (230)	Inhibits GC B cell apoptosis and promotes GC B cell proliferation (175, 188, 231).
IL-21 (pre-T _{FH} and T _{FH} cells (224))	IL-21R (activated and GC B cells (224))	STAT1/3 (232)	Promotes GC B cell proliferation and plasma cell differentiation at the expense of memory B cells (233, 234).
SLAM (pre-T _{FH} and T _{FH} cells (235))	SLAM (Activated and GC B cells (235))	Integrins, NFκB (236)	Promotes IL-4 production in T _{FH} cells and plasma cell differentiation (237).
CD84 (pre-T _{FH} and T _{FH} cells (235))	CD84 (Activated and GC B cells (235))	Integrins (238)	Needed for optimal GC formation, optimal antibody responses, and T _{FH} cell maintenance (235).
Ly108 (pre-T _{FH} and T _{FH} cells (235))	Ly108 (Activated and GC B cells (235))	Integrins (238)	Inhibits GC induction and maintenance by promoting short B-T interactions until this receptor is engaged (239).

1.9 Thesis overview

This thesis characterizes the progression of autoreactive GCs directed against MOG protein and establishes rules controlling its progression. This was accomplished by developing a new MOG expression system that can be easily manipulated to change the properties of the immunizing Ag. The **primary goal** of this thesis was to characterize the basic rules that control B cell differentiation in GC responses and to apply these rules to an autoimmune GC model that has a pathogenic B cell component. I **hypothesized** that B cells participating in GCs directed against an autoAg would make different fate choices relative to a standard model Ag and that T cells would control these fate choices.

1.9.1 *Chapter 2: Simple and Efficient Production and Purification of Mouse Myelin Oligodendrocyte Glycoprotein for Experimental Autoimmune Encephalomyelitis Studies*

Herein, I describe the process of production and purification of the model autoAg I use throughout this thesis, mMOG_{tag} protein. I show that mMOG_{tag} protein obtains the correct 3-D conformation and can be recognized by MOG-specific B and T cells. I also show that mMOG_{tag} protein is amenable to modification for experimental purposes by creating a new MOG protein that manipulates T cell Ag-affinity, called haMOG_{tag}. Both mMOG_{tag} and haMOG_{tag} induce EAE through protein immunization including the incorporation of pathogenic B and T cells confirming that both induce adaptive immune responses that contribute to CNS demyelination. Overall, the mMOG_{tag} expression system has proven to be an effective system for purifying large amounts of MOG protein making it possible to characterize how autoreactive B cell responses are initiated and how they contribute to EAE.

1.9.2 *Chapter 3: Autoreactive T cells preferentially drive differentiation of short-lived memory B cells at the expense of germinal center maintenance.*

In this chapter, the tools developed in the previous chapter are used to determine whether B cell responses directed against an autoAg are different from those of a model foreign-Ag. I show that GCs directed against mMOG_{tag} protein collapse early and instead form large numbers of memory B cells. While robust immune memory was generated in

the foreign-Ag driven GC response, in the form of memory B cells and long-lived plasma cells, MOG-specific memory B cells are short lived and few long-lived plasma cells are generated through mMOG_{tag} immunization. Collapse of the autoreactive GC was largely under the control of the autoreactive T cells. However, GC collapse could be partially corrected when T cells were stimulated with a high-affinity T cell Ag. Despite clear evidence for T cell control of the GC response, autoreactive and foreign-Ag specific T cells did not differ in phenotype but rather, differed only by the absolute number of T cells controlling in the GC response. Altogether, this chapter characterizes the development of the anti-MOG GC response and shows that T cells are capable of influencing some aspects of the GC response, but not others.

1.9.3 *Chapter 4: Reporters for in vivo and in vitro monitoring of NFκB and NFAT signaling*

For the final chapter, I describe the generation of fluorescent reporters capable of monitoring intracellular signaling in real-time for the purposes of understanding how signals are exchanged between interacting cognate pairs of B and T cells. I show that by combining a fluorescent marker of the nuclei of cells with fluorescently labelled NFκB or NFAT proteins, I can monitor intracellular signaling in living cells. Using the Clustered regularly interspaced short palindromic repeats (CRISPR)/Cas9 genomic editing tool, I show that I can edit mouse genomes to express my reporters but generation of a reporter mouse was unsuccessful. This issue was addressed by constructing a new reporter for NFAT activity that is compatible with conventional gene knock-in methods and will be used to generate a reporter mouse. Overall, this project demonstrates the potential of a reporter capable of determining the timing and kinetics of signal exchange between B and T cells during their interactions.

Chapter 2

2 Simple and Efficient Production and Purification of Mouse Myelin Oligodendrocyte Glycoprotein for Experimental Autoimmune Encephalomyelitis Studies

Multiple sclerosis is a chronic inflammatory disease of the CNS, thought to occur as a result of autoimmune responses targeting myelin. Experimental autoimmune encephalomyelitis is the most common animal model of CNS autoimmune disease and is typically induced via immunization with short peptides representing immunodominant CD4⁺ T cell epitopes of myelin proteins. However, B cells recognize unprocessed protein directly, and immunization with short peptide does not activate B cells that recognize the native protein (240). As recent clinical trials of B cell-depleting therapies in MS have suggested a role for B cells in driving disease in humans, there is an urgent need for animal models that incorporate B cell-recognition of autoAg. To this end, I have generated a new fusion protein containing the extracellular domain of the mouse version of MOG as well as N-terminal fusions of a His-tag for purification purposes and the thioredoxin protein to improve solubility (mMOG_{tag}). A tobacco etch virus (TEV) protease cleavage site was incorporated to allow, if desired, the removal of all tag sequences, leaving only the enriched MOG₁₋₁₂₅ extracellular domain. Here, I describe a simple protocol using only standard laboratory equipment to produce large quantities of enriched mMOG_{tag} or MOG₁₋₁₂₅. This protocol consistently generates over 200 mg of mMOG_{tag} protein. Additionally, the same purification protocol successfully purified a family of modified mMOG_{tag} proteins, one of which is described in detail here, high-affinity MOG (haMOG_{tag}), which incorporates a high-affinity T cell epitope and is capable of stimulating potent MOG-specific T cell responses. Immunization with either mMOG_{tag}, MOG₁₋₁₂₅, or haMOG_{tag} generates an autoimmune response that includes pathogenic B and T cells that recognize the native mouse MOG Ag. Furthermore, it was found that haMOG_{tag} immunization potentiated EAE development. Together, this protein expression system has proven to be reliable and amenable to modification permitting the study of how B cells contribute to EAE and how manipulating B and T cells affects EAE development.

2.1 Introduction

MS is a human disease characterized by chronic inflammation and neurodegeneration of the CNS which is thought to be driven by an autoimmune response directed towards myelin. The loss of myelin and axons over time result in the gradual decline of cognitive and motor function (241). "Experimental Autoimmune Encephalomyelitis" is an umbrella term for animal models of autoimmune disease directed towards CNS myelin. Like human MS, EAE is typically characterized by immune cell infiltration of the CNS and, in some cases, demyelination (38). However, the degree to which any given EAE model resembles human MS in part depends on the species or strain used and on the complexity of the underlying anti-myelin autoimmune response.

Anti-myelin autoimmunity can be experimentally induced in several ways, but the most common method used today is to immunize mice with a short peptide of amino acids mimicking the immunodominant CD4⁺ T cell epitope of a myelin protein. This represents the minimum requirement to induce a pathogenic immune response. Perhaps the most common of these is a 21 amino acid peptide derived from myelin oligodendrocyte glycoprotein (MOG₃₅₋₅₅), which is used to induce EAE in C57Bl/6 mice (242). However, for some experimental purposes it is desirable or even necessary to immunize with larger protein Ags and indeed there are several advantages to this over immunization with short peptides. First, due to MHC restriction, short peptides are usually only effective in a very limited number of animal strains, while larger protein Ags representing either the whole protein or a specific domain can be processed normally for presentation in multiple inbred mouse strains or even in different species (243). Second, a larger protein Ag is capable of inducing a more complex immune response by incorporating additional types of lymphocytes through Ag recognition of a broader array of epitopes, rather than limiting Ag recognition to a small population of CD4⁺ T cells responding to a single peptide. For example, B cells via their BCR interact directly with whole protein rather than processed peptides. We and others have shown that B cells activated by MOG₃₅₋₅₅ immunization do not recognize whole MOG protein (240). Since

B cells were recently demonstrated to play a pathogenic role in human MS (244), EAE models that incorporate B cells in autoimmune pathology are increasingly important.

Despite the advantages of using larger protein Ags to induce EAE, there remain few commercially available sources for such proteins. Indeed, while short peptides like MOG₃₅₋₅₅ can be synthesized very quickly and at a relatively low cost, the commercial options for MOG protein are limited and cost substantially more to purchase. Currently, there are several expression vectors available that research groups can use to generate MOG extracellular domain (MOG₁₋₁₂₅). However, all of the expression systems that I have identified in the literature are based on older technologies that have since been replaced with more efficient expression systems (245). Further, most are based on rat or human MOG (246). For some investigations of autoimmunity in mice, an Ag based on the mouse MOG (mMOG) autoAg is preferable. In addition to the problems highlighted above, a new expression system would ideally be modular as this would allow for the manipulation of variables associated with the Ag. Indeed, several studies have made use of specific point mutations in Ags to manipulate B cell Ag-affinity (247, 248) as well as T cell Ag-affinity (249-251). Thus, a modular MOG expression system would permit an in depth characterization of how B and T cell Ag-affinity contributes to the progression and maintenance of the EAE autoimmune response. Finally, all expression vectors of MOG-based proteins that I have identified are fusion proteins containing additional amino acids to the MOG₁₋₁₂₅ base (245, 252). These include a tag for purification and usually other sequences as well, many of which with a function I was unable to identify, which in some cases may need to be removed for experimental purposes.

To address these limitations, I generated a family of proteins based on the mouse MOG extracellular domain fused to a tag containing thioredoxin to combat the known insolubility of MOG protein (240). The tag sequence also contains a 6xHis sequence for purification and a TEV protease cleavage site that allows for the complete removal of all tag sequences, if desired. This is the only method that I am aware of that efficiently generates enriched MOG₁₋₁₂₅ protein. To facilitate production of large amounts of protein, the MOG₁₋₁₂₅ sequence was codon-optimized for bacterial expression and the mMOG_{tag} fusion protein was inserted into the pET-32 expression system. Additionally,

the mMOG_{tag}-pET-32a vector contains several restriction enzyme sites and is easily polymerase chain reaction (PCR) amplified permitting manipulation through cloning techniques. An example of this is given here through the production of ‘high-affinity’ mMOG_{tag} (haMOG_{tag}) Ag, which incorporates a high-affinity T cell epitope recognized by MOG-specific CD4⁺ T cells, allowing for the experimental manipulation of the CD4⁺ T cell response. Here, I show that I can produce and purify large quantities of mMOG_{tag} protein, enriched MOG₁₋₁₂₅, and haMOG_{tag} using non-specialized equipment available to most immunology laboratories. I then show that these proteins are capable of inducing MOG-specific B and T cell responses in the context of EAE and that the haMOG_{tag} Ag can manipulate MOG-specific T cell responses.

2.2 Results

2.2.1 A protocol for expressing mMOG_{tag} protein

To develop a system with which I could produce large amounts of mMOG protein, I took advantage of the pET-32a protein expression system in BL21 *E.coli*. This was accomplished by inserting bacterial codon optimized mMOG extracellular domain (amino acids 1-125) sequence (based upon GenBank NM_010814.2) into the pET-32a vector along with an N-terminal TEV protease cleavage site. The mMOG₁₋₁₂₅ and TEV protease sequences are expressed in frame with the preceding sequences in the pET-32a vector including *E.coli* thioredoxin protein, an S-Tag, and a 6xHis tag to make the mMOG_{tag} protein (Figure 2.1).

To make the mMOG_{tag} protein, BL21 bacteria transformed with the pET-32a mMOG_{tag} vector are induced to express mMOG_{tag} with Isopropyl β-D-1-thiogalactopyranoside (IPTG) overnight. This resulted in a substantial increase in mMOG_{tag} expression as seen by the appearance of a 31.86 kilodalton (kDa) band on sodium dodecyl sulfate-polyacrylamide gel electrophoresis (SDS-PAGE) after induction (T_{O/N}) relative to pre-induction (T₀) (Figure 2.2A and 2.2B). The BL21 bacteria are then lysed and pelleted to collect inclusion bodies primarily containing the mMOG_{tag} protein (253). Inclusion bodies are then solubilized with guanidine, a chaototropic agent that

disrupts protein folding (254), to produce a crude solution of mMOG_{tag} prior to purification (Figure 2.2B). The protein is then purified through four rounds of incubation with nickel resin, that can be used to purify His-tag labelled proteins (255), followed by elution to collect our 6xHis tag labelled mMOG_{tag} protein. As guanidine prevents the mMOG_{tag} protein from folding, dialysis is used to slowly remove guanidine from the purified protein allowing the protein to slowly fold into the correct 3-D protein conformation. Once folded, the protein is concentrated to 5 mg/ml using PEG3350 and PEG8000 to generate enriched and concentrated mMOG_{tag} protein. Purity of mMOG_{tag} protein was confirmed by SDS-PAGE (Figure 2.2B).

To determine whether the mMOG_{tag} protein produced had acquired the correct 3-D conformation, I took advantage of a mouse strain called the IgH^{MOG} mouse, which expresses a heavy chain BCR that confers MOG specificity to B cells in this mouse (256). I hypothesized that if mMOG_{tag} had acquired the correct conformation, it should preferentially bind to IgH^{MOG} B cells over wild type C57Bl/6 B cells. Lymph node cells from either IgH^{MOG} or C57Bl/6 mice were incubated with mMOG_{tag} Ag, to label MOG-specific B cells, then labelled with a secondary anti-His antibody and a tertiary anti-IgG1 antibody. Binding of mMOG_{tag} to B cells was then assessed by flow cytometry. As shown in Figure 2.2C, mMOG_{tag}-specific B cells could be detected in both WT C57Bl/6 mice and IgH^{MOG} mice however mMOG_{tag} preferentially bound to IgH^{MOG} cells, often labelling between 20-30% of the B cells in these mice well above the background level seen in the fluorescence minus one (FMO) control.

Figure 2.1. mMOG_{tag} protein.

Linear structure, and amino acid and DNA sequences of the mMOG_{tag} fusion protein. The DNA sequence for the extracellular domain of mouse MOG (MOG₁₋₁₂₅, lower sequence in blue) was codon-optimized for expression in bacteria (black). This sequence was synthesized and inserted into a vector to create an N-terminal fusion to a tag containing *E.coli* thioredoxin and an S-Tag to counteract the known insolubility of the MOG protein (253, 257), as well as a 6x His Tag for purification (258). A TEV protease cleavage site separates the MOG₁₋₁₂₅ from the tag sequences. TEV-mediated cleavage between glutamine-164 and glycine-165 using an alternative consensus TEV cleavage site (258) results in removal of all non-MOG amino acids.

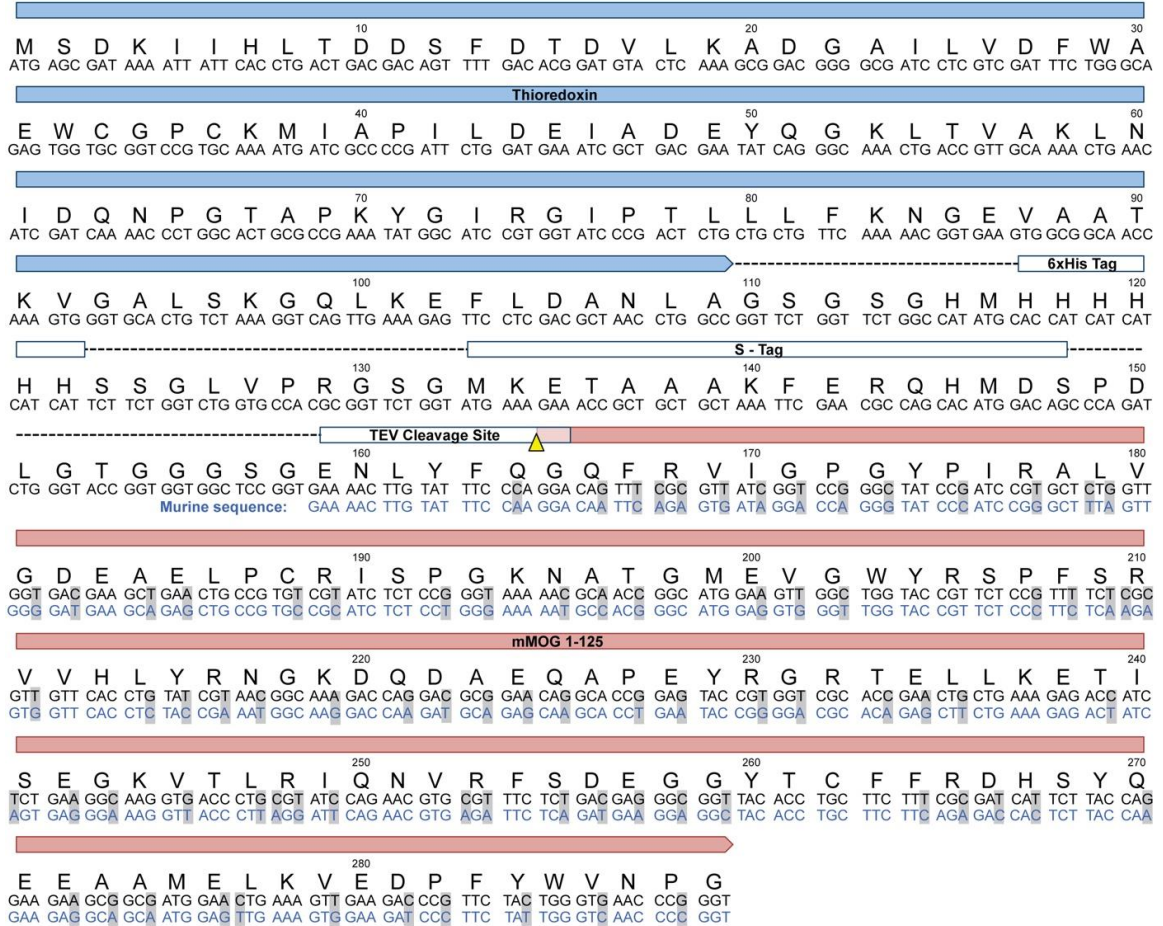
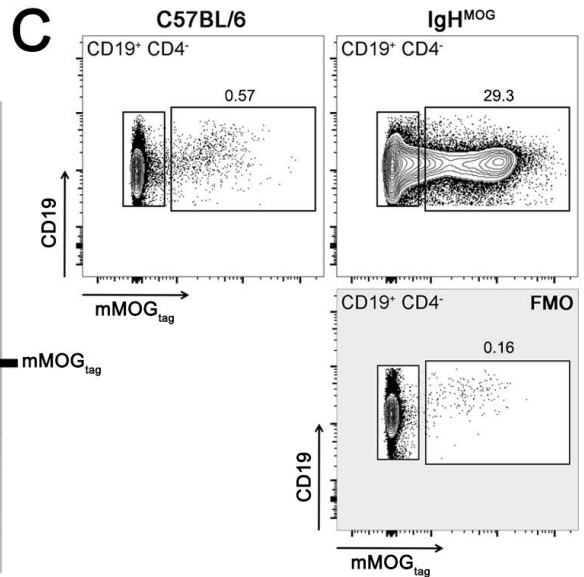
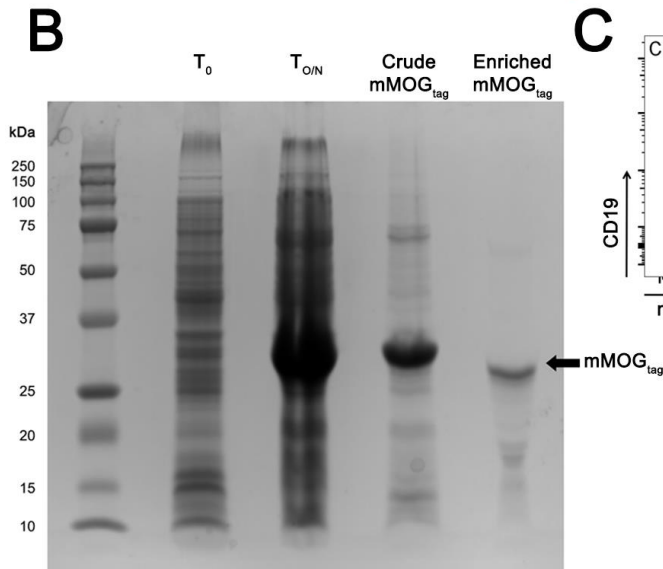
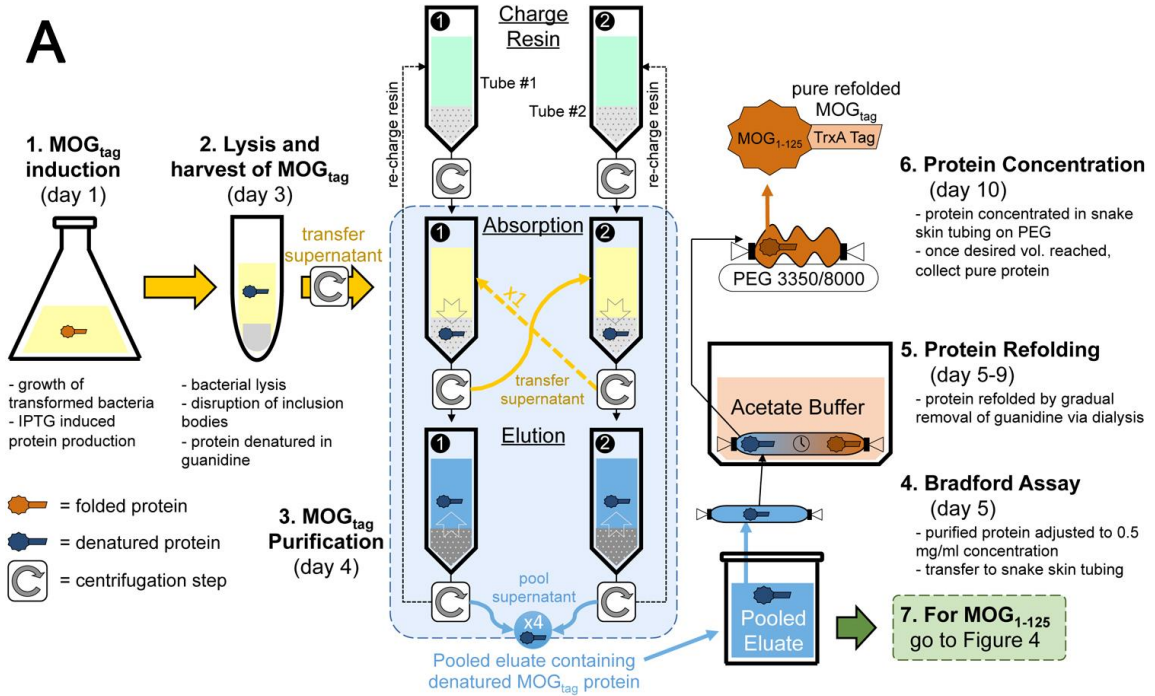


Figure 2.2. Purification of mMOG_{tag}.

(A) To generate mMOG_{tag} protein, bacteria expressing the mMOG_{tag} protein are grown to high densities then induced to express mMOG_{tag} using IPTG. After an overnight culture, the bacteria are lysed and through a series of pelleting steps the protein fraction containing inclusion bodies, which contains mMOG_{tag}, is extracted. mMOG_{tag} is then purified from the crude protein fraction through four cycles of absorption onto charged nickel resin and elution of the mMOG_{tag} protein. A portion of the pooled eluate is then taken for a Bradford assay to determine the yield of mMOG_{tag} protein and the rest of the eluate is dialyzed into acetate buffer over the course of several days. Lastly, the protein is concentrated using PEG3350 and PEG8000 to a final concentration of 5 mg/ml based upon the yield of mMOG_{tag} determined in the Bradford assay. (B) Shown are protein samples that were collected from various points across the protein purification procedure and analyzed by SDS-PAGE gel. T₀= BL21 bacteria prior to protein induction, T_{O/N}= BL21 bacteria post-induction of protein expression, Crude mMOG_{tag}= Solubilized mMOG_{tag} protein prior to protein purification, Enriched mMOG_{tag}= mMOG_{tag} protein after purification. (C) Binding of the mMOG_{tag} protein to CD19⁺ CD4⁻ naive B cells from lymph nodes from either wild type C57Bl/6 mice or IgH^{MOG} mice that express an immunoglobulin heavy chain specific for MOG protein (245, 256) was assessed using flow cytometry. mMOG_{tag}-specific B cells were identified by staining LN cells with mMOG_{tag} followed by a secondary anti-His tag antibody and a fluorescent tertiary anti-IgG1 antibody. Staining of cells from C57Bl/6 or IgH^{MOG} mice is shown along with a mMOG_{tag} FMO control stain of IgH^{MOG} cells. The proportion of IgH^{MOG} B cells binding mMOG_{tag} protein is written above the gating displaying mMOG_{tag} binding.

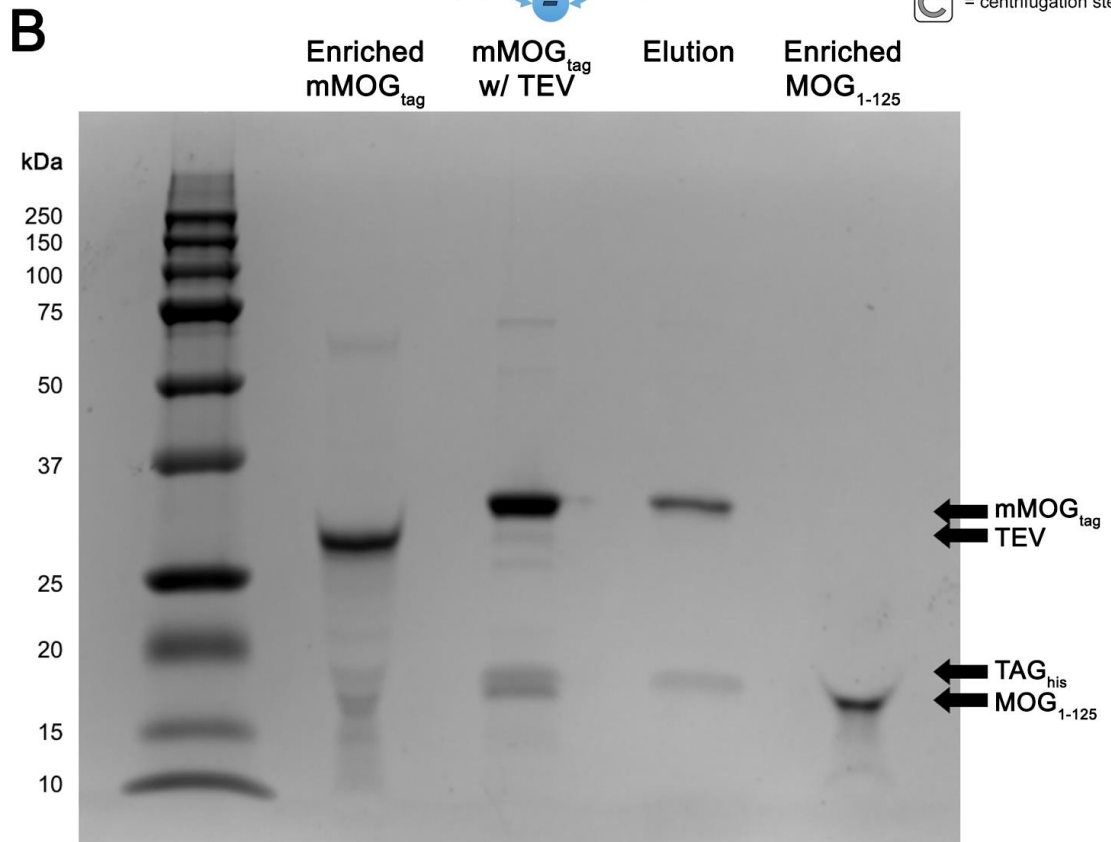
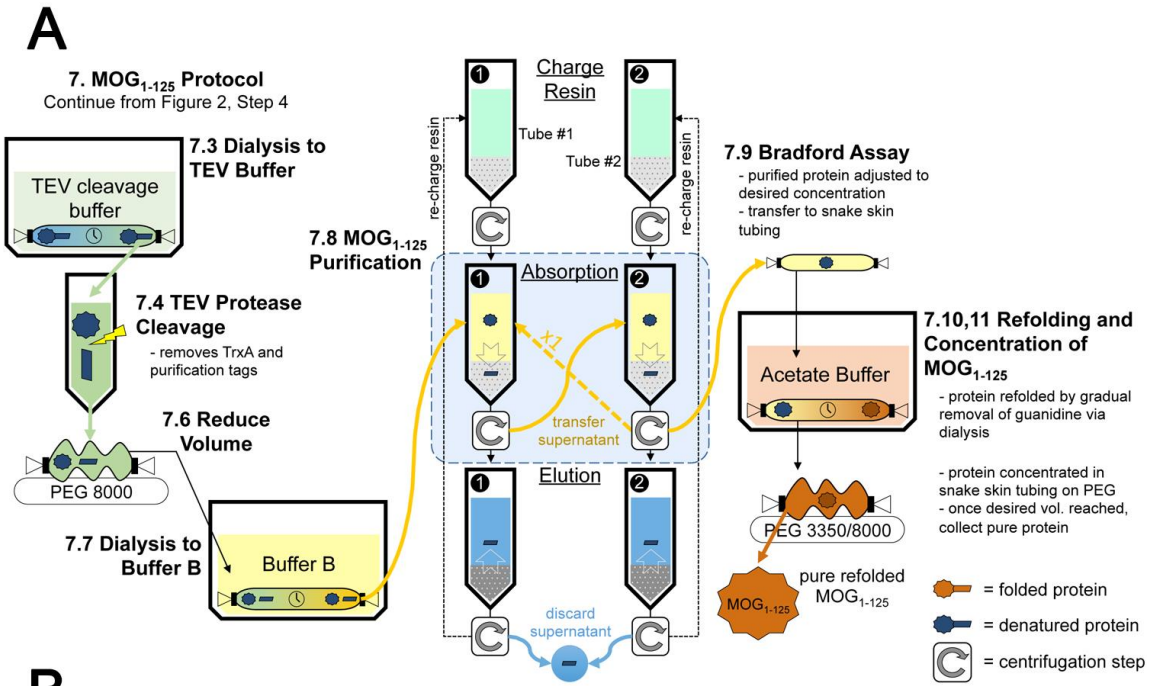


2.2.2 TEV protease can remove the tag sequence to generate enriched MOG₁₋₁₂₅ that can be purified

As the tag sequence is derived from foreign-Ags, some experiments or protocols may have need of enriched MOG₁₋₁₂₅ Ag. To accomplish this, I developed a protocol to remove all of the exogenous sequence associated with the mMOG_{tag} Ag to make enriched MOG₁₋₁₂₅ (summarized in Figure 2.3A). In this protocol, purified mMOG_{tag} protein is dialyzed into TEV protease cleavage buffer then TEV protease is mixed with the mMOG_{tag} protein to remove the tag sequence. After cleavage, the buffer is changed and the volume is reduced by dialysis. Then nickel resin is used to remove impurities from MOG₁₋₁₂₅, namely the tag sequence, uncut mMOG_{tag}, and the TEV protease. After four rounds of absorption onto nickel resin, the protein left in the original solution is then folded similarly to mMOG_{tag} and concentrated to 2.24 mg/ml to be equimolar with mMOG_{tag} at 5 mg/ml. As shown in Figure 2.3B, this protocol can be used to generate enriched MOG₁₋₁₂₅ as seen by the prominent band at 14.28 kDa on an SDS-PAGE gel.

Figure 2.3. Generation of MOG₁₋₁₂₅.

(A) After collecting the mMOG_{tag} eluate from the mMOG_{tag} purification described in Figure 2.2A, the mMOG_{tag} protein is dialyzed into TEV protease cleavage buffer. Once the dialysis is complete, TEV protease is added to the mMOG_{tag} solution resulting in the cleavage of mMOG_{tag} into the MOG₁₋₁₂₅ protein and the associated tag sequence. The volume of the cleavage solution is then reduced and dialyzed into buffer B prior to protein purification. Impurities from the cleavage solution are removed by four successive rounds of absorption onto charged nickel resin and elution of the impurities ultimately resulting in a solution of enriched MOG₁₋₁₂₅. The concentration of the MOG₁₋₁₂₅ protein is determined through a Bradford assay and the protein is folded over the course of several days through dialysis. Once dialysis is complete, the MOG₁₋₁₂₅ protein is concentrated to 2.24 mg/ml using PEG3350 and PEG8000. (B) Shown are protein samples run on a SDS-PAGE gel demonstrating purification of MOG₁₋₁₂₅. Enriched mMOG_{tag} = mMOG_{tag} protein prior to TEV cleavage, mMOG_{tag} w/ TEV = Protein fraction that was collected after 72 hr of incubation of mMOG_{tag} with TEV protease, Elution = Protein fraction that remained bound to the nickel resin during the MOG₁₋₁₂₅ purification protocol, Enriched MOG₁₋₁₂₅ = MOG₁₋₁₂₅ protein after purification.



2.2.3 Generation of haMOG_{tag}, a variation of mMOG_{tag} that alters T cell antigen affinity

In addition to studying the immune response induced against mMOG protein, the mMOG_{tag} expression system provides a general platform to easily produce manipulated versions of the protein to investigate how properties of the immunizing Ag affect developing immune responses. For example, T cell affinity for Ag is a central component of T cell activation (19) but is not well characterized in the context of GCs. To this end, I have generated several variations of the mMOG_{tag} Ag: a version based on the rat MOG protein (rMOG_{tag}), a humanized version of mMOG that I call B cell dependent MOG (bMOG_{tag}), and lastly a version that manipulates Ag-affinity called haMOG_{tag}. Although the bMOG_{tag} and rMOG_{tag} Ags have been purified and validated, I will only focus on haMOG_{tag} in this thesis.

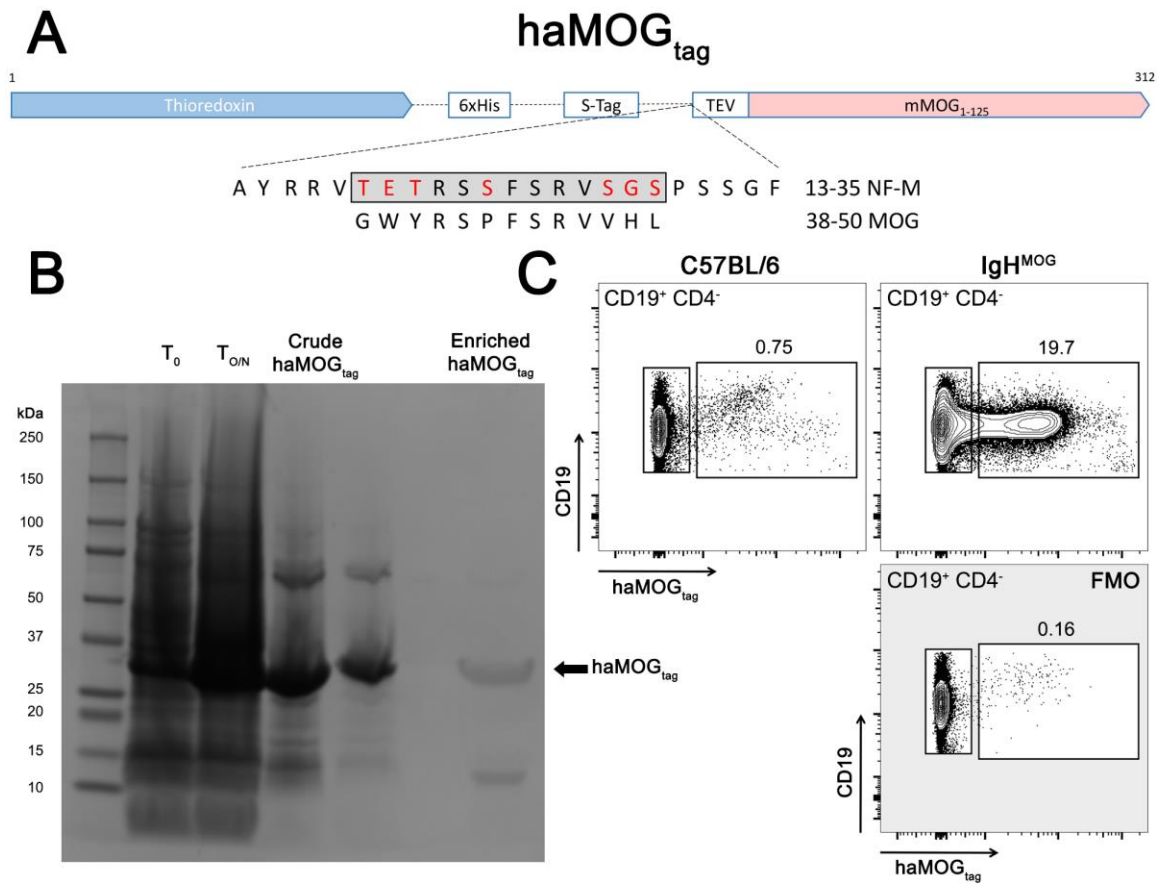
The haMOG_{tag} protein is based upon manipulating the mMOG_{tag} Ag to incorporate a high-affinity T cell epitope, thereby altering the affinity of T cell recognition, by taking advantage of a common feature of TCRs known as polyreactivity (259) that is especially prevalent in autoreactive T cells (260). Polyreactivity is a feature of TCRs where a single TCR molecule can recognize more than one Ag with different Ag-affinities. Autoreactive TCRs, including TCRs that recognize the MOG₃₅₋₅₅ peptide such as the 2D2 TCR, tend to bind peptide:MHC with relatively low affinity (261). However, analysis of the MOG₃₅₋₅₅-specific 2D2 TCR revealed that it also recognizes a second peptide derived from amino acids 18-30 from the Neurofilament-M protein (NF-M₁₈₋₃₀) (262), and in fact binds NF-M₁₈₋₃₀ with higher affinity than it does MOG₃₅₋₅₅ (261). Of note, this property is not just an artifact of the 2D2 TCR, as cross reactivity between MOG₃₅₋₅₅ and NF-M₁₈₋₃₀ is common in C57Bl/6 mice (263). The usage of polyreactivity to assess how T cell Ag-affinity affects immune responses is highly desirable because it involves stimulating the same T cell to different degrees. Other models that use different T cell clones to look at affinity will always have the confounding factor that the two T cells could simply be generally different beyond their affinity.

I took advantage of the polyreactivity of the 2D2 TCR to generate a modified mMOG_{tag} Ag that incorporates amino acids 13-35 from NF-M, containing the NF-M₁₈₋₃₀

epitope, in between the N-terminal tag and the TEV protease cleavage site in the original mMOG_{tag} Ag (Figure 2.4A – referred to as haMOG_{tag}). Incorporation of the haMOG_{tag} pET-32a vector into BL21 bacteria and purification of the haMOG_{tag} protein were both successful using our protocol as seen by the prominent 34.36 kDa band on an SDS-PAGE gel (Figure 2.4B). Enriched haMOG_{tag} protein was further confirmed to have acquired the correct 3-D conformation as haMOG_{tag}, much like mMOG_{tag}, bound IgH^{MOG} B cells (between 20-25% of the IgH^{MOG} B cells depending on the experiment) to a greater degree than wild type C57Bl/6 B cells (Figure 2.4C).

Figure 2.4. Structure and purification of the haMOG_{tag} protein.

(A) Schematic of the haMOG_{tag} protein. The haMOG_{tag} protein is structurally similar to the mMOG_{tag} protein however amino acids 13-35 derived from NF-M were inserted inbetween the TEV protease site and the S-tag in the original mMOG_{tag} protein. Below the amino acid sequence of NF-M₁₃₋₃₅ and MOG₃₈₋₅₀ are shown where the sequences highlighted in grey represent the minimal amino acid sequence required to induce 2D2 T cell responses (262) and amino acids highlighted in red represent amino acids that change between NF-M₁₈₋₃₀ and MOG₃₈₋₅₀. (B) Shown are protein samples that were collected from various points across the protein purification procedure and run on a SDS-PAGE gel. T₀= BL21 bacteria prior to protein induction, T_{O/N}= BL21 bacteria post-induction of protein expression, Crude haMOG_{tag}= Solubilized haMOG_{tag} protein prior to protein purification, Enriched haMOG_{tag}= haMOG_{tag} protein after purification. (C) Binding of the haMOG_{tag} protein to CD19⁺ CD4⁻ naive B cells from LN's from either wild type C57Bl/6 mice or IgH^{MOG} mice was assessed using flow cytometry. haMOG_{tag}-specific B cells were identified by staining LN cells with haMOG_{tag} followed by a secondary anti-his tag antibody and a fluorescent tertiary anti-IgG1 antibody. Staining of cells from C57Bl/6 or IgH^{MOG} mice is shown along with a haMOG_{tag} FMO control stain of IgH^{MOG} cells. The proportion of IgH^{MOG} B cells binding haMOG_{tag} protein is written above the gating displaying haMOG_{tag} binding.



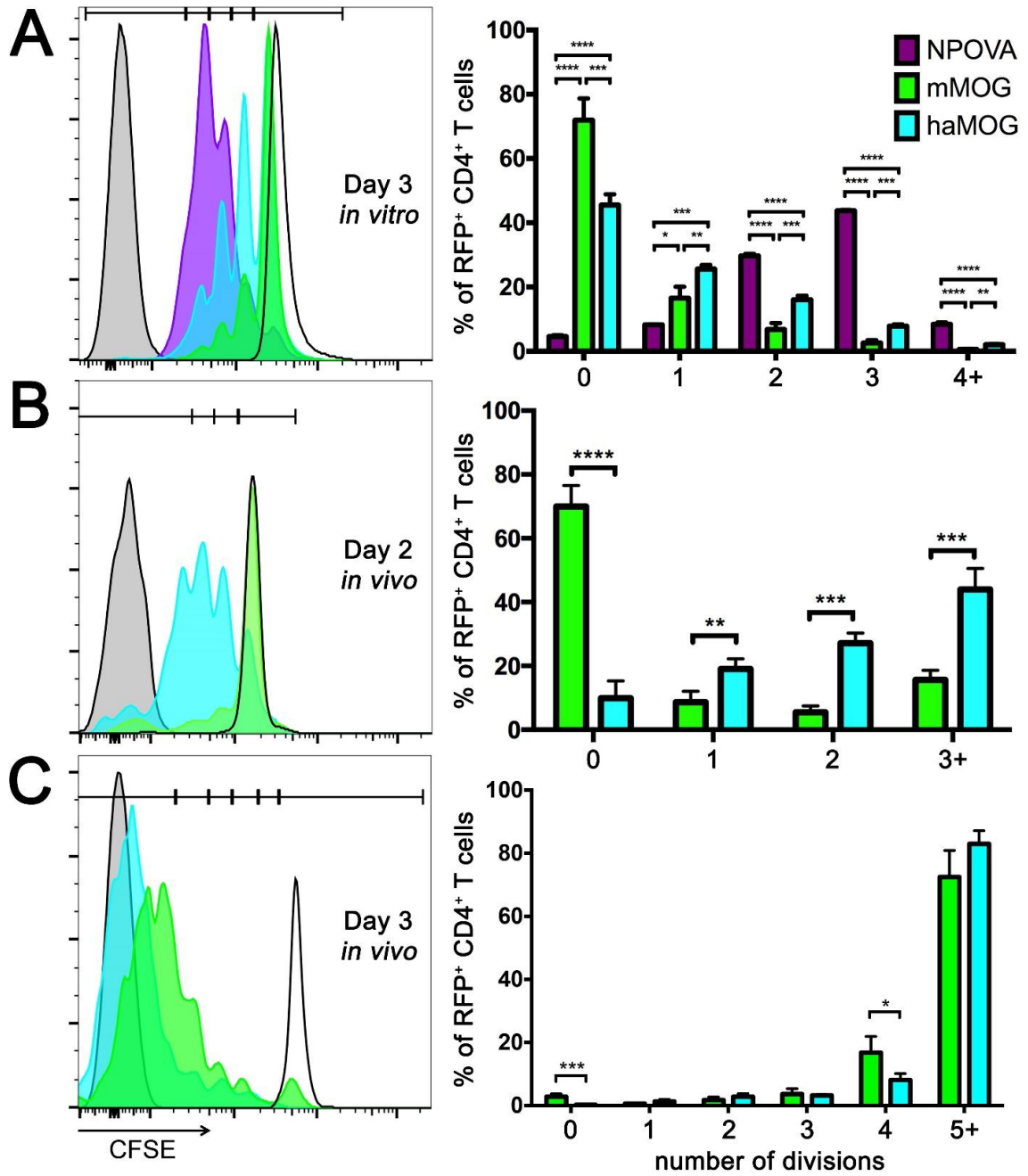
2.2.4 haMOG_{tag} induces greater MOG-specific T cell responses relative to mMOG_{tag} *in vitro* and *in vivo*

Having confirmed that I could produce both mMOG_{tag} and haMOG_{tag}, I sought to determine whether these proteins could induce different myelin-specific T cell responses. I hypothesized that haMOG_{tag} would induce larger T cell responses based on higher-affinity engagement of the TCR. To accomplish this, I set up an *in vitro* T cell stimulation assay where splenocytes from wild type C57Bl/6 mice were loaded with either mMOG_{tag} or haMOG_{tag}. Unloaded splenocytes were used as a negative control and splenocytes loaded with the model foreign-Ag nitrophenyl conjugated ovalbumin (NPOVA) were used as a positive control. Splenocytes were then incubated with Carboxyfluorescein succinimidyl ester (CFSE) labelled T cells from 2D2 (MOG specific T cells (264)) or OTII (OVA specific T cells (265)) mice. After three days of incubation, T cell proliferation was assessed by flow cytometry looking for CFSE dilution. All Ags induced proliferation of T cells relative to the no Ag control confirming that each Ag was capable of being properly presented (Figure 5A - left). Of the three Ags, NPOVA induced the greatest degree of proliferation with a large percentage of OTII T cells having undergone 2, 3, and 4 cell divisions relative to 2D2 T cells incubated with either MOG-based Ag (Figure 2.5A). Proliferation induced with haMOG_{tag} Ag was intermediate between that of NPOVA and mMOG_{tag} where a greater proportion of T cells had undergone proliferation relative to mMOG_{tag} (Figure 2.5A). Thus, *in vitro* haMOG_{tag} was capable of inducing a larger 2D2 T cell response relative to mMOG_{tag}.

To determine whether this was true *in vivo*, a similar assay was set up where CFSE labelled red fluorescent protein (RFP) positive 2D2 T cells were transferred into wild type C57Bl/6 mice. Mice were then immunized by flank injections with either mMOG_{tag} or haMOG_{tag} and T cell proliferation and differentiation in the draining inguinal LNs was assessed d2 and d3 post-immunization. Proliferation of 2D2 T cells as seen by CFSE dilution was greater at the d2 time point in haMOG_{tag} immunized mice relative to mMOG_{tag} however by the d3 time point these two populations were no longer different (Figure 2.5B and 2.5C). Thus, proliferation of MOG-specific T cells towards mMOG_{tag} was not compromised but rather delayed.

Figure 2.5. haMOG_{tag} induces greater MOG-specific T cell proliferation than mMOG_{tag}

(A) *In vitro* proliferation assay assessing T cell proliferation to NPOVA, mMOG_{tag}, and haMOG_{tag}. Splenocytes loaded with either NPOVA, mMOG_{tag}, or haMOG_{tag} were incubated with CFSE labelled OTII T cells (NPOVA) or 2D2 T cells (mMOG_{tag} and haMOG_{tag}) for three days. On the third day, CFSE dilution was assessed by flow cytometry. A representative FACS plot is shown on the left and the quantification of proliferation is shown on the right. Data is representative of three independent experiments with three technical replicates, error bars represent standard deviation. (B and C) CFSE labelled RFP⁺ 2D2 T cells were transferred into non-fluorescent C57Bl/6 recipients then immunized in the flanks with mMOG_{tag} or haMOG_{tag} and CFSE dilution in RFP⁺ CD4⁺ CD8⁻ CD19⁻ T cells in the draining inguinal LN was assessed by flow cytometry on d2 (B) or d3 (C) post-immunization. (B and C) Data is based on one experiment. Error bars represent standard deviation for panels B (n=4 mMOG_{tag}, n=3 haMOG_{tag}) and C (n=5 mMOG_{tag}, n=4 haMOG_{tag}). Comparisons between multiple groups were done using a one-way ANOVA with a Bonferroni correction and comparisons between single groups were done using a Student's T-test, *p<0.05, **p<0.01, ***p<0.001, ****p<0.0001.



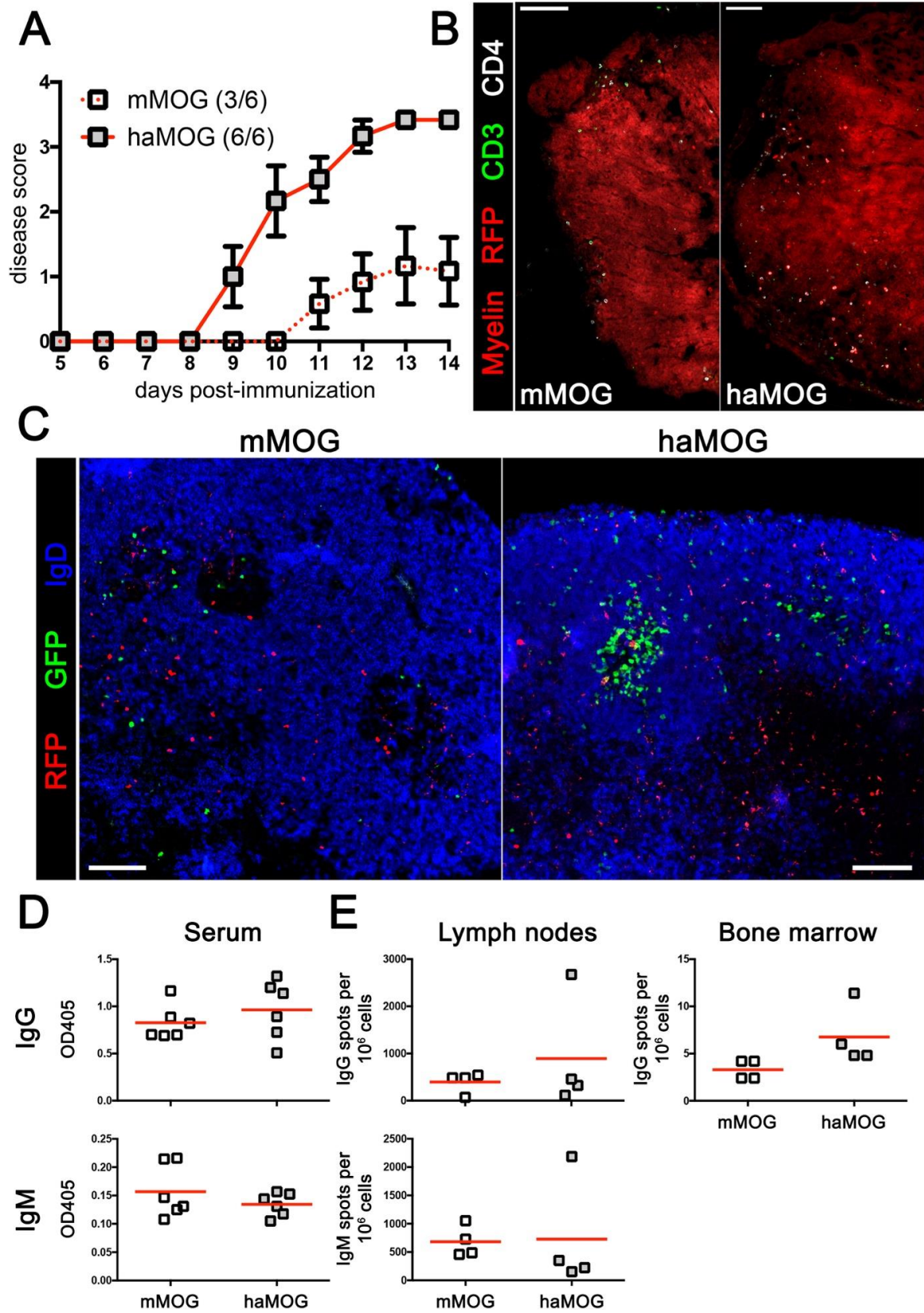
2.2.5 mMOG_{tag} and haMOG_{tag} can both induce EAE incorporating anti-myelin B and T cells

MOG proteins are commonly used for the induction of EAE where there is considerable interest in understanding how B cell responses contribute to EAE progression. To determine whether the mMOG_{tag} and haMOG_{tag} proteins can induce EAE with associated myelin-specific B and T cell responses, I transferred green fluorescent protein (GFP) positive IgH^{MOG} B cells and RFP⁺ 2D2 T cells into non-fluorescent C57Bl/6 recipients then immunized the recipients with mMOG_{tag} or haMOG_{tag} via flank injections. On d0 and d2, pertussis toxin (PTX) was administered to promote EAE induction (266) and mice were scored daily based on disease severity. Mice immunized with either Ag were capable of developing EAE where haMOG_{tag} immunized mice developed EAE with greater incidence (Figure 2.6A). Spinal cords taken from these mice demonstrated inflammation and demyelination within the CNS (Figure 2.6B). Furthermore, histological analysis of draining inguinal LNs of these mice showed that MOG-specific GFP⁺ B and RFP⁺ T cells could be seen within GCs confirming that these cells were activated through immunization and were actively participating in anti-myelin autoimmunity (Figure 2.6C).

To determine if haMOG_{tag} immunization impacts the B cell antibody response, serum from the above mice were analyzed for circulating IgM and IgG anti-MOG₁₋₁₂₅ specific antibodies using an enzyme-linked immunosorbent assay (ELISA). No difference in either IgM or IgG anti-MOG antibodies were observed (Figure 2.6D). This finding was confirmed in a separate experiment where wild type C57Bl/6 mice were immunized with mMOG_{tag} or haMOG_{tag} to induce EAE. Then, the number of anti-MOG₁₋₁₂₅ specific plasma cells in the draining inguinal LNs and bone marrow was assessed using an enzyme linked immuno-spot (ELISpot) assay. Equivalent numbers of IgM⁺ and IgG⁺ plasma cells were confirmed to be present in the draining inguinal LNs and bone marrow of mMOG_{tag} and haMOG_{tag} immunized mice (Figure 2.6E).

Figure 2.6. mMOG_{tag} and haMOG_{tag} both induce EAE incorporating myelin-specific B and T cells.

(A-D) RFP⁺ 2D2 T cells and GFP⁺ IgH^{MOG} B cells were transferred into non-fluorescent C57Bl/6 recipients then immunized with either mMOG_{tag} or haMOG_{tag}. Mice were injected with intraperitoneal (i.p.) PTX on d0 and d2 post-immunization and were scored daily to assess their physical disability. Then, d14 post-immunization the draining inguinal LNs and spinal cords were taken for histology and blood was taken to analyze the serum for anti-MOG₁₋₁₂₅ antibodies. (A) Disease curves of mMOG_{tag} and haMOG_{tag} immunized mice are shown, the disease incidence for each group is shown on the legend (n=6 per group). Errors bars represent standard error of the mean (SEM). (B) Shown are representative histological sections of spinal cords from mMOG_{tag} and haMOG_{tag} immunized mice stained with the antibodies shown on the left and FluoroMyelin to stain myelin. (C) Shown are representative images of inguinal LNs from mMOG_{tag} and haMOG_{tag} immunized mice, LN sections were stained with IgD to outline the B cell follicle. (B and C) Scale bars represent 100 μm. (D) Serum from mMOG_{tag} and haMOG_{tag} immunized mice were analyzed for IgM and IgG anti-MOG₁₋₁₂₅ antibodies. (E) C57Bl/6 mice were immunized with either mMOG_{tag} or haMOG_{tag} and injected with PTX i.p. d0 and d2 post-immunization. Day 18 post-immunization draining inguinal LNs and bone marrow were extracted and assessed for MOG₁₋₁₂₅ specific IgM⁺ or IgG⁺ plasma cells using an ELISpot assay. Data is representative of 1-3 independent experiments. A Student's T-test was used for single comparisons.



2.3 Discussion

Here, I have described a protocol for the production of mMOG_{tag} protein and how to generate enriched MOG₁₋₁₂₅ from mMOG_{tag}. This protocol is based both on standard His-tag based protein purification methods, as well as a previously described protocol for the generation of an older MOG-based protein (245). Previously we demonstrated that immunization with mMOG_{tag} or MOG₁₋₁₂₅ not only induces EAE with greater spinal cord inflammation and demyelination compared to the standard MOG₃₅₋₅₅ peptide, but also that pathogenic IgH^{MOG} B cells that recognize MOG protein are activated to produce a germinal center in response to mMOG_{tag} or MOG₁₋₁₂₅, but not to MOG₃₅₋₅₅ (240). Thus, our mMOG_{tag} protein successfully incorporates MOG-specific B cells into an immune response directed against the brain and spinal cord allowing us to study how autoreactive B cells differentiate and contribute to EAE.

One major difference between the mMOG_{tag} protein described here and previously published forms of recombinant MOG protein is that these studies use the extracellular domain of human MOG protein (246, 247, 267). This is significant because mMOG and human MOG have different properties and induce different forms of EAE. In particular, human MOG induces a B cell dependent form of EAE (49) whereas rodent versions of MOG induce T-cell dependent EAE that is complemented by Ag-specific B cells (41, 240, 268). The change from T cell-dependent to B cell-dependent EAE can be attributed to a single amino acid change, a S42P mutation in the human MOG protein (268, 269). This mutation resides within the immunodominant MOG₃₅₋₅₅ epitope (243) and induces delayed proliferation of MOG-specific T cells relative to MOG₃₅₋₅₅ (data not shown). As T cell priming is less efficient in human MOG immunized mice, it is unclear whether studies using human MOG are inducing a potent enough T cell response for them to make a major contribution to EAE progression. Thus, one major advantage of the mMOG_{tag} protein over the human MOG version is that T cells are unambiguously being primed with the endogenous autoAg, which leads to potent T cell responses that can drive inflammation.

The other form of MOG commonly used in EAE models is the extracellular domain of rat MOG protein. The rat MOG and mMOG proteins share the same MOG₃₅₋₅₅

immunodominant epitope and both induce T cell-dependent EAE (41, 270). Although rat MOG and mMOG induce similar effector T cell responses, they do differ in Treg activation (271). In particular, rat MOG differs from mMOG at 6 amino acids that reside in subdominant T cell epitopes recognized by Treg cells, ultimately impacting their ability to respond to rat MOG. As a result of inefficient Treg activation, rat MOG induces more severe EAE than mMOG (271). Ideally, EAE models should not exclude regulatory processes that would normally be present in MS patients (272, 273), as overcoming these regulatory processes would be expected to be a part of the development of autoimmune disease. As a result, EAE induced with mMOG protein better recapitulates regulatory processes expected to be a part of MS. Nonetheless, rat MOG can still be useful experimentally to manipulate regulatory T cell responses.

In addition to manipulating Treg responses, I have also shown here that I could generate a version of the mMOG_{tag} protein that manipulates Ag-affinity, haMOG_{tag}, to promote MOG-specific T cell responses using a high-affinity T cell epitope recognized by MOG-specific T cells. In the EAE experiment described here, haMOG_{tag} induced EAE with greater incidence relative to mMOG_{tag} immunized mice, a finding that has been repeated several times. This may be related to my finding that 2D2 T cells proliferate faster in response to haMOG_{tag} relative to mMOG_{tag} consistent with previously published work showing faster signaling kinetics in 2D2 T cells stimulated with NF-M₁₈₋₃₀ relative to MOG₃₅₋₅₅ (261). It is therefore possible that stronger T cell responses are better at priming T cells to induce EAE where I may expect that inducing a weaker T cell response would reduce disease incidence. Indeed, we have previously shown that a version of our mMOG_{tag} protein containing the S42P mutation described above, bMOG_{tag}, that induces even slower kinetics of T cell activation relative to mMOG_{tag}, cannot induce EAE through T cell stimulation alone whereas mMOG_{tag} and haMOG_{tag} can (268). This shows how our modular mMOG_{tag} platform can be manipulated for experimental needs to answer basic questions about immunology and EAE induction. Indeed, in Chapter 3 of this thesis I will use the tools produced here to determine factors that limit the initiation and progression of GC responses directed against the MOG protein.

In addition to the ability to manipulate the autoimmune B and T cell responses, the mMOG_{tag} system is valuable as a system to identify and study MOG-specific B cells. The first way that this can be done is using the MOG₁₋₁₂₅ Ag as a reagent for an ELISpot to identify MOG-specific plasma cells in a tissue. Indeed, here I was able to show that MOG₁₋₁₂₅-specific plasma cells are found in draining LNs and bone marrow post-immunization with mMOG_{tag}. The mMOG_{tag} Ag can also be used as a flow cytometry reagent to identify MOG-specific B cells. In the experiments shown in this chapter, MOG-specific B cells were identified by staining them with mMOG_{tag} followed by a secondary anti-his antibody and a tertiary anti-mouse IgG1 antibody. This method has the flaw that it identifies IgG1⁺ B cells in addition to identifying mMOG_{tag}-specific B cells. This can be addressed through direct conjugation of the mMOG_{tag} protein to a fluorophore, thereby removing the need for the tertiary anti-IgG1 antibody, a method that we have validated previously (240) and will use in Chapter 3 of this thesis. Similar methods have been used to study GC responses induced with nitrophenyl (NP) haptened proteins but, the NP system has one major advantage over our MOG based system, the ability to study antibody/BCR-affinity by manipulating the conjugation ratio of NP to protein to increase or decrease Ag-avidity (274). Thus, although mMOG_{tag} is a useful tool for studying MOG-specific B cells and plasma cells, it does not have the same utility as previously established methods for studying GC responses to other Ags.

In summary, here I have described a simple protocol for producing and purifying large quantities of mMOG_{tag} protein. Furthermore, the addition of a TEV protease cleavage site to our mMOG_{tag} protein provides the opportunity to generate enriched MOG₁₋₁₂₅ that can be used to identify MOG-specific antibodies in serum or detect MOG-specific plasma cells. I have also shown that our expression system is modular by producing haMOG_{tag}, an Ag that successfully manipulated the induction of EAE and the underlying T cell response by stimulating autoreactive T cells with a high-affinity T cell epitope. Furthermore, as both mMOG_{tag} and haMOG_{tag} are recognized and bound by anti-myelin autoimmune B cells, EAE induced with these proteins incorporates myelin-specific B cell-mediated contributions into their pathology. Therefore, this protein expression system allows us to not only begin to study how B cells contribute to EAE,

but also how manipulations of B cells or T cells modify how the underlying autoimmune response develops and by extension how EAE progresses.

2.4 Materials and Methods

2.4.1 Mice

C57Bl/6, 2D2 TCR-transgenic (264), SMARTA TCR-transgenic (4694;Tg(TcrLCMV)327Sdz/JDvsJ), and OTII TCR-transgenic mice (4194;Tg(TcraTcrb)425Cbn/J) were purchased from Jackson Laboratories, Bar Harbor, Maine. IgH^{MOG} MOG-specific BCR knock-in mice (256) were received as a gift from Dr. H Wekerle. Mice expressing fluorescent proteins within all nucleated cells, either dsRed (RFP; 6051; Tg(CAG-DsRedpMST)1Nagy/J) under control of the β -Actin promoter or eGFP via the ubiquitin promoter (4353; Tg(UBCGFP)30Scha/J) were obtained from the Jackson Laboratory. Mice were housed in a specific pathogen-free barrier at the University of Western Ontario's West Valley Barrier Facility (London, Ontario). All animal protocols (2011-047 and 2015-090) were approved by the Western University Animal Use Subcommittee.

2.4.2 Antibodies used for flow cytometry or histology

The following antibodies were purchased from BD Biosciences (Franklin Lakes, New Jersey): anti-CD4-V450 and A647 (RM4-5), anti-CD19-BV711 (1D3), and anti-IgG1-APC (A85-1). The following antibody was purchased from BioLegend (San Diego, California): anti-His Tag-purified (J099B12). The following antibodies were purchased from Thermo Fisher Scientific (Waltham, Massachusetts): anti-IgD-eF450 (11-26), anti-CD3-FITC (145-SC11), and anti-CD4-PE-Cy5 (RM4-5). FluoroMyelin Red for myelin staining was purchased from Invitrogen (Carlsbad, California).

2.4.3 Recombinant mMOG_{tag} and haMOG_{tag} vector design and purification

The mMOG_{tag} insert was designed using SnapGene software (Chicago, Illinois) to include the following: a TEV cleavage sequence site (ENLYFQ/G), the extracellular

immunoglobulin domain of mouse MOG (residues 1–125), a TAA stop codon and BglIII and EcoRI restriction sites added to the 5' and 3' ends, respectively. The mMOG_{tag} insert sequence was codon optimized for bacterial protein expression in *E. coli* then synthesized in the pQE-12 vector (Celtek Genes, Franklin, Tennessee). The insert was then cloned into the pET-32a(+) vector containing the gene for thioredoxin (Novagen, Madison, Wisconsin) and then transformed into BL21 *E. coli* using standard transformation procedures(275).

A protocol for purification of mMOG_{tag} protein was adapted from previous systems (245) and is described in more detail in a Jain *et al.* 2016 (276). pET-32a(+) mMOG_{tag} BL21 *E. coli* were cultured in LB medium at 37 °C to an O.D. of 0.6, when protein expression was induced overnight with 1 mM IPTG. Bacterial cells were pelleted and suspended in lysis buffer (0.1 mg/mL hen egg lysozyme, 0.1% Triton-X (v/v) in PBS) then lysed to collect inclusion bodies. The inclusion body pellet was suspended in 500 mM NaCl, 20 mM Tris–HCl, 5 mM imidazole, pH 7.9 (Buffer A) and incubated at 4 °C, then denatured with the addition of 6 M guanidine (Buffer B). The protein suspension was centrifuged at 4 °C to collect the supernatant containing the solubilized proteins. Before protein absorption, His-Bind nickel resin (Novagen, Madison, Wisconsin) was prepared according to the manufacturer's instructions. Briefly, the nickel resin was washed and treated with distilled water and 100 mM NiSO₄, then equilibrated with Buffer B. The solubilized proteins containing mMOG_{tag} was incubated with the charged nickel resin in a standard 50 mL centrifuge tube at 4 °C. Following centrifugation, the supernatant was kept for further rounds of purification and mMOG_{tag} was eluted from the pelleted resin with 500 mM imidazole, 500 mM NaCl, 6 M guanidine and 20 mM Tris–HCl pH 7.9. Elutions were pooled and exchanged by overnight dialysis at 4 °C into the storage buffer containing 0.115% glacial acetic acid, 3 mM sodium acetate and concentrated with PEG3350 and PEG8000 to 5 mg/mL before storage at -80 °C. Unless otherwise stated, reagents were purchases from Bioshop (Burlington, Ontario). Protein expression and quantification were confirmed using standard SDS-PAGE and Bradford assay kits (Bio-Rad, Hercules, California) according to manufacturer's instructions.

To generate haMOG_{tag}, the pET-32 mMOG_{tag} vector was mutated by PCR using the following primers: 5'-TCTTCTTTTTCTCGCGTTTCTGGTTCTCCGTCTTCTGGTTTTGAAAACCTTGATT TCCAAGGACAGTTTTCGCG 3' and the reverse primer 5'-GCGAGAAAAAGAAGAACGGGTTTTCGGTAACACGACGATATGCACCGGAGCC ACCACCGGTAC 3'. The resulting vector was sequenced to confirm the insertion of the 13-35 NF-M sequence (based on NCBI Reference Sequence: NP_032717.2) and transformed into BL21 bacteria for expression. Expression of the haMOG_{tag} protein is similar to what was listed above for mMOG_{tag}. However, haMOG_{tag} was concentrated to 5.394 mg/mL to be equimolar with mMOG_{tag}.

2.4.4 TEV protease cleavage of mMOG_{tag} protein

Purified mMOG_{tag} was dialyzed into 50 mM Tris-HCl, 0.5 mM EDTA and 5 mM 2-Mercaptoethanol pH 8. Then, AcTEV protease (Thermo Fisher Scientific, Waltham, Massachusetts) was added to mMOG_{tag} protein at a 1:20 ratio and incubated at room temperature for 72 hrs. The protein was then dialysed into pure water then concentrated with PEG8000 to a final volume of 35 mL. The protein was then dialyzed into buffer B and the tag, AcTEV protease, and uncut mMOG_{tag} impurities were removed through incubation with charged nickel resin as described above. After four rounds of incubation with nickel, the original volume was then dialyzed into 0.115% glacial acetic acid and concentrated using PEG3350 and PEG8000 to 2.24 mg/ml before storage at -80 °C. Unless otherwise stated, reagents were purchases from Bioshop (Burlington, Ontario). Protein expression and quantification were confirmed using standard SDS-PAGE and Bradford assay kits (Bio-Rad, Hercules, California) according to manufacturer's instructions.

2.4.5 Adoptive transfer of B and T cells and immunization

Naïve Ag-specific T cells were isolated from RFP⁺ 2D2 mice and naïve Ag-specific B cells were isolated from GFP⁺ IgH^{MOG} mice as previously described (78). Briefly, LNs and spleens of RFP⁺ T cell and GFP⁺ B cell mice were dissociated and B and T cells were isolated using EasySep Negative selection Mouse B and T cell

Enrichment Kits (StemCell Technologies, Vancouver, Canada). Five million GFP⁺ IgH^{MOG} B cells and 5×10^5 2D2 T cells were transferred i.v into C57Bl/6 or SMARTA recipients 2 days prior to immunization. Mice were immunized in each flank with equimolar amounts of the given Ag (250 μ g mMOG_{tag} and 270 μ g haMOG_{tag}) in complete Freund's adjuvant (CFA) and injected with 250 ng PTX on days 0 and 2 post-immunization. Draining inguinal LNs were harvested at the indicated time points for analysis.

2.4.6 Flow cytometry

Draining popliteal LNs were harvested from mice for flow cytometric analysis as previously described (78). Briefly, LN cell suspensions were blocked with an anti-Fc γ receptor, CD16/32 2.4G2 (BD biosciences, Franklin Lakes, New Jersey), in PBS containing 2% FBS before further incubation with the indicated antibodies. Dead cells were excluded by staining with either the Fixable Viability Dye eFluor506 or propidium iodide (Thermo Fisher Scientific, Waltham, Massachusetts). Flow cytometry was performed on a BD Immunocytometry Systems LSRII cytometer and analyzed with FlowJo software (Tree Star, Ashland, Oregon).

2.4.7 Induction of EAE

Six to 8 week old mice were immunized s.c. on d0 at two sites on the hind flanks with a total of either 0.5 mg of mMOG_{tag} or 0.54 mg of haMOG_{tag} mixed 1:1 with 4 mg/mL desiccated *M. tuberculosis* (H37 Ra) in incomplete Freund's adjuvant (Sigma-Aldrich, St. Louis, Missouri). At the same time mice were also administered 250 ng of pertussis toxin (List Biological Laboratories, Campbell, California) i.p. and again on d2. Clinical disease was monitored daily and was scored according to standard conventions (277) as follows: 0, no clinical signs; 1, tail paralysis; 2, tail paralysis and hind limb weakness; 3, hind limb paralysis; and 4, complete hind limb paralysis and front limb weakness. Half points were given for intermediate scores.

2.4.8 Immunofluorescence histology

At the end of the experiment, spinal cords and inguinal LNs were extracted from mice and prepared as previously described (78). Briefly, spinal cords and LNs were extracted and incubated overnight in 1% paraformaldehyde (PFA), 95 mM L-Lysine, 10 mM sodium periodate, pH 7.2 (Bioshop, Burlington, Ontario). Tissues were then incubated in solutions of increasingly concentrated sucrose until a final concentration of 30% sucrose (Bioshop, Burlington, Ontario). Then, 5–9 evenly spaced spinal cord tissues spanning the lumbar to cervical regions were cut and frozen in OCT (Tissue-Tek, St. Torrance, California) media or directly frozen in OCT media for inguinal LNs. Serial cryostat sections (7 μ m) were blocked in PBS containing 1% Bovine Serum Albumin, 0.1% Tween-20 and 10% rat serum before proceeding with staining. Sections were mounted with ProLong Gold Antifade Reagent (Invitrogen, Carlsbad, California) and stored at -20°C . Tiled images of whole spinal cord sections or inguinal LNs (20 \times) were imaged using DM5500B fluorescence microscope (Leica microsystems, Concord, ON, Canada).

2.4.9 *In vitro* and *in vivo* T cell proliferation assays

RFP⁺ OTII or 2D2 CD4⁺ T cells were enriched through negative selection as described above. Splenocytes of wild type C57Bl/6 mice were depleted of red blood cells using ACK lysis buffer (Thermo Fisher Scientific, Waltham, Massachusetts). The cells were then transferred into 10% FBS RPMI with L-glutamine (Thermo Fisher Scientific, Waltham, Massachusetts) supplemented with 1x penicillin/streptomycin (WISENT, Saint-Bruno, Quebec, Canada). One million splenocytes were then added to individual wells of a sterile 48-well plate and were incubated with either 35 μ g NP-OVA, 25 μ g mMOG_{tag}, or 27 μ g haMOG_{tag} for one hour at 37 $^{\circ}\text{C}$ 5% CO₂. OTII or 2D2 T cells were CFSE (Thermo Fisher Scientific, Waltham, Massachusetts) labelled as described in (278) and 4 x 10⁵ T cells were added to the Ag loaded splenocytes. After three days of co-culture, CFSE labeling of Ag-specific T cells was analyzed by flow cytometry. For the *in vivo* assays, T cells were CFSE labelled as listed above and transferred into mice, also listed above.

2.4.10 ELISpots and ELISA

96-well plates were coated overnight at 4°C with 0.5 µg MOG₁₋₁₂₅. Wells were blocked with 1% (wt/vol) BSA in PBS, then incubated with serial diluted bone marrow or LN cells at 37°C in 5% CO₂. Spots were detected using a goat alkaline phosphatase-conjugated anti-mouse IgM or IgG antibody (MABTECH, Nacka Strand, Sweden) and 5-bromo-4-chloro-3-indolyl-phosphate substrate (Sigma-Aldrich, St. Louis, Missouri) and counted under a Leica M80 dissection microscope. To detect circulating antibodies against MOG₁₋₁₂₅, 96-well plates were incubated with MOG₁₋₁₂₅ and blocked with BSA as written above. Blood was extracted from mice using a cardiac puncture into preloaded syringes with 0.5 M EDTA and spun at 4500 x g for 15 minutes. Plasma was extracted and incubated with the 96-well plate for one hour at room temperature. Plates were incubated with anti-IgM or IgG antibodies and then the alkaline phosphatase yellow (pNPP; Sigma-Aldrich, St. Louis, Missouri) substrate. OD405 was measured using an Eon microplate spectrophotometer (BioTek, Winooski, Vermont).

2.4.11 Statistical analyses

PRISM software (GraphPad Software, La Jolla, California) was used to analyze flow cytometry and histology data. For statistical comparisons, a Student's T-test was used for single comparisons and a one-way ANOVA followed by a T test with Bonferroni correction was used for multiple comparisons.

Chapter 3

3 Autoreactive T cells preferentially drive differentiation of short-lived memory B cells at the expense of germinal center maintenance.

B cell fate decisions within a GC are critical to determining the outcome of the immune response to a given Ag. Here, I characterize GC kinetics and B cell fate choices in response to the autoAg MOG, and compare them to the response to a standard model of foreign Ag (NP-haptenated ovalbumin, NPOVA). Both Ags generated productive primary responses, as evidenced by GC development, circulating Ag-specific antibodies, and differentiation of memory B cells. However, in the MOG response the status of the cognate T cell partner drove preferential B cell differentiation to a memory phenotype at the expense of GC maintenance, resulting in a small ongoing GC. Indeed, placing the same NP-specific B cells under the control of either OVA or MOG-specific T cells, I identified that preferential memory B cell differentiation over GC maintenance was instructed by the MOG-specific T cell. Furthermore, the MOG-specific T cell could not efficiently expand the early low-affinity plasmablast response although plasma cell differentiation occurred similarly within the GC under the control of either T cell. The collapse of MOG-driven GCs, but not plasmablast expansion, could be partially reversed by hyperactivating MOG-specific T cells with a high-affinity Ag suggesting low T cell Ag-affinity limits the MOG-driven GC response. Despite this, T_{FH} cells exhibited no observed differences in the expression of cytokines or surface receptors previously identified as controlling memory B cell differentiation in the different model systems. Interestingly, memory B cells formed in the MOG GC were short-lived leading to the failure of secondary challenges with Ag to induce GC responses. The short-lived nature of memory B cells was not programmed by the autoreactive T cell. Overall these results highlight properties of B and T cells that contribute to B cell fate choices in GC responses and how these are relevant to an autoimmune response.

3.1 Introduction

Tailoring the immune response to a given Ag is a crucial function of the immune system, as the quality and nature of the response impacts the success of pathogen clearance as well as subsequent long-lived immunity. This is further complicated in cases where the response directly targets or cross reacts with an autoAg. Nearly all naturally occurring immune responses incorporate both B and T cell recognition of the Ag, and collaboration between B and T cells specific for said Ag produces a GC response (94, 279, 280). Throughout the GC response, B cell survival, proliferation, and differentiation to either antibody-producing plasma cells or memory B cells is dependent upon, and informed by, direct interactions with T cells specific for the same Ag (cognate interactions) (58). However, the signals that drive differential fate choices made by B cells responding to different Ags and how they are influenced by features of the Ag itself are not well understood.

Interactions with cognate T cells are critical during two distinct phases of the developing B cell response. The first phase occurs shortly after exposure to a new Ag, but prior to GC formation. During this phase, cognate B-T interactions are essential to the initiation of Ag-stimulated B cell proliferation and also to driving B cell differentiation along three distinct pathways: 1st, short-lived plasmablasts that produce low-affinity largely IgM antibodies; 2nd, early (mostly) IgM memory B cells; and 3rd, GC B cells that reenter the follicle to initiate a new GC (281). The second phase of B-T cell interactions occurs within the mature GC itself. GC B cells undergo clonal expansion and SHM largely within the DZ, before migrating to the LZ to compete for survival signals supplied through interactions with specialized cognate T_{FH} cells (58). Evidence also suggests that T_{FH} cells provide signals that, in addition to maintaining the GC by selecting GC B cells for survival and additional rounds of proliferation and mutation in the DZ, further influence GC B cell differentiation into memory B cells or plasma cells. GC-derived plasma cells and long-lived plasma cells produce the high-affinity, class-switched antibodies critical to pathogen clearance and long-term immunity; while different subpopulations of GC-derived memory B cells are able to rapidly differentiate into plasma cells or re-initiate the GC upon re-exposure to Ag.

Several T_{FH}-derived signals have been identified that can, through genetic deletion or antibody blockade, influence B cell differentiation. These include the cytokines IL-4 and IL-21 (177, 233) and receptors PD-1 and ICOS (218, 223). It is possible that differential expression of these factors is the mechanism by which the immune system tailors the B cell response to different Ags, but this has not been explored. B cell receptor affinity for Ag is known to influence B cell fate choice, with higher-affinity being linked to preferential plasma cell differentiation (248), but how or if an Ag can influence the cognate T cell partner or the signal it provides to B cells is not known.

Recent advances in understanding GC development and the cognate B-T interactions that drive them have benefited from model Ag systems in which B and T cells specific for the Ag can be identified and their activation and differentiation tracked over the course of the response. For example, we and others have transferred fluorescent protein-marked ovalbumin (OVA)-specific T cells isolated from OTII mice and nitrophenyl hapten (NP)-specific B cells from B1-8 mice to non-fluorescent protein-marked mice to track both cell types in the developing GC following immunization with NPOVA (78, 106). Similar models based on other (mostly) foreign-Ags produce GCs with similar kinetics and patterns of B cell differentiation. A model system based on an autoAg may provide a tool with which to dissect the mechanisms by which the immune system itself controls differential outcomes, without relying on external blockade or deletion of candidate factors. Yet comparable models that examine the development of the autoimmune GC remain under explored.

MOG is a well characterized autoAg associated with anti-myelin autoimmunity of the CNS, both in human MS and the well-characterized animal model EAE. In MS, anti-myelin B cells and antibodies show evidence of SHM, indicating that they are GC-derived (72, 282). Currently, the most common way to induce MOG autoimmunity in C57Bl/6 mice is to immunize with the MOG₃₅₋₅₅ peptide that corresponds to the CD4⁺ T cell epitope, a method that excludes B cell targeting of the MOG protein (240). However, as I have showed earlier (Chapter 2), immunization with a larger peptide corresponding with the MOG-extracellular domain does indeed result in GC development incorporating

anti-MOG B cells (240, 283). Therefore, using the tools assembled and developed in Chapter 2, we can use our MOG-based model Ag system in an analogous manner to the NPOVA system described above for investigation of differential B cell fate choice under the control of notably different Ags.

Here, I demonstrate that the GC develops very differently in response to MOG compared to the well characterized NPOVA system. In comparison to the NPOVA response, B cell fate choice in the MOG GC response was heavily biased against plasma cells. Further, while the initial stages of the MOG GC developed normally, it was not sustained and instead collapsed early, producing a large number of memory-phenotype B cells. By manipulating the T cell controlling the same B cell response, I determined that, while plasma cell differentiation was largely independent of T cell influence, immunoglobulin class-switching, GC maintenance, and B cell differentiation into a memory-phenotype were largely under the control of the T cell partner. By manipulating the Ag itself, I, for the first time, found the T cell affinity for Ag impacts B cell fate choice. Finally, we determined that memory-phenotype B cells derived from the MOG GC are not long-lived, resulting in a failed memory response to secondary-challenge. Finally, the short-lived nature of MOG-specific memory B cells is not due to education by the autoimmune T cell.

3.2 Results

3.2.1 Immunization with MOG autoAg results in an atypical, unsustainable GC response

In order to identify and track responding B and T cells throughout an immune response to two different Ags, GFP⁺ B cells (either NP-specific B1-8⁺ J κ ^{-/-} (284, 285) or MOG-specific IgH^{MOG} (256)) and RFP⁺ T cells (either OVA-specific OTII (265) or MOG-specific 2D2 (264)) were isolated from transgenic mice and transferred into wild type C57Bl/6, non-fluorescent protein-marked recipients (Figure 3.1A). Two days post-transfer, mice were immunized in the footpad with the appropriate Ag (NPOVA for recipients of B1-8 B cells and OTII T cells, or mMOG_{tag} for recipients of IgH^{MOG} B cells

and 2D2 T cells) in CFA. Lymph nodes were harvested for histological analysis 5d post-immunization, representing the outcomes of early, pre-GC cognate interactions between responding B and T cells, or 10d post-immunization, representing a mature GC time point.

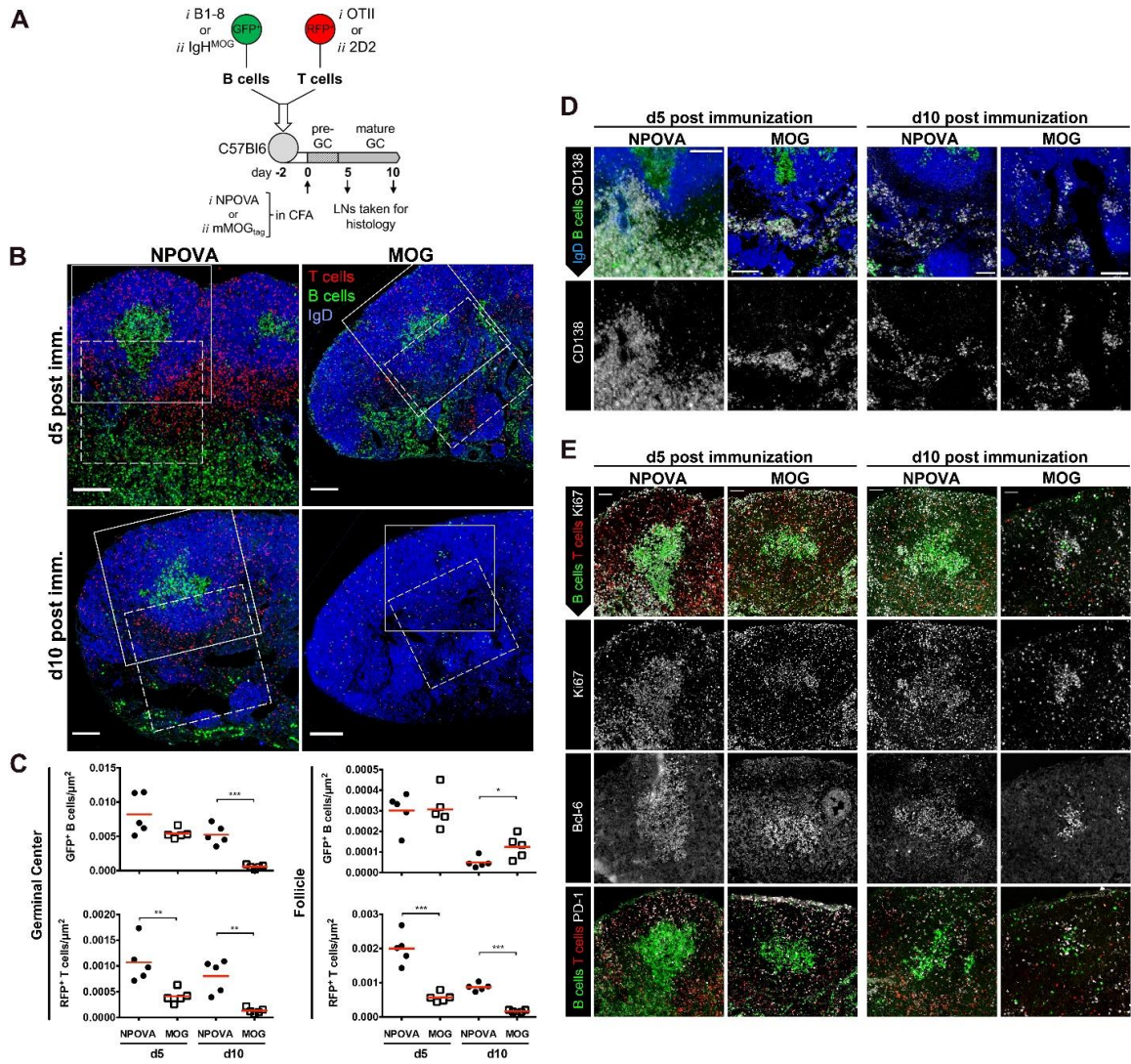
While virtually no transferred fluorescent cells could be observed in LNs from unimmunized mice (data not shown), large numbers of fluorescent B and T cells derived from the original transferred populations were readily evident at the 5d time point in both Ag systems (Figure 3.1B, top and 3.1C). Consistent with previous observations (78), PD-1⁺ RFP⁺ T_{FH} cells were distributed throughout the follicle and GC in both model systems, although the density of RFP⁺ T cells was significantly lower in mMOG_{tag}-immunized mice (Figure 3.1B, 3.1C, 3.1E).

Very large numbers of GFP⁺ CD138⁺ cells, representing the early short-lived plasmablast response, were evident outside of the follicles and within medullary cords of NPOVA- but not mMOG_{tag}-immunized mice (Figure 3.1D). By 10d post immunization fewer, but equivalent numbers of plasma cells were within medullary cords in both model systems.

Within B cell follicles, dense clusters of GFP⁺ cells (Figure 3.1B and 3.1C) that were also IgD^{lo}, Ki67⁺, and Bcl-6⁺ (Figure 3.1A and 3.1E) were evident in both systems 5d post-immunization, indicating that early pre-GC B-T interactions were sufficient to drive GC B cell differentiation and establishment of a new GC. However, by 10d post-immunization, the GC in the MOG Ag system had largely disappeared, while this time point corresponded with the full development of a mature and organized GC in the NPOVA system (Figure 3.1B, bottom and 3.1C). Small clusters of Ki67⁺ and Bcl-6⁺ cells could still be observed in follicles of mMOG_{tag}-immunized mice, however these were much smaller and less dense than those observed in NPOVA mice (Figure 3.1E). Instead, greater numbers of individual GFP⁺ cells were scattered throughout the follicle (Figure 3.1B and 3.1C). Very few individual GFP⁺ cells were evident in the follicle in the NPOVA system, and virtually all remained confined in the GC.

Figure 3.1. Differential GC development in the NPOVA and MOG model Ag systems.

(A) Fluorescent protein-marked B and CD4⁺ T cells specific for NPOVA or MOG were isolated and transferred into wild type, non-fluorescent protein-marked recipients. Two days post-transfer, mice were immunized with either NPOVA or mMOG_{tag} in CFA in the footpad. Draining popliteal LNs were harvested for histology d5 and d10 post-immunization, representing the early and mature GCs. (B) Immunofluorescence of LNs from NPOVA and mMOG_{tag} immunized mice to visualize RFP⁺ T cells and GFP⁺ B cells derived from transferred Ag-specific cells. Sections were also stained for IgD to outline B cell follicles. Scale bars represent 100 μm. (C) The density of GFP⁺ or RFP⁺ cells in the GC or follicle was quantified. Each data point represents the average value across one histological section for a single mouse. * p<0.05, **p<0.01, ***p<0.001. A Student's T-test was used for single comparisons. (D) Higher magnification of the regions of interest outlined by the dashed lines in panel B showing CD138 staining for plasma cells. (E) Higher magnification of the regions of interest outlined by the solid white line in panel B were further examined for Ki67, Bcl6, and PD-1 expression. Data is representative of 1 of 2 experiments.



3.2.2 Preferential differentiation of B cells with a memory phenotype in response to MOG autoAg

The developing GC response was analyzed by flow cytometry in a separate, identical experiment. Consistent with our histological observations, the early CD19^{int} CD138⁺ plasma cell response was nearly absent in mMOG_{tag}-immunized mice compared to a very large response in the NPOVA system (Figure 3.2A-3.2C). This was true of both the GFP⁺ response derived from transferred, Ag-specific B cells and the endogenous GFP⁻ response (Figure 3.2C bottom), confirming that this is a feature of the anti-MOG response.

While Ag-specific GFP⁺ CD95^{hi} CD38^{lo} GC B cells were evident in both the NPOVA and MOG systems at the d5 time point, they made up a significantly smaller proportion of the total GFP⁺ B cell population in the MOG system (Figure 3.2A-3.2C), and most dramatically at the d10 time point, consistent with the collapse of the GC response observed by histology. A similar collapse of the endogenous, GFP⁻ GC was also observed in mMOG_{tag} immunized mice (Figure 3.2C bottom). The proportional loss of GFP⁺ Ag-specific GC B cells and plasma cells in the MOG response was offset by a large increase in the proportion of CD95^{lo} CD38^{hi} cells, a phenotype shared by naïve and memory B cells (Figure 3.2C, top right).

Evaluation of immunoglobulin class-switching in the GC B cell population 8d post immunization, prior to complete collapse of the MOG GC, revealed that the ratio of IgG1 to IgM-expressing GC B cells was significantly higher in NPOVA-immunized mice (Figure 3.2E). Nevertheless, and despite the bias against plasma cell development (Figure 3.2A and 3.2C), mMOG_{tag}-immunized mice were still capable of mounting an Ag-specific antibody response, albeit smaller than observed to NPOVA. Indeed, by ELISpot the number of anti-MOG IgM and IgG producing cells was significantly lower in LN's 14d post immunization compared to anti-NP producing cells (Figure 3.2D, middle). Similar analysis of bone marrow revealed a reduction in anti-MOG IgM, but not IgG-producing cells (Figure 3.2D, right). This was reflected by reduced levels of circulating anti-MOG compared to anti-NP IgM but not IgG, as measured by ELISA of serum from the same mice (Figure 3.2D, left).

As the anti-MOG GC response is an autoimmune response, it was possible that regulatory processes, such as the induction of Bregs (44), Tregs (286), or T_{FR} cells (187), could have contributed to the collapse of the MOG GC response. In a separate experiment, there was no difference between the MOG and NPOVA systems in IL-10 production by GFP⁺ or GFP⁻ B cells, a measure of Breg cells, or by T cells (Figure 3.2F). Neither were there any differences in the proportion of Treg or T_{FR} cells. Therefore, an enhanced regulatory response was not responsible for the failed GC in the MOG system. It has also been suggested that administration of PTX, which is often used in conjunction with MOG-immunization to induce EAE, could modify regulatory responses and by extension, potentially affect the GC (287). However, I found that PTX administration did not rescue the MOG GC (Figure 3.3A) and had no effect on circulating antibody titers (Figure 3.3B).

Figure 3.2. Early collapse of the MOG GC to a memory B cell phenotype.

(A-C and F) Fluorescent protein-marked B and CD4⁺ T cells specific for NPOVA or MOG were transferred into non-fluorescent protein-marked C57Bl/6 mice that were then immunized with NPOVA or mMOG_{tag}. Draining LNs were harvested for analysis by flow cytometry d5 and d10 post-immunization. (A) Representative gating of GFP⁺ cells for plasma cells (PC), GC B cells, and memory/naive B cells (M/N). (B) Shown is the absolute number of GFP⁺ cells per LN. (C) Quantification from panel A showing size of each cell subset (as defined in panel A, gating shown above each plot) derived from the transferred GFP⁺ B cells (top row) or from endogenous GFP⁻ cells (bottom row). Data is expressed as the percentage of all GFP⁺ cells for Plasma cells, or percentage of all GFP⁺ B cells (CD19⁺ CD138⁻) for GC and Memory/Naïve B cells. One representative of two separate experiments is shown. Of note, the difference between GFP⁻ plasma cells at d5 was not seen using a non-parametric test. (D) C57Bl/6 mice were immunized with either NPOVA or mMOG_{tag} in CFA. Day 14 post-immunization, draining popliteal LNs and bone marrow were taken for ELISpot analysis of NP- or MOG-specific IgM or IgG. Blood serum from the same mice was assayed by ELISA for circulating anti-NP or -MOG IgM or IgG antibodies. Data is representative of 1 of 2 experiments. Of note, no statistically significant difference is seen in the number of IgM plasma cells in the bone marrow when using a non-parametric test. (E) The ratio of IgG1 expressing cells over IgM expressing GC B cells d8 post-immunization is shown. Data is representative of 1 of 2 experiments. (of note, there was no statistically significant difference between the groups when using a non-parametric test). (F) The percentage of all T cells expressing IL-10 (top) or FoxP3 (top middle), the percentage of Bcl6⁺ PD-1^{high} expressing FoxP3 (middle), and the percentage of B cells expressing IL-10 for GFP⁺ cells (bottom middle) and GFP⁻ cells (bottom) are shown d10 post-immunization. Data is based on one experiment. In all graphs, each data point represents an individual mouse. * p<0.05, **p<0.01, ***p<0.001. A Student's T-test was used for single comparisons.

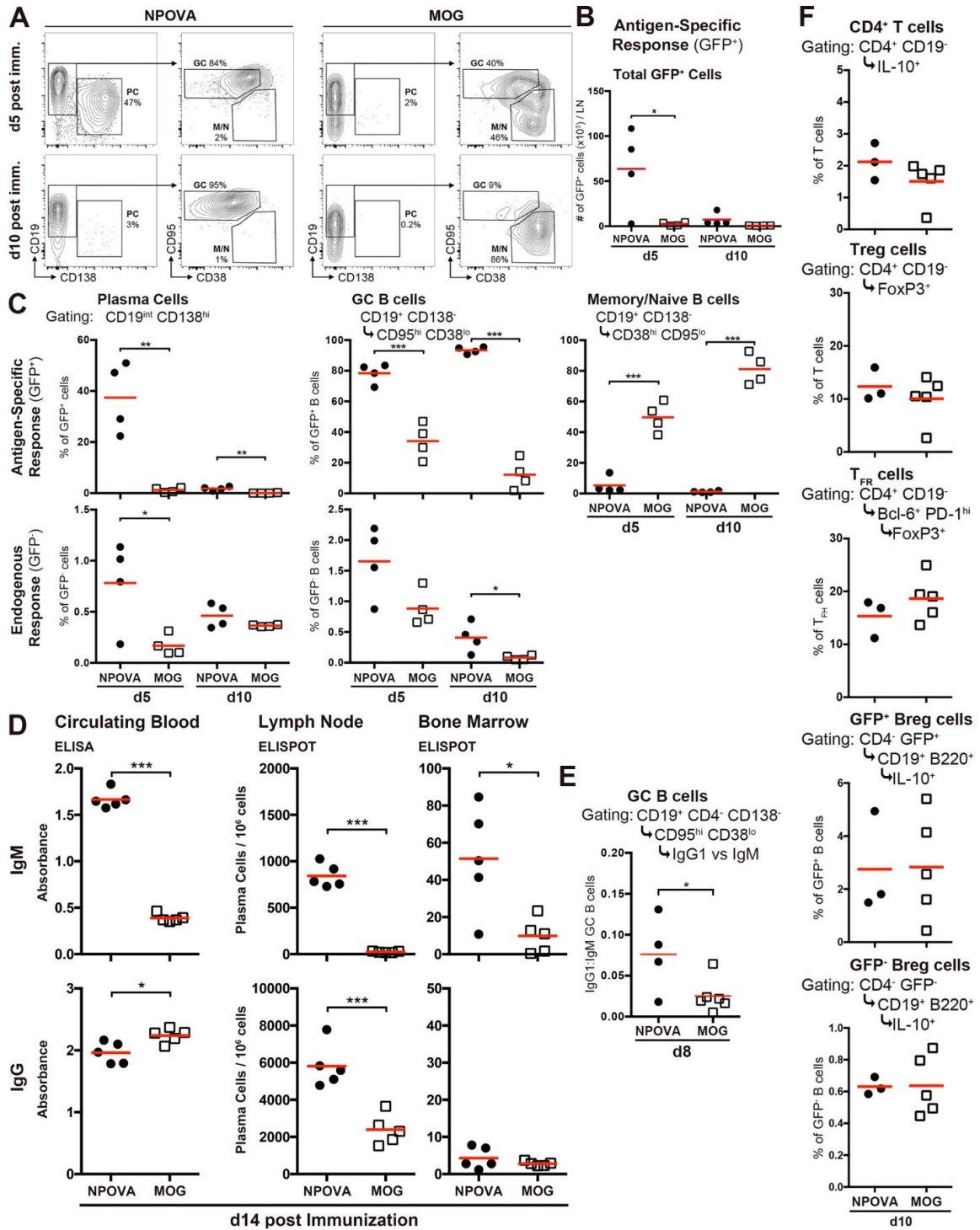
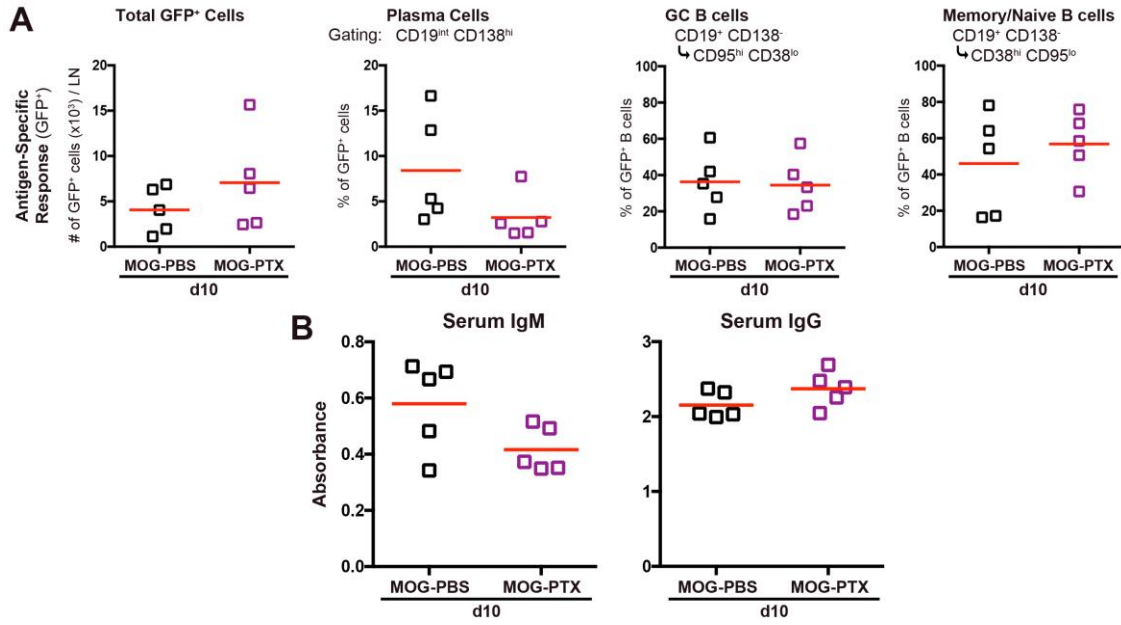


Figure 3.3. Administration of pertussis toxin does not save the MOG-induced GC from collapse

(A and B) Fluorescent protein-marked MOG-specific B and CD4⁺ T cells were transferred into non-fluorescent protein-marked C57Bl/6 mice that were then immunized with mMOG_{tag}. On days 0 and 2, mice were injected i.p. with either PBS or PTX. Draining LNs were harvested for analysis by flow cytometry d10 post-immunization. (A) Shown is the absolute number of GFP⁺ cells per LN (left) and each cell subset derived from the transferred GFP⁺ B cells is expressed as the percentage of all GFP⁺ cells for Plasma cells, or percentage of all GFP⁺ B cells (CD19⁺ CD138⁻) for GC and Memory/Naiïve B cells. (B) Blood serum from the same mice was assayed by ELISA for circulating anti-mMOG_{tag} IgM or IgG antibodies. Data is based on one experiment. In all graphs, each data point represents an individual mouse. A Student's T-test was used for single comparisons.



3.2.3 Ag-specific GFP⁺ CD95^{lo} CD38^{hi} B cells are Ag experienced

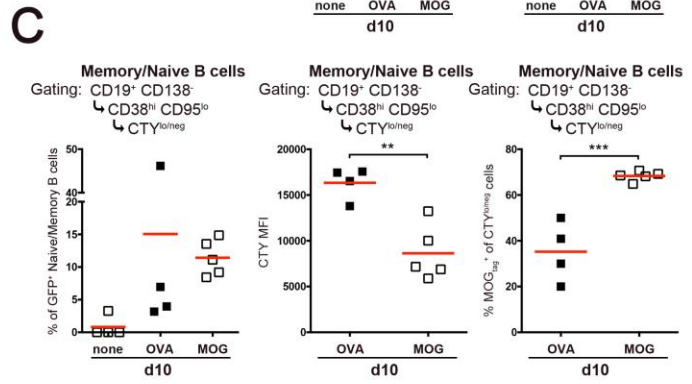
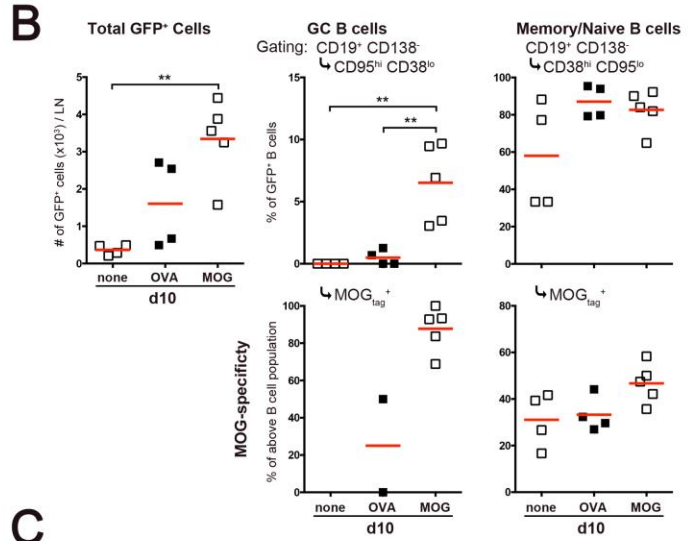
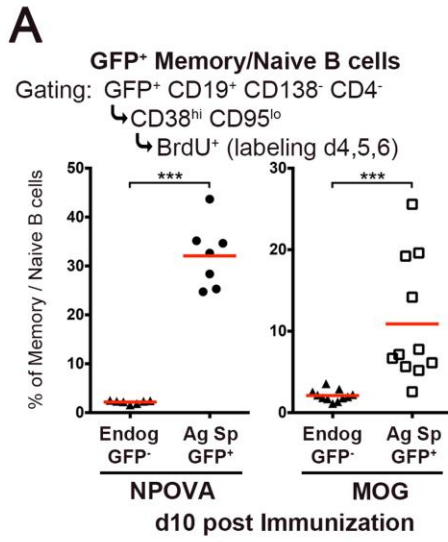
To confirm that the GFP⁺ CD95^{lo} CD38^{hi} B cells observed above derive from previously activated and proliferating cells, bromodeoxyuridine (BrdU) was injected d4, d5, and d6 post-immunization to label proliferating cells. On d10 post-immunization, LNs were harvested for flow cytometry analysis. In this way, only cells that were actively proliferating during the labeling period (note that only a proportion of actively proliferating cells would be labeled, due to the short half-life of free BrdU in mice), but had then become quiescent would retain BrdU labeling (126). Indeed, neither non-proliferating endogenous GFP⁻ CD95^{lo} CD38^{hi} follicular B cells (Figure 3.4A), nor proliferative GFP⁺ CD95^{hi} CD38^{lo} GC B cells (data not shown) stained with BrdU. In contrast, a proportion of GFP⁺ CD95^{lo} CD38^{hi} memory/naïve B cells were BrdU⁺ in both model systems, confirming that some of them derived from previously activated cells. Nonetheless, a relatively smaller portion of MOG-specific memory-phenotype B cells had labelled with BrdU, making it unclear how many of these cell had actually expanded due to mMOG_{tag}-immunization.

To more precisely establish whether GFP⁺ CD95^{lo} CD38^{hi} B cells in the MOG system had indeed derived from previously activated cells, GFP⁺ IgH^{MOG} B cells were isolated and labeled with Cell Tracker Yellow (CTY) prior to transfer along with either OVA or MOG-specific T cells. The CTY dye was used to monitor proliferation as the fluorescent signal from this dye halves whenever cells proliferate. Furthermore, this dye was used in combination with fluorescently labelled mMOG_{tag} protein to identify mMOG_{tag}-specific B cells. Recipients expressing an irrelevant transgenic TCR (SMARTA) were used as recipients to limit the endogenous T cell response. Control mice were left unimmunized or, to measure Ag-non-specific expansion, recipients of OVA-specific T cells were immunized with OVA to generate a GC response to an irrelevant Ag. Compared to unimmunized mice at the same time point, immunization with OVA protein resulted in a small, non-significant increase in GFP⁺ cells in draining LNs d10 post-immunization and, as expected, they did not participate in the GC response (Figure 3.4B, top). Immunization of mice with mMOG_{tag} that received MOG-specific T cells however, resulted in an increase in GFP⁺ cells. Consistent with above (Figure 3.2C),

the majority had a CD95^{lo} CD38^{hi} naïve/memory B cell phenotype, but some CD95^{hi} CD38^{lo} GC B cells were still evident. Approximately 90% of these GFP⁺ GC B cells bound fluorescently-labelled mMOG_{tag} antigen (Figure 3.4B, bottom), and all had fully diluted out the CTY dye (data not shown). Among the GFP⁺ CD95^{lo} CD38^{hi} naïve/memory B cell population, ~50% bound mMOG_{tag} Ag (Figure 3.4B, bottom). Further, a proportion of these cells had at least partly diluted CTY, indicating that they derived from proliferating cells (Figure 3.4C, left). While some non-specific expansion and CTY dilution was observed in the OVA-immunized mice, compared to expanded GFP⁺ memory B cells in MOG-immunized mice, they had a higher mean fluorescence intensity (MFI) for CTY, indicating that immunization with OVA did not induce the same extent of proliferation (Figure 3.4C, middle). Furthermore, CTY dilution was concentrated in the mMOG_{tag}-binding population in MOG-immunized but not OVA-immunized mice, indicating that expansion of the CD95^{lo} CD38^{hi} had been driven by Ag (Figure 3.4C, right).

Figure 3.4. Memory-phenotype B cells generated in response to MOG are Ag-experienced

(A) Fluorescent protein-marked OVA or MOG-specific B and T cells were transferred into non-fluorescent protein-marked SMARTA recipient mice and immunized with NPOVA or mMOG_{tag}, respectively. Mice were injected i.p. with BrdU d4, d5, and d6 post-immunization and BrdU incorporation in the GFP⁺ or GFP⁻ memory/naïve B cell populations was assessed by flow cytometry d10 post-immunization. Each graph represents a separate experiment and the data points in the mMOG graph were pooled from two separate experiments. (B and C) IgH^{MOG} GFP⁺ B cells were labelled with CTY then transferred into SMARTA recipient mice along 2D2 or OTII T cells. Mice were then immunized with either mMOG_{tag}, OVA (for those that received OTII T cells), or given no immunization and the GC response was assessed by flow cytometry d10 post-immunization. (B) Data is expressed as the absolute number of GFP⁺ cells, as the percentage of all GFP⁺ B cells (CD19⁺ CD138⁻) for GC and Memory/Naïve B cells (top panels), or as the percentage of all GFP⁺ GC or Memory/Naïve B cell that are mMOG_{tag}⁺ (bottom panels). Of note, the difference in the percentage of GFP⁺ B cells as GC B cells between the OVA and MOG groups was not seen in a non-parametric ANOVA. (C) Data is expressed as the percentage of GFP⁺ Memory/Naïve B cells that are CTY^{low/neg} (left) (of note, one data point in the ‘none’ group was identified as an outlier; furthermore, a statistically significant difference is seen between the ‘none’ group and MOG group when using a non-parametric ANOVA), the MFI CTY of CTY^{low/neg} Memory/Naïve B cells (middle), or the percentage of CTY^{low/neg} Memory/Naïve B cells that are MOG_{tag}⁺ (right). Data is based on one experiment. In all graphs, each data point represents an individual mouse. *p<0.05, **p<0.01, ***p<0.001. A Student’s T-test was used for single comparisons and a one-way ANOVA was used for multiple comparisons.



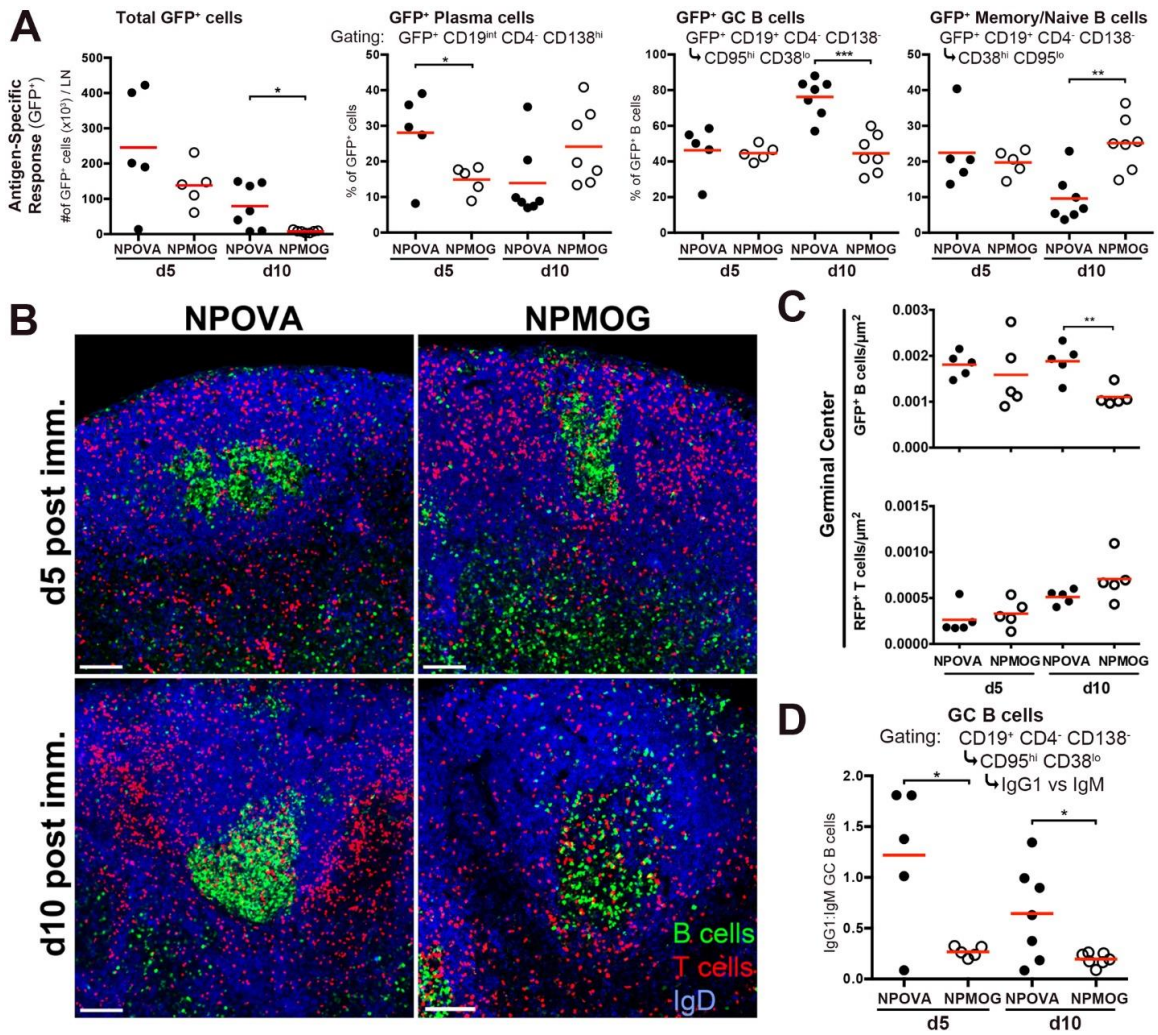
3.2.4 T cells partially control the outcome of the germinal center response to MOG

To begin to decipher the role for the cognate T cell partner in instructing differential B cell fate choice and the failure of GC maintenance in the MOG vs NPOVA systems, we took advantage of the modular nature of the hapten Ag system to place NP-specific B1-8⁺ J κ ^{-/-} B cells under control of either OVA-specific OTII T cells (NPOVA) or MOG-specific 2D2 T cells (NPMOG). Fluorescent protein-marked NP-specific B cells were transferred to non-fluorescent protein-marked SMARTA recipients and either OVA or MOG-specific T cells were transferred at the same time. Recipients were immunized 2d later with NPOVA for mice that received OTII T cells or NPMOG for those that received 2D2 T cells and LNs were harvested d5 or d10 post-immunization for analysis by flow cytometry or, in a separate experiment, histology.

Five days post-immunization, there was no significant difference in the number of GFP⁺ cells, but short-lived plasmablasts made up a smaller proportion of the NP-specific GFP⁺ response under control of MOG-specific T cells compared to OVA specific T cells (Figure 3.5A). However, similar results were not seen at the d10 time point suggesting plasma cell numbers had fully recovered by d10. A large population of GC B cells was evident d5 post-immunization by flow cytometry (Figure 3.5A) and large GCs were seen by histology (Figure 3.5B and 3.5C) in both systems, indicating that OVA and MOG-specific T cells are capable of supporting the early formation of a GC. However, by d10 post-immunization there was evidence that the NPMOG GC had begun to collapse, as reflected by the significant drop in numbers of GFP⁺ cells and that GC B cells made up a smaller proportion of the total Ag-specific population compared to the NPOVA response (Figure 3.5A), and GCs were less dense (Figure 3.5B and 3.5C). This was balanced by a significant increase in the proportion of Ag-specific B cells with a memory/naïve CD38^{hi} CD95^{lo} phenotype (Figure 3.5A). Furthermore, the immunoglobulin class-switching on GC B cells was also significantly reduced under the control of MOG-specific T cells (Figure 3.5D). Therefore, ongoing maintenance rather than initiation of the GC, as well as the immunoglobulin class-switching, are in part controlled by the T cell partner of the cognate B-T pairing.

Figure 3.5. MOG-specific T cells induce early GC collapse to a memory B cell phenotype.

Fluorescent protein-marked NP-specific B cells and either OVA or MOG-specific CD4⁺ T cells were transferred into non-fluorescent protein-marked SMARTA recipients that were then immunized with either NPOVA or NPMOG. Draining popliteal LNs were harvested for analysis by flow cytometry or, in a separate experiment, histology at d5 and d10 post-immunization. (A) The absolute numbers of GFP⁺ cells and size of the given cell subset is shown as a percentage of all GFP⁺ cells (Plasma cells) or all GFP⁺ B cells (GC B cells and Memory/Naïve B cells). The d5 and d10 time points were assessed in separate experiments, data shown is representative of 2 to 3 individual experiments. Of note, no statistically significant difference is seen in the proportion of GFP⁺ plasma cells between groups at the d5 time point when using a non-parametric test. Furthermore one of the data points at the d10 time point in the NPOVA group was identified as an outlier. (B) Representative histological sections from NPOVA or NPMOG-immunized mice to visualize NP-specific GFP⁺ B cells and either RFP⁺ OVA-specific or MOG-specific T cells, respectively. Sections were stained for IgD to outline B cell follicles. Data is representative of one experiment. Scale bars represent 100 μ m. (C) The density of GFP⁺ or RFP⁺ cells in the GC was quantified from histological images. (D) The ratio of IgG1-over IgM-expressing GC B cells d5 and d10 post-immunization is shown. Of note, differences in class-switching were not seen when using a non-parametric test. Each data point represents an individual mouse. * $p < 0.05$, ** $p < 0.01$, *** $p < 0.001$. A Student's T-test was used for single comparisons.



3.2.5 Low T cell Ag-affinity limits the MOG GC response

A common feature of autoimmune TCRs, including TCRs that recognize the MOG₃₅₋₅₅ peptide, is that they tend to bind peptide:MHC with relatively low-affinity (288, 289). Additionally, many are also polyreactive including the MOG₃₅₋₅₅-specific 2D2 TCR that also recognizes the NF-M₁₈₋₃₀ peptide with higher-affinity than it does MOG₃₅₋₅₅ (261, 262). I took advantage of polyreactivity of the 2D2 TCR to determine if TCR affinity for Ag influences B cell fate choice and maintenance of the GC response by using our modified haMOG_{tag} Ag that incorporates the NF-M₁₈₋₃₀ epitope.

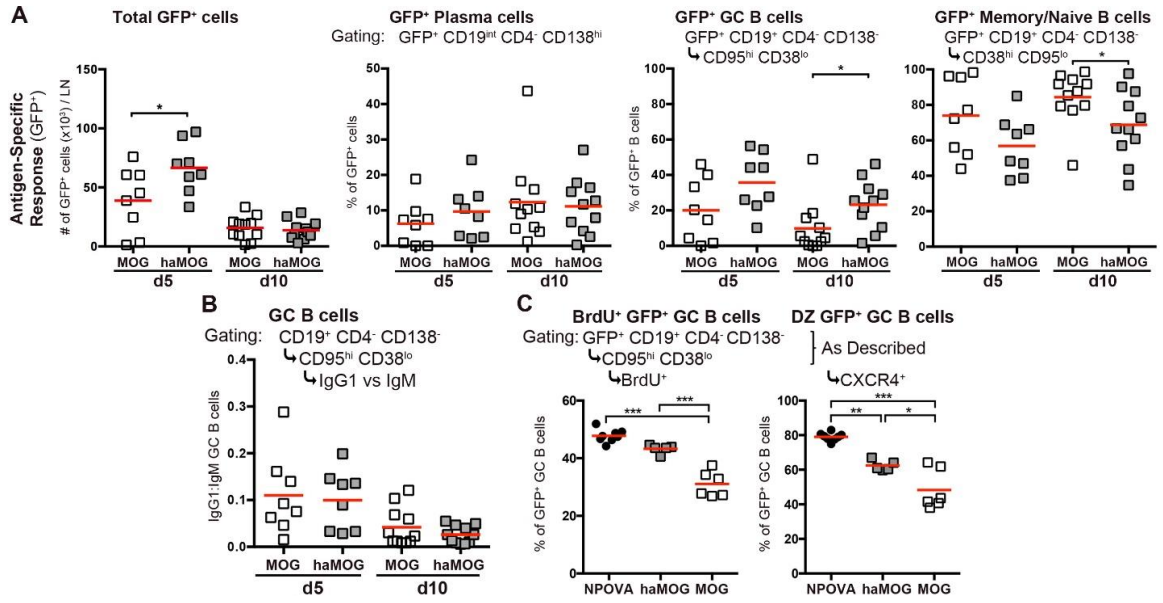
Fluorescent protein-marked MOG-specific B and T cells were transferred to SMARTA recipients which were then immunized with either mMOG_{tag} or haMOG_{tag}. Lymph nodes were harvested d5 or d10 post-immunization for analysis by flow cytometry. No differences in plasma cell differentiation were observed at either time point (Figure 3.6A). However, consistent with the hypothesis that the TCR affinity of the T cell partner in the cognate pair influences GC maintenance vs B cell differentiation, partial recovery of the GC with a corresponding decrease in the proportion of memory-phenotype B cells was observed 10d post-immunization with haMOG_{tag}. In contrast to our observations where NP-specific B cells were placed under control of two different T cells (Figure 3.5), T cells responding to haMOG_{tag} did not affect immunoglobulin class-switching in the GC (Figure 3.6B), suggesting that these outcomes are controlled separately or that they represent a gradient of potential outcomes influenced by different levels of T cell activation and signal production.

In the cyclic re-entry model of the GC response (280), GC B cells undergo repeated rounds of proliferation and SHM, largely in the DZ, followed by migration to the LZ to receive survival and differentiation signals, primarily from T_{FH} cells. We hypothesized that the collapse of the MOG GC was due to the inability of T_{FH} cells to drive LZ B cells to maintain GC status and reenter the DZ, instead resulting in differentiation to a memory phenotype. To test this, proliferation of GC B cells was analyzed by BrdU uptake, along with the expression of CXCR4 as a marker of DZ GC B cells. Consistent with our hypothesis, BrdU labeling of GC B cells was significantly higher in mice immunized with NPOVA and haMOG_{tag} compared to mMOG_{tag}, and more

GC B cells were of the CXCR4⁺ DZ phenotype in mice immunized with NPOVA, while haMOG_{tag}-induced GCs were intermediate (Figure 3.6C).

Figure 3.6. Increasing T cell Ag-affinity partly rescues the MOG GC from early collapse.

(A and B) Fluorescent protein-marked MOG-specific B and T cells were transferred into non-fluorescent protein-marked SMARTA recipients that were then immunized with mMOG_{tag} or haMOG_{tag}. Draining popliteal LNs were harvested for analysis by flow cytometry at d5 and d10 post-immunization. The d5 and d10 time points were assessed in separate experiments, data shown is the combination of two separate experiments. (A) The absolute numbers of GFP⁺ cells and size of the given cell subset at both d5 and d10 post-immunization is shown as a percentage of all GFP⁺ cells (Plasma cells) or all GFP⁺ B cells (GC B cells and Memory/Naïve B cells). Of note, no statistically significant difference is seen in the number of GFP⁺ cells per LN at the d5 time point when using a non-parametric test. Additionally, one data point in the d10 MOG group comparing the percentage GC B cells amongst GFP⁺ B cells was identified as an outlier. (B) The ratio of IgG1- over IgM-expressing cells was determined for GC B cells. (C) Fluorescent protein-marked Ag-specific B and T cells were transferred into non-fluorescent protein-marked SMARTA recipients that were then immunized with NPOVA, mMOG_{tag}, or haMOG_{tag}. Mice were injected i.p. with BrdU 7d post-immunization, and draining popliteal and inguinal LNs were harvested for analysis by flow cytometry 12hrs later. The percentage of GFP⁺ GC B cells that are BrdU⁺ (left) or CXCR4⁺ (right) is shown. Of note, no statistically significant differences between the haMOG and MOG groups when using a non-parametric test. Data is based on one experiment. Each data point represents an individual mouse. * p<0.05, **p<0.01, ***p<0.001. A Student's T-test was used for single comparisons and a one-way ANOVA was used for multiple comparisons.



3.2.6 Levels of T cell activation do not explain the differential B cell response between the different model systems

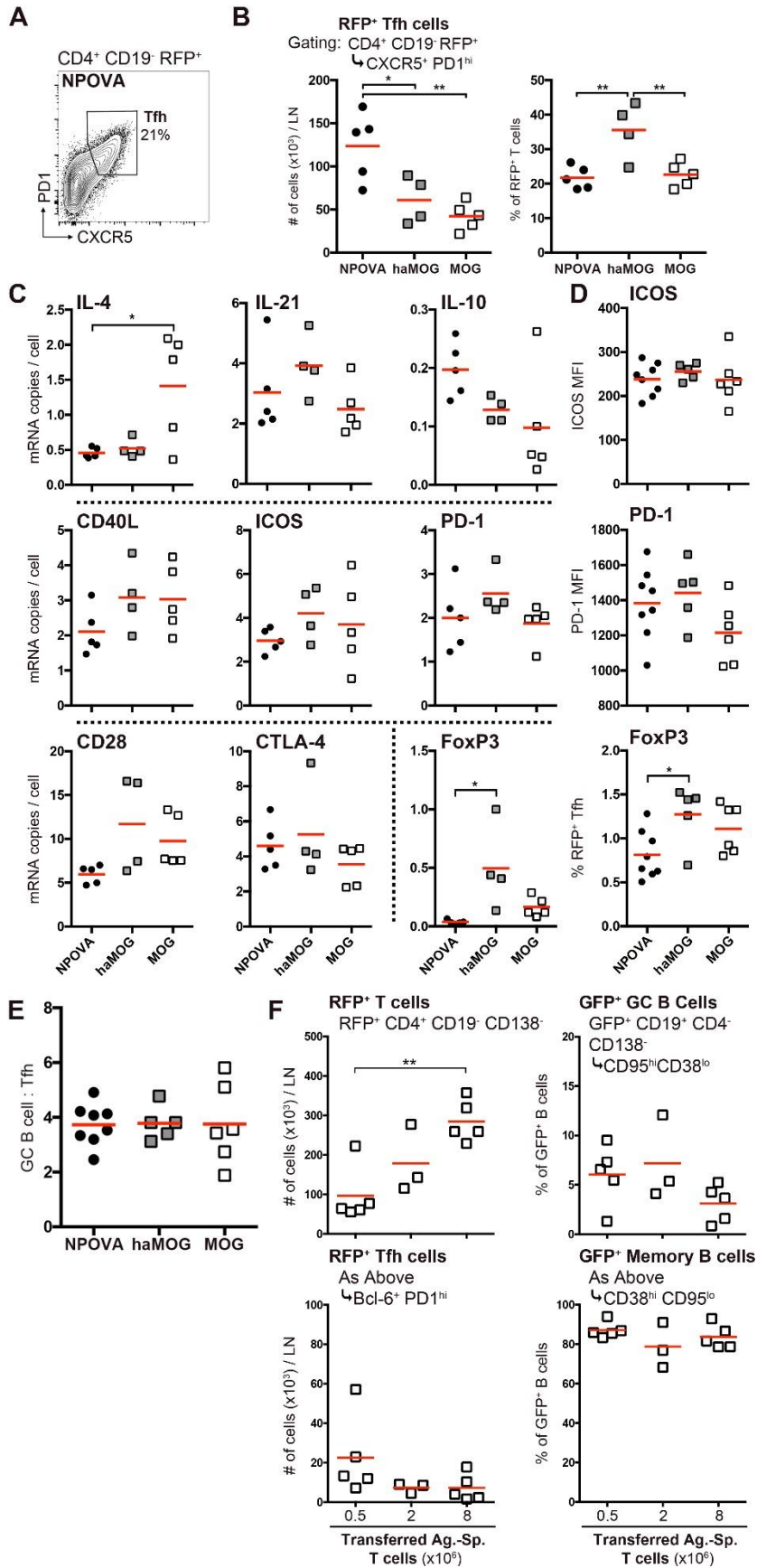
In an attempt to understand the underlying mechanism behind the differential outcome of the GC response in the different model Ag systems, Ag-specific T_{FH} cells (CXCR5⁺ PD-1^{hi} RFP⁺) were isolated by FACS from LNs of mice 10d post-immunization with NPOVA, mMOG_{tag}, or haMOG_{tag} (Figure 3.7A and 3.7B). Messenger RNA was isolated for quantitative digital droplet PCR analysis of the expression of genes with a known role in providing T cell help and differentiation signals to GC B cells. Surprisingly, little difference was observed in mRNA expression levels of the canonical T_{FH} cytokines IL-4 and IL-21 (Figure 3.7C – note that the small difference in IL-4 expression was not consistent across experiments). Again, there was no difference in the expression of IL-10 (Figure 3.7C, top). Neither were there differences in the mRNA expression of the surface receptors CD40L, ICOS, PD-1, CD28 and CTLA-4 (Figure 3.7C, middle). Equivalent surface expression of ICOS and PD-1 by Ag-specific T_{FH} cells was confirmed in a separate experiment by flow cytometry (Figure 3.7D). Interestingly, the master regulator of regulatory T cells, FoxP3, mRNA was expressed at significantly higher levels by T_{FH} cells from haMOG_{tag}-immunized mice (Figure 3.7C bottom), a finding confirmed by flow cytometry (Figure 3.7D). The significance of this observation is not clear, as an increased ratio of T_{FR} cells would seem to counter the larger GC response in haMOG_{tag} vs mMOG_{tag}-immunized mice. Nevertheless, this finding was consistent across three separate ddPCR and flow cytometry experiments. Thus, differences in gene expression by T_{FH} cells cannot explain why B cells in the NPOVA, mMOG_{tag}, and haMOG_{tag} induced GCs make different fate decisions.

I consistently observed that the absolute number of T_{FH} cells was greater in the NPOVA vs MOG systems (Figure 3.7B, and also reflected in Figure 3.1C) and that haMOG_{tag} immunization produced intermediate numbers of T_{FH} cells (Figure 3.7B). This resulted in an identical GC B cell:T_{FH} cell ratio across model Ag systems (one example presented in Figure 3.7E). To determine if the size of the GC response was simply linked to the size of the T cell response to a given Ag, different numbers of 2D2 T cells were transferred along with equal numbers of MOG-specific B cells into SMARTA recipient

mice. While immunization with mMOG_{tag} resulted in a significantly larger Ag-specific T cell response in mice that received more cells, there was no similar increase in the number of T_{FH} cells, nor was there an alteration in the GC response (Figure 3.7F).

Figure 3.7. T_{FH} cell phenotype is not altered by Ag.

(A-C) RFP⁺ OVA or MOG-specific T cells were transferred along with non-fluorescent protein-marked NP or MOG-specific B cells into non-fluorescent protein-marked SMARTA recipient mice that were then immunized with NPOVA, mMOG_{tag}, or haMOG_{tag} in CFA. Draining popliteal and inguinal LNs were harvested 10d later and T_{FH} cells (CD4⁺ CD19⁻ RFP⁺ CXCR5⁺ PD-1^{hi}) were sorted by FACS sorted for subsequent analysis of gene expression by digital droplet PCR. One representative of two independent experiments is shown. (A) An example of gating for CXCR5⁺ PD-1^{hi} T_{FH} cells is shown. (B) The absolute number of T_{FH} cells per LN is shown (left panel), along with size of the T_{FH} population as a percentage of total RFP⁺ T cells (right panel). Of note, no statistically significant differences are seen between the NPOVA and haMOG groups in the left graph or between any groups on the right graph when using a non-parametric test. (C) Digital droplet PCR analysis of mRNA levels (copies per cell) for the listed gene. Of note, between the NPOVA and MOG groups, no statistically significant difference is seen in IL-4 copies and a statistically significant difference is seen in CD28 copies when using a non-parametric test. (D-E) Fluorescent protein-marked Ag-specific B and T cells were transferred into non-fluorescent protein-marked SMARTA recipients that were then immunized with NPOVA, mMOG_{tag}, or haMOG_{tag}. Draining popliteal and inguinal LNs were harvested d8 post-immunization for analysis by FACS. (D) MFI for ICOS and PD-1 on RFP⁺ CXCR5⁺ PD-1^{hi} T_{FH} cells (top two panels) and the percent of T_{FH} cells (Bcl6⁺ PD-1^{hi}) that were FoxP3⁺ (bottom panel) are shown. Data is based on one experiment. (E) Ratio of GC B cells to T_{FH} cells in the different Ag systems. (F) Fluorescent protein-marked MOG-specific B cells and different numbers of MOG-specific T cells (0.5, 2, or 8 x 10⁶ 2D2 T cells) were transferred into non-fluorescent protein-marked SMARTA recipients that were then immunized with mMOG_{tag}. Draining popliteal LNs were harvested 10d post immunization for FACS analysis. The absolute number of RFP⁺ T cells per LN (top left panel) and RFP⁺ T_{FH} cells per LN is shown (bottom left panel). The percentage of the GFP⁺ B cells with a GC B cell (top right panel) or memory B cell (bottom right panel) phenotype is shown. Data is based on one experiment. Each data point represents an individual mouse. * p<0.05, **p<0.01. A one-way ANOVA was used for multiple comparisons.



3.2.7 The MOG-induced GC does not generate effective B cell memory

The primary function of memory B cells is to respond to secondary immune challenge (100). To determine if CD38^{hi} CD95^{lo} memory phenotype B cells generated from the MOG GC are responsive to Ag challenge, we performed an experiment that isolates the primary and secondary responses within the same mouse (Figure 3.8A). B and T cells specific for NPOVA protein were transferred into groups of SMARTA recipients and MOG-specific cells were transferred into a third group of SMARTA mice. Recipients were then immunized in the left footpad only with NPOVA or mMOG_{tag} depending on the cells transferred into them. Then 34 days later, mice were immunized in the right footpad with NPOVA or PBS if they had originally been immunized with NPOVA, or again immunized with mMOG_{tag}. Left and right draining LNs were analyzed separately by flow cytometry 5d post-secondary challenge. Control mice immunized with NPOVA in CFA in the left footpad but “challenged” with PBS alone showed an ongoing primary (but small in absolute terms - Figure 3.8B, top) GFP⁺ GC response in the left but not right draining LNs (Figure 3.8B, middle bottom). This confirmed that the lymphatics on the left and right sides of the animal were indeed separate allowing for separate analysis of the primary and secondary immune responses within the same animal. As expected, memory phenotype B cells made up the vast majority of GFP⁺ cells on the right side, confirming that memory B cells generated in the primary GC properly circulate and home to lymphatic tissues (Figure 3.8B, bottom). As expected, secondary-challenge with NPOVA resulted in generation of plasmablasts (Figure 3.8B, middle top) and initiation of a GC response on the right side. This contrasted starkly with the secondary challenge response in mMOG_{tag}-immunized mice. Consistent with previous observations, the primary GC response on the left side in mMOG_{tag}-immunized mice had disappeared, along with evidence of plasma cells at the d39 time point, leaving GFP⁺ cells with exclusively a CD38^{hi} CD95^{lo} phenotype. Despite the clear presence of memory-phenotype GFP⁺ cells in the right LN, secondary-challenge with mMOG_{tag} Ag did not produce a new GC response or plasma cells.

Recently, subsets of memory B cells have been identified based on differential expression of PD-L2 and CD80 (290). Double negative memory cells are associated with

the establishment of a new GC (135). Nevertheless, CD38^{hi} CD95^{lo} GFP⁺ B cells in mMOG_{tag}-immunized mice were almost entirely double negative, while a significant proportion of memory cells in NPOVA immunized mice expressed PD-L2 and/or CD80 (Figure 3.10A). Immunoglobulin class-switching remained reduced on GFP⁺ memory cells in the MOG system compared to the NPOVA system (Figure 3.10B), and significantly fewer IgG-producing long-lived plasma cells were recovered from the bone marrow (Figure 3.10C).

In the above experiment, it is possible that the B cell memory response in MOG-immunized mice failed due to the lack of T cells capable of responding to secondary challenge. Therefore, we performed a separate experiment where new naïve MOG-specific T cells were transferred 2d prior to secondary-challenge with mMOG_{tag} (groups iv and v, Figure 3.8C). Transfer of new naïve T cells did not result in an appreciable secondary GC response suggesting the secondary GC response was not limited by a lack of T cell help (Figure 3.8D). Nevertheless, the large majority of the very-rare GC B cells induced by secondary immunization bound mMOG_{tag}, as expected (Figure 3.9A, top). Interestingly, only ~12% of memory-phenotype B cells in either LN were MOG-specific at this late time point (Figure 3.9A, bottom), which is a considerable reduction from the ~50% observed d10 post-immunization (Figure 3.4B). This raised the possibility that the memory B cell response in the MOG system fails due to the selective loss of MOG-specific memory B cells over time. Therefore, we repeated the experiment using the NPOVA and mMOG_{tag} systems, but performed secondary-challenge d19 post-immunization (Figure 3.9B). At this intermediate time point, the GC response to secondary-challenge in LNs on the right side were equivalent between the NPOVA and MOG systems (groups vi and vii, respectively, Figure 3.9C) although, as with the primary response (Figure 3.2C), the plasma cell response was significantly lower with mMOG_{tag} challenge (Figure 3.9C). As expected, the large majority of GC B cells bound appropriate Ag (NP and MOG, respectively) in the secondary-response (Figure 3.9D). Importantly, ~60% of memory-phenotype B cells in either LN in the MOG-system bound mMOG_{tag}, which is similar to the proportion of MOG-specific memory B cells d10 post-immunization (Figure 3.4B), and considerably greater than observed d39 post-primary immunization (Figure 3.9A). While this percentage of Ag-binding cells was lower than

observed in the NPOVA system (Figure 3.9D), it suggests that a threshold number of Ag-binding cells are required to respond to Ag and that, over time, MOG-binding cells are lost and B cell memory fails.

To test whether MOG-specific memory B cells could respond in small numbers, GFP⁺ Ag-specific CD38^{hi} CD95^{lo} memory phenotype cells were sorted by FACS from mMOG_{tag} or NPOVA immunized mice. Ten days post-immunization, a small number of naïve/memory-phenotype B cells, 7.5×10^3 , were transferred to new SMARTA recipients along with naïve T cells specific for the relevant Ag. Following secondary-challenge, small numbers of GFP⁺ NP-specific cells were recovered, the majority of which were plasma cells or GC B cells (Figure 3.10D). In contrast, MOG-specific cells were either completely undetectable or exclusively of the CD38^{hi} CD95^{lo} phenotype, indicating that they had not responded to secondary-challenge. This suggests that NP-specific memory-phenotype B cells could respond in small numbers; however, MOG-specific memory-phenotype B cells could not.

Figure 3.8. Memory B cells produced by the MOG-induced GC response are unresponsive during secondary immune responses.

(A and B) Fluorescent protein-marked Ag-specific B and T cells were transferred into non-fluorescent protein-marked SMARTA recipients that were then immunized in their left footpad with either NPOVA or mMOG_{tag} in CFA. Thirty-four days post-immunization, mice were immunized in their right footpad with NPOVA, PBS, or mMOG_{tag} in CFA in the right footpad, as shown. (B and D) The primary response in the left draining popliteal and inguinal LNs and secondary response in the right LNs were analyzed separately by flow cytometry 5d post-secondary challenge. The absolute numbers of GFP⁺ cells and size of the given Ag-specific subsets as a percentage of the total GFP⁺ cells (Plasma cells) or GFP⁺ B cells (GC and Memory/Naïve B cells) is shown for the left and right sides separately. (B) No statistically significant differences are seen between the NPOVA-NPOVA and MOG-MOG groups on the left f.p. for the GC B cells and memory B cell subsets using a non-parametric test. Furthermore, on the right f.p. there were no differences between the NPOVA-NPOVA and MOG-MOG groups by absolute numbers, and between the NPOVA-NPOVA and NPOVA-PBS groups for GC B cells, plasma cells, or memory B cells when using a non-parametric test. (C and D) Fluorescent protein-marked MOG-specific B and T cells were transferred into non-fluorescent protein-marked SMARTA recipients that were then immunized in their left footpad with mMOG_{tag} in CFA. Thirty-two days post-immunization 5×10^5 naïve 2D2 T cells were transferred then d34 post-immunization, mice were immunized in their right footpad with PBS or mMOG_{tag} in CFA, as shown. Of note, a statistically significant difference between the MOG-PBS and MOG-MOG groups in the proportion of GFP⁺ B cells as GC B cells is seen when using a non-parametric test. Data shown is based on one experiment. Each data point represents an individual mouse. * $p < 0.05$, ** $p < 0.01$, *** $p < 0.001$. A Student's T-test was used for single comparisons and a one-way ANOVA was used for multiple comparisons.

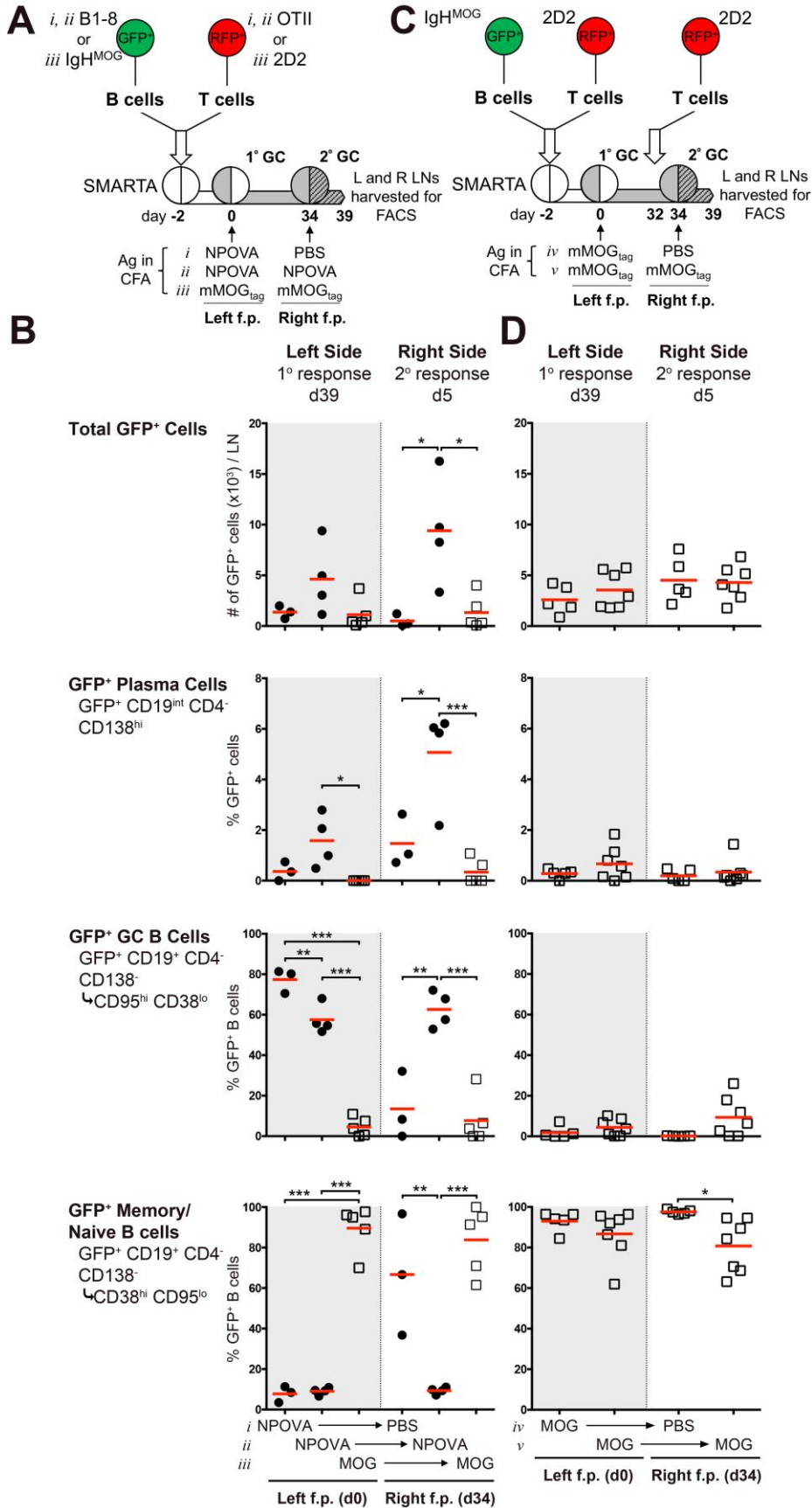
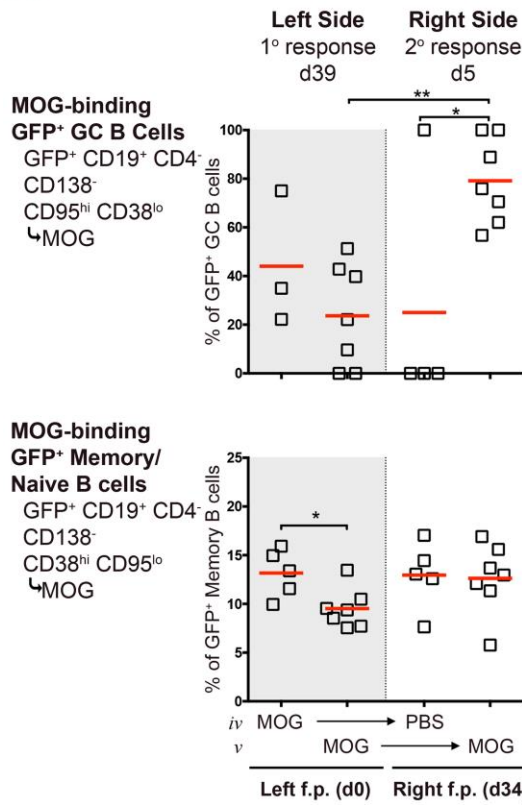


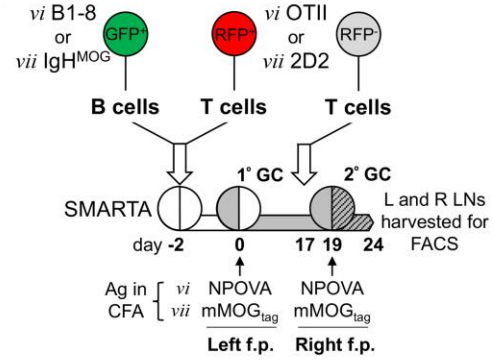
Figure 3.9. MOG-specific memory B cells are responsive but they are short-lived.

(A) Is from the experiment described in Figure 3.8C. (A and D) The proportion of GFP⁺ B cells (GC and Memory/Naïve B cells) that are Ag-specific is shown for the left and right sides separately. (B-D) Fluorescent protein-marked Ag-specific B and T cells were transferred into non-fluorescent protein-marked SMARTA recipients that were then immunized with either NPOVA or mMOG_{tag} in CFA in their left footpad. Seventeen days post-immunization 5 x 10⁵ naïve Ag-specific T cells were transferred then d19 post-immunization, mice were immunized in their right footpad with NPOVA or mMOG_{tag} in CFA, as shown. (C) The primary response in the left draining popliteal and inguinal LNs and secondary response in the right LNs were analyzed separately by flow cytometry 5d post-secondary challenge. The absolute numbers of GFP⁺ cells and size of the given Ag-specific subsets as a percentage of the total GFP⁺ cells (Plasma cells) or GFP⁺ B cells (GC and Memory/Naïve B cells) is shown for the left and right sides separately. Of note, no statistically significant difference is seen between the NPOVA-NPOVA and MOG-MOG groups in the left f.p. for absolute numbers of GFP⁺ cells when using a non-parametric test. Data shown is based on one experiment. Each data point represents an individual mouse. * p<0.05, **p<0.01, ***p<0.001. A Student's T-test was used for single comparisons and a one-way ANOVA was used for multiple comparisons.

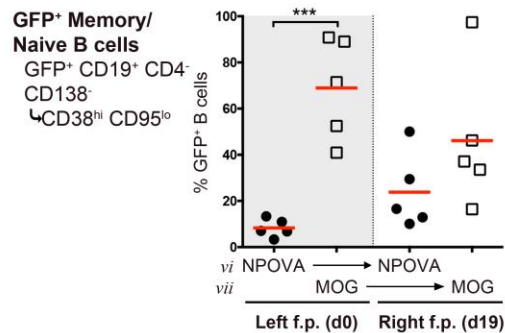
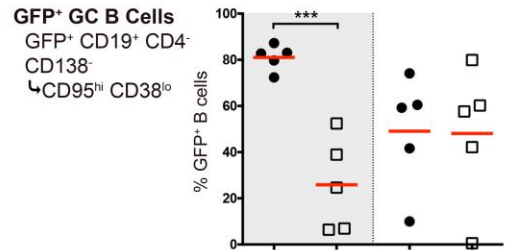
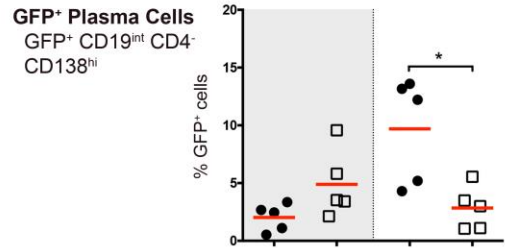
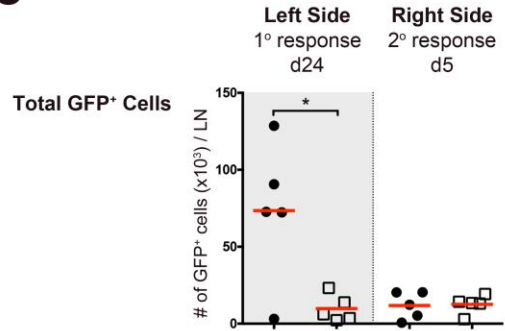
A



B



C



D

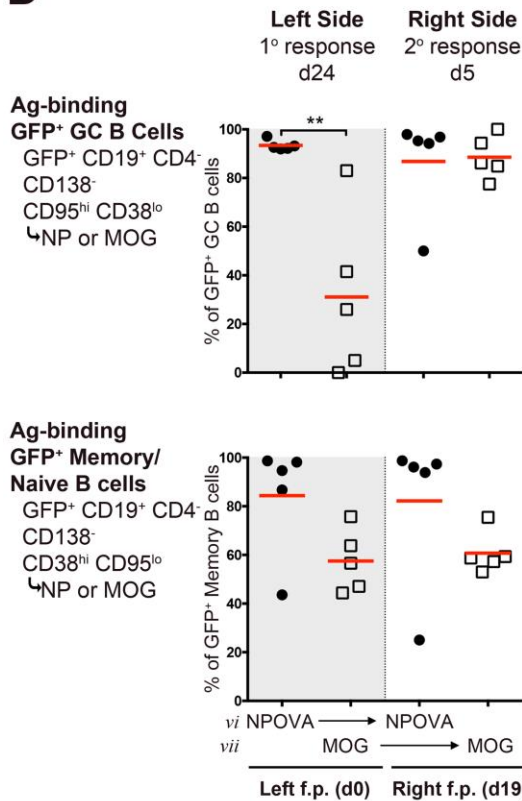
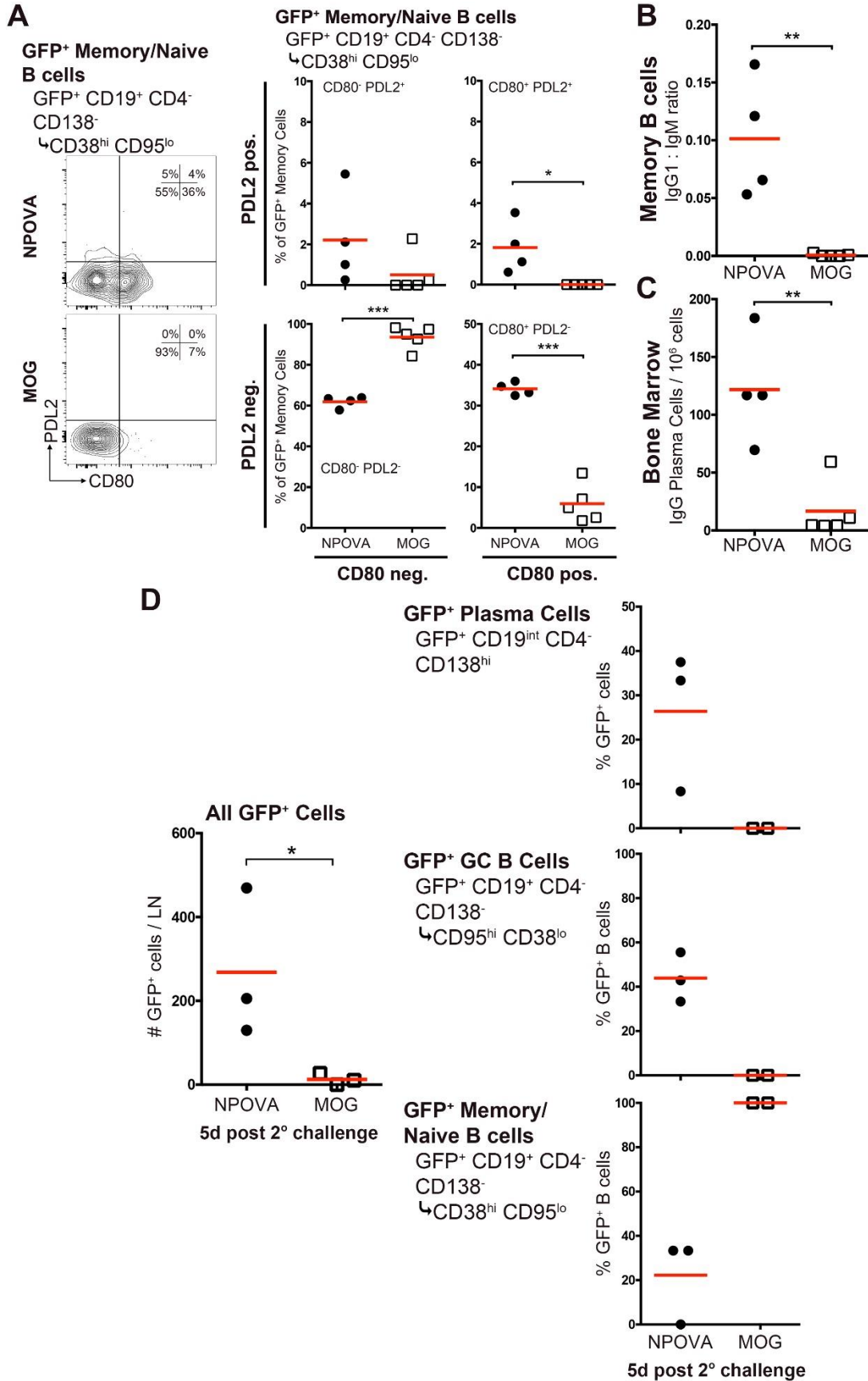


Figure 3.10. Characterization of MOG-specific memory B cells and their functionality.

(A) Fluorescent protein-marked NPOVA or MOG-specific B and T cells were transferred into non-fluorescent protein-marked SMARTA recipients that were then immunized in their left footpad with either NPOVA or mMOG_{tag} in CFA, respectively. Thirty-four days post-immunization, mice were immunized in their right footpad with NPOVA, PBS, or mMOG_{tag} in CFA in the right footpad, as shown in Figure 3.7A. Representative staining and quantification for CD80 and PD-L2 on NPOVA and MOG GFP⁺ memory/naïve B cell subsets. Groups shown are for the NPOVA-NPOVA and MOG-MOG groups. (B) The ratio of IgG1 B expressing cells over IgM expressing B cells amongst GFP⁺ memory/naïve B cells is shown. (C) At the same time, bone marrow was harvested for ELISpot quantification of NP- or MOG-specific IgG producing plasma cells. (D) Fluorescent protein-marked NPOVA or MOG-specific B and T cells were transferred into non-fluorescent protein-marked SMARTA recipients that were then immunized with NPOVA or mMOG_{tag} in CFA, respectively. Draining popliteal and inguinal LNs were harvested d10 post-immunization and CD19⁺ CD4⁻ CD138⁻ CD38^{hi} CD95^{lo} GFP⁺ memory/naïve B cells were sorted. Seventy five hundred NP or MOG-specific B cells were transferred along with 5×10^5 naïve OVA or MOG specific T cells into new non-fluorescent protein-marked SMARTA recipient mice. These were immunized with NPOVA or mMOG_{tag} and 5d later draining popliteal and inguinal LNs were analyzed by flow cytometry. The absolute numbers of GFP⁺ cells per LN (shown on the left) and size of the given Ag-specific subsets as a percentage of the total GFP⁺ cells (Plasma cells) or GFP⁺ B cells (GC and Memory/Naïve B cells) is shown on the right. Of note, no difference is seen between the NPOVA and MOG groups when using a non-parametric test. Data shown is based on one experiment. Each data point represents an individual mouse. *p<0.05, **p<0.01, ***p<0.001. A Student's T-test was used for single comparisons.

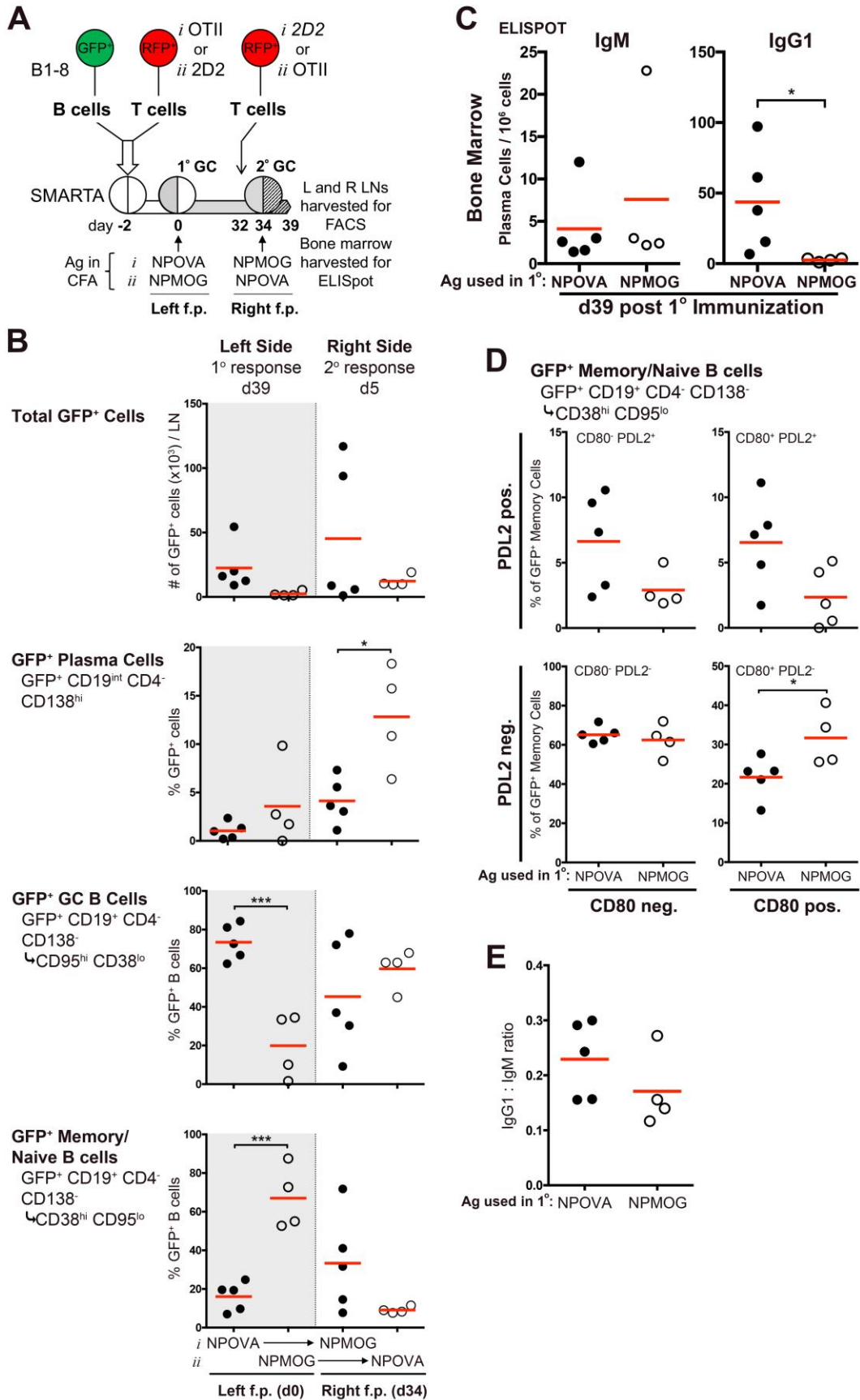


3.2.8 Memory B cell responsiveness is not programmed by the MOG-specific T cell

To determine if the failure of MOG-specific B cell memory was due to education from MOG-specific T cells, an experiment was performed to determine if MOG-specific T cells could instruct short-lived memory into NP-specific memory B cells. Nitrophenyl-specific B cells were transferred along with either OVA or MOG-specific T cells into SMARTA recipient mice. Mice were then immunized with NPOVA, if they receive OVA-specific T cells, or NPMOG, if they received MOG-specific T cells, in the left footpad only. Thirty-two days later, naive T cells specific for the opposite Ag (mice that originally received OVA-specific T cells had a new transfer of MOG-specific T cells or *vice versa*) were transferred; then mice were challenged with Ag in the right footpad 2d later such that the NP-conjugated protein matched with the cells of the secondary transfer (Figure 3.11A). This was done to eliminate any potential confounding factors associated with differences in the generation of T cell memory or regulatory cells from the primary immune response. Left and right draining LNs were analyzed separately by flow cytometry d5 post-secondary challenge. Analysis of the primary response in the left LN revealed that, as at d10 (Figure 3.5), the NP-specific B cell response under control of MOG-specific T cells was heavily biased to memory-phenotype cells at the expense of GC B cells (Figure 3.11B). The presence of IgG-producing long-lived plasma cells in the bone marrow was also reduced (Figure 3.11C). In contrast, and as opposed to the MOG-specific B cells in the previous experiment (Figure 3.10A), there was no difference in the proportion of CD80 PDL2 double negative memory NP-specific B cells under the control of either T cell (Figure 3.11D), nor was there a defect in immunoglobulin class-switching of memory cells (Figure 3.11E). Also, analysis of the right LN clearly demonstrated that NP-specific B cells educated by MOG-specific T cells in the primary response were able to respond to secondary-challenge (Figure 3.11B). Overall, this confirmed that the failure of MOG-specific memory B cells was not due to T cell education, but, rather was something intrinsic to the B cell or its environment.

Figure 3.11. Autoimmune T cells do not induce short-lived memory in MOG-specific B cells during the GC response.

(A) Fluorescent protein-marked NP-specific B cells and OVA or MOG-specific T cells were transferred into non-fluorescent protein-marked SMARTA recipients that were then immunized in their left footpad with either NPOVA or NPMOG. Thirty-two days post-immunization, naïve T cells of the reciprocal specificity were transferred to these recipient mice, as shown, followed two days later by immunization with that Ag in the right footpad. (B) The primary response in the left draining popliteal and inguinal LNs and secondary response in the right LNs were analyzed separately by flow cytometry d5 post-challenge. The absolute numbers of GFP⁺ cells and size of the given Ag-specific subsets as a percentage of the total GFP⁺ cells (Plasma cells) or GFP⁺ B cells (GC and Memory/Naïve B cells) is shown for the left and right sides separately. Of note, a statistically significant difference is seen between the groups in the left f.p. when using a non-parametric test. (C-E) Groups shown are based upon what they were immunized with for the primary immunization. (C) At the same time, bone marrow was harvested for ELISpot quantification of NP-specific IgM or IgG producing plasma cells (the Ag used to coat plates was based on the primary immunogen). (D) Memory/naïve phenotype GFP⁺ B cells were analyzed for expression of CD80 and PD-L2. Of note, no statistically significant differences between groups are seen when using a non-parametric test. (E) The ratio of IgG1 over IgM expressing B cells amongst GFP⁺ memory/naïve B cells is shown. Data shown is based on one experiment. Each data point represents an individual mouse. *p<0.05, **p<0.01, ***p<0.001. A Student's T-test was used for single comparisons.



3.3 Discussion

Here, I manipulated Ag model systems as a novel approach to investigate how the immune system controls B cell fate choice and differentiation to produce different GC outcomes tailored to the specific Ag in an autoimmune setting. The response to NPOVA and other NP-haptenated proteins is well characterized (126, 291), and in many ways is considered to represent the default response to a foreign-Ag. Myself and others have shown that the anti-NP GC consistently forms 4-5d after exposure to Ag, peaks ~2 wks post exposure, and remains active for several weeks after that (78, 135). I show here that, while the GC response to MOG develops with similar kinetics, it is not sustained and instead dissipates early. This should not be interpreted as a failed GC response, however, as it still produces measurable levels of circulating, class switched anti-MOG antibody. Further, subcutaneous immunization with MOG protein is a well-established method to induce the anti-myelin autoimmune model EAE. In my hands, mice immunized with mMOG_{tag} develop a robust disease with evidence that GC-derived anti-MOG B cells contribute to both disease severity and chronic disease course (240, 283). Therefore, although short-lived, the MOG GC is productive.

The GC response is sustained by interactions between GC B cells and T_{FH} cells, predominantly in the LZ of the GC. The outcome of these interactions can select B cells to maintain their GC status and cycle back into the DZ for additional rounds of cell division, mutation, and return to the LZ for selection (58). Alternatively, GC B cells can be driven to memory or plasma cell fates (292). The first major finding of this study is that, in the MOG GC response, early failure of the GC is associated with preferential differentiation to a memory phenotype at the expense of maintaining the GC. Indeed, within the small GC B cell population in the collapsing MOG response there is a clear bias to a LZ phenotype, suggesting that B cells are not being selected to return to the DZ for proliferation. A similar bias to memory cell differentiation is seen for B cells defective in CXCR4, which is required for proper DZ B cell homing (108). By histology, this manifests as a small, less-organized GC with a large number of individual GFP⁺ cells distributed throughout the follicle. In the GC response to a foreign-Ag, memory B cell differentiation has been shown to occur predominantly in the early stages, shortly after

GC formation, with plasma cell differentiation preferentially occurring later in the response (126). Therefore, it is possible that the early dissolution of the MOG GC to generate memory B cells represents an extreme acceleration of this same process.

It is clear from my observations that the status of the cognate T cell partner strongly influences the dichotomy between GC maintenance and memory B cell differentiation, along with immunoglobulin class-switching. Indeed, MOG-reactive T cells induced a similar GC outcome when paired with NP-specific B cells and enhanced T cell activation via high-affinity Ag partly rescued the MOG GC from collapse and reduced memory B cell differentiation. In this case, immunoglobulin class-switching was not impacted, suggesting that there is a gradient to the GC parameters that are influenced by T cell status. Interestingly, while BCR affinity has previously been linked to plasma cell differentiation (128, 248) (see below), this is the first report that I am aware of that demonstrates that TCR affinity for Ag can impact B cell fate choice.

It is not clear what signals the cognate T cell partners use to drive differential GC maintenance vs memory B cell differentiation in the two model systems. Previously identified T cell signals that influence GC formation and memory differentiation include ICOS and PD-1 (218, 223). T_{FH}-produced cytokines, IL-21, IL4, and IL-10 have also been shown to be required for proper GC development (175, 177, 233). Nevertheless, I did not find evidence that these are differentially expressed by T_{FH} cells in the NPOVA and MOG systems. Therefore, the immune system may employ other signals to modulate GC outcome in response to different Ags. The size of the T_{FH} cell pool itself may be one of these “signals”, as we consistently observed a direct correlation between the number of T_{FH} and GC B cells in our different model systems. An attempt to modulate this by increasing the total T cell response was not successful, suggesting that other factors limit the size of the T_{FH} cell niche in an Ag-dependent way. Indeed, maintenance of the PD-1^{hi} phenotype on T_{FH} cells is dependent on their ongoing cognate interactions with B cells (78, 293). Therefore, it is difficult to separate cause and effect with regards to the GC B cell:T_{FH} cell ratio.

While the balance between GC maintenance and memory B cell differentiation, along with immunoglobulin class-switching, were heavily influenced by the status of the cognate T cell partner, plasma cell differentiation and memory B cell unresponsiveness were not. Plasma cell differentiation has been linked to BCR affinity (128, 248). Further, plasma cells preferentially differentiate later in the GC response compared to memory cells (126). It is possible that the MOG GC doesn't last long enough to produce BCRs with sufficiently high-affinity to promote plasma cell differentiation. The accumulation of somatic mutations in anti-MOG B cells and BCR affinity for Ag will need to be explored in future studies. However, this would not explain the almost complete absence of early, short lived plasmablasts that typically derive from pre-GC interactions. The starting affinity for Ag in the Ig-heavy chain knockin (IgH^{MOG}) B cells is clearly sufficient to allow for B cell activation to proliferate and initiate the GC. Additional investigation will be required to determine if (potentially) low BCR affinity accounts for reduced plasma cell formation, or if the few (but productive) plasma cells that do form in the MOG GC response represent clones that attained a threshold affinity that allowed for their differentiation.

Finally, it is clear from our studies that, despite the preference for differentiation to memory phenotype B cells in the MOG system, this differentiation may not be complete as the cells are not long-lived, resulting in a failure to respond to secondary-challenge. Our Ag-binding studies demonstrate that the primary GC response is indeed driven by specific Ag, as virtually all GC B cells bind mMOG_{tag}. Among naïve/memory phenotype cells, the proportion that bound specific Ag was lower in the MOG compared to NPOVA systems, which may be in part explained by the properties of the IgH^{MOG} mouse. The heavy chain knock-in for the IgH^{MOG} mouse combines with endogenous light chains resulting in ~30% of cells being specific for MOG, while the B1.8 heavy chain paired exclusively with the lambda light chain in a kappa chain-deficient mice results in ~90% of cells binding NP (294). Nevertheless, the large majority of proliferated memory-phenotype B cells bound to MOG Ag at the d10 time point, confirming that they derived from the Ag-response. However, over time there was a selective loss of these MOG-binding cells. Intriguingly, capacity to bind MOG Ag also appeared to be lost among the rare remnants of the MOG GC at later time points (compare Figure 3.3B to 3.7H) and

therefore, there may be an active selection against MOG-binding not observed in the NPOVA system. Further study will be required to determine if this is the case.

In conclusion, I showed here that different Ags can drive GC responses with very different outcomes. Further, I identify GC maintenance vs memory B cell differentiation as a fate decision dichotomy that is regulated independently from plasma cell differentiation, and that the status of the cognate T cell partner heavily influences the former, but not the latter. Finally, I show that, despite a preference for memory B cell formation in the MOG system, differentiation may not be complete as the Ag-specific cells are not long-lived. My findings have implications both for our fundamental understanding of how B cell fate choice is regulated in the GC response, and for our understanding of how autoimmune B cells participate in autoimmune responses, and anti-myelin responses in particular.

3.4 Materials and Methods

3.4.1 Mice

C57Bl/6, 2D2 TCR-transgenic (264), SMARTA TCR-transgenic (4694; Tg(TcrLCMV)327Sdz/JDvsJ), and OTII TCR-transgenic mice (4194; Tg(TcraTcrb)425Cbn/J) were purchased from Jackson Laboratories, Bar Harbor, Maine. B1-8 mice (285) with a homozygous deletion of the $J\kappa$ locus (284) were a generous gift from Dr. Ann Haberman. IgH^{MOG} MOG-specific BCR knock-in mice (256) were received as a gift from Dr. H Wekerle. Mice expressing fluorescent proteins within all nucleated cells, either dsRed (RFP; 6051; Tg(CAG-DsRedpMST)1Nagy/J) under control of the β -Actin promoter or eGFP via the ubiquitin promoter (4353; Tg(UBCGFP)30Scha/J) were obtained from the Jackson Laboratory. Mice were housed in a specific pathogen-free barrier at West Valley Barrier. All animal protocols (2011-047) were approved by the Western University Animal Use Subcommittee.

3.4.2 Antibodies for histology/flow cytometry

The following antibodies were purchased from BD Biosciences, Franklin Lakes, New Jersey: anti-Bcl6 A647 or v450 (K112-91), anti-CD138 BV421 or biotin (281-2), anti-CXCR5 APC (2G8), anti-CD19 BV711 (1D3), anti-CD4 v450 (RM4-5), anti-CD62L A700 (Mel14), anti-CD95 PE-Cy7 (Jo2), anti-IgG1 APC (A85-1), anti-B220 PE-Cy7 (RA3-6B2), Streptavidin v450 or APC-Cy7, and anti-CD80 PE (16-10A1). The following antibodies were purchased from Thermo Fisher Scientific, Waltham, Massachusetts: anti-BrdU A647 (MoBU-1), anti-IgM A568 (polyclonal), anti-CXCR4 PE (2B11), Streptavidin A568, anti-Ki67 unconjugated. The following antibodies were purchased from eBioscience, Waltham, Massachusetts: anti-PD-1 biotin (RMP1-30), anti-CD38 PE or PE-Cy5 (90), anti-CD4 PE-Cy5 (RM4-5), anti-FoxP3 eF660 (FJK-16s), anti-IgD eF450 (11-26c), anti-IgG1 PerCP-eF710 (M1-14D12), Streptavidin APC, anti-ICOS biotin (C398.4A), and anti-PD-L2 biotin (TY25). The following antibodies were purchased from BioLegend, San Diego, California: anti-His Tag purified (J099B12), anti-PD-1 PE-Cy7 (RMP1-30), anti-rabbit IgG Dylight 649 (polyclonal), anti-IL10 A647 (JES5-16E3), anti-CD4 A647 (RM4-5), and anti-CD4 A700 (RM4-5).

3.4.3 MOG production and purification

mMOG_{tag} and haMOG_{tag} proteins were produced and purified as described in Chapter 2. The final equimolar concentrations were 5 mg/mL for mMOG_{tag} and 5.394 mg/mL for haMOG_{tag} with no detectable impurities as determined by SDS-PAGE.

3.4.4 Adoptive transfer of B and T cells and immunization

Naïve Ag-specific T cells were isolated from RFP⁺ 2D2 and OTII mice and naïve Ag-specific B cells were isolated from GFP⁺ IgH^{MOG} and B1-8 Jκ^{-/-} mice as previously described (78). Briefly, LNs and spleens of RFP⁺ Ag-specific T cell and GFP⁺ Ag-specific B cell mice were dissociated and B and T cells were isolated using EasySep Negative selection Mouse B and T cell Enrichment Kits (StemCell Technologies, Vancouver, Canada). Unless otherwise stated, 5×10^5 RFP⁺ T cells and either 1×10^6 GFP⁺ B1-8 Jκ^{-/-} or 5×10^6 GFP⁺ IgH^{MOG} B cells (to account for the fact that only 20% are MOG-specific (240)) were transferred i.v into C57Bl/6 or SMARTA recipients 2d prior

to immunization. In experiments using CellTrace Yellow (ThermoFisher), 5×10^6 B cells were labelled according to the manufacturer's protocol prior to transfer. Mice were immunized in the footpad with equimolar amounts of the given Ag (125 μ g mMOG_{tag}, 175 μ g NPOVA, 125 μ g NPMOG_{tag} (both at a 1:25 protein:NP ratio), 135 μ g haMOG_{tag}) in CFA (of note, unless otherwise stated mice were not injected with PTX, in the scenario where PTX is used, 250 ng were injected on days 0 and 2 post-immunization). Unless otherwise stated, draining popliteal LNs were harvested at the indicated time points for analysis. In experiments using BrdU, 1.5 mg of BrdU was injected i.p at the specified time points.

3.4.5 Flow cytometry

Draining popliteal LNs were harvested from mice for flow cytometry analysis as previously described (240). Briefly, LN cell suspensions were stained with A647 conjugated mMOG_{tag} (conjugated using Alexa Fluor 647 antibody labelling kit, ThermoFisher) or NP₃₀PE (Biosearch Technologies) then blocked with an anti-Fc γ receptor, CD16/32 2.4G2 (BD biosciences), in PBS containing 2% FBS before further incubation with the indicated antibodies. Dead cells were excluded by staining with either the Fixable Viability Dye eFluor506 (eBioscience), propidium iodide (Thermoscientific), or 7-AAD (Biolegend). Flow cytometry was performed on a BD Immunocytometry Systems LSRII cytometer and analyzed with FlowJo software (Tree Star, Ashland, Oregon). For cytokine staining, 2×10^6 freshly isolated cells were stimulated with cell activation cocktail with brefeldin A (Biolegend) for 4 hrs at 37°C then stained as listed above. For intracellular stains of IL-10, FoxP3 or Bcl6, cells were fixed and permeabilized with Cytofix / Cytoperm solution (BD Bioscience) after cell surface staining. Fixed cells were then intracellularly stained for IL-10, FoxP3, and Bcl6 at 4°C overnight. For BrdU staining, cells were fixed in 2% PFA then permeabilized in 0.1% Tween 20 for two nights at 4°C. The DNA within the fixed cells was degraded using DNase I (Sigma-Aldrich, St. Louis, Missouri) then stained with anti-BrdU antibody. Cell sorting was performed using a BD FACS ARIAIII where cells were sorted into 100% FBS.

3.4.6 Immunofluorescent histology

Tissues were prepared for histology as previously described (240). Briefly, whole popliteal LNs were fixed in periodate–lysine–paraformaldehyde (PLP), subsequently passed through sucrose gradients to protect from freezing artifacts and then frozen in OCT (TissueTek, Torrance, California) media. Serial cryostat sections (7 µm) were blocked in PBS containing 1% Bovine Serum Albumin, 0.1% Tween-20 and 10% rat serum before proceeding with staining. Sections were mounted with ProLong Gold Antifade Reagent (Invitrogen, Carlsbad, California). Tiled images of whole LN sections (20×) were imaged using DM5500B fluorescence microscope (Leica, Wetzlar, Germany).

3.4.7 Digital Droplet PCR (ddPCR)

T follicular helper and naïve T cells were sorted by flow and RNA was extracted from cells using a RNeasy Plus Micro Kit (QIAGEN, Hilden, Germany) and immediately converted into cDNA using a Superscript VILO cDNA Synthesis Kit (Invitrogen).

ddPCR reactions were set up using ddPCR EvaGreen 2x Supermix (Bio-Rad, Hercules, California) and the following primers: IL-4 Sense – 5'

AGATGGATGTGCCAAACGTCCTCA 3', IL-4 Antisense – 5'

AATATGCGAAGCACCTTGGAAGCC 3', IL-10 Sense – 5'

GGTTGCCAAGCCTTATCGGA 3', IL-10 Antisense – 5'

ACCTGCTCCACTGCCTTGCT 3', IL-21 Sense – 5'

TGAAAGCCTGTGGAAGTGCAAACC 3', IL-21 Antisense – 5'

AGCAGATTCATCACAGGACACCCA 3', CD40L Sense – 5'

GTGAGGAGATGAGAAGGCAA 3', CD40L Antisense – 5'

CACTGTAGAACGGATGCTGC 3', ICOS Sense – 5' TGACCCACCTCCTTTTCAAG

3', ICOS Antisense – 5' TTAGGGTCATGCACACTGGA 3', PD-1 Sense – 5'

CGTCCCTCAGTCAAGAGGAG 3', PD-1 Antisense – 5'

GTCCCTAGAAGTGCCCAACA 3', CD28 Sense – 5' TGACACTCAGGCTGCTGTTC

3', CD28 Antisense – 5' TTCCTTTGCGAGAAGGTTGT 3', CTLA4 Sense – 5'

GCTTCCTAGATTACCCCTTCTGC 3', CTLA4 Antisense – 5'

CGGGCATGGTTCTGGATCA 3', FoxP3 Sense – 5'

CCCAGGAAAGACAGCAACCTT 3', FoxP3 Antisense – 5'

TTCTCACAACCAGGCCACTTG 3'. ddPCR reactions were run on a QX200 Droplet Digital PCR System (Bio-Rad) and analyzed using QuantaSoft software (Bio-Rad). Gene expression was normalized to the number of sorted cells and expressed as mRNA copies per cell.

3.4.8 ELISpots and ELISA

96-well plates were coated overnight at 4°C with 0.5 µg NPOVA, NPMOG_{tag}, or mMOG_{tag}. Wells were blocked with 1% (wt/vol) BSA in PBS, then incubated with serial diluted bone marrow or lymph node cells at 37°C in 5% CO₂. Spots were detected using a goat alkaline phosphatase-conjugated anti-mouse IgM or IgG antibody (MABTECH, Nacka Strand, Sweden) and 5-bromo-4-chloro-3-indolyl-phosphate substrate (Sigma-Aldrich) and counted under a Leica M80 dissection microscope. To detect circulating antibodies using an ELISA, 96-well plates were incubated with Ag and blocked with BSA as written above. Blood was extracted from mice using a cardiac puncture and spun at 4500 x g for 15 minutes. Serum plasma was extracted and incubated with the 96-well plate for one hour at room temperature. Plates were incubated with anti-IgM or IgG antibodies and then the alkaline phosphatase yellow (pNPP; Sigma-Aldrich) substrate. OD405 was measured using an Eon microplate spectrophotometer (BioTek, Winooski, Vermont).

3.4.9 Image and statistical analyses

Histology images were analyzed using ImageJ software to quantify the density of B and T cells in germinal centers (Bcl6⁺ IgD⁻) and B cell follicles (IgD⁺ cells excluding five cells deep worth of the outermost perimeter of the B cell follicle near the capsule). PRISM software (GraphPad Software, La Jolla, California) was used to analyze flow cytometry and histology data. For statistical comparisons, a Student's T-test was used for single comparisons and a one-way ANOVA followed by a T test with Bonferroni correction was used for multiple comparisons. Additionally, data sets were also analyzed using non-parametric a Mann-Whitney test for single comparisons and a Kruskal-Wallis test with a Dunn's correction for multiple comparisons. Unless otherwise stated, the results were the same with each test. Outliers were identified using ROUT method.

Chapter 4

4 Reporters for *in vivo* and *in vitro* monitoring of NF κ B and NFAT signaling

The development of a high-affinity class-switched B cell response is absolutely dependent on cognate interactions between B and T cells. Signals are exchanged between B and T cells during these interactions that inform B cell fate choices however, the precise timing of signal exchange has never been established. This is important as cognate interactions can differ substantially in duration over the course of the immune response and between individual B-T pairings making it difficult to establish how long and short B-T interactions may uniquely contribute to the immune response. Studying the relationship between intracellular signaling and interaction duration is complicated by the lack of tools available for visualizing intracellular signaling in individual cells in living tissue. To address this issue, I sought to generate reporters that were capable of visualizing signaling by monitoring the activity of two key transcription factors: p65 (NF κ B) and NFAT1. These proteins integrate signaling through multiple different receptors involved with B and T cell activation. To monitor p65 and NFAT1 activity, two fluorescent reporters were constructed using a histone 2 B-GFP fusion protein, which will label the nuclei of cells, coupled to the expression of the mCherry fluorescent protein linked to the N-terminus of the p65 or NFAT1 proteins. *In vitro* stimulation of macrophage cell lines transfected with these reporters revealed that mCherry labelled p65 or NFAT1 were excluded from the nucleus in the steady state but could be induced to translocate into the nucleus when stimulated. Using the CRISPR/Cas9 genomic editing system, these reporters were adapted for insertion of the mCherry labelled p65 or NFAT1 constructs into the *NFAT1* or *p65* loci to allow expression from their endogenous loci. Although I was not successful in editing the *p65* locus, initial experiments editing the *NFAT1* locus *in vitro* were successful. However, this was not successfully translated into making reporter mice carrying the reporter. I am now adapting the reporter to be inserted into the *Rosa26* locus and single cell zygote injections will be used to generate a reporter mouse controlled by Cre recombinase expression.

4.1 Introduction

Communication between immune cells is essential in shaping an immune response and can determine if a pathogen infection persists or if it is successfully cleared. A critical component of immunity is the B cell response that is coordinated by communication between B and T cells specific for the same Ag through direct physical interactions that occur at the pre-GC phase and throughout the GC response (78, 206). Interactions between B and T cells are coordinated through cytokines and the engagement of multiple cell surface receptors that initiate intracellular signaling (295). The induction of cellular signaling is responsible for informing cells to become activated, differentiate, or undergo cell death and, thus, determines the output of the immune response. As a result, B and T cell interactions are essential for the duration of a GC response. Yet, the duration of interactions formed between B and T cells varies considerably over the course of the immune response, where pre-GC interactions are longer than those that occur in the GC, and between individual B-T pairings at each time point (78, 106). Indeed, in our lab we have seen at the pre-GC phase, B-T interactions occurring in MOG immunized mice are significantly shorter than those that occur in NPOVA immunized mice (Parham KA *et al.* in progress). Thus, B-T cell interaction length may contribute to the different fate choices seen in these two systems. However, it is difficult to address this hypothesis because we still do not understand the basics of how signaling kinetics and interaction kinetics are related to one another. Additionally, as GC B-T interactions are shorter than pre-GC interactions, it is not clear whether the kinetics of signal exchange change over the course of the response.

Traditional methods of monitoring intracellular signaling, such as western blots, rely on pooling millions of cells and analyzing in bulk and are therefore inappropriate for analyzing individual events amongst a variable pool of cells. Furthermore, fate decisions are made at the single cell level and thus can only be studied by analyzing individual cells (296). Direct imaging of cells during their interactions using two-photon intravital microscopy solves this problem, however this technology requires fluorescent reporters (297). This is problematic as most fluorescent activation reporters currently rely on *de novo* expression of a fluorescent protein driven by a promoter which requires time to

transcribe, translate, and fold the fluorescent protein (298, 299). This results in a delay between the time of signal initiation and the time of visible reporter activity making it impossible to determine the kinetics of activation using transcription-based reporters (298, 299). Commercially available fluorescent Ca^{2+} signaling reporters, that fluoresce when binding to intracellular Ca^{2+} (300), allow real-time visualization of signaling and could address this issue (301). However, these reporters are not retained in cells over long periods of time and can be diluted out of cells as they proliferate making their use impractical in rapidly expanding immune responses (302). Ideally, an activation reporter should continuously provide instantaneous information about cellular signaling.

Designing a reporter that provides real-time signaling information is possible by taking advantage of how immune signaling becomes integrated: through the activation of transcription factors. Signaling cascades initiated at the cell membrane rely on a wide variety of adaptor proteins and signaling enzymes to initiate intracellular signaling. These signaling pathways tend to converge on a much more limited number of common transcription factors. In this way, the signals from various surface receptors can be integrated to refine the signal that is transmitted to the nucleus to alter the expression of specific genes. Nuclear factor of activated T cells and NF κ B are two key transcription factors that are downstream of receptors involved in both B and T cell activation (195, 303). Both are maintained in the cytosol and upon activation translocate into the nucleus where they can initiate gene transcription (196, 304). Thus, by monitoring the cellular location of NF κ B and NFAT, we can obtain real-time evidence of ongoing signaling that is relevant to cellular immune activation.

The NFAT family consists of 5 related proteins where NFAT1, NFAT2, and NFAT4 are expressed in B and T cells (305). Of these, NFAT1 and NFAT2 have considerable overlap in function where deletion of either gene alone leads to subtle changes in B and T cell responses (306-308) and double deletion leads to accelerated differentiation of B cells and the inability of T cells to function (309). As both of NFAT proteins are expressed in and affect B and T cells across an immune response, either could act as a potential reporter of B and T cell activation. Of these two proteins, I

focused on NFAT1 as fusion proteins using NFAT1 have been described previously (310).

The NF κ B family includes 5 proteins: p65, Rel-B, c-Rel, p105/p50, and p100/52 that form homo- or heterodimers in order to be transcriptionally active (304). Only the p65, RelB, and c-Rel proteins have C-terminal transactivation domains that promote transcription whereas the p50 and p52 proteins do not directly promote transcription but rather competitively inhibit NF κ B binding sites and are not associated cellular activation (304). Amongst the NF κ B proteins that have transactivation potential and could act as reporters for activation, the Rel-B gene is only expressed transiently in B cells during the GC response and thus would not act as good reporter of B cell activity (311). In contrast, c-Rel and p65 are both expressed in mature B cells and the GC (312). Thus, either could act as a reporter of activation. However, fusion proteins of p65 have already been described making p65 a more appealing target (313).

Here, I describe the generation of fluorescent reporters based on the NFAT1 and p65 proteins. This was accomplished by making fusion proteins of the NFAT1 and p65 proteins where the N-terminus of each is fused to the mCherry fluorescent protein. The fluorescently tagged reporters were then combined with a nuclear marker, Histone 2 B-GFP (H2B-GFP), for accurate quantification of nuclear versus cytoplasmic localization. These reporters proved to be functional and useful for quantifying intracellular signaling. However, when attempting to generate reporter mice using the CRISPR/Cas9 system by inserting my reporter constructs into the endogenous *p65* or *NFAT1* loci, I was unable to generate any founder mice. Therefore, I have generated a new version of the reporter that has been adapted for insertion into the *Rosa26* locus and will be used to generate an NFAT1 reporter mouse whose expression of the reporter will be under the control of Cre recombinase. Overall, this reporter mouse will extend what is currently possible with intravital two-photon microscopy by allowing us to see signaling in real-time within immune cells *in vivo*.

4.2 Results

4.2.1 Fusion of p65 or NFAT1 to fluorescent proteins generates functional reporters capable of monitoring their nuclear and cytoplasmic localization

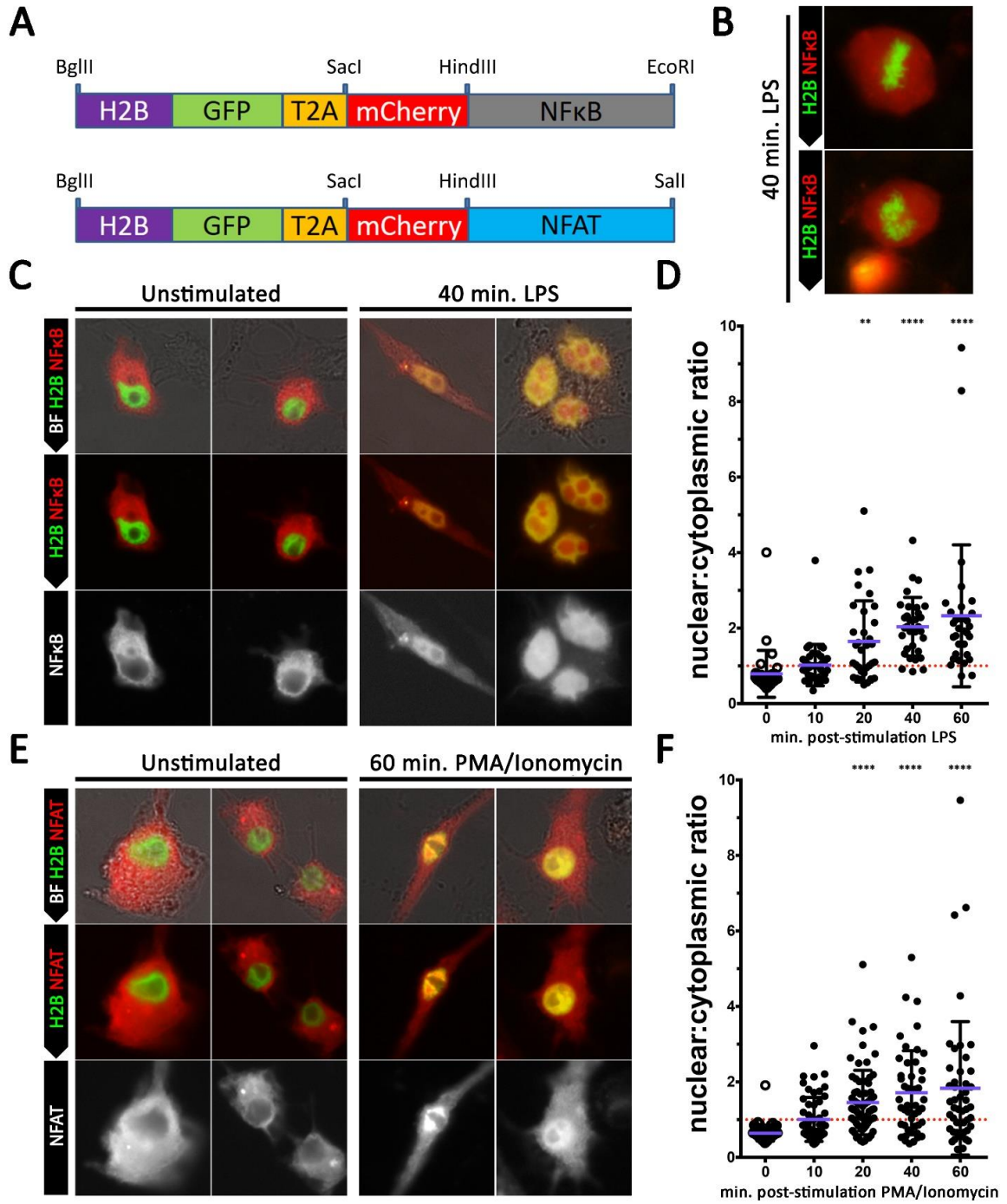
To construct the p65 and NFAT1 reporters, cDNA sequences for mouse *p65* or *NFAT1* were cloned into the pEGFP-N1 vector along with the DNA sequence encoding the mCherry fluorescent protein. The mCherry gene was inserted upstream of the *p65* or *NFAT1* sequences creating N-terminal fusions. To unambiguously determine whether p65 or NFAT1 are in the nucleus, the mCherry fusion proteins were combined with a nuclear marker, histone 2 B (H2B) fused to the N-terminus of GFP (H2B-GFP). By using a nuclear marker, the nucleus can be identified with GFP and the ratio of nuclear vs cytosolic mCherry can be calculated with certainty. As only 1 protein can be expressed from a single mRNA transcript, and the H2B-GFP and mCherry fusion proteins must be expressed as separate proteins, a T2A site was incorporated between into the fusion proteins allowing both proteins to be expressed separately from a single mRNA transcript at a 1:1 ratio (314). Altogether, the reporters were constructed such that the H2B-GFP gene was followed by a T2A site allowing for expression of a second mCherry-p65 fusion protein (H2B-GFP-T2A-mCh-p65) or a mCherry-NFAT1 fusion protein (H2B-GFP-T2A-mCh-NFAT1) as shown in Figure 4.1A.

To determine whether the T2A site separates the two fusion proteins into functional reporters, RAW267.4 macrophages were transfected with either the H2B-GFP-T2A-mCh-p65 or the H2B-GFP-T2A-mCh-NFAT1 vectors. Cells were stimulated with lipopolysaccharide (LPS) (known to induce p65 signaling (315)) or phorbol 12-myristate 13-acetate (PMA) + ionomycin (known to induce NFAT signaling (316)), respectively. Cells were then fixed at 0, 10, 20, 40, or 60 min time intervals and imaged by fluorescent microscopy. For both the p65 and NFAT1 reporters, the T2A site effectively split the H2B-GFP fusion protein from the mCherry fusion proteins as seen by the separation of green and red fluorescence in unstimulated cells (Figure 4.1C and 4.1E). In addition to the H2B-GFP protein properly localizing to the nucleus, the H2B-GFP protein was seen to effectively monitor proliferation through the visualization of chromosomes condensing

during mitosis, a feature and advantage of H2B-GFP over other nuclear markers (317) further confirming that this protein was functional (Figure 4.1B). The p65 and NFAT1 fusion proteins were also seen to be functional as the stimulation of RAW267.4 macrophages resulted in p65 and NFAT1 translocating from the cytoplasm to nucleus as seen by GFP and mCherry co-localization (Figure 4.1C and 4.1E) and a shift in the ratio of mCherry in the cytoplasm to mCherry in the nucleus (Figure 4.1D and 4.1F). Together, these results confirm that the p65 and NFAT1 reporters are functional and capable of providing quantitative information on cytoplasmic to nuclear translocations.

Figure 4.1. Reporters capable of monitoring the cytoplasmic and nuclear localization of the p65 and NFAT1 proteins.

(A) Schematics of the H2B-GFP-T2A-mCh-p65 or NFAT1 constructs that were inserted into the pEGFP-N1 vector using the indicated restriction sites. (B-F) RAW macrophage were transfected with H2B-GFP-T2A-mCherry-p65 then stimulated with 1 $\mu\text{g/ml}$ LPS (B-D) or transfected with H2B-GFP-T2A-mCherry-NFAT1 then stimulated with 1 $\mu\text{g/ml}$ ionomycin and 0.25 $\mu\text{g/ml}$ PMA (E and F) for the indicated periods of time. Cells were then fixed and imaged in bright field, GFP, and mCherry channels. (B) Shown are two images of RAW macrophage undergoing proliferation as seen by the condensation of chromosomes visualized by H2B-GFP. (C and E) Representative images of unstimulated and stimulated RAW macrophage are shown. (D and F) Quantification of average mCherry MFI in the nucleus (defined by GFP fluorescence) over the average mCherry MFI in the cytoplasm where each data point represents a single cell. Data shown is representative of three individual experiments. For panel D: n=31 for time 0, n=38 for time 10, n=30 for time 20, n=22 for time 40, n=28 for time 60. For panel F: n=71 for time 0, n=66 for time 10, n=97 for time 20, n=55 for time 40, n=57 for time 60. **p<0.01, ****p<0.0001. A one-way ANOVA comparing time 0 to the other time points was used for multiple comparisons.



4.2.2 Using the CRISPR/Cas9 system to generate a reporter knock-in at the *p65* locus *in vitro*

The purpose for constructing these reporters is to visually monitor signaling within primary B and T cells during immune responses. However, the forms described above are based upon overexpression of the p65 and NFAT1 proteins. This is problematic as the overexpression of p65 protein is known to affect the biology of cells (318, 319). To avoid problems associated with overexpression, the p65 reporter was adapted to insert the H2B-GFP-T2A-mCh construct into the genome of mouse cells ahead of the *p65* gene in the *p65* locus to be expressed off of the endogenous promoter. To insert DNA into the genome in a site directed fashion, arms of homology that consist of DNA segments that are homologous to the DNA in either direction of the insertion site direct the homologous recombination pathway to insert the DNA contained between the arms of homology into the genome (320). Based on this, a DNA donor vector containing two ~1 kbp arms of homology corresponding to the DNA sequence of the *p65* locus upstream and downstream of the ATG start codon was constructed. In between the two arms of homology, the H2B-GFP-T2A-mCh reporter was inserted upstream of the *p65* gene resulting in a fusion of the fluorescent reporters to the N-terminus of the p65 protein (Figure 4.2A).

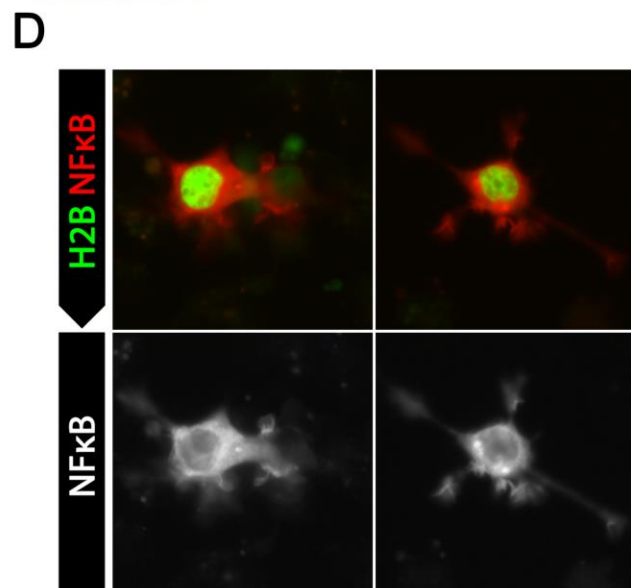
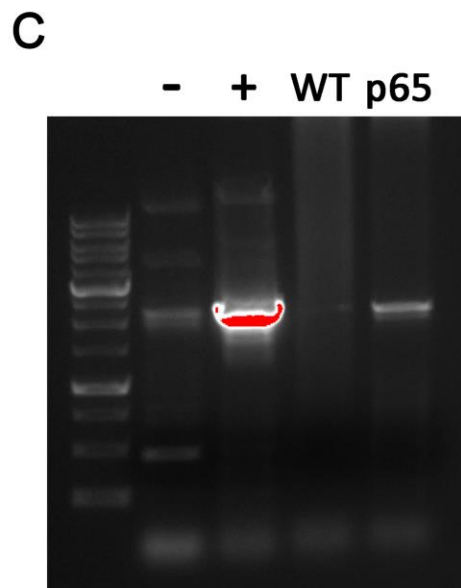
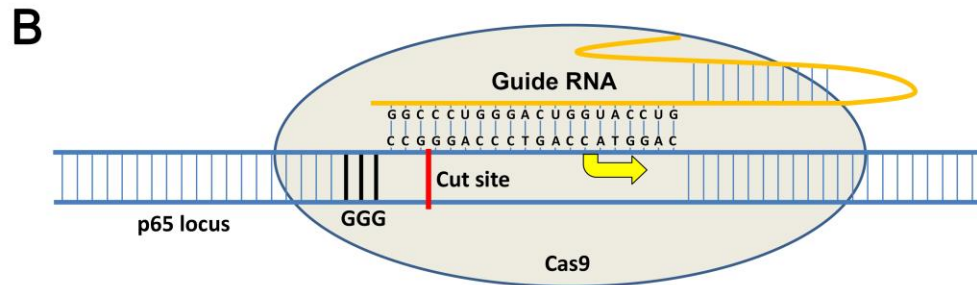
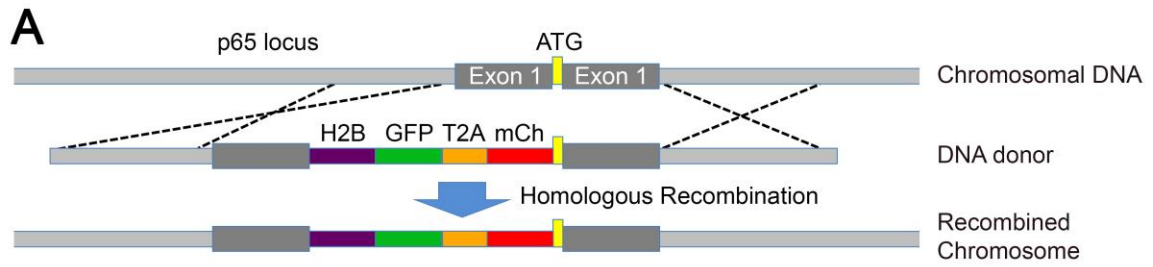
As DNA donor vectors do not incorporate into DNA in a site directed fashion unless the homologous recombination DNA repair pathway is induced, the CRISPR/Cas9 system was used to create targeted DNA damage at the *p65* locus to enhance incorporation efficiency. The Cas9 enzyme is a RNA guided DNA endonuclease that can be used to induce double stranded DNA breaks at any site in the genome that has been targeted by a RNA guide (321). As homologous recombination is one of the pathways used to repair double stranded DNA damage (322), the CRISPR/Cas9 system can be used to promote recombination of a DNA donor vector into the genome. To target the *p65* locus using the CRISPR/Cas9 system, a guide RNA was designed based on available tools (323) (Figure 4.2B) and incorporated into the pX330 vector that expresses the Cas9 enzyme as well as the associated guide RNA.

To test the efficacy of the CRISPR/Cas9 system to facilitate incorporation of the *p65* DNA donor vector into the genome of cells, J774 macrophages were transfected with the *p65* DNA donor vector along with its associated pX330 vector. Two days post-transfection, cells were either fixed for fluorescent microscopy or their genomic DNA was isolated for genotyping. Insertion of the p65 reporter in the *p65* locus was not detected in wild type J774 macrophage however, insertion of the reporter was detected in transfected cells although this was not consistent across repeat experiments (no band was observed in 2 of 4 experiments) (Figure 4.2C).

By microscopy, a small proportion of observed cells were fluorescent, indication that they had incorporated the p65 donor vector (Figure 4.2D). Due to the low incorporation rate, further characterization of the functionality of the p65 reporter was not possible. Although not shown here, several guide RNAs were tested. However, none of these guide RNAs proved to be efficient in facilitating insertion into the *p65* locus. Thus, although the p65 reporter can insert into the *p65* locus, it does not occur efficiently.

Figure 4.2. CRISPR/Cas9-mediated editing of the *p65* locus.

(A) Targeting strategy for inserting the H2B-GFP-T2A-mCherry construct into exon 1 of the *p65* locus. Shown is the DNA donor vector consisting of two ~1 kbp arms of homology, corresponding to the sequence around the ATG start codon in the *p65* locus, surrounding the H2B-GFP-T2A-mCherry DNA construct. Upon recombination with the *p65* locus, transcription begins at a new start codon at the start of the H2B gene and continues through to the *p65* gene. (B) Diagram showing the CRISPR/Cas9 cut site. The guide RNA is shown in orange including the nucleotide sequence used to target the *p65* locus, the location of the double stranded break is shown in red, the site of translation initiation is shown in yellow, and in black is the protospacer associated motif that is required CRISPR mediated cutting (324). (C and D) J774 macrophage were transfected with the *p65* DNA donor vector and a pX330 vector containing the Cas9 gene and sequence encoding the guide RNA specific for the *p65* locus. Two days post-transfection, DNA was isolated to detect incorporation of the *p65* vector into the *p65* locus by PCR (C), or cells were fixed and imaged in the GFP and mCherry channels (D). (C) To detect site-specific incorporation into the *p65* locus two primers were used, one specific for the *p65* locus and the other specific for the mCherry gene. The negative control is pure *p65* donor vector DNA, the positive control is pure *p65* donor vector DNA with ~2 kbp arms of homology, WT is untransfected J774 macrophage, and *p65* is J774 macrophage transfected with the *p65* donor vector and pX330 vector (Representative of 2 of 4 experiments).



4.2.3 The CRISPR/Cas9 system can be used to generate a reporter knock-in at the *NFAT1* locus *in vitro*

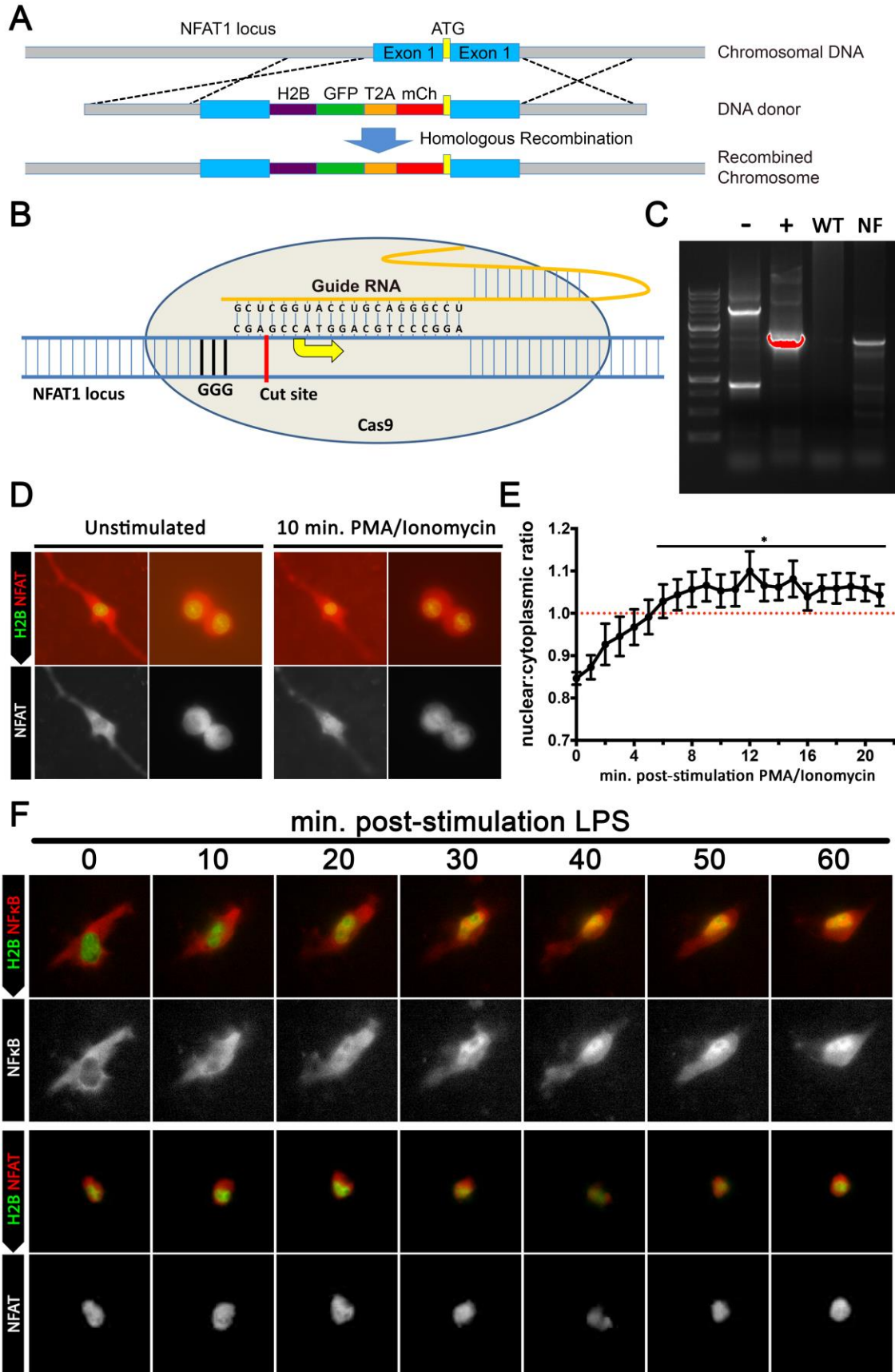
Similar to the approach described above, the NFAT1 reporter was adapted for incorporation into the *NFAT1* locus such that ~1 kbp arms of homology derived from the sequence surrounding the ATG start codon in the *NFAT1* locus were cloned around the H2B-GFP-T2A-mCh reporter (Figure 4.3A). Additionally, a guide RNA was designed to target the *NFAT1* locus to facilitate homologous recombination and was cloned into the pX330 vector (Figure 4.3B).

To test whether the CRISPR/Cas9 system can facilitate insertion of the NFAT1 reporter into the *NFAT1* locus, J774 macrophages were transfected with NFAT1 DNA donor vector and associated pX330 vector and cultured for two days. After two days, the cells were processed for genotyping or fixed for microscopy. Incorporation of the DNA donor vector into transfected cells was observed by genotyping as a 2 kbp band was present in transfected J774 macrophage but not wild type controls (Figure 4.3C). Additionally, by microscopy many cells were observed to be fluorescent and this was above background levels of incorporation in cells transfected with donor alone (data not shown).

To determine whether the reporter remains functional when expressed from the endogenous *NFAT1* promoter, J774 macrophages were transfected as indicated above. Two days post-transfection, the cells were imaged over time in a live cell fluorescent microscope after the addition of PMA and ionomycin. At time 0, NFAT1 reporter cells had the proper distribution of H2B-GFP in the nucleus and mCh-NFAT1 in the cytoplasm (Figure 4.3D). Over time mCh-NFAT1 began to accumulate in the nucleus resulting in a shift of mCherry fluorescence in the cytoplasm to the nucleus confirming that the knock-in at the endogenous locus was still responsive (Figure 4.3D and 4.3E). Of note, nuclear accumulation did not occur unless the cells were stimulated with ionomycin as unstimulated or LPS stimulation did not result in nuclear accumulation of NFAT1 (Figure 4.3F, bottom) using a protocol that induced robust p65 translocation (Figure 4.3F, top).

Figure 4.3. CRISPR/Cas9 mediated editing of the *NFAT1* locus

(A) Targeting strategy for inserting the H2B-GFP-T2A-mCherry construct into exon 1 of the *NFAT1* locus. Shown is the DNA donor vector consisting of two ~1 kbp arms of homology, corresponding to the sequence around the ATG start codon in the *NFAT1* locus, surrounds the H2B-GFP-T2A-mCherry DNA construct. Upon recombination with *NFAT1* locus, transcription begins at a new start codon at the start of the H2B gene and continues through to the *NFAT1* gene. (B) Diagram showing the CRISPR/Cas9 cut site. The guide RNA shown in orange is used to target the *NFAT1* locus, the location of the double stranded break is shown in red, the site of translation initiation is shown in yellow, and in black is the protospacer associated motif. (C-E) J774 macrophage were transfected with the *NFAT1* DNA donor vector and a pX330 vector containing the Cas9 gene and sequence for the guide RNA for the *NFAT1* locus. Two days post-transfection, DNA was isolated to detect incorporation of the *NFAT1* vector by PCR (C), or live cells were imaged in the GFP and mCherry channels (D and E). (C) To detect site-specific incorporation into the *NFAT1* locus two primers were used, one specific for the *NFAT1* locus and the other specific for the mCherry gene. The negative control is pure *NFAT1* donor vector DNA, the positive control is pure *NFAT1* donor vector DNA with ~2 kbp arms of homology, WT is untransfected J774 macrophage, and *NFAT1* is J774 macrophage transfected with the *NFAT1* donor vector and pX330 vector (representative of 3 of 4 experiments). (D and E) Transfected cells were stimulated with 1 $\mu\text{g/ml}$ ionomycin and 0.25 $\mu\text{g/ml}$ PMA then imaged once every minute for 21 mins. (D) GFP and mCherry fluorescence is shown at the 10 min time point. (E) Quantification of average mCherry MFI in the nucleus (defined by GFP fluorescence) over the average mCherry MFI in the cytoplasm at each time point is shown. Data is from a combination of two independent experiments. A one-way ANOVA was used to compare values at each time point to time 0, errors bars are SEM, $n=7$, $*p<0.05$. (F) J774 macrophage were transfected with pEGFP-N1 H2B-GFP-T2A-mCh-p65 (top panel) or *NFAT1* DNA donor vector and a pX330 vector containing the Cas9 gene and sequence for the guide RNA for the *NFAT1* locus (bottom panel). Two days post-transfection, live cells were imaged in the GFP and mCherry channels after stimulation with 1 $\mu\text{g/ml}$ LPS over the course of an hour (D and E). Representative cells are shown for two individual experiments.



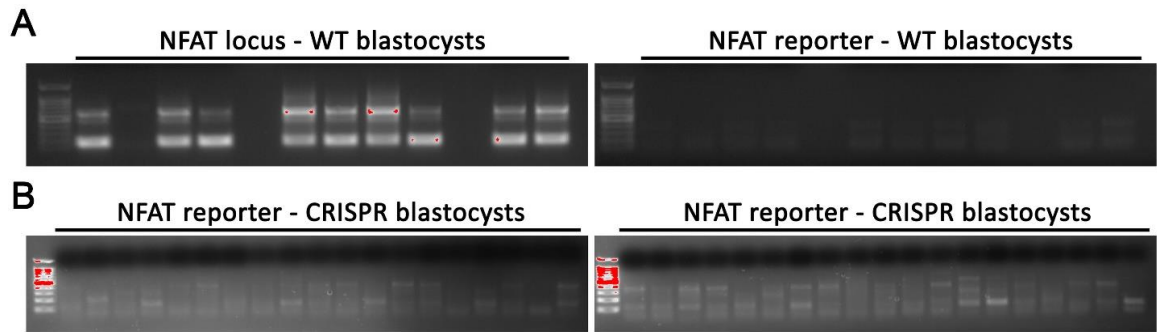
4.2.4 Generating knock-in mice using the CRISPR/Cas9 system

Having confirmed that the *NFAT1* locus can be modified to generate a functional reporter, I sought to use the CRISPR/Cas9 system to genetically modify mouse zygotes, a prerequisite to making a reporter mouse. To determine whether mouse zygotes could be edited to incorporate the NFAT1 reporter, single C57Bl/6 mouse zygotes were given nuclear microinjections with guide RNA, DNA donor vector, and Cas9 mRNA and grown *in vitro* into blastocysts. Individual blastocysts were then processed for genotyping.

The PCR protocol was first validated to be capable of detecting small amounts of DNA by detecting the *NFAT1* locus in wild type blastocysts and confirmed not to produce false positives when using primers specific for the NFAT1 reporter (Figure 4.4A). Then, 65 viable blastocysts were genotyped as an initial measure of incorporation frequency. Unfortunately, there was no evidence of incorporation of the reporter in any of the blastocysts, suggesting that this approach to insert a large segment of DNA is not reliable enough to proceed with generating mice (Figure 4.4B). Indeed, in a second attempt where live blastocysts were implanted to produce pups, no positive mice were identified by genotyping (data not shown).

Figure 4.4. Insertion of the NFAT1 reporter into C57Bl/6 blastocysts.

(A) A protocol for detecting DNA from blastocysts was tested on 10 wild type C57Bl/6 blastocysts using a nested PCR approach. Primers specific for either the NFAT1 locus (left) or specific for a site specific incorporation of our reporter (right) were used. (B) Incorporation of the NFAT1 reporter into blastocysts injected with the NFAT1 CRISPR components was assessed using PCR (38 of 65 shown).



4.2.5 An overexpression-based NFAT1 reporter

As inserting the NFAT1 reporter into the endogenous locus was not viable, I attempted an alternative approach where a transcriptionally inactive reporter, thus unable to affect the biology of the cell, would be overexpressed in cells. This was accomplished by taking advantage of the structure of the NFAT1 protein. The NFAT1 protein has an N-terminal transactivation domain followed by a regulatory domain that contains the nuclear localization sequence as well as phosphorylation sites that regulate the availability of the nuclear localization sequence (325). Following this is the Rel-homology domain that is responsible for DNA binding and the final domain is the C-terminal domain. Of key significance, the regulatory domain of NFAT1 is entirely separate from its DNA binding domain. Thus, it is possible to express the regulatory domain of NFAT1, which is responsible for dictating NFAT1 import and export from the nucleus, without its DNA binding domain that would be required for this protein to act as a transcription factor.

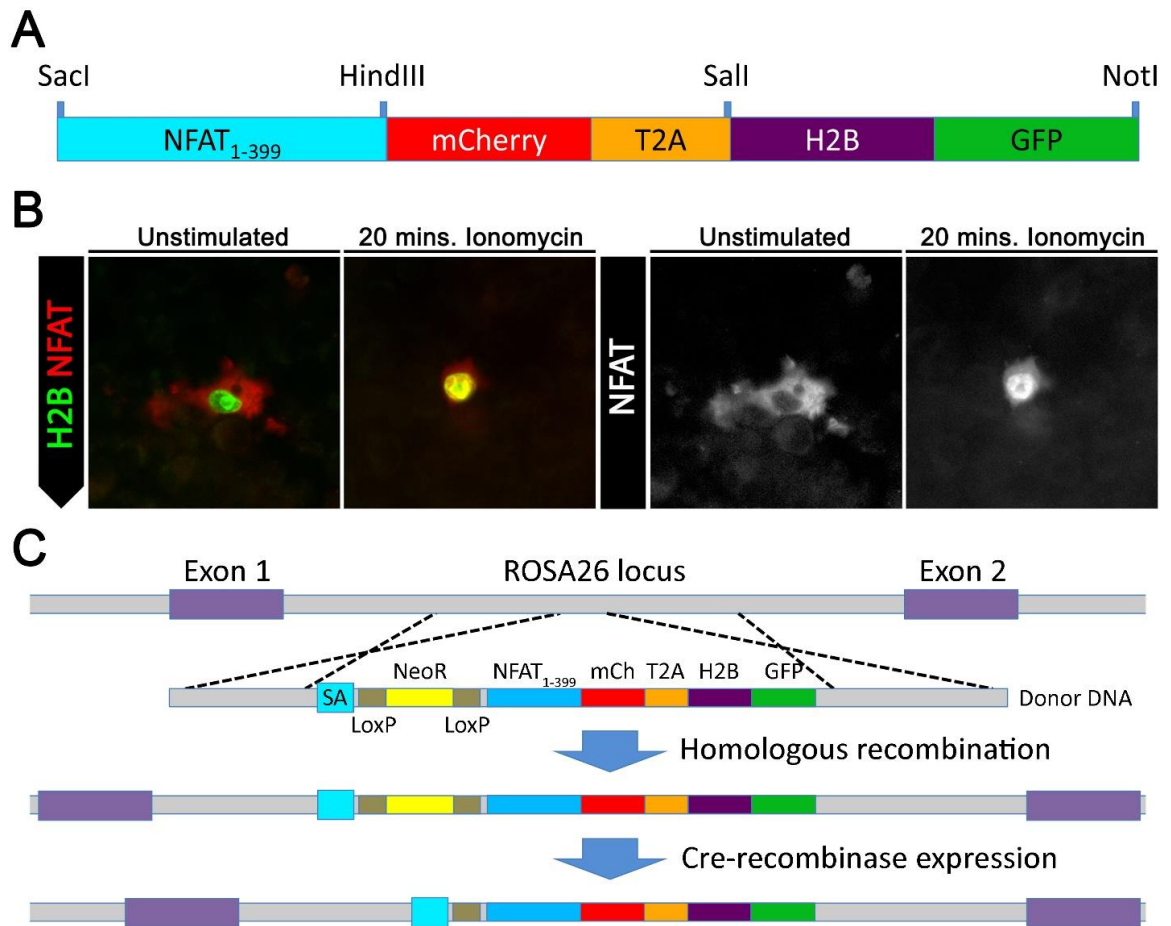
To construct this reporter, amino acids 1-399 from NFAT1, corresponding to the N-terminal transactivation domain and regulatory domains, were used in place of the full length NFAT1 protein. The *NFAT1*₁₋₃₉₉ gene was then combined with mCherry, the H2B-GFP gene, and T2A site in a pEGFP-N1 vector (Figure 4.5A). To test whether this form of the reporter was functional, J774 macrophages were transfected with the NFAT1₁₋₃₉₉ reporter and then stimulated with PMA and ionomycin for 20 mins prior to fixation for fluorescent microscopy. Transfected cells that were unstimulated had no evidence of nuclear accumulation of the NFAT1₁₋₃₉₉ reporter whereas the reporter accumulated in the nucleus of stimulated cells confirming the reporter was functional (Figure 4.5B).

To adapt the reporter for insertion into the mouse genome, I took advantage of a commonly targeted locus known as the *Rosa26* locus. This locus constitutively expresses a non-coding RNA, with no known function, uniformly across the body (326). Genes of interest can be expressed from this locus by inserting them into the intron between exon 1 and 2 of this locus along with a gene trap (327). A gene trap involves the usage of a splice acceptor site to ‘steal’ the splice donor site from the previous exon, preventing the second exon from being spliced into the mRNA transcript, resulting in your gene of

interest becoming the next exon. To take advantage of this system, the NFAT₁₋₃₉₉ reporter was inserted into the ROSA26TV vector, a plasmid that already contains the splice acceptor site and arms of homology required for insertion into the *Rosa26* locus (Figure 4.5C). Additionally, this plasmid also has a neomycin resistance gene flanked by loxP sites ahead of the NFAT1 reporter such that expression through the construct will result in the production of the neomycin resistance protein before production of the NFAT1 reporter. This organization of genes is useful as the expression of the NFAT1 reporter is inducible in this system through the expression Cre recombinase in cells. When Cre recombinase is expressed, it will use the LoxP sites to remove the neomycin resistance gene (328) resulting in the first start codon to then reside at the start of the NFAT1 reporter construct. Thus, this construct not only expresses the NFAT1 reporter, but can do so in a cell-specific manner depending on Cre recombinase expression.

Figure 4.5. Construction of an NFAT1 reporter that can be overexpressed.

(A) Schematic of the NFAT1₁₋₃₉₉-mCherry-T2A-H2B-GFP construct that was inserted into the pEGFP-N1 vector using the indicated restriction sites. (B) J774 macrophages were transfected with NFAT1₁₋₃₉₉-mCherry-T2A-H2B-GFP and then stimulated with PMA + ionomycin for 20 mins prior to fixation for fluorescent microscopy. Cells were imaged in the GFP and mCherry channels. Shown are representative images. (C) Shown is a diagram outlining the targeting strategy for inserting the NFAT1₁₋₃₉₉-mCherry-T2A-H2B-GFP construct into the *Rosa26* locus. A donor vector consisting of two arms of homology, corresponding to the intron sequence in between exon 1 and 2 of the *Rosa26* locus, surrounds the DNA construct. The DNA construct contains a splice acceptor (SA) site, that upon recombination into the locus, interrupts splicing between exon 1 and 2 of the *Rosa26* locus and instead leads to the reporter construct being incorporated into the mRNA transcript. Ahead of the NFAT1 reporter, a neomycin resistance gene flanked by LoxP sites is expressed and prevents expression of the NFAT1 reporter. Using Cre-LoxP mediated recombination, the neomycin gene can be removed allowing expression of the NFAT1 reporter.



4.3 Discussion

Our understanding of how intracellular signaling induced through B and T cell interactions contributes to B cell fate choices is limited by the inability to visualize signaling as it occurs *in vivo*. Here, I address this issue by constructing fluorescent reporters capable of monitoring NF κ B and NFAT signaling *in vivo*, in real-time, and in individual cells using reporters compatible with intravital imaging. Despite the reporters being functional, I was unable to generate reporter mice using a knock-in approach to modify the *p65* and *NFAT1* loci. Nonetheless, insertion into the *Rosa26* locus holds potential for generating an NFAT1 reporter mouse. This will be accomplished through either conventional knock-in methods (320) or aided using the CRISPR/Cas9 system (329).

As the generation of new mouse strains is never guaranteed, additional options can be explored in the case where a mouse cannot be made. This is easier for the NFAT1 reporter as I have made a form of this reporter that can be overexpressed in cells. Indeed, the use of a retroviral vector to introduce a transcriptionally inactive NFAT1 reporter into cells has already been used with success (310, 330). One major limitation to retroviral vectors however, is that they do not readily transduce quiescent cells such as naïve B and T cells (310, 330, 331). This problem can be overcome through *in vitro* activation of cells and transducing the cells as they begin to proliferate. However, in the context of studying foreign or autoAg driven GCs, *in vitro* activation of B and T cells would pose several problems: First, it is not clear whether *in vitro* activated cells would behave similarly to cells activated exclusively *in vivo*. Second, *in vitro* activation may allow autoreactive B and T cells to subvert regulatory pathways that would normally suppress their activation (332, 333). Lastly, although *in vitro* activation of T cells is well established (334), *in vitro* expansion of B cells is relatively new and is likely to affect the phenotype of the cultured B cells (335). Thus, to study naive B and T cell responses, a reporter mouse is needed and may require the use of methods that are less than ideal for generating a transgenic mouse. Transgenic mice can be generated by injecting zygotes with linear DNA that incorporates at random into the genome where the linear DNA contains your gene of interest as well as a promoter to drive its expression (336). This method is quite robust for generating

founder mice, although, it suffers from several problems: 1st, variable expression of the transgene; 2nd, loss or gain of function mutations in genes already in the genome as a result of transgene insertion; and 3rd, insertion of multiple copies of the transgene. The combination of these problems makes it difficult to be confident that the founder mice generated are truly correct as these factors could act as confounding factors in interpreting the data acquired by studies using mice with incorrect transgenes. Thus, although there are alternative methods available for generating a useable NFAT1 reporter, these methods have significant limitations.

Ideally these studies would be conducted using both the NFAT1 and p65 reporters as transcription factors do not work alone. Instead, they work in coordination with other transcription factors influencing their activity (337) and the NFAT1 and p65 proteins are no exception to this (338-340). For example, NFAT1 induces an anergic transcriptional program unless it is complemented by other transcription factors (341, 342). Additionally, as particular transcription factors are preferentially activated by certain pathways (see Chapter 1.8.2), the usage of multiple reporters of activation would integrate a greater range of signaling allowing us to more confidently determine whether signals are being exchanged. I was able to construct a reporter of NFAT1 activity by taking advantage of the monomeric nature and structure of the NFAT1 protein (325) to express a transcriptionally inactive reporter. A similar approach is not possible with p65 or the other NF κ B proteins as the same domain is responsible for regulating cytoplasmic:nuclear shuttling and DNA binding making these functions inseparable (343). Indeed, even if the p65 protein was mutated to abolish its capacity to bind DNA and act as a transcription factor (344), the transgene would create a dominant negative mutation. Cytoplasmic and nuclear shuttling of NF κ B proteins requires them to form dimers (304), and given that NF κ B proteins form homo- and heterodimers, inactive forms of p65 would inactivate any other NF κ B proteins they dimerized with. Thus, a reporter of NF κ B activity requires modification of the endogenous locus.

The major factor limiting the generation of a p65 reporter mouse was the low incorporation rate of my p65 donor DNA. In the time since we had completed the injections, the field of genomic modifications using the CRISPR/Cas9 system has moved

forward generating several technologies that could have aided my approach. Although I will not provide an exhaustive list of new methods, the following represent easily adaptable methods that could be employed in the future. The first is the use of single stranded DNA donor vectors over double stranded DNA. For some applications, single stranded DNA donor vectors have been able to achieve high levels of incorporation relative to double stranded DNA vectors (345). Second, the stability of the guide RNA can also be limiting (321). The stability of RNAs can be increased by incorporating chemically modified nucleotides at the ends of the RNA molecules to limit their degradation and can have substantial effects on incorporation rates (346). Lastly, inhibition of the non-homologous end joining pathway can promote usage of the homologous recombination pathway. In this study, I used the SCR7 inhibitor of non-homologous end joining (347). However, additional small inhibitors of non-homologous end joining have been identified and could be used to further promote homologous recombination over non-homologous recombination (348). Thus, there are several methods that could be used in the future to try to improve incorporation into the *p65* locus.

The generation of these reporters is of great interest to us as this will allow us to answer many basic questions about the GC response. Throughout the GC response B and T cells form interactions that are essential for GC induction and maintenance (78, 204). We know that individual interactions can differ substantially in length and this has been associated with B cells making different fate choices (112, 117, 161). Nonetheless, we still do not understand at a molecular level what makes a long and short interaction different. It is for example, unclear whether a short interaction represents a ‘failed’ interaction in which signaling in the B or T cell fails to be induced or is a less potent version of the longer interaction. Furthermore, although interactions can be quite long at the pre-GC phase, interactions within the GC are exclusively short. Thus, it is not clear how signaling in B and T cells has changed between these two time points. Beyond questions about the basic biology of B and T cell interactions, there are also several applications of this reporter in our MOG-induced GC model. At the pre-GC phase, it was observed that B and T cells in MOG-immunized mice form substantially shorter interactions than those in NPOVA-immunized mice (unpublished observations, Parham

KA *et al.*). Currently, it is not clear whether the short interactions in both systems are equivalent or, perhaps, if the short interactions are unique in each Ag model. Indeed, using these signaling reporters would give us the first clues for identifying whether the developing B cell response is controlled through unique signals being exchanged during interactions to different Ag's or if perhaps, B cell differentiation is controlled by a universal code of interaction duration.

In conclusion, the reporters developed here will require additional optimization. Fortunately, several different avenues are available to address this. By creating fluorescent mouse strains capable of monitoring the activity of the NF κ B and NFAT proteins, an understanding of the molecular events responsible for directing B cell differentiation at a cellular level can be defined. This will ultimately give us a more precise understanding of B cell differentiation that is not currently possible with bulk analysis of B cells.

4.4 Materials and Methods

4.4.1 Cloning

Primers referenced in Table 4.1 (Integrated DNA Technologies, Carolville, Iowa, and Sigma, St. Louis, Missouri) were used in PCR reactions using either Pfu polymerase (Gbiosciences, St. Louis, Missouri) or Phusion polymerase (Thermo Fisher Scientific, Waltham, Massachusetts). PCR products were run through agarose gel electrophoresis and bands corresponding to the correct PCR products were purified using either E.Z.N.A. Gel Extraction Kit (OMEGA Bio-Tek, Norcross, Georgia) or Gel/ PCR DNA Fragments Extraction Kit (Geneaid, New Taipei City, Taiwan) using manufacturers protocols. Purified PCRs were digested using combinations of Sall, HindIII, EcoRI, MfeI, NotI, XmaI, AscI, SacI, XhoI, and BglII (New England Biolabs, Ipswich, Massachusetts) or BbsI (Thermo Fisher Scientific, Waltham, Massachusetts) then purified using GeneClean II Kit (MPbiomedicals, Santa Ana, California) according to manufacturers protocol. Digested products were then ligated into pEGFP-N1 (Clontech, Mountain View, California), pX330-U6-Chimeric_BB-CBh-hSpCas9 (Addgene 42230), pCAGGS

(Belgian Co-Ordinated Collections of Micro-Organisms), or STOP-eGFP-ROSA26TV vector (Addgene 11739) using T4 DNA ligase (New England Biolabs, Ipswich, Massachusetts).

The following plasmids were used for PCR templates: pBABE-H2BGFP (Addgene 26790) was used for amplification of H2B-GFP, RelA cFlag pcDNA3 (Addgene 20012) was used for amplification of the p65 subunit of NF κ B, WT NFAT1 (Addgene 11100) was used for amplification of NFAT1, pmCherryN1 (Clontech, Mountain View, California) was used for amplification of mCherry, RP23-30E22 Bacterial Artificial Chromosome (Invitrogen, Carlsbad, California) containing the p65 locus was used for amplification of arms of homology for the p65 locus, RP23-135N9 Bacterial Artificial Chromosome (Invitrogen, Carlsbad, California) containing the NFAT1 locus was used for amplification of arms of homology for the NFAT1 locus. BACs were purified using NucleoBond Xtra BAC (Clontech, Mountain View, California) as listed in manufacturers protocol.

In brief, the H2B-GFP-T2A-mCh-p65/NFAT1 reporters were constructed by PCR amplifying H2B-GFP and cutting the PCR transcript with BglII and HindIII. This was ligated into the pEGFP-N1 vector along with annealed primers corresponding to the T2A sequence. The mCherry gene was then PCR amplified and cut with SacI and HindIII. This was cloned into the same pEGFP-N1 vector along with PCR amplified NFAT1 (cut with HindIII and SalI) or p65 (cut with HindIII and EcoRI).

The p65 donor DNA plasmids were constructed by first modifying the pCAGGs vector using EcoRI and BglII to incorporate annealed primers encoding a multiple cloning site. The left arm of homology for the p65 locus was PCR amplified to make a long version (1938 bp) or a short version (961 bp) and cloned into the pCAGGs vector using the SalI and MfeI restriction sites. The H2B-GFP-T2A-mCh reporter was PCR amplified (cut with MfeI and XhoI) and ligated into the same pCAGGs vector. Finally, the right arm of homology for the p65 locus was amplified to make a long version (1942 bp) or a short version (988 bp) then cut with XhoI and HindIII before ligation into the pCAGGs vector. The NFAT1 donor plasmids were similarly constructed by PCR

amplifying the right arm of homology to make a long version (1999 bp) and a short version (952 bp) that were cut with NotI and BglIII for insertion into the pCAGGs vector. Then the H2B-GFP-T2A-mCh reporter was PCR amplified and cut with NotI and XhoI for insertion into the same pCAGGs vector. Lastly, the left arm of homology was PCR amplified to make a long version (1976 bp) or short version (937 bp) that were cut with Sall and XhoI before ligation into the pCAGGs vector.

The DNA sequences coding the guide RNAs responsible for targeting the p65 and NFAT1 locus were generated by annealing DNA primers and ligating them into pX330 vectors cut with BbsI.

Cloning of the NFAT1₁₋₃₉₉-mCh-T2A-H2B-GFP construct was accomplished by PCR amplifying NFAT1₁₋₃₉₉ (cut with SacI and HindIII) and mCherry (cut with HindIII and AgeI) then ligating them into the pEGFP-N1 vector. Then H2B-GFP (cut with Sall and NotI) was ligated into the same vector along with two annealed primers forming the T2A site. This reporter construct was then PCR amplified (cut with AscI and NotI) and cloned into the STOP-eGFP-ROSA26TV vector along with anneal primers to act as an adaptor between the XmaI restriction site and the NotI restriction site.

Ligated plasmids were transformed into competent *E. coli* (DH5 α) using standard techniques (275). Plasmids were collected from these cells using the High-Speed Plasmid Mini Kit (Geneaid, New Taipei City, Taiwan) according to manufacturers protocol. Finalized vectors were sent for sequencing (London Regional Genomics Centre, London, Ontario) and upon confirmation plasmids were purified using Plasmid Maxiprep kit (Geneaid, New Taipei City, Taiwan).

Table 4.1. Forward and reverse primers used for cloning

Primer name	DNA sequence (5' to 3')	Product size
<i>H2B-GFP</i> fwd	5'-AAA AAA AGA TCT ATG CCA GAG CCA GCG AAG T-3'	1137 bp
rev	5'-AAA AAA AAG CTT CTT GTA CAG CTC GTC CAT GCC-3'	
<i>T2A</i> fwd	5'-AGC TGG AGG GCA GAG GAA GTC TTC TAA CAT GCG GTG ACG TGG AGG AGA ATC CCG GCC CTG AGC T-3'	64 bp
rev	5'-CAG GGC CGG GAT TCT CCT CCA CGT CAC CGC ATG TTA GAA GAC TTC CTC TGC CCT CC-3'	
<i>mCherry</i> fwd	5'-AAA AAA GAG CTC ATG GTG AGC AAG GGC GAG G-3'	732 bp
rev	5'-TTT TTT AAG CTT CTT GTA CAG CTC GTC CAT GCC-3'	
<i>p65</i> fwd	5'-AAA AAA AAG CTT ATG GAC GAT CTG TTT CCC CTC ATC-3'	1674 bp
rev	5'-TTT TTT GAA TTC TTA GGA GCT GAT CTG ACT CAA AAG AGC AG-3'	
<i>NFAT1</i> fwd	5'-AAA AAA AAG CTT ATG GAC GTC CCG GAG CCG CAG C-3'	2808 bp
rev	5'-AAA AAA GTC GAC CTA GGT CTG ATT TCG GGA GGG AG-3'	

<i>p65</i> guide RNA fwd	5'-CAC CGT CCA TGG TCA GGG TCC CGG-3'	24 bp
rev	5'-AAA CCC GGG ACC CTG ACC ATG GAC-3'	
<i>NFAT1</i> guide RNA fwd	5'-CAC CGT CCG GGA CGT CCA TGG CTC G-3'	25 bp
rev	5'-AAA CCG AGC CAT GGA CGT CCC GGA C-3'	
multiple cloning site pCAGGs fwd	5'-AAT TCC AAT TGC AGG TTC TCG AGT CGT GTG AGC TCA ACT GAG CGG CCG CAT GTC GA-3'	60 bp
rev	5'-GAT CTC GAC ATG CGG CCG CTC AGT TGA GCT CAC ACG ACT CGA GAA CCT GCA ATT GG-3'	
long left arm <i>p65</i> fwd	5'-TTT TTT GTC GAC CTA GCC CCT GCT GGT CCA GAG CTC-3'	1968 bp
short left arm <i>p65</i> fwd	5'-TGC CAC CTG GTC GAC GCC AGA GTC CCC ACA CTC AAT CTG CA-3'	985 bp
rev	5'-GCT TTT CAA TTG GGT CAG GGT CCC GGG AGC GGG GCC GGG GT-3'	
<i>p65</i> reporter fwd	5'-AAA AAA CAA TTG ATG CCA GAG CCA GCG AAG T-3'	1900 bp

rev	5'-TTT TTT CTC GAG CTT GTA CAG CTC GTC CAT GCC GCC GGT GGA G-3'	
right arm <i>p65</i> fwd	5'-GAA CCG CTC GAG ATG GAC GGT GAG GCT GCC CTC TGG CTC G-3'	
long rev	5'-GAA CCC AAG CTT CTT CCC ACT CCT TAC CCA CTG GCA AGT-3'	1966 bp
short rev	5'-GAT TAC GCC AAG CTT CAA TCC CTA ATC TGG CTC TTA GAC ACA GGG C-3'	1012 bp
long left arm <i>NFAT1</i> fwd	5'-GAA CGC GTC GAC TGT GGG TCA TGA CTG ACC CCT TCG GGT ATG TCA AAA GAC CC-3'	2000 bp
short left arm <i>NFAT1</i> fwd	5'-TGC CAC CTG GTC GAC TCA GGG AGC ACT GCC CAT CTC C-3'	961 bp
rev	5'-GAA CCG CTC GAG GGC TCG GAG CGT TCG GGA TGC GGG TTC GTA TAG AG-3'	
<i>NFAT1</i> reporter fwd	5'-AAA AAA CTC GAG ATG CCA GAG CCA GCG AAG T-3'	1911 bp
rev	5'-AAG GAA AAA AGC GGC CGC CCT TGT ACA GCT CGT CCA TGC CGC CGG TGG AG-3'	
right arm <i>NFAT1</i> fwd	5'-TTT TTT GCG GCC GCA TGG ACG TCC CGG AGC CGC A-3'	
long rev	5'-TTT TTT AGA TCT CAG CAG GAC AGG AGA AGG GAA TGG CC-3'	2023 bp

short rev	5'-GAG GGA AAA AGA TCT ATC TGG AAG CTG CCA GCA GGC T-3'	976 bp
<i>p65</i> genotyping fwd	5'-CAT GGA CGA GCT GTA CAA GCT CGA G-3'	1041 bp
rev	5'-CCA AAG TAC AGA GTA CTC TAG TGG CCA G-3'	
<i>NFAT1</i> locus genotyping fwd	5'-ATG GAC GTC CCG GAG CCG CA-3'	985 bp
<i>NFAT1</i> reporter genotyping fwd	5'-ACG AGC TGT ACA AGG GCG GCC GC-3'	1008 bp
<i>NFAT1</i> locus rev	5'-ACC AGA TGC CCG CAA GCC CGC AG-3'	
nested fwd	5'-AGA GGT AGA GGG GCG TGT GC-3'	121 bp
rev	5'-AAG TCC CCA ACA ACC GGC TC-3'	
<i>NFAT1</i> ₁₋₃₉₉ fwd	5'-AAA AAA GAG CTC ATG GAC GTC CCG GAG CCG CAG C-3'	1221 bp
rev	5'-CAA GGC AAG CTT GAG TGG TGG GAG GGA TGC AGT C-3'	
<i>mCherry</i> fwd	5'-GAA CCG AAG CTT ATG GTG AGC AAG GGC GAG G-3'	732 bp

rev	5'-GAA GCC ACC GGT CTT GTA CAG CTC GTC CAT GCC G-3'	
<i>T2A</i> fwd	5'-CCG GAG AGG GCA GAG GAA GTC TTC TAA CAT GCG GTG ACG TGG AGG AGA ATC CCG GCC CT-3'	60 bp
rev	5'-TCG ACA GGG CCG GGA TTC TCC TCC ACG TCA CCG CAT GTT AGA AGA CTT CCT CTG CCC TC-3'	
<i>H2B-GFP</i> fwd	5'-GAA CGC GTC GAC ATG CCA GAG CCA GCG AAG TCT G-3'	1144 bp
rev	5'-AAG GAA AAA AGC GGC CGC TTA CTT GTA CAG CTC GTC CAT GCC GAG AG-3'	
reporter <i>ROSA26</i> fwd	5'-GTC GAA GAG CTC GGC GCG CCA TGG ACG TCC CGG AGC CGC AGC-3'	3117 bp
rev	5'-GTA AGC GCG GCC GCA TTA ATT TAC TTG TAC AGC TCG TCC ATG CCG-3'	
<i>ROSA26- TV adaptor</i> fwd	5'-GGC CCA CAC TTG CCT GGT AAG CTG CAC TCT GCT C-3'	38 bp
rev	5'-CCG GGA GCA GAG TGC AGC TTA CCA GGC AAG TGT G-3'	
Genotype GFP fwd	5'-GCG AGG GCG ATG CCA CCT ACG GCA-3'	450 bp
rev	5'-GGG TGT TCT GCT GGT AGT GGT CGG-3'	

4.4.2 Cell culture and transfections

RAW264.7 macrophage or J774 macrophage were cultured in 12-well plates with 1 ml RPMI Medium 1640 with L-glutamine (WISENT, Saint-Bruno, Quebec) and 10% FBS (WISENT, Saint-Bruno, Quebec) at 37°C, 5% CO₂. Cells were plated at 5x10⁵ cells per well and grown on coverslips overnight until approximately 30-50% confluency at which point they were transfected with 1 µg of total DNA per well using Fugene HD (Promega, Madison, Wisconsin) as listed in manufacturer's protocol (for CRISPR experiments, cells were transfected at a 3:1 ratio of DNA donor plasmid:pX330 vector). After 4-5 hours, the media on the transfected cells was replaced by 1 ml of fresh media and incubated for 1 day for overexpression experiments and 2 days for CRISPR experiments where the media was supplemented with 0.1 µM SCR7 (Xcessbio, San Diego, California). For the p65 stimulation experiments, p65 transfected cells were then stimulated with LPS from *S. enterica* (Sigma, St. Louis, Missouri) in 10% FBS RPMI and MEM Non-Essential Amino Acids Solution 100x (Thermo Fisher Scientific, Waltham, Massachusetts). For NFAT1 stimulation experiments cells were stimulated with PMA (Tocris Biosciences, Bristol, United Kingdom) and ionomycin (Sigma, St. Louis, Missouri) in 1 mL serum free RPMI with MEM non-essential amino acids after a PBS wash.

4.4.3 Fixed and live cell microscopy

Cells were fixed onto coverslips after a PBS wash using a 20 minute incubation in 4% PFA (Electron Microscopy Sciences, Hatfield, Pennsylvania). Fixed cells were then washed again with PBS and mounted onto glass slides using PermaFluor Mountant (Thermo Fisher Scientific, Waltham, Massachusetts). These slides were then imaged using a DM5500B fluorescence microscope (Leica microsystems, Concord, ON, Canada) with a 40x objective lens in the Bright Field, GFP, and mCherry filters.

For live cell experiments, coverslips with transfected macrophage (described in 4.4.2) were transferred to a Leiden chamber in a Leica DM16000B microscope equipped with a 37°C heated stage perfused with 5% CO₂, a 40x objective, photometrics Evolve-512 delta EM-CCD camera, Chroma Sedat Quad filter set, and the Leica Application

Suite X software platform (Leica microsystems, Concord, ON, Canada). The locations of 2-3 reporter positive cells were tracked using the mark-and-find feature then the Leiden chamber was opened to add PMA + ionomycin to a final concentration of 0.25 µg/ml PMA and 1 µg/ml ionomycin in serum free RPMI. Cells were then imaged once every minute for 22 minutes in the GFP and mCherry channels.

4.4.4 Genotyping of CRISPR transfected cells and mouse pups

Two days post-transfection, J774 macrophage were scraped off the bottom of 12-well plates then centrifuged at 1500 rpm for 8 minutes at 4°C. The pellet was then suspended in permeabilization buffer (50 mM Tris, 50 mM KCl, 2.5 mM EDTA, 0.45% Igepal, 0.45% Tween-20 (Bioshop, Burlington, Ontario), and 0.15 mg/ml proteinase K (Biobasic, Markham, Ontario)) and incubated overnight at 55°C then frozen at -20°C until needed. To set up the genotyping reactions, Phusion polymerase (Thermo Fisher Scientific, Waltham, Massachusetts) was used with 2% DMSO and either 1 µl of genomic DNA or 0.5 µg of purified donor DNA plasmids were used as templates. The cyclor conditions used were: 98°C for 3 mins then 45 cycles of (0.5 mins 98°C, 0.5 mins 62°C, and 3 mins 72°C) followed by 10 mins 72°C. Finished PCR reactions were then loaded onto a 1% agarose gel. For the genotyping of mouse pups, small tail snips were used instead of transfected cells.

4.4.5 Guide RNA design

Suitable guide RNAs were identified for both the p65 and NFAT1 loci using the CRISPR design tool provided at (<http://crispr.mit.edu/>) which is described in (323). Guide RNAs were selected based on specificity where the p65 guide RNA had a score of 82 and the NFAT1 guide RNA had a score of 94.

4.4.6 Nuclear injections

The protocol for nuclear injections was based on (349). In brief, 4 week old C57Bl/6 females were injected with pregnant mare serum gonadotrophin (Sigma, St. Louis, Missouri) and two days later mice were injected with human chorionic gonadotrophin (Sigma, St. Louis, Missouri) then mated with male C57Bl/6 mice. Single

embryos were then collected from female mice, washed, then cultured briefly in M2 media (Millipore, Burlington, Massachusetts) at 37°C and 5% CO₂. An injection mixture of 100 ng/μl Cas9 mRNA (TriLink Biotechnologies), 50 ng/μl guide RNA (Integrated DNA Technologies, Carolville, Iowa), and 200 ng/μl donor DNA was mixed at a 1:3:3 ratio with M2 media supplemented with Cytochalasin B 10 μg/ml (Sigma, St. Louis, Missouri) and M2 media supplemented with 10% (wt/vol) Polyvinylpyrrolidone 360 kDa (Sigma, St. Louis, Missouri). Zygotes were then injected with this mixture and cultured in KOSM media (Millipore, Burlington, Massachusetts) supplemented with 0.1 μM SCR7 until the two cell stage for transfers into pseudopregnant females to generate whole mice, or cultured to the blastocyst stage for genotyping.

4.4.7 Blastocyst genotyping

To isolate DNA from blastocysts a DNeasy blood and tissue kit (Qiagen, Hilden, Germany) was used. To detect blastocysts DNA, an initial set of primers specific for the NFAT1 locus or specific for a site-specific insertion of the NFAT1 reporter was used in combination with Q5 high-fidelity polymerase (New England Biolabs, Ipswich, Massachusetts) according to the manufacturer's protocol. Then, 1 μl of the PCR was used to seed a second PCR reaction using two primers that formed a nested PCR within the first set of primers. Again the PCR reaction was conducted with Q5 high-fidelity polymerase according to the manufacturer's protocol. Once complete, the PCRs were run on a 2% agarose gel.

4.4.8 Image analysis

Tiled images from microscopy were analyzed using the ImageJ program. The cell counter add-on for this program was used to quantify the number of cells in a tiled image that displayed a nuclear translocation of a transcription factor where a nuclear translocation was defined as visible fluorescence in the area defined by the nuclear marker. The nuclear to cytoplasmic fluorescence ratio was calculated by measuring the fluorescence in the nuclei of cells defined by the nuclear marker and dividing this by the fluorescence measured in a representative portion of cytoplasm near the nucleus.

4.4.9 Statistical analysis

Prism software (Graphpad, La Jolla, California) was used to graph the data and for calculation of statistical significance. A student's T test was used to compare two groups, while multiple comparisons were compared using an ANOVA followed by a T test with a Bonferroni correction.

Chapter 5

5 Overall discussion and future directions

In this thesis, I describe factors that influence the initiation and progression of GCs directed against the autoAg MOG. The hypothesis that the MOG-induced GC would be short-lived and less productive than foreign-Ag driven GCs is addressed.

5.1 Summary of the major findings of this thesis

In Chapter 2 of this thesis, I developed a novel protein expression system to express large amounts of mMOG_{tag} protein. I show that the mMOG_{tag} expression system is amenable to manipulation through the generation of haMOG_{tag}, which alters T cell Ag-affinity and induces accelerated proliferation of MOG-specific T cells. Both mMOG_{tag} and haMOG_{tag} were confirmed to be capable of inducing EAE incorporating autoreactive B and T cells confirming that these Ags can induce GC responses in the context of relevant autoimmune disease. In Chapter 3, I used the tools developed in Chapter 2 to determine factors that influence B cell differentiation in the context of autoimmune GC responses. I found that immunization with MOG protein results in a short-lived GC that produces few plasma cells relative to the model foreign-Ag, NPOVA. Instead, the MOG-induced immune response produces predominantly memory B cells; however, these cells are short-lived. I then showed that the collapse of the MOG-induced GC response is instructed by the autoreactive T cell and could be attributed to their low-affinity for Ag. However, the short-lived nature of MOG-specific memory B cells was not under T cell control. Despite evidence of T cells contributing to B cell fate choices in these Ag-models, I saw no evidence that T_{FH} cells are differentially expressing molecules associated with B cell differentiation. Instead, T_{FH} cells differed only in absolute number, a property that appears to be instructed by the Ag itself. Increases in T_{FH} cell numbers were also associated with an expansion of DZ B cells suggesting that absolute T_{FH} cell numbers influence the fate decision between staying in the GC and memory B cell differentiation. Altogether, the MOG-induced autoreactive GC response is limited by properties of the MOG-autoAg including low T cell Ag-affinity. One hypothesis that could link the fate choices B cells make in immune responses to the properties of Ags, is

that Ag-properties influence how signals are exchanged during B and T cell interactions. This hypothesis was addressed in Chapter 4 by developing a tool to investigate the kinetics of signal exchange between B and T cells during their interactions. I showed that I can monitor the activation status of cells by monitoring the cytoplasmic to nuclear translocations of the NFAT1 and p65 proteins. The reporter of NFAT1 activity was successfully adapted for insertion into the endogenous *NFAT1* locus using the CRISPR/Cas9 system; however, this did not translate into successful generation of a reporter mouse. The NFAT1 reporter has since been adapted for insertion into the *Rosa26* locus and this construct should generate a functional reporter mouse.

5.2 A model of the autoreactive germinal center

Overall, the results of this thesis reinforce the current models of GC initiation and progression but also extend them. One of the key findings in Chapter 3 was that MOG-induced GCs are biased towards centrocytes over centroblasts as a result of not maintaining a DZ in the GC. Indeed, the lack of a DZ in the MOG-induced GC response can potentially explain why I do not see efficient plasma cell production and why there is preferential memory differentiation. In particular, differentiation into plasma cells is favored in B cells that acquire a high-affinity BCR, where the acquisition of a high-affinity BCR is facilitated by SHM, whereas memory B cell differentiation is favored by low-affinity BCRs (58, 108, 128, 152). As SHM occurs in the DZ of the GC (108), it seems likely that the lack of selection of centrocytes to enter the DZ of the MOG-induced GC would contribute to preferential memory B cell differentiation although, further analysis of SHM in the MOG-induced GC would be required to validate this.

I also showed that when immunizing with haMOG_{tag} instead of mMOG_{tag}, which incorporates a high-affinity T cell epitope, MOG-specific B cells favored staying in the GC over memory B cell differentiation and this was associated with an expansion in the DZ of the GC and increased proliferation. This result is also supported by the cyclic re-entry model of the LZ and DZ of the GC and by studies looking at how Ag-presentation affects B cell differentiation. In particular, several reports have shown that when additional Ag is targeted towards a population of GC B cells, that population is preferentially selected to enter the DZ of the GC over memory B cell differentiation (112,

127). This is similar to my experiments with haMOG_{tag}, where manipulation of T cell Ag-affinity promoted the transition of GC B cells to enter the DZ, opposed to Ag-avidity that was used in the studies mentioned above. One key difference between our model and the studies mentioned above, is that in my experiments all GC B cells are presenting a higher-affinity Ag whereas in their experiments they are targeting Ag towards a small population of GC B cells within the GC. Thus, in their studies they are manipulating the competitiveness of a specific population of GC B cells whereas in my experiments I am manipulating the whole GC, as all GC B cells would present the exact same Ag. Indeed, my results would suggest that B cell fate choices are influenced by not only competition between B cells for Ag, but also that presentation of higher-affinity Ags can affect B cell fate choices across the entire GC.

While I was able to show that T cell Ag-affinity affected the balance between memory B cells and GC B cells, manipulation of T cell Ag-affinity in our MOG system did not affect plasma cell generation unlike the manipulation of Ag-avidity in other studies (112, 127). However, it should be noted that, although haMOG_{tag} does contain a higher-affinity peptide than mMOG_{tag}, the affinity of this peptide is still much lower than the affinity of many foreign Ag-derived peptides typically used in such studies (261, 350). Furthermore, the NF-M₁₈₋₃₀ peptide used in haMOG_{tag} has a relatively low affinity for MHC class II molecules resulting in incomplete presentation of this peptide (351). Thus, it is likely that haMOG_{tag} only partially enhanced T cell Ag-affinity in B-T interactions, perhaps explaining its modest effects. Consistent with this, in our experiments using NPOVA and NPMOG, where there is a substantial difference in T cell affinity, the results were more striking. Relative to NPOVA, NPMOG was characterized by reduced early plasmablast expansion and reduced long-lived plasma cell generation. Based on these results and the results of others (112), it seems likely that there is a continuum where low levels of T cell help promotes memory B cell differentiation, while intermediate levels of T cell help promotes GC maintenance and T cells imparting the highest level of help promote plasma cell expansion.

An unexpected finding in this thesis was that T_{FH} cells in the NPOVA, mMOG_{tag}, and haMOG_{tag} responses had the same expression of cytokines and surface receptors

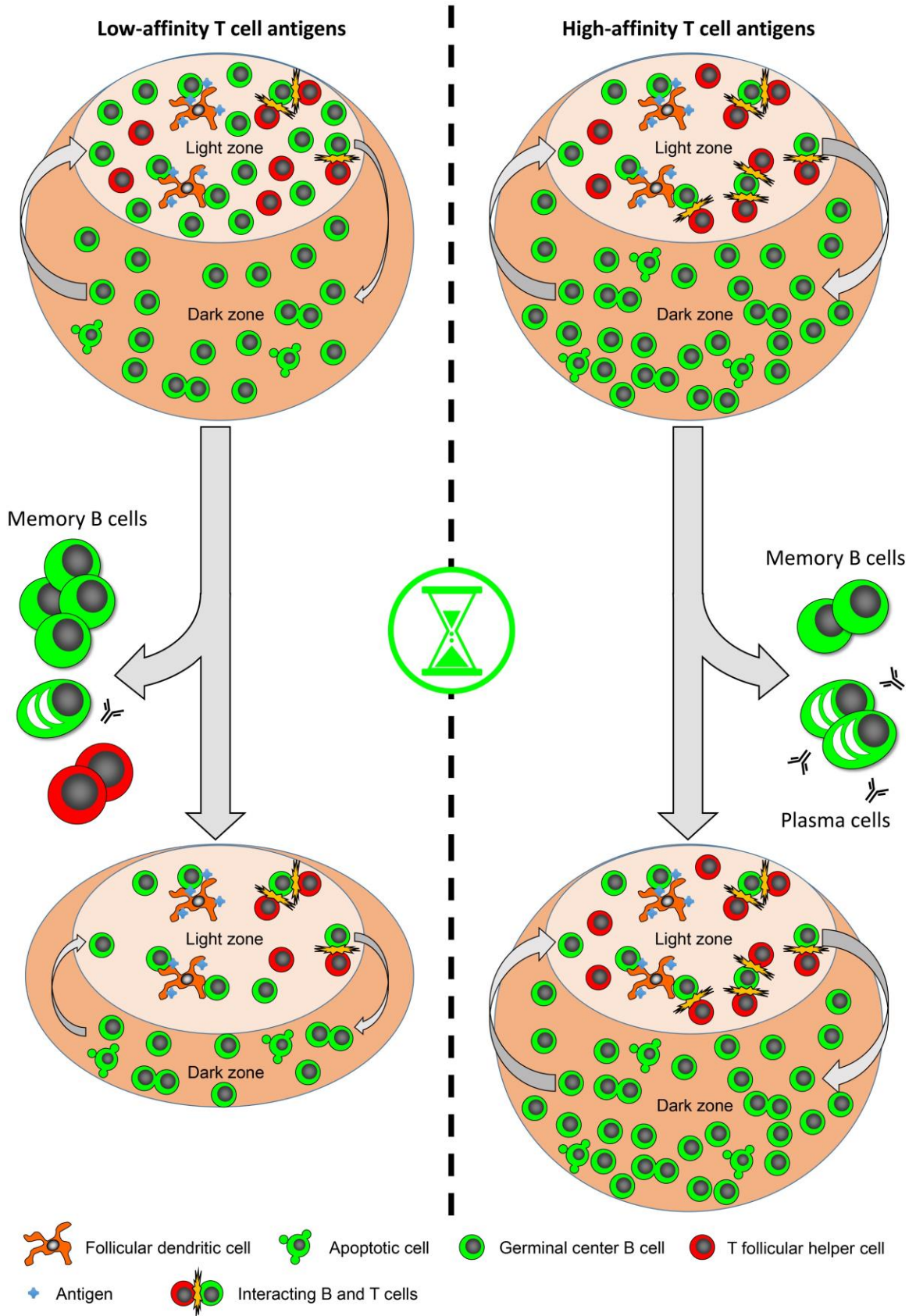
known to influence B cell fate choices, despite clear evidence of B cells making different fate decisions. The only major difference between these Ags, was the absolute number of T_{FH} cells that each Ag could induce. It is possible however, that the differing numbers of T_{FH} cells may alone be sufficient to change B cell fate choices. In all of the experiments conducted in this study, the ratio of GC B cells to T_{FH} cells remained the same, a finding also supported by the results of others (170, 352), suggesting that the absolute numbers of T_{FH} cells by itself may determine the size of the GC B cell response. Furthermore, based upon the experiments in this thesis and the results of others (170), Ag can be a limiting factor in GCs by controlling the maintenance of T_{FH} cells (170). In particular, Ag-presentation by GC B cells is required for T_{FH} cells to maintain PD-1 expression. This is important because PD-1 signaling is required to suppress the expression of the CXCR3 chemokine receptor that normally directs T_{FH} cells to leave the GC environment (180). Thus, it seems likely that a combination of Ag-affinity and Ag-avidity may influence the number of T_{FH} cells that can be maintained in the GC, which in turn may determine the number of GC B cells that can be supported. Nonetheless, it should be noted that Ag-affinity can also affect the initial differentiation of pre-T_{FH} cells (353, 354) and thus, increased initial differentiation of pre-T_{FH} cells could contribute to my findings.

Based upon the literature cited above, there are general rules established for how B cell differentiation is instructed during GC responses: first, low BCR-affinity promotes memory differentiation over GC B cell or plasma cell differentiation and high-BCR affinity promotes plasma cell differentiation over GC B cell or memory B cell differentiation; second, the acquisition of a high-affinity BCR is dependent on acquiring high-affinity mutations through SHM that is largely influenced by the time GC B cells stay within the DZ of the GC; lastly, presentation of larger amounts of Ag leads to preferential plasma cell expansion and increased LZ to DZ transitions leading to better GC retention of particular B cell clones in increased DZ dwell time. I have contributed to these rules by expanding the last point. In particular, I have shown that in addition to the absolute amount of Ag being presented, it is important to consider the cumulative affinities of those Ags as this functions similarly to the presentation of more Ag.

Altogether, these results suggest a model where the absolute number of T_{FH} cells controls LZ to DZ transitions. In particular, when T_{FH} cells are limited, T_{FH} cell help would also be limited making it difficult for GC B cells to gain access to the DZ of the GC (112). However, when T_{FH} cells are in abundance, T_{FH} cell help would be expected to be plentiful resulting in many B cells being selected to enter the DZ of the GC. As discussed above, how T cell Ag-affinity and the absolute number of T_{FH} cells would affect plasma cell differentiation is less clear. The decision to become a plasma cell is B cell intrinsic (128). However, T cells can influence plasmablast proliferation (128, 156) and influence the long-term production of plasma cells indirectly by maintaining GCs over a longer period of time (126). Thus, the absolute number of T_{FH} cells may influence plasmablast proliferation or the accumulation of plasma cells over time; however, additional experiments will be required to determine how this occurs. Putting all of these ideas together, a model was generated and is summarized and described in Figure 5.1. In the next sections I will address unresolved questions and the significance of this research.

Figure 5.1. A model of how T cell antigen-affinity affects germinal center progression

Based on the results of this thesis, the initiation of GC responses is similar regardless of the T cell controlling the GC. However, for low-affinity Ags, the low number of T_{FH} cells is limiting leading to fewer B cells acquiring sufficient T cell help. This leads to inefficient plasma cell expansion and failure of centrocytes to be selected to enter the DZ of the GC. Furthermore, this leads to B cells accumulating and persisting in the LZ of the GC leading to preferential memory B cell differentiation. Limited interactions between B and T cells also limits the maintenance of T_{FH} cells, resulting in T_{FH} cells losing their PD-1^{high} phenotype and leaving the GC. Then at the mature GC time point, an equilibrium is reached between the small number of GC B cells and T_{FH} cells allowing the maintenance of a small GC response. In contrast, high-affinity Ags maintain themselves over longer periods of time by maintaining a larger T_{FH} cell pool that can support plasma cell differentiation and LZ to DZ transitions in the GC.



5.3 Future directions

5.3.1 Somatic hypermutation in the MOG-induced germinal center

One of the main functions of the GC, in particular the DZ of the GC, is to drive SHM (58). Differences in SHM between the NPOVA and MOG GC responses could potentially partially explain the collapse of MOG-induced GCs and inefficient plasma cell differentiation. However, SHM was not addressed in this thesis. Studying SHM is complicated by the need to sequence individual BCRs of GC B cells to identify mutations in their BCRs. These mutations also need to be mapped, cloned, and expressed to test how each mutation contributes to the affinity of the antibody/BCR. Mutations and their affinities have been mapped for the NP system using B1-8 mice, indeed, the NP-system has been used extensively for the study of SHM (355). In this study, we could not conduct similar research as mutations in the IgH^{MOG} BCR have not been mapped, which requires a significant amount of work and was beyond what could be accomplished in this thesis. Nonetheless, preliminary experiments to determine how autoreactive T cells affect SHM could make use of the NPOVA and NPMOG systems, as the tools for analyzing the NP response are already available (274).

This avenue of research would be of interest in the future as this could help solidify the GC model I suggested above. In particular, I would expect that the MOG-induced GC would be characterized by low SHM and that SHM would be restored upon immunizing with haMOG_{tag}, as haMOG_{tag} could support a sizable DZ. Presumably, centroblasts would have a sufficiently longer DZ dwell time to permit efficient induction of SHM (112). It should be noted however, that in some scenarios excessive T_{FH} cell support can inhibit SHM as a result of excessive selection of centrocytes for entry into the DZ of the GC making it difficult to specifically expand high-affinity B cell clones (356). Thus, it possible that additional T cell help would not promote SHM. Nonetheless, based upon the results of Chapter 3, immunization with haMOG_{tag} approached but did not exceed the DZ proportions of the NPOVA GC, which effectively supports SHM and the selection of high-affinity GC B cells (123), suggesting that immunization with haMOG_{tag} would not represent excessive T cell help.

Another unresolved finding of this thesis is that although MOG-specific GCs start as being predominantly MOG-specific, over time MOG-specificity appears to decrease, something that is not seen with the NPOVA system. A similar phenomenon has been described before where GC B cells undergo SHM to mutate their autoreactive BCRs to become non-autoreactive (104, 357-359). In these scenarios, autoreactive B cells first mutate their BCR to decrease their affinity for epitopes on the endogenously expressed autoAg, then mutate their BCRs towards any foreign-epitopes on the immunizing-Ag. Of key significance, as this process had been described to be dependent on the endogenous expression of the autoAg, we can test whether this process is occurring in our autoreactive GCs by taking advantage of MOG deficient mice (351), thereby eliminating the endogenous Ag.

Another scenario where using MOG-deficient mice would be useful is in understanding why MOG-specific memory B cells have a short life-span. In Figure 3.9, I showed that autoreactive T cells were not responsible for programming unstable B cell memory suggesting that the reduced life-span of autoreactive memory B cells was due to some factor intrinsic to the autoreactive B cell or its environment. Using MOG-deficient mice, we could determine whether endogenously expressed MOG, available in tissues such as the deep cervical LNs (69, 70), is leading to activation-induced cell death of MOG-reactive B cells as I would expect MOG-specific memory to be more stable in a setting where no endogenous MOG is available. Additionally, if the MOG-deficient background was crossed onto the IgH^{MOG} mouse to generate MOG-specific B cells that pass through immune tolerance unaffected, we could assess whether the reduced life-span of MOG-specific memory B cells is as a result of anergy induced during development (30). Indeed, we cannot be sure at this time that MOG-specific B cells do not start in an anergic state and that being drawn into an immune response would reverse anergy in these cells.

5.3.2 T cell antigen-affinity and the germinal center

In Chapter 3 of this thesis, there were unaddressed confounding factors influencing the interpretation of how T cell Ag-affinity affects the GC: 1st, Many of my experiments make use of two different T cells that differ in autoreactivity making it

unclear whether autoreactivity or low T cell Ag-affinity was affecting my results; 2nd, in my experiments using haMOG_{tag} the differences in affinity were not substantial and lead to only modest changes in the GC response. Thus, to more firmly establish how T cell Ag-affinity affects the GC response, I would need to make use of an Ag-model system that eliminates autoimmunity and has a greater range of T cell Ag-affinities that can be manipulated. Both of these issues could be addressed using the NPOVA system using B1-8 B cells and OTII T cells. The NP-based system is useful as NP can be attached to any protein allowing for the B cell side of the immune response to be standardized to any protein (360). The OTII T cell is also useful as it recognizes the OVA₃₂₃₋₃₃₉ peptide with a high-affinity (250) and it is easier to design mutated peptides (known as altered peptide ligands) that lower T cell Ag-affinity than it is to increase T cell Ag-affinity. Indeed, several altered peptide ligands of the OVA₃₂₃₋₃₃₉ peptide have been described making it possible to clone and express a series of OVA proteins exhibiting a gradient of T cell Ag-affinities (250, 251). Overall, this system would not only provide more precise control of T cell Ag-affinity, but it will also eliminate the confounding factor of autoreactivity. Nonetheless, these results could also be validated using the haMOG_{tag} system if done on a MOG-deficient background to eliminate autoreactivity in IgH^{MOG} B cells, 2D2 T cells, and eliminate endogenous MOG-expression in the recipient environment.

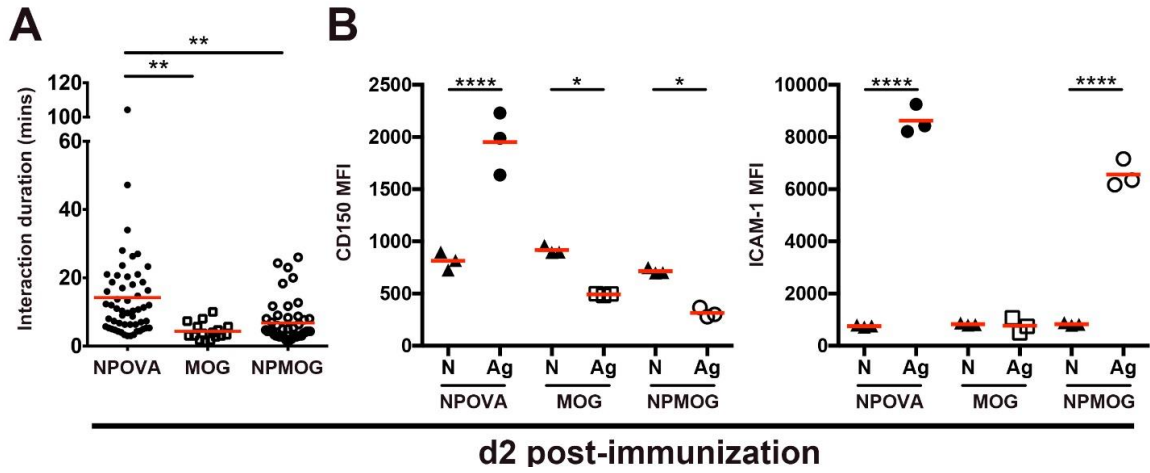
5.3.3 Signal exchange and interaction duration of B and T cell conjugates

As I elaborated on in Chapter 4 of this thesis, there are several basic aspects of the B and T cell interaction that are still not understood. In particular, it is not known what the kinetics of signal exchange between B and T cells is during their interactions. This is important as interactions can differ substantially in duration (78). Thus, it is not clear whether signals can be effectively exchanged within a short-interaction or that signals continue to be exchanged during long-interactions. This question requires the usage of reporters such as the ones I had attempted to make in Chapter 4 of this thesis, which would allow for real-time quantification of signaling in B and T cells as they interact in living tissue. Indeed, if these reporter mice are successfully generated in the future, they will be used to answer these questions.

Beyond understanding the basic rules that govern B cell differentiation during B and T cell interactions, these results are also likely relevant to the GC responses I have characterized in this thesis. A promising explanation for how Ag-properties influence B cell fate choices is that Ag-properties affect signal exchange between B and T cells during their interactions. Indeed, the Kerfoot laboratory has found that during the pre-GC phase of the immune response, B and T cells form shorter interactions in response to MOG relative to NPOVA (Figure 5.2A). Furthermore, when we immunize with NPMOG, we get an intermediate phenotype consistent with the intermediate phenotype I saw in Chapter 3. Consistent with our results, others have seen that increased interaction duration promotes GC B cell differentiation over memory B cell differentiation and promotes ASC differentiation over GC B cell differentiation (112, 127). Thus, interaction length may play a key role in determining B cell differentiation to these different Ags. The maintenance of physical interactions between B and T cells is dependent on the expression of SLAM proteins and ICAMs (160). Preliminary evidence suggests that SLAM and ICAM-1 are upregulated on B cells when immunizing with NPOVA; however, this fails to occur on MOG specific B cells and NPMOG immunization results in an intermediate phenotype (Figure 5.2B). Thus, differential expression of ICAM-1 molecules and SLAM receptors that modify cellular adhesion may be responsible for the differences in interaction length that we have seen. Further work will need to characterize explicitly how Ag-properties influence the upregulation of these molecules on B cells, whether these differences in receptor expression on B cells are truly determining interaction length, and by extension, influencing how B cells are differentiating.

Figure 5.2. Pre-GC B and T cell interactions are influenced by properties of immunizing Ags.

(A and B) Fluorescent protein-marked Ag-specific B and T cells were transferred into non-fluorescent protein-marked SMARTA recipient mice then immunized with the indicated Ag two days post-transfer. Two days post-immunization, the popliteal LN was exposed for intravital two-photon microscopy to track Ag-specific B and T cell interactions over time (A) or LNs were processed for flow cytometry analysis (B). (B) N is IgD⁻ CD19⁺ GFP⁻ B cells, Ag is IgD⁻ CD19⁺ GFP⁺ B cells. *p<0.05, **p<0.01, ***p<0.0001. Data courtesy of Dr. Parham.



5.4 B cells in MS and EAE

In addition to acquiring a better understanding of the basic biology of GC responses, the results of this thesis have important implications to the autoimmune disease MS and its animal model EAE. In particular, there is the idea that myelin-specific B cells are activated in the deep cervical LNs and that these cells are fueling a myelin-specific B cell response in the CNS (68-70). Nonetheless, despite evidence of myelin-specific GCs occurring in MS (62), no other study beyond the work in this thesis has characterized a myelin-specific GC. Indeed, the short-lived nature of myelin-specific GCs is likely to have several implications in how we look at MS.

Currently, the memory B cell subset appears to be a promising candidate for the pathogenic subset in MS (5, 361). In this thesis, I found MOG-specific GCs produced memory B cells in abundance at the early stages of the GC response; however, these cells were short-lived. Given that memory B cells have recently been shown to be potent inducers of myelin-specific T cell responses (361), then it would be expected that their short life span would represent a major limitation in driving the disease. Indeed, this would suggest that myelin-specific B cells would need constant replenishment to continue to fuel the autoimmune response and thus, would be therapeutically targetable throughout MS. Consistent with the idea autoreactive GCs require replenishment, MS relapses are associated increased numbers of circulating memory T_{FH} cells, that are generated during the initiation of GCs and throughout GCs (94), suggesting the induction of autoreactive GCs coincides with disease progression (362, 363).

One possibility that was not fully addressed in this thesis or in the MS literature in general, is that some of the cells that we are defining as memory B cells may actually be ABCs. This population is produced from GC responses to most Ags (166) and has a tendency to localize to the B cell follicle-T cell zone border where they can interact with T cells and promote T helper 17 cell differentiation (148), a T cell subset associated with the promotion of MS and EAE (364-367). Indeed, when looking at GC histology, many GFP⁺ B cells can be seen at the B cell follicle-T cell zone interface although presently it cannot be definitively determined whether these cells are ABCs. Nonetheless, knowing whether ABCs are being generated in GCs would be of interest as this population appears

to be expanded in MS patients and also shows evidence of disproportionate representation in the cerebral spinal fluid of MS patients relative to peripheral blood suggesting these cells actively accumulate in the inflamed CNS (141).

Beyond my analysis of GCs and memory B cells, I also found that when immunizing with our MOG Ag, I could induce Ag-specific plasma cell responses including the generation of long-lived plasma cells that could be detected as late as d39 post-immunization. This would suggest that even a single GC response directed against a myelin autoAg is sufficient to drive an antibody response including the generation of long-lived cells that can maintain antibody production over time. Although antibodies are not the main driving factor in MS (368), they can exacerbate damage (61-63) and thus, should ideally be suppressed. However, if these plasma cells are actually long-lived, then halting their production is unlikely to appreciably affect their numbers as it would require a great deal of time for the long-lived plasma cells to die off. Altogether, these results would suggest that the therapeutic targeting of autoreactive GCs to induce a full collapse would quickly lead to the deterioration of myelin-specific memory B cells as these cells would not be renewed; however, long-lived plasma cells would persist.

5.5 Concluding remarks

The focus of the research conducted in the Kerfoot laboratory is to understand the basic rules governing B cell differentiation and establishing the role of B cells in MS. The work in this thesis bridges the gap between these two goals by establishing the rules that govern myelin-specific GC development, but also doing this in a model that is relevant to CNS autoimmune disease. Indeed, relative to the development of GCs towards foreign-Ags, the GC response against MOG diverges significantly from the expected trajectory of a foreign-Ag resulting in plenty of opportunities to look at factors that influence B cell differentiation. This thesis focused predominantly of how T cells contribute to the collapse of autoreactive GCs. However, as shown in the above sections, there may also be differences between MOG and foreign-Ag specific B cells that may be contributing to the differential GC progression I have seen. Furthermore, I do not know how the autoreactive origins of the B and T cells I studied or how the expression of endogenous autoAg may be contributing to GC progression. Both of these issues will need to be

studied in more detail. Thus, the results of this thesis points to several different avenues of research on basic B cell biology that will need to be addressed in the future.

Additional work is also needed to characterize how myelin-specific B cells contribute to EAE. I have shown that MOG-specific B cells can be expanded through immunization with MOG and I and others have shown that MOG-specific B cells contribute to EAE. Nonetheless, it is still not known how or where MOG-specific B cells contribute to EAE. Thus, future research will need to characterize how the subsets of B cells produced in MOG-specific GCs, are contributing to EAE. Overall, the research in this thesis into the manipulation of B cell responses may be valuable in vaccine design, but also for understanding how autoreactive B cell responses initiate and progress.

References

1. Esposito, S., E. Franco, G. Gavazzi, A. G. de Miguel, R. Hardt, G. Kassianos, I. Bertrand, M. C. Levant, B. Soubeyrand, and J. A. Lopez Trigo. 2018. The public health value of vaccination for seniors in Europe. *Vaccine* 36: 2523-2528.
2. Fisher, C. R., H. J. Sutton, J. A. Kaczmarek, H. A. McNamara, B. Clifton, J. Mitchell, Y. Cai, J. N. Dups, N. J. D'Arcy, M. Singh, A. Chuah, T. S. Peat, C. J. Jackson, and I. A. Cockburn. 2017. T-dependent B cell responses to Plasmodium induce antibodies that form a high-avidity multivalent complex with the circumsporozoite protein. *PLoS Pathog* 13: e1006469.
3. Havenar-Daughton, C., A. Sarkar, D. W. Kulp, L. Toy, X. Hu, I. Deresa, O. Kalyuzhniy, K. Kaushik, A. A. Upadhyay, S. Menis, E. Landais, L. Cao, J. K. Diedrich, S. Kumar, T. Schiffner, S. M. Reiss, G. Seumois, J. R. Yates, J. C. Paulson, S. E. Bosinger, I. A. Wilson, W. R. Schief, and S. Crotty. 2018. The human naive B cell repertoire contains distinct subclasses for a germline-targeting HIV-1 vaccine immunogen. *Sci Transl Med* 10.
4. Good-Jacobson, K. L., and J. R. Groom. 2018. Tailoring Immune Responses toward Autoimmunity: Transcriptional Regulators That Drive the Creation and Collusion of Autoreactive Lymphocytes. *Front Immunol* 9: 482.
5. Li, R., K. R. Patterson, and A. Bar-Or. 2018. Reassessing B cell contributions in multiple sclerosis. *Nat Immunol*.
6. Chung, J. B., M. Silverman, and J. G. Monroe. 2003. Transitional B cells: step by step towards immune competence. *Trends Immunol* 24: 343-349.
7. Germain, R. N. 2002. T-cell development and the CD4-CD8 lineage decision. *Nat Rev Immunol* 2: 309-322.
8. Jackson, K. J., M. J. Kidd, Y. Wang, and A. M. Collins. 2013. The shape of the lymphocyte receptor repertoire: lessons from the B cell receptor. *Front Immunol* 4: 263.
9. Treanor, B. 2012. B-cell receptor: from resting state to activate. *Immunology* 136: 21-27.
10. Natarajan, K., J. Jiang, N. A. May, M. G. Mage, L. F. Boyd, A. C. McShan, N. G. Sgourakis, A. Bax, and D. H. Margulies. 2018. The Role of Molecular Flexibility in Antigen Presentation and T Cell Receptor-Mediated Signaling. *Front Immunol* 9: 1657.
11. Zinkernagel, R. M., and P. C. Doherty. 1973. Cytotoxic thymus-derived lymphocytes in cerebrospinal fluid of mice with lymphocytic choriomeningitis. *J Exp Med* 138: 1266-1269.

12. Loo, T. T., Y. Gao, and V. Lazarevic. 2018. Transcriptional regulation of CD4(+) TH cells that mediate tissue inflammation. *J Leukoc Biol.*
13. Ueno, H., J. Banchereau, and C. G. Vinuesa. 2015. Pathophysiology of T follicular helper cells in humans and mice. *Nat Immunol* 16: 142-152.
14. Pores-Fernando, A. T., and A. Zweifach. 2009. Calcium influx and signaling in cytotoxic T-lymphocyte lytic granule exocytosis. *Immunol Rev* 231: 160-173.
15. Nurieva, R. I., Y. Chung, D. Hwang, X. O. Yang, H. S. Kang, L. Ma, Y. H. Wang, S. S. Watowich, A. M. Jetten, Q. Tian, and C. Dong. 2008. Generation of T follicular helper cells is mediated by interleukin-21 but independent of T helper 1, 2, or 17 cell lineages. *Immunity* 29: 138-149.
16. Nikolich-Zugich, J., M. K. Slifka, and I. Messaoudi. 2004. The many important facets of T-cell repertoire diversity. *Nat Rev Immunol* 4: 123-132.
17. Batista, F. D., and M. S. Neuberger. 1998. Affinity dependence of the B cell response to antigen: a threshold, a ceiling, and the importance of off-rate. *Immunity* 8: 751-759.
18. Salmond, R. J., R. J. Brownlie, V. L. Morrison, and R. Zamoyska. 2014. The tyrosine phosphatase PTPN22 discriminates weak self peptides from strong agonist TCR signals. *Nat Immunol* 15: 875-883.
19. Huang, J., V. I. Zarnitsyna, B. Liu, L. J. Edwards, N. Jiang, B. D. Evavold, and C. Zhu. 2010. The kinetics of two-dimensional TCR and pMHC interactions determine T-cell responsiveness. *Nature* 464: 932-936.
20. Klein, L., B. Kyewski, P. M. Allen, and K. A. Hogquist. 2014. Positive and negative selection of the T cell repertoire: what thymocytes see (and don't see). *Nat Rev Immunol* 14: 377-391.
21. Gay, D., T. Saunders, S. Camper, and M. Weigert. 1993. Receptor editing: an approach by autoreactive B cells to escape tolerance. *J Exp Med* 177: 999-1008.
22. Nemazee, D., and K. Buerki. 1989. Clonal deletion of autoreactive B lymphocytes in bone marrow chimeras. *Proc Natl Acad Sci U S A* 86: 8039-8043.
23. Rolink, A. G., J. Andersson, and F. Melchers. 1998. Characterization of immature B cells by a novel monoclonal antibody, by turnover and by mitogen reactivity. *Eur J Immunol* 28: 3738-3748.
24. Wardemann, H., S. Yurasov, A. Schaefer, J. W. Young, E. Meffre, and M. C. Nussenzweig. 2003. Predominant autoantibody production by early human B cell precursors. *Science* 301: 1374-1377.

25. Pelanda, R., and R. M. Torres. 2012. Central B-cell tolerance: where selection begins. *Cold Spring Harb Perspect Biol* 4: a007146.
26. Huang, H., J. F. Kearney, M. J. Grusby, C. Benoist, and D. Mathis. 2006. Induction of tolerance in arthritogenic B cells with receptors of differing affinity for self-antigen. *Proc Natl Acad Sci U S A* 103: 3734-3739.
27. Goodnow, C. C., J. Crosbie, S. Adelstein, T. B. Lavoie, S. J. Smith-Gill, R. A. Brink, H. Pritchard-Briscoe, J. S. Wotherspoon, R. H. Loblay, K. Raphael, and et al. 1988. Altered immunoglobulin expression and functional silencing of self-reactive B lymphocytes in transgenic mice. *Nature* 334: 676-682.
28. Cambier, J. C., S. B. Gauld, K. T. Merrell, and B. J. Vilen. 2007. B-cell anergy: from transgenic models to naturally occurring anergic B cells? *Nat Rev Immunol* 7: 633-643.
29. Cooke, M. P., A. W. Heath, K. M. Shokat, Y. Zeng, F. D. Finkelman, P. S. Linsley, M. Howard, and C. C. Goodnow. 1994. Immunoglobulin signal transduction guides the specificity of B cell-T cell interactions and is blocked in tolerant self-reactive B cells. *J Exp Med* 179: 425-438.
30. Fulcher, D. A., and A. Basten. 1994. Reduced life span of anergic self-reactive B cells in a double-transgenic model. *J Exp Med* 179: 125-134.
31. Legoux, F. P., J. B. Lim, A. W. Cauley, S. Dikiy, J. Ertelt, T. J. Mariani, T. Sparwasser, S. S. Way, and J. J. Moon. 2015. CD4+ T Cell Tolerance to Tissue-Restricted Self Antigens Is Mediated by Antigen-Specific Regulatory T Cells Rather Than Deletion. *Immunity* 43: 896-908.
32. Malhotra, D., J. L. Linehan, T. Dileepan, Y. J. Lee, W. E. Purtha, J. V. Lu, R. W. Nelson, B. T. Fife, H. T. Orr, M. S. Anderson, K. A. Hogquist, and M. K. Jenkins. 2016. Tolerance is established in polyclonal CD4(+) T cells by distinct mechanisms, according to self-peptide expression patterns. *Nat Immunol* 17: 187-195.
33. Malchow, S., D. S. Leventhal, V. Lee, S. Nishi, N. D. Socci, and P. A. Savage. 2016. Aire Enforces Immune Tolerance by Directing Autoreactive T Cells into the Regulatory T Cell Lineage. *Immunity* 44: 1102-1113.
34. Xing, Y., and K. A. Hogquist. 2012. T-cell tolerance: central and peripheral. *Cold Spring Harb Perspect Biol* 4.
35. Sabatino, J. J., Jr., J. Huang, C. Zhu, and B. D. Evavold. 2011. High prevalence of low affinity peptide-MHC II tetramer-negative effectors during polyclonal CD4+ T cell responses. *J Exp Med* 208: 81-90.
36. Reich, D. S., C. F. Lucchinetti, and P. A. Calabresi. 2018. Multiple Sclerosis. *N Engl J Med* 378: 169-180.

37. International Multiple Sclerosis Genetics, C., A. H. Beecham, N. A. Patsopoulos, D. K. Xifara, M. F. Davis, A. Kemppinen, C. Cotsapas, T. S. Shah, C. Spencer, D. Booth, A. Goris, A. Oturai, J. Saarela, B. Fontaine, B. Hemmer, C. Martin, F. Zipp, S. D'Alfonso, F. Martinelli-Boneschi, B. Taylor, H. F. Harbo, I. Kockum, J. Hillert, T. Olsson, M. Ban, J. R. Oksenberg, R. Hintzen, L. F. Barcellos, C. Wellcome Trust Case Control, I. B. D. G. C. International, C. Agliardi, L. Alfredsson, M. Alizadeh, C. Anderson, R. Andrews, H. B. Sondergaard, A. Baker, G. Band, S. E. Baranzini, N. Barizzzone, J. Barrett, C. Bellenguez, L. Bergamaschi, L. Bernardinelli, A. Berthele, V. Biberacher, T. M. Binder, H. Blackburn, I. L. Bomfim, P. Brambilla, S. Broadley, B. Brochet, L. Brundin, D. Buck, H. Butzkueven, S. J. Caillier, W. Camu, W. Carpentier, P. Cavalla, E. G. Celius, I. Coman, G. Comi, L. Corrado, L. Cosemans, I. Cournu-Rebeix, B. A. Cree, D. Cusi, V. Damotte, G. Defer, S. R. Delgado, P. Deloukas, A. di Sapio, A. T. Dillet, P. Donnelly, B. Dubois, M. Duddy, S. Ekins, I. Elovaara, F. Esposito, N. Evangelou, B. Fiddes, J. Field, A. Franke, C. Freeman, I. Y. Frohlich, D. Galimberti, C. Gieger, P. A. Gourraud, C. Graetz, A. Graham, V. Grummel, C. Guaschino, A. Hadjixenofontos, H. Hakonarson, C. Halfpenny, G. Hall, P. Hall, A. Hamsten, J. Harley, T. Harrower, C. Hawkins, G. Hellenthal, C. Hillier, J. Hobart, M. Hoshi, S. E. Hunt, M. Jagodic, I. Jelcic, A. Jochim, B. Kendall, A. Kermode, T. Kilpatrick, K. Koivisto, I. Konidari, T. Korn, H. Kronsbein, C. Langford, M. Larsson, M. Lathrop, C. Lebrun-Frenay, J. Lechner-Scott, M. H. Lee, M. A. Leone, V. Leppa, G. Liberatore, B. A. Lie, C. M. Lill, M. Linden, J. Link, F. Luessi, J. Lycke, F. Macciardi, S. Mannisto, C. P. Manrique, R. Martin, V. Martinelli, D. Mason, G. Mazibrada, C. McCabe, I. L. Mero, J. Mescheriakova, L. Moutsianas, K. M. Myhr, G. Nagels, R. Nicholas, P. Nilsson, F. Piehl, M. Pirinen, S. E. Price, H. Quach, M. Reunanen, W. Robberecht, N. P. Robertson, M. Rodegher, D. Rog, M. Salvetti, N. C. Schnetz-Boutaud, F. Sellebjerg, R. C. Selter, C. Schaefer, S. Shaunak, L. Shen, S. Shields, V. Siffrin, M. Slee, P. S. Sorensen, M. Sorosina, M. Sospedra, A. Spurkland, A. Strange, E. Sundqvist, V. Thijs, J. Thorpe, A. Ticca, P. Tienari, C. van Duijn, E. M. Visser, S. Vucic, H. Westerlind, J. S. Wiley, A. Wilkins, J. F. Wilson, J. Winkelmann, J. Zajicek, E. Zindler, J. L. Haines, M. A. Pericak-Vance, A. J. Ivinson, G. Stewart, D. Hafler, S. L. Hauser, A. Compston, G. McVean, P. De Jager, S. J. Sawcer, and J. L. McCauley. 2013. Analysis of immune-related loci identifies 48 new susceptibility variants for multiple sclerosis. *Nat Genet* 45: 1353-1360.
38. Baxter, A. G. 2007. The origin and application of experimental autoimmune encephalomyelitis. *Nat Rev Immunol* 7: 904-912.
39. Lassmann, H., and M. Bradl. 2017. Multiple sclerosis: experimental models and reality. *Acta Neuropathol* 133: 223-244.
40. Rangachari, M., and V. K. Kuchroo. 2013. Using EAE to better understand principles of immune function and autoimmune pathology. *J Autoimmun* 45: 31-39.

41. Fillatreau, S., C. H. Sweeney, M. J. McGeachy, D. Gray, and S. M. Anderton. 2002. B cells regulate autoimmunity by provision of IL-10. *Nat Immunol* 3: 944-950.
42. Matsushita, T., K. Yanaba, J. D. Bouaziz, M. Fujimoto, and T. F. Tedder. 2008. Regulatory B cells inhibit EAE initiation in mice while other B cells promote disease progression. *J Clin Invest* 118: 3420-3430.
43. Shen, P., T. Roch, V. Lampropoulou, R. A. O'Connor, U. Stervbo, E. Hilgenberg, S. Ries, V. D. Dang, Y. Jaimes, C. Daridon, R. Li, L. Jouneau, P. Boudinot, S. Wilantri, I. Sakwa, Y. Miyazaki, M. D. Leech, R. C. McPherson, S. Wirtz, M. Neurath, K. Hoehlig, E. Meinel, A. Grutzkau, J. R. Grun, K. Horn, A. A. Kuhl, T. Dorner, A. Bar-Or, S. H. E. Kaufmann, S. M. Anderton, and S. Fillatreau. 2014. IL-35-producing B cells are critical regulators of immunity during autoimmune and infectious diseases. *Nature* 507: 366-370.
44. Yoshizaki, A., T. Miyagaki, D. J. DiLillo, T. Matsushita, M. Horikawa, E. I. Kountikov, R. Spolski, J. C. Poe, W. J. Leonard, and T. F. Tedder. 2012. Regulatory B cells control T-cell autoimmunity through IL-21-dependent cognate interactions. *Nature* 491: 264-268.
45. Hauser, S. L., E. Waubant, D. L. Arnold, T. Vollmer, J. Antel, R. J. Fox, A. Bar-Or, M. Panzara, N. Sarkar, S. Agarwal, A. Langer-Gould, C. H. Smith, and H. T. Group. 2008. B-cell depletion with rituximab in relapsing-remitting multiple sclerosis. *N Engl J Med* 358: 676-688.
46. Montalban, X., S. L. Hauser, L. Kappos, D. L. Arnold, A. Bar-Or, G. Comi, J. de Seze, G. Giovannoni, H. P. Hartung, B. Hemmer, F. Lublin, K. W. Rammohan, K. Selmaj, A. Traboulsee, A. Sauter, D. Masterman, P. Fontoura, S. Belachew, H. Garren, N. Mairon, P. Chin, J. S. Wolinsky, and O. C. Investigators. 2017. Ocrelizumab versus Placebo in Primary Progressive Multiple Sclerosis. *N Engl J Med* 376: 209-220.
47. Knippenberg, S., E. Peelen, J. Smolders, M. Thewissen, P. Menheere, J. W. Cohen Tervaert, R. Hupperts, and J. Damoiseaux. 2011. Reduction in IL-10 producing B cells (Breg) in multiple sclerosis is accompanied by a reduced naive/memory Breg ratio during a relapse but not in remission. *J Neuroimmunol* 239: 80-86.
48. Li, R., A. Rezk, Y. Miyazaki, E. Hilgenberg, H. Touil, P. Shen, C. S. Moore, L. Michel, F. Althekair, S. Rajasekharan, J. L. Gommerman, A. Prat, S. Fillatreau, A. Bar-Or, and B. c. i. M. S. T. Canadian. 2015. Proinflammatory GM-CSF-producing B cells in multiple sclerosis and B cell depletion therapy. *Sci Transl Med* 7: 310ra166.
49. Molnarfi, N., U. Schulze-Topphoff, M. S. Weber, J. C. Patarroyo, T. Prod'homme, M. Varrin-Doyer, A. Shetty, C. Linington, A. J. Slavin, J. Hidalgo, D. E. Jenne, H. Wekerle, R. A. Sobel, C. C. Bernard, M. J. Shlomchik, and S. S.

- Zamvil. 2013. MHC class II-dependent B cell APC function is required for induction of CNS autoimmunity independent of myelin-specific antibodies. *J Exp Med* 210: 2921-2937.
50. Dubey, D., T. Forsthuber, E. P. Flanagan, S. J. Pittock, and O. Stuve. 2017. B-cell-targeted therapies in relapsing forms of MS. *Neurol Neuroimmunol Neuroinflamm* 4: e405.
 51. Salzer, J., R. Svenningsson, P. Alping, L. Novakova, A. Bjorck, K. Fink, P. Islam-Jakobsson, C. Malmstrom, M. Axelsson, M. Vagberg, P. Sundstrom, J. Lycke, F. Piehl, and A. Svenningsson. 2016. Rituximab in multiple sclerosis: A retrospective observational study on safety and efficacy. *Neurology* 87: 2074-2081.
 52. Hess, C., A. Winkler, A. K. Lorenz, V. Holecska, V. Blanchard, S. Eiglmeier, A. L. Schoen, J. Bitterling, A. D. Stoehr, D. Petzold, T. Schommartz, M. M. Mertes, C. T. Schoen, B. Tiburzy, A. Herrmann, J. Kohl, R. A. Manz, M. P. Madaio, M. Berger, H. Wardemann, and M. Ehlers. 2013. T cell-independent B cell activation induces immunosuppressive sialylated IgG antibodies. *J Clin Invest* 123: 3788-3796.
 53. Bowers, P. M., P. Verdino, Z. Wang, J. da Silva Correia, M. Chhoa, G. Macondray, M. Do, T. Y. Neben, R. A. Horlick, R. L. Stanfield, I. A. Wilson, and D. J. King. 2014. Nucleotide insertions and deletions complement point mutations to massively expand the diversity created by somatic hypermutation of antibodies. *J Biol Chem* 289: 33557-33567.
 54. Hwang, J. K., F. W. Alt, and L. S. Yeap. 2015. Related Mechanisms of Antibody Somatic Hypermutation and Class Switch Recombination. *Microbiol Spectr* 3: MDNA3-0037-2014.
 55. Surova, E., and H. Jumaa. 2014. The role of BCR isotype in B-cell development and activation. *Adv Immunol* 123: 101-139.
 56. Yang, Z., M. J. Robinson, X. Chen, G. A. Smith, J. Taunton, W. Liu, and C. D. Allen. 2016. Regulation of B cell fate by chronic activity of the IgE B cell receptor. *Elife* 5.
 57. Liu, W., T. Meckel, P. Tolar, H. W. Sohn, and S. K. Pierce. 2010. Intrinsic properties of immunoglobulin IgG1 isotype-switched B cell receptors promote microclustering and the initiation of signaling. *Immunity* 32: 778-789.
 58. Mesin, L., J. Ersching, and G. D. Victora. 2016. Germinal Center B Cell Dynamics. *Immunity* 45: 471-482.
 59. Probstel, A. K., K. Dornmair, R. Bittner, P. Sperl, D. Jenne, S. Magalhaes, A. Villalobos, C. Breithaupt, R. Weissert, U. Jacob, M. Krumbholz, T. Kuempfel, A. Blaschek, W. Stark, J. Gartner, D. Pohl, K. Rostasy, F. Weber, I. Forne, M.

- Khademi, T. Olsson, F. Brilot, E. Tantsis, R. C. Dale, H. Wekerle, R. Hohlfeld, B. Banwell, A. Bar-Or, E. Meinl, and T. Derfuss. 2011. Antibodies to MOG are transient in childhood acute disseminated encephalomyelitis. *Neurology* 77: 580-588.
60. Mariotto, S., S. Ferrari, S. Monaco, M. D. Benedetti, K. Schanda, D. Alberti, A. Farinazzo, R. Capra, C. Mancinelli, N. De Rossi, R. Bombardi, L. Zuliani, M. Zoccarato, R. Tanel, A. Bonora, M. Turatti, M. Calabrese, A. Polo, A. Pavone, L. Grazian, G. Sechi, E. Sechi, D. Urso, R. Delogu, F. Janes, L. Deotto, M. Cadaldini, M. R. Bianchi, G. Cantalupo, M. Reindl, and A. Gajofatto. 2017. Clinical spectrum and IgG subclass analysis of anti-myelin oligodendrocyte glycoprotein antibody-associated syndromes: a multicenter study. *J Neurol* 264: 2420-2430.
61. Reindl, M., F. Di Pauli, K. Rostasy, and T. Berger. 2013. The spectrum of MOG autoantibody-associated demyelinating diseases. *Nat Rev Neurol* 9: 455-461.
62. Zhou, D., R. Srivastava, S. Nessler, V. Grummel, N. Sommer, W. Bruck, H. P. Hartung, C. Stadelmann, and B. Hemmer. 2006. Identification of a pathogenic antibody response to native myelin oligodendrocyte glycoprotein in multiple sclerosis. *Proc Natl Acad Sci U S A* 103: 19057-19062.
63. Blauth, K., J. Soltys, A. Matschulat, C. R. Reiter, A. Ritchie, N. L. Baird, J. L. Bennett, and G. P. Owens. 2015. Antibodies produced by clonally expanded plasma cells in multiple sclerosis cerebrospinal fluid cause demyelination of spinal cord explants. *Acta Neuropathol* 130: 765-781.
64. Quintana, F. J., B. Patel, A. Yeste, M. Nyirenda, J. Kenison, R. Rahbari, D. Fetco, M. Hussain, J. O'Mahony, S. Magalhaes, M. McGowan, T. Johnson, S. Rajasekharan, S. Narayanan, D. L. Arnold, H. L. Weiner, B. Banwell, A. Bar-Or, and N. Canadian Pediatric Demyelinating Disease. 2014. Epitope spreading as an early pathogenic event in pediatric multiple sclerosis. *Neurology* 83: 2219-2226.
65. Galicia, G., D. S. W. Lee, V. Ramaglia, L. A. Ward, J. Y. Yam, L. Y. T. Leung, R. Li, M. Handy, J. Zhang, P. C. Drohomyrecky, E. Lancaster, A. Bar-Or, A. Martin, and J. L. Gommerman. 2018. Isotype-Switched Autoantibodies Are Necessary To Facilitate Central Nervous System Autoimmune Disease in *Aicda*(^{-/-}) and *Ung*(^{-/-}) Mice. *J Immunol* 201: 1119-1130.
66. Krishnamoorthy, G., H. Lassmann, H. Wekerle, and A. Holz. 2006. Spontaneous opticospinal encephalomyelitis in a double-transgenic mouse model of autoimmune T cell/B cell cooperation. *J Clin Invest* 116: 2385-2392.
67. Parker Harp, C. R., A. S. Archambault, J. Sim, M. J. Shlomchik, J. H. Russell, and G. F. Wu. 2018. B cells are capable of independently eliciting rapid reactivation of encephalitogenic CD4 T cells in a murine model of multiple sclerosis. *PLoS One* 13: e0199694.

68. de Vos, A. F., M. van Meurs, H. P. Brok, L. A. Boven, R. Q. Hintzen, P. van der Valk, R. Ravid, S. Rensing, L. Boon, B. A. t Hart, and J. D. Laman. 2002. Transfer of central nervous system autoantigens and presentation in secondary lymphoid organs. *J Immunol* 169: 5415-5423.
69. Fabriek, B. O., J. N. Zwemmer, C. E. Teunissen, C. D. Dijkstra, C. H. Polman, J. D. Laman, and J. A. Castelijns. 2005. In vivo detection of myelin proteins in cervical lymph nodes of MS patients using ultrasound-guided fine-needle aspiration cytology. *J Neuroimmunol* 161: 190-194.
70. Louveau, A., I. Smirnov, T. J. Keyes, J. D. Eccles, S. J. Rouhani, J. D. Peske, N. C. Derecki, D. Castle, J. W. Mandell, K. S. Lee, T. H. Harris, and J. Kipnis. 2015. Structural and functional features of central nervous system lymphatic vessels. *Nature* 523: 337-341.
71. Palanichamy, A., L. Apeltsin, T. C. Kuo, M. Sirota, S. Wang, S. J. Pitts, P. D. Sundar, D. Telman, L. Z. Zhao, M. Derstine, A. Abounasr, S. L. Hauser, and H. C. von Budingen. 2014. Immunoglobulin class-switched B cells form an active immune axis between CNS and periphery in multiple sclerosis. *Sci Transl Med* 6: 248ra106.
72. Stern, J. N., G. Yaari, J. A. Vander Heiden, G. Church, W. F. Donahue, R. Q. Hintzen, A. J. Huttner, J. D. Laman, R. M. Nagra, A. Nylander, D. Pitt, S. Ramanan, B. A. Siddiqui, F. Vigneault, S. H. Kleinstein, D. A. Hafler, and K. C. O'Connor. 2014. B cells populating the multiple sclerosis brain mature in the draining cervical lymph nodes. *Sci Transl Med* 6: 248ra107.
73. Chang, J. E., and S. J. Turley. 2015. Stromal infrastructure of the lymph node and coordination of immunity. *Trends Immunol* 36: 30-39.
74. Steiniger, B. S. 2015. Human spleen microanatomy: why mice do not suffice. *Immunology* 145: 334-346.
75. Choi, I., S. Lee, and Y. K. Hong. 2012. The new era of the lymphatic system: no longer secondary to the blood vascular system. *Cold Spring Harb Perspect Med* 2: a006445.
76. Qian, C., and X. Cao. 2018. Dendritic cells in the regulation of immunity and inflammation. *Semin Immunol* 35: 3-11.
77. Cyster, J. G. 2010. B cell follicles and antigen encounters of the third kind. *Nat Immunol* 11: 989-996.
78. Kerfoot, S. M., G. Yaari, J. R. Patel, K. L. Johnson, D. G. Gonzalez, S. H. Kleinstein, and A. M. Haberman. 2011. Germinal center B cell and T follicular helper cell development initiates in the interfollicular zone. *Immunity* 34: 947-960.

79. Dufaud, C. R., L. J. McHeyzer-Williams, and M. G. McHeyzer-Williams. 2017. Deconstructing the germinal center, one cell at a time. *Curr Opin Immunol* 45: 112-118.
80. Sixt, M., N. Kanazawa, M. Selg, T. Samson, G. Roos, D. P. Reinhardt, R. Pabst, M. B. Lutz, and L. Sorokin. 2005. The conduit system transports soluble antigens from the afferent lymph to resident dendritic cells in the T cell area of the lymph node. *Immunity* 22: 19-29.
81. Carrasco, Y. R., and F. D. Batista. 2007. B cells acquire particulate antigen in a macrophage-rich area at the boundary between the follicle and the subcapsular sinus of the lymph node. *Immunity* 27: 160-171.
82. Qi, H., J. G. Egen, A. Y. Huang, and R. N. Germain. 2006. Extrafollicular activation of lymph node B cells by antigen-bearing dendritic cells. *Science* 312: 1672-1676.
83. Heesters, B. A., P. Chatterjee, Y. A. Kim, S. F. Gonzalez, M. P. Kuligowski, T. Kirchhausen, and M. C. Carroll. 2013. Endocytosis and recycling of immune complexes by follicular dendritic cells enhances B cell antigen binding and activation. *Immunity* 38: 1164-1175.
84. Suzuki, K., I. Grigorova, T. G. Phan, L. M. Kelly, and J. G. Cyster. 2009. Visualizing B cell capture of cognate antigen from follicular dendritic cells. *J Exp Med* 206: 1485-1493.
85. Braun, A., T. Worbs, G. L. Moschovakis, S. Halle, K. Hoffmann, J. Bolter, A. Munk, and R. Forster. 2011. Afferent lymph-derived T cells and DCs use different chemokine receptor CCR7-dependent routes for entry into the lymph node and intranodal migration. *Nat Immunol* 12: 879-887.
86. Denton, A. E., E. W. Roberts, M. A. Linterman, and D. T. Fearon. 2014. Fibroblastic reticular cells of the lymph node are required for retention of resting but not activated CD8+ T cells. *Proc Natl Acad Sci U S A* 111: 12139-12144.
87. Liu, C., X. V. Yang, J. Wu, C. Kuei, N. S. Mani, L. Zhang, J. Yu, S. W. Sutton, N. Qin, H. Banie, L. Karlsson, S. Sun, and T. W. Lovenberg. 2011. Oxysterols direct B-cell migration through EBI2. *Nature* 475: 519-523.
88. Muller, G., and M. Lipp. 2003. Shaping up adaptive immunity: the impact of CCR7 and CXCR5 on lymphocyte trafficking. *Microcirculation* 10: 325-334.
89. Hannedouche, S., J. Zhang, T. Yi, W. Shen, D. Nguyen, J. P. Pereira, D. Guerini, B. U. Baumgarten, S. Roggo, B. Wen, R. Knochenmuss, S. Noel, F. Gessier, L. M. Kelly, M. Vanek, S. Laurent, I. Preuss, C. Miault, I. Christen, R. Karuna, W. Li, D. I. Koo, T. Suply, C. Schmedt, E. C. Peters, R. Falchetto, A. Katopodis, C. Spanka, M. O. Roy, M. Detheux, Y. A. Chen, P. G. Schultz, C. Y. Cho, K.

- Seuwen, J. G. Cyster, and A. W. Sailer. 2011. Oxysterols direct immune cell migration via EBI2. *Nature* 475: 524-527.
90. Mempel, T. R., S. E. Henrickson, and U. H. Von Andrian. 2004. T-cell priming by dendritic cells in lymph nodes occurs in three distinct phases. *Nature* 427: 154-159.
 91. Benson, R. A., M. K. MacLeod, B. G. Hale, A. Patakas, P. Garside, and J. M. Brewer. 2015. Antigen presentation kinetics control T cell/dendritic cell interactions and follicular helper T cell generation in vivo. *Elife* 4.
 92. Schmitt, N., and H. Ueno. 2015. Regulation of human helper T cell subset differentiation by cytokines. *Curr Opin Immunol* 34: 130-136.
 93. Shiner, E. K., B. C. Holbrook, and M. A. Alexander-Miller. 2014. CD4⁺ T cell subset differentiation and avidity setpoint are dictated by the interplay of cytokine and antigen mediated signals. *PLoS One* 9: e100175.
 94. Vinuesa, C. G., M. A. Linterman, D. Yu, and I. C. MacLennan. 2016. Follicular Helper T Cells. *Annu Rev Immunol* 34: 335-368.
 95. Wang, X., B. Cho, K. Suzuki, Y. Xu, J. A. Green, J. An, and J. G. Cyster. 2011. Follicular dendritic cells help establish follicle identity and promote B cell retention in germinal centers. *J Exp Med* 208: 2497-2510.
 96. Qi, H., X. Chen, C. Chu, P. Lu, H. Xu, and J. Yan. 2014. Follicular T-helper cells: controlled localization and cellular interactions. *Immunol Cell Biol* 92: 28-33.
 97. Okada, T., M. J. Miller, I. Parker, M. F. Krummel, M. Neighbors, S. B. Hartley, A. O'Garra, M. D. Cahalan, and J. G. Cyster. 2005. Antigen-engaged B cells undergo chemotaxis toward the T zone and form motile conjugates with helper T cells. *PLoS Biol* 3: e150.
 98. Deenick, E. K., A. Chan, C. S. Ma, D. Gatto, P. L. Schwartzberg, R. Brink, and S. G. Tangye. 2010. Follicular helper T cell differentiation requires continuous antigen presentation that is independent of unique B cell signaling. *Immunity* 33: 241-253.
 99. Blink, E. J., A. Light, A. Kallies, S. L. Nutt, P. D. Hodgkin, and D. M. Tarlinton. 2005. Early appearance of germinal center-derived memory B cells and plasma cells in blood after primary immunization. *J Exp Med* 201: 545-554.
 100. Weisel, F., and M. Shlomchik. 2017. Memory B Cells of Mice and Humans. *Annu Rev Immunol* 35: 255-284.
 101. Bohannon, C., R. Powers, L. Satyabhama, A. Cui, C. Tipton, M. Michaeli, I. Skountzou, R. S. Mittler, S. H. Kleinstein, R. Mehr, F. E. Lee, I. Sanz, and J.

- Jacob. 2016. Long-lived antigen-induced IgM plasma cells demonstrate somatic mutations and contribute to long-term protection. *Nat Commun* 7: 11826.
102. Pape, K. A., J. J. Taylor, R. W. Maul, P. J. Gearhart, and M. K. Jenkins. 2011. Different B cell populations mediate early and late memory during an endogenous immune response. *Science* 331: 1203-1207.
103. Stavnezer, J., and C. E. Schrader. 2014. IgH chain class switch recombination: mechanism and regulation. *J Immunol* 193: 5370-5378.
104. Burnett, D. L., D. B. Langley, P. Schofield, J. R. Hermes, T. D. Chan, J. Jackson, K. Bourne, J. H. Reed, K. Patterson, B. T. Porebski, R. Brink, D. Christ, and C. C. Goodnow. 2018. Germinal center antibody mutation trajectories are determined by rapid self/foreign discrimination. *Science* 360: 223-226.
105. Cui, A., R. Di Niro, J. A. Vander Heiden, A. W. Briggs, K. Adams, T. Gilbert, K. C. O'Connor, F. Vigneault, M. J. Shlomchik, and S. H. Kleinstein. 2016. A Model of Somatic Hypermutation Targeting in Mice Based on High-Throughput Ig Sequencing Data. *J Immunol* 197: 3566-3574.
106. Shulman, Z., A. D. Gitlin, J. S. Weinstein, B. Lainez, E. Esplugues, R. A. Flavell, J. E. Craft, and M. C. Nussenzweig. 2014. Dynamic signaling by T follicular helper cells during germinal center B cell selection. *Science* 345: 1058-1062.
107. Klein, U., and R. Dalla-Favera. 2008. Germinal centres: role in B-cell physiology and malignancy. *Nat Rev Immunol* 8: 22-33.
108. Bannard, O., R. M. Horton, C. D. Allen, J. An, T. Nagasawa, and J. G. Cyster. 2013. Germinal center centroblasts transition to a centrocyte phenotype according to a timed program and depend on the dark zone for effective selection. *Immunity* 39: 912-924.
109. Haynes, N. M., C. D. Allen, R. Lesley, K. M. Ansel, N. Killeen, and J. G. Cyster. 2007. Role of CXCR5 and CCR7 in follicular Th cell positioning and appearance of a programmed cell death gene-1high germinal center-associated subpopulation. *J Immunol* 179: 5099-5108.
110. Heesters, B. A., R. C. Myers, and M. C. Carroll. 2014. Follicular dendritic cells: dynamic antigen libraries. *Nat Rev Immunol* 14: 495-504.
111. Luo, W., F. Weisel, and M. J. Shlomchik. 2018. B Cell Receptor and CD40 Signaling Are Rewired for Synergistic Induction of the c-Myc Transcription Factor in Germinal Center B Cells. *Immunity* 48: 313-326 e315.
112. Vitorica, G. D., T. A. Schwickert, D. R. Fooksman, A. O. Kamphorst, M. Meyer-Hermann, M. L. Dustin, and M. C. Nussenzweig. 2010. Germinal center dynamics revealed by multiphoton microscopy with a photoactivatable fluorescent reporter. *Cell* 143: 592-605.

113. Zaretsky, I., O. Atrakchi, R. D. Mazor, L. Stoler-Barak, A. Biram, S. W. Feigelson, A. D. Gitlin, B. Engelhardt, and Z. Shulman. 2017. ICAMs support B cell interactions with T follicular helper cells and promote clonal selection. *J Exp Med* 214: 3435-3448.
114. Rodda, L. B., O. Bannard, B. Ludewig, T. Nagasawa, and J. G. Cyster. 2015. Phenotypic and Morphological Properties of Germinal Center Dark Zone Cxcl12-Expressing Reticular Cells. *J Immunol* 195: 4781-4791.
115. Gitlin, A. D., Z. Shulman, and M. C. Nussenzweig. 2014. Clonal selection in the germinal centre by regulated proliferation and hypermutation. *Nature* 509: 637-640.
116. Hauser, A. E., T. Junt, T. R. Mempel, M. W. Sneddon, S. H. Kleinstein, S. E. Henrickson, U. H. von Andrian, M. J. Shlomchik, and A. M. Haberman. 2007. Definition of germinal-center B cell migration in vivo reveals predominant intrazonal circulation patterns. *Immunity* 26: 655-667.
117. Gitlin, A. D., C. T. Mayer, T. Y. Oliveira, Z. Shulman, M. J. Jones, A. Koren, and M. C. Nussenzweig. 2015. HUMORAL IMMUNITY. T cell help controls the speed of the cell cycle in germinal center B cells. *Science* 349: 643-646.
118. Taylor, J. J., K. A. Pape, H. R. Steach, and M. K. Jenkins. 2015. Humoral immunity. Apoptosis and antigen affinity limit effector cell differentiation of a single naive B cell. *Science* 347: 784-787.
119. Engels, N., L. M. Konig, C. Heemann, J. Lutz, T. Tsubata, S. Griep, V. Schrader, and J. Wienands. 2009. Recruitment of the cytoplasmic adaptor Grb2 to surface IgG and IgE provides antigen receptor-intrinsic costimulation to class-switched B cells. *Nat Immunol* 10: 1018-1025.
120. Wan, Z., X. Chen, H. Chen, Q. Ji, Y. Chen, J. Wang, Y. Cao, F. Wang, J. Lou, Z. Tang, and W. Liu. 2015. The activation of IgM- or isotype-switched IgG- and IgE-BCR exhibits distinct mechanical force sensitivity and threshold. *Elife* 4.
121. Brink, R., T. G. Phan, D. Paus, and T. D. Chan. 2008. Visualizing the effects of antigen affinity on T-dependent B-cell differentiation. *Immunol Cell Biol* 86: 31-39.
122. Dal Porto, J. M., A. M. Haberman, M. J. Shlomchik, and G. Kelsoe. 1998. Antigen drives very low affinity B cells to become plasmacytes and enter germinal centers. *J Immunol* 161: 5373-5381.
123. Tas, J. M., L. Mesin, G. Pasqual, S. Targ, J. T. Jacobsen, Y. M. Mano, C. S. Chen, J. C. Weill, C. A. Reynaud, E. P. Browne, M. Meyer-Hermann, and G. D. Victora. 2016. Visualizing antibody affinity maturation in germinal centers. *Science* 351: 1048-1054.

124. Cirelli, K. M., and S. Crotty. 2017. Germinal center enhancement by extended antigen availability. *Curr Opin Immunol* 47: 64-69.
125. Greczmiel, U., N. J. Krautler, A. Pedrioli, I. Bartsch, P. Agnellini, G. Bedenikovic, J. Harker, K. Richter, and A. Oxenius. 2017. Sustained T follicular helper cell response is essential for control of chronic viral infection. *Sci Immunol* 2.
126. Weisel, F. J., G. V. Zuccarino-Catania, M. Chikina, and M. J. Shlomchik. 2016. A Temporal Switch in the Germinal Center Determines Differential Output of Memory B and Plasma Cells. *Immunity* 44: 116-130.
127. Shinnakasu, R., T. Inoue, K. Kometani, S. Moriyama, Y. Adachi, M. Nakayama, Y. Takahashi, H. Fukuyama, T. Okada, and T. Kurosaki. 2016. Regulated selection of germinal-center cells into the memory B cell compartment. *Nat Immunol* 17: 861-869.
128. Krautler, N. J., D. Suan, D. Butt, K. Bourne, J. R. Hermes, T. D. Chan, C. Sundling, W. Kaplan, P. Schofield, J. Jackson, A. Basten, D. Christ, and R. Brink. 2017. Differentiation of germinal center B cells into plasma cells is initiated by high-affinity antigen and completed by Tfh cells. *J Exp Med* 214: 1259-1267.
129. Toyama, H., S. Okada, M. Hatano, Y. Takahashi, N. Takeda, H. Ichii, T. Takemori, Y. Kuroda, and T. Tokuhsa. 2002. Memory B cells without somatic hypermutation are generated from Bcl6-deficient B cells. *Immunity* 17: 329-339.
130. Choi, Y. S., J. A. Yang, and S. Crotty. 2013. Dynamic regulation of Bcl6 in follicular helper CD4 T (Tfh) cells. *Curr Opin Immunol* 25: 366-372.
131. Fukuda, T., T. Yoshida, S. Okada, M. Hatano, T. Miki, K. Ishibashi, S. Okabe, H. Koseki, S. Hirosawa, M. Taniguchi, N. Miyasaka, and T. Tokuhsa. 1997. Disruption of the Bcl6 gene results in an impaired germinal center formation. *J Exp Med* 186: 439-448.
132. Tomayko, M. M., S. M. Anderson, C. E. Brayton, S. Sadanand, N. C. Steinle, T. W. Behrens, and M. J. Shlomchik. 2008. Systematic comparison of gene expression between murine memory and naive B cells demonstrates that memory B cells have unique signaling capabilities. *J Immunol* 181: 27-38.
133. Klein, U., R. Kuppers, and K. Rajewsky. 1997. Evidence for a large compartment of IgM-expressing memory B cells in humans. *Blood* 89: 1288-1298.
134. Inamine, A., Y. Takahashi, N. Baba, K. Miyake, T. Tokuhsa, T. Takemori, and R. Abe. 2005. Two waves of memory B-cell generation in the primary immune response. *Int Immunol* 17: 581-589.
135. Zuccarino-Catania, G. V., S. Sadanand, F. J. Weisel, M. M. Tomayko, H. Meng, S. H. Kleinstein, K. L. Good-Jacobson, and M. J. Shlomchik. 2014. CD80 and

- PD-L2 define functionally distinct memory B cell subsets that are independent of antibody isotype. *Nat Immunol* 15: 631-637.
136. Isnardi, I., Y. S. Ng, L. Menard, G. Meyers, D. Saadoun, I. Srdanovic, J. Samuels, J. Berman, J. H. Buckner, C. Cunningham-Rundles, and E. Meffre. 2010. Complement receptor 2/CD21- human naive B cells contain mostly autoreactive unresponsive clones. *Blood* 115: 5026-5036.
 137. Portugal, S., C. M. Tipton, H. Sohn, Y. Kone, J. Wang, S. Li, J. Skinner, K. Virtaneva, D. E. Sturdevant, S. F. Porcella, O. K. Doumbo, S. Doumbo, K. Kayentao, A. Ongoiba, B. Traore, I. Sanz, S. K. Pierce, and P. D. Crompton. 2015. Malaria-associated atypical memory B cells exhibit markedly reduced B cell receptor signaling and effector function. *Elife* 4.
 138. Moir, S., J. Ho, A. Malaspina, W. Wang, A. C. DiPoto, M. A. O'Shea, G. Roby, S. Kottlil, J. Arthos, M. A. Proschan, T. W. Chun, and A. S. Fauci. 2008. Evidence for HIV-associated B cell exhaustion in a dysfunctional memory B cell compartment in HIV-infected viremic individuals. *J Exp Med* 205: 1797-1805.
 139. Dauby, N., C. Kummert, S. Lecomte, C. Liesnard, M. L. Delforge, C. Donner, and A. Marchant. 2014. Primary human cytomegalovirus infection induces the expansion of virus-specific activated and atypical memory B cells. *J Infect Dis* 210: 1275-1285.
 140. Charles, E. D., C. Brunetti, S. Marukian, K. D. Ritola, A. H. Talal, K. Marks, I. M. Jacobson, C. M. Rice, and L. B. Dustin. 2011. Clonal B cells in patients with hepatitis C virus-associated mixed cryoglobulinemia contain an expanded anergic CD21^{low} B-cell subset. *Blood* 117: 5425-5437.
 141. Claes, N., J. Fraussen, M. Vanheusden, N. Hellings, P. Stinissen, B. Van Wijmeersch, R. Hupperts, and V. Somers. 2016. Age-Associated B Cells with Proinflammatory Characteristics Are Expanded in a Proportion of Multiple Sclerosis Patients. *J Immunol* 197: 4576-4583.
 142. Thorarinsdottir, K., A. Camponeschi, I. Gjertsson, and I. L. Martensson. 2015. CD21^{-/low} B cells: A Snapshot of a Unique B Cell Subset in Health and Disease. *Scand J Immunol* 82: 254-261.
 143. Seifert, M., M. Przekopowicz, S. Taudien, A. Lollies, V. Ronge, B. Drees, M. Lindemann, U. Hillen, H. Engler, B. B. Singer, and R. Kuppers. 2015. Functional capacities of human IgM memory B cells in early inflammatory responses and secondary germinal center reactions. *Proc Natl Acad Sci U S A* 112: E546-555.
 144. Dal Porto, J. M., A. M. Haberman, G. Kelsoe, and M. J. Shlomchik. 2002. Very low affinity B cells form germinal centers, become memory B cells, and participate in secondary immune responses when higher affinity competition is reduced. *J Exp Med* 195: 1215-1221.

145. Davey, A. M., and S. K. Pierce. 2012. Intrinsic differences in the initiation of B cell receptor signaling favor responses of human IgG(+) memory B cells over IgM(+) naive B cells. *J Immunol* 188: 3332-3341.
146. Rubtsov, A. V., K. Rubtsova, A. Fischer, R. T. Meehan, J. Z. Gillis, J. W. Kappler, and P. Marrack. 2011. Toll-like receptor 7 (TLR7)-driven accumulation of a novel CD11c(+) B-cell population is important for the development of autoimmunity. *Blood* 118: 1305-1315.
147. Rubtsova, K., A. V. Rubtsov, M. P. Cancro, and P. Marrack. 2015. Age-Associated B Cells: A T-bet-Dependent Effector with Roles in Protective and Pathogenic Immunity. *J Immunol* 195: 1933-1937.
148. Rubtsov, A. V., K. Rubtsova, J. W. Kappler, J. Jacobelli, R. S. Friedman, and P. Marrack. 2015. CD11c-Expressing B Cells Are Located at the T Cell/B Cell Border in Spleen and Are Potent APCs. *J Immunol* 195: 71-79.
149. Kenderes, K. J., R. C. Levack, A. M. Papillion, B. Cabrera-Martinez, L. M. Dishaw, and G. M. Winslow. 2018. T-Bet(+) IgM Memory Cells Generate Multi-lineage Effector B Cells. *Cell Rep* 24: 824-837 e823.
150. Wang, Y., J. Shi, J. Yan, Z. Xiao, X. Hou, P. Lu, S. Hou, T. Mao, W. Liu, Y. Ma, L. Zhang, X. Yang, and H. Qi. 2017. Germinal-center development of memory B cells driven by IL-9 from follicular helper T cells. *Nat Immunol* 18: 921-930.
151. Good-Jacobson, K. L. 2018. Strength in diversity: Phenotypic, functional, and molecular heterogeneity within the memory B cell repertoire. *Immunol Rev* 284: 67-78.
152. Suan, D., N. J. Krautler, J. L. V. Maag, D. Butt, K. Bourne, J. R. Hermes, D. T. Avery, C. Young, A. Statham, M. Elliott, M. E. Dinger, A. Basten, S. G. Tangye, and R. Brink. 2017. CCR6 Defines Memory B Cell Precursors in Mouse and Human Germinal Centers, Revealing Light-Zone Location and Predominant Low Antigen Affinity. *Immunity* 47: 1142-1153 e1144.
153. Crowe, J. E., Jr. 2017. Principles of Broad and Potent Antiviral Human Antibodies: Insights for Vaccine Design. *Cell Host Microbe* 22: 193-206.
154. Romanelli, E., D. Merkler, A. Mezydlo, M. T. Weil, M. S. Weber, I. Nikic, S. Potz, E. Meinl, F. E. Matznick, M. Kreutzfeldt, A. Ghanem, K. K. Conzelmann, I. Metz, W. Bruck, M. Routh, M. Simons, D. Bishop, T. Misgeld, and M. Kerschensteiner. 2016. Myelinosome formation represents an early stage of oligodendrocyte damage in multiple sclerosis and its animal model. *Nat Commun* 7: 13275.
155. Ribatti, D. 2017. The discovery of plasma cells: An historical note. *Immunol Lett* 188: 64-67.

156. Chan, T. D., D. Gatto, K. Wood, T. Camidge, A. Basten, and R. Brink. 2009. Antigen affinity controls rapid T-dependent antibody production by driving the expansion rather than the differentiation or extrafollicular migration of early plasmablasts. *J Immunol* 183: 3139-3149.
157. Goldfinger, M., M. Shmuel, S. Benhamron, and B. Tirosh. 2011. Protein synthesis in plasma cells is regulated by crosstalk between endoplasmic reticulum stress and mTOR signaling. *Eur J Immunol* 41: 491-502.
158. Lee, S. K., R. J. Rigby, D. Zotos, L. M. Tsai, S. Kawamoto, J. L. Marshall, R. R. Ramiscal, T. D. Chan, D. Gatto, R. Brink, D. Yu, S. Fagarasan, D. M. Tarlinton, A. F. Cunningham, and C. G. Vinuesa. 2011. B cell priming for extrafollicular antibody responses requires Bcl-6 expression by T cells. *J Exp Med* 208: 1377-1388.
159. Odegard, J. M., B. R. Marks, L. D. DiPlacido, A. C. Poholek, D. H. Kono, C. Dong, R. A. Flavell, and J. Craft. 2008. ICOS-dependent extrafollicular helper T cells elicit IgG production via IL-21 in systemic autoimmunity. *J Exp Med* 205: 2873-2886.
160. Ise, W., K. Fujii, K. Shiroguchi, A. Ito, K. Kometani, K. Takeda, E. Kawakami, K. Yamashita, K. Suzuki, T. Okada, and T. Kurosaki. 2018. T Follicular Helper Cell-Germinal Center B Cell Interaction Strength Regulates Entry into Plasma Cell or Recycling Germinal Center Cell Fate. *Immunity* 48: 702-715 e704.
161. Schwickert, T. A., G. D. Victora, D. R. Fooksman, A. O. Kamphorst, M. R. Mugnier, A. D. Gitlin, M. L. Dustin, and M. C. Nussenzweig. 2011. A dynamic T cell-limited checkpoint regulates affinity-dependent B cell entry into the germinal center. *J Exp Med* 208: 1243-1252.
162. Sciammas, R., A. L. Shaffer, J. H. Schatz, H. Zhao, L. M. Staudt, and H. Singh. 2006. Graded expression of interferon regulatory factor-4 coordinates isotype switching with plasma cell differentiation. *Immunity* 25: 225-236.
163. Tellier, J., W. Shi, M. Minnich, Y. Liao, S. Crawford, G. K. Smyth, A. Kallies, M. Busslinger, and S. L. Nutt. 2016. Blimp-1 controls plasma cell function through the regulation of immunoglobulin secretion and the unfolded protein response. *Nat Immunol* 17: 323-330.
164. Xu, H., V. K. Chaudhri, Z. Wu, K. Biliouris, K. Dienger-Stambaugh, Y. Rochman, and H. Singh. 2015. Regulation of bifurcating B cell trajectories by mutual antagonism between transcription factors IRF4 and IRF8. *Nat Immunol* 16: 1274-1281.
165. Johnston, R. J., A. C. Poholek, D. DiToro, I. Yusuf, D. Eto, B. Barnett, A. L. Dent, J. Craft, and S. Crotty. 2009. Bcl6 and Blimp-1 are reciprocal and antagonistic regulators of T follicular helper cell differentiation. *Science* 325: 1006-1010.

166. Koutsakos, M., A. K. Wheatley, L. Loh, E. B. Clemens, S. Sant, S. Nussing, A. Fox, A. W. Chung, K. L. Laurie, A. C. Hurt, S. Rockman, M. Lappas, T. Loudovaris, S. I. Mannering, G. P. Westall, M. Elliot, S. G. Tangye, L. M. Wakim, S. J. Kent, T. H. O. Nguyen, and K. Kedzierska. 2018. Circulating TFH cells, serological memory, and tissue compartmentalization shape human influenza-specific B cell immunity. *Sci Transl Med* 10.
167. Shapiro-Shelef, M., and K. Calame. 2005. Regulation of plasma-cell development. *Nat Rev Immunol* 5: 230-242.
168. Xiang, Z., A. J. Cutler, R. J. Brownlie, K. Fairfax, K. E. Lawlor, E. Severinson, E. U. Walker, R. A. Manz, D. M. Tarlinton, and K. G. Smith. 2007. FcγRIIb controls bone marrow plasma cell persistence and apoptosis. *Nat Immunol* 8: 419-429.
169. Vinuesa, C. G., M. C. Cook, C. Angelucci, V. Athanasopoulos, L. Rui, K. M. Hill, D. Yu, H. Domasch, B. Whittle, T. Lambe, I. S. Roberts, R. R. Copley, J. I. Bell, R. J. Cornall, and C. C. Goodnow. 2005. A RING-type ubiquitin ligase family member required to repress follicular helper T cells and autoimmunity. *Nature* 435: 452-458.
170. Baumjohann, D., S. Preite, A. Reboldi, F. Ronchi, K. M. Ansel, A. Lanzavecchia, and F. Sallusto. 2013. Persistent antigen and germinal center B cells sustain T follicular helper cell responses and phenotype. *Immunity* 38: 596-605.
171. Arnold, C. N., D. J. Campbell, M. Lipp, and E. C. Butcher. 2007. The germinal center response is impaired in the absence of T cell-expressed CXCR5. *Eur J Immunol* 37: 100-109.
172. Qi, H. 2016. T follicular helper cells in space-time. *Nat Rev Immunol* 16: 612-625.
173. Hollister, K., S. Kusam, H. Wu, N. Clegg, A. Mondal, D. V. Sawant, and A. L. Dent. 2013. Insights into the role of Bcl6 in follicular Th cells using a new conditional mutant mouse model. *J Immunol* 191: 3705-3711.
174. He, J., L. M. Tsai, Y. A. Leong, X. Hu, C. S. Ma, N. Chevalier, X. Sun, K. Vandenberg, S. Rockman, Y. Ding, L. Zhu, W. Wei, C. Wang, A. Karnowski, G. T. Belz, J. R. Ghali, M. C. Cook, D. S. Riminton, A. Veillette, P. L. Schwartzberg, F. Mackay, R. Brink, S. G. Tangye, C. G. Vinuesa, C. R. Mackay, Z. Li, and D. Yu. 2013. Circulating precursor CCR7(lo)PD-1(hi) CXCR5(+) CD4(+) T cells indicate Tfh cell activity and promote antibody responses upon antigen reexposure. *Immunity* 39: 770-781.
175. Laidlaw, B. J., Y. Lu, R. A. Amezcua, J. S. Weinstein, J. A. Vander Heiden, N. T. Gupta, S. H. Kleinstein, S. M. Kaech, and J. Craft. 2017. Interleukin-10 from CD4(+) follicular regulatory T cells promotes the germinal center response. *Sci Immunol* 2.

176. Luthje, K., A. Kallies, Y. Shimohakamada, G. T. Belz, A. Light, D. M. Tarlinton, and S. L. Nutt. 2012. The development and fate of follicular helper T cells defined by an IL-21 reporter mouse. *Nat Immunol* 13: 491-498.
177. Weinstein, J. S., E. I. Herman, B. Lainez, P. Licona-Limon, E. Esplugues, R. Flavell, and J. Craft. 2016. TFH cells progressively differentiate to regulate the germinal center response. *Nat Immunol* 17: 1197-1205.
178. Moriyama, S., N. Takahashi, J. A. Green, S. Hori, M. Kubo, J. G. Cyster, and T. Okada. 2014. Sphingosine-1-phosphate receptor 2 is critical for follicular helper T cell retention in germinal centers. *J Exp Med* 211: 1297-1305.
179. Shulman, Z., A. D. Gitlin, S. Targ, M. Jankovic, G. Pasqual, M. C. Nussenzweig, and G. D. Victora. 2013. T follicular helper cell dynamics in germinal centers. *Science* 341: 673-677.
180. Shi, J., S. Hou, Q. Fang, X. Liu, X. Liu, and H. Qi. 2018. PD-1 Controls Follicular T Helper Cell Positioning and Function. *Immunity* 49: 264-274 e264.
181. Ramsdell, F., and S. F. Ziegler. 2014. FOXP3 and scurfy: how it all began. *Nat Rev Immunol* 14: 343-349.
182. Maceiras, A. R., S. C. P. Almeida, E. Mariotti-Ferrandiz, W. Chaara, F. Jebbawi, A. Six, S. Hori, D. Klatzmann, J. Faro, and L. Graca. 2017. T follicular helper and T follicular regulatory cells have different TCR specificity. *Nat Commun* 8: 15067.
183. Aloulou, M., E. J. Carr, M. Gador, A. Bignon, R. S. Liblau, N. Fazilleau, and M. A. Linterman. 2016. Follicular regulatory T cells can be specific for the immunizing antigen and derive from naive T cells. *Nat Commun* 7: 10579.
184. Wing, J. B., Y. Kitagawa, M. Locci, H. Hume, C. Tay, T. Morita, Y. Kidani, K. Matsuda, T. Inoue, T. Kurosaki, S. Crotty, C. Coban, N. Ohkura, and S. Sakaguchi. 2017. A distinct subpopulation of CD25(-) T-follicular regulatory cells localizes in the germinal centers. *Proc Natl Acad Sci U S A* 114: E6400-E6409.
185. Wu, H., Y. Chen, H. Liu, L. L. Xu, P. Teuscher, S. Wang, S. Lu, and A. L. Dent. 2016. Follicular regulatory T cells repress cytokine production by follicular helper T cells and optimize IgG responses in mice. *Eur J Immunol* 46: 1152-1161.
186. Sage, P. T., A. M. Paterson, S. B. Lovitch, and A. H. Sharpe. 2014. The coinhibitory receptor CTLA-4 controls B cell responses by modulating T follicular helper, T follicular regulatory, and T regulatory cells. *Immunity* 41: 1026-1039.

187. Wollenberg, I., A. Agua-Doce, A. Hernandez, C. Almeida, V. G. Oliveira, J. Faro, and L. Graca. 2011. Regulation of the germinal center reaction by Foxp3+ follicular regulatory T cells. *J Immunol* 187: 4553-4560.
188. Levy, Y., and J. C. Brouet. 1994. Interleukin-10 prevents spontaneous death of germinal center B cells by induction of the bcl-2 protein. *J Clin Invest* 93: 424-428.
189. Xie, M. M., and A. L. Dent. 2018. Unexpected Help: Follicular Regulatory T Cells in the Germinal Center. *Front Immunol* 9: 1536.
190. Fazilleau, N., and M. Aloulou. 2018. Several Follicular Regulatory T Cell Subsets With Distinct Phenotype and Function Emerge During Germinal Center Reactions. *Front Immunol* 9: 1792.
191. D'Alessio, A. C., Z. P. Fan, K. J. Wert, P. Baranov, M. A. Cohen, J. S. Saini, E. Cohick, C. Charniga, D. Dadon, N. M. Hannett, M. J. Young, S. Temple, R. Jaenisch, T. I. Lee, and R. A. Young. 2015. A Systematic Approach to Identify Candidate Transcription Factors that Control Cell Identity. *Stem Cell Reports* 5: 763-775.
192. Basso, K., and R. Dalla-Favera. 2012. Roles of BCL6 in normal and transformed germinal center B cells. *Immunol Rev* 247: 172-183.
193. Alinikula, J., and O. Lassila. 2011. Gene interaction network regulates plasma cell differentiation. *Scand J Immunol* 73: 512-519.
194. Feske, S. 2007. Calcium signalling in lymphocyte activation and disease. *Nat Rev Immunol* 7: 690-702.
195. Vallabhapurapu, S., and M. Karin. 2009. Regulation and function of NF-kappaB transcription factors in the immune system. *Annu Rev Immunol* 27: 693-733.
196. Hogan, P. G., L. Chen, J. Nardone, and A. Rao. 2003. Transcriptional regulation by calcium, calcineurin, and NFAT. *Genes Dev* 17: 2205-2232.
197. Zanoni, I., and F. Granucci. 2012. Regulation and dysregulation of innate immunity by NFAT signaling downstream of pattern recognition receptors (PRRs). *Eur J Immunol* 42: 1924-1931.
198. Rathmell, J. C., S. Fournier, B. C. Weintraub, J. P. Allison, and C. C. Goodnow. 1998. Repression of B7.2 on self-reactive B cells is essential to prevent proliferation and allow Fas-mediated deletion by CD4(+) T cells. *J Exp Med* 188: 651-659.
199. Liu, Y. J., C. Barthelemy, O. de Bouteiller, C. Arpin, I. Durand, and J. Banchereau. 1995. Memory B cells from human tonsils colonize mucosal

- epithelium and directly present antigen to T cells by rapid up-regulation of B7-1 and B7-2. *Immunity* 2: 239-248.
200. Guegan, J. P., and P. Legembre. 2018. Nonapoptotic functions of Fas/CD95 in the immune response. *FEBS J* 285: 809-827.
 201. Butt, D., T. D. Chan, K. Bourne, J. R. Hermes, A. Nguyen, A. Statham, L. A. O'Reilly, A. Strasser, S. Price, P. Schofield, D. Christ, A. Basten, C. S. Ma, S. G. Tangye, T. G. Phan, V. K. Rao, and R. Brink. 2015. FAS Inactivation Releases Unconventional Germinal Center B Cells that Escape Antigen Control and Drive IgE and Autoantibody Production. *Immunity* 42: 890-902.
 202. Hao, Z., G. S. Duncan, J. Seagal, Y. W. Su, C. Hong, J. Haight, N. J. Chen, A. Elia, A. Wakeham, W. Y. Li, J. Liepa, G. A. Wood, S. Casola, K. Rajewsky, and T. W. Mak. 2008. Fas receptor expression in germinal-center B cells is essential for T and B lymphocyte homeostasis. *Immunity* 29: 615-627.
 203. Takahashi, Y., H. Ohta, and T. Takemori. 2001. Fas is required for clonal selection in germinal centers and the subsequent establishment of the memory B cell repertoire. *Immunity* 14: 181-192.
 204. Lee, B. O., J. Moyron-Quiroz, J. Rangel-Moreno, K. L. Kusser, L. Hartson, F. Sprague, F. E. Lund, and T. D. Randall. 2003. CD40, but not CD154, expression on B cells is necessary for optimal primary B cell responses. *J Immunol* 171: 5707-5717.
 205. Elgueta, R., M. J. Benson, V. C. de Vries, A. Wasiuk, Y. Guo, and R. J. Noelle. 2009. Molecular mechanism and function of CD40/CD40L engagement in the immune system. *Immunol Rev* 229: 152-172.
 206. Han, S., K. Hathcock, B. Zheng, T. B. Kepler, R. Hodes, and G. Kelsoe. 1995. Cellular interaction in germinal centers. Roles of CD40 ligand and B7-2 in established germinal centers. *J Immunol* 155: 556-567.
 207. Hennino, A., M. Berard, P. H. Krammer, and T. Defrance. 2001. FLICE-inhibitory protein is a key regulator of germinal center B cell apoptosis. *J Exp Med* 193: 447-458.
 208. Wikenheiser, D. J., and J. S. Stumhofer. 2016. ICOS Co-Stimulation: Friend or Foe? *Front Immunol* 7: 304.
 209. Lenschow, D. J., A. I. Sperling, M. P. Cooke, G. Freeman, L. Rhee, D. C. Decker, G. Gray, L. M. Nadler, C. C. Goodnow, and J. A. Bluestone. 1994. Differential up-regulation of the B7-1 and B7-2 costimulatory molecules after Ig receptor engagement by antigen. *J Immunol* 153: 1990-1997.
 210. Esensten, J. H., Y. A. Helou, G. Chopra, A. Weiss, and J. A. Bluestone. 2016. CD28 Costimulation: From Mechanism to Therapy. *Immunity* 44: 973-988.

211. Good-Jacobson, K. L., E. Song, S. Anderson, A. H. Sharpe, and M. J. Shlomchik. 2012. CD80 expression on B cells regulates murine T follicular helper development, germinal center B cell survival, and plasma cell generation. *J Immunol* 188: 4217-4225.
212. Salek-Ardakani, S., Y. S. Choi, M. Rafii-El-Idrissi Benhnia, R. Flynn, R. Arens, S. Shoenberger, S. Crotty, M. Croft, and S. Salek-Ardakani. 2011. B cell-specific expression of B7-2 is required for follicular Th cell function in response to vaccinia virus. *J Immunol* 186: 5294-5303.
213. Engelhardt, J. J., T. J. Sullivan, and J. P. Allison. 2006. CTLA-4 overexpression inhibits T cell responses through a CD28-B7-dependent mechanism. *J Immunol* 177: 1052-1061.
214. Rudd, C. E., A. Taylor, and H. Schneider. 2009. CD28 and CTLA-4 coreceptor expression and signal transduction. *Immunol Rev* 229: 12-26.
215. Wang, C. J., F. Heuts, V. Ovcinnikovs, L. Wardzinski, C. Bowers, E. M. Schmidt, A. Kogimtzis, R. Kenefeck, D. M. Sansom, and L. S. Walker. 2015. CTLA-4 controls follicular helper T-cell differentiation by regulating the strength of CD28 engagement. *Proc Natl Acad Sci U S A* 112: 524-529.
216. Wing, J. B., W. Ise, T. Kurosaki, and S. Sakaguchi. 2014. Regulatory T cells control antigen-specific expansion of Tfh cell number and humoral immune responses via the coreceptor CTLA-4. *Immunity* 41: 1013-1025.
217. Xu, H., X. Li, D. Liu, J. Li, X. Zhang, X. Chen, S. Hou, L. Peng, C. Xu, W. Liu, L. Zhang, and H. Qi. 2013. Follicular T-helper cell recruitment governed by bystander B cells and ICOS-driven motility. *Nature* 496: 523-527.
218. Liu, D., H. Xu, C. Shih, Z. Wan, X. Ma, W. Ma, D. Luo, and H. Qi. 2015. T-B-cell entanglement and ICOSL-driven feed-forward regulation of germinal centre reaction. *Nature* 517: 214-218.
219. Weber, J. P., F. Fuhrmann, R. K. Feist, A. Lahmann, M. S. Al Baz, L. J. Gentz, D. Vu Van, H. W. Mages, C. Haftmann, R. Riedel, J. R. Grun, W. Schuh, R. A. Kroczek, A. Radbruch, M. F. Mashreghi, and A. Hutloff. 2015. ICOS maintains the T follicular helper cell phenotype by down-regulating Kruppel-like factor 2. *J Exp Med* 212: 217-233.
220. Dai, S., R. Jia, X. Zhang, Q. Fang, and L. Huang. 2014. The PD-1/PD-Ls pathway and autoimmune diseases. *Cell Immunol* 290: 72-79.
221. Jiang, T. T., T. Martinov, L. Xin, J. M. Kinder, J. A. Spanier, B. T. Fife, and S. S. Way. 2016. Programmed Death-1 Culls Peripheral Accumulation of High-Affinity Autoreactive CD4 T Cells to Protect against Autoimmunity. *Cell Rep* 17: 1783-1794.

222. Sage, P. T., L. M. Francisco, C. V. Carman, and A. H. Sharpe. 2013. The receptor PD-1 controls follicular regulatory T cells in the lymph nodes and blood. *Nat Immunol* 14: 152-161.
223. Good-Jacobson, K. L., C. G. Szumilas, L. Chen, A. H. Sharpe, M. M. Tomayko, and M. J. Shlomchik. 2010. PD-1 regulates germinal center B cell survival and the formation and affinity of long-lived plasma cells. *Nat Immunol* 11: 535-542.
224. McGuire, H. M., A. Vogelzang, J. Warren, C. Loetsch, K. D. Natividad, T. D. Chan, R. Brink, M. Batten, and C. King. 2015. IL-21 and IL-4 Collaborate To Shape T-Dependent Antibody Responses. *J Immunol* 195: 5123-5135.
225. Ul-Haq, Z., S. Naz, and M. A. Mesaik. 2016. Interleukin-4 receptor signaling and its binding mechanism: A therapeutic insight from inhibitors tool box. *Cytokine Growth Factor Rev* 32: 3-15.
226. Dufort, F. J., B. F. Bleiman, M. R. Gumina, D. Blair, D. J. Wagner, M. F. Roberts, Y. Abu-Amer, and T. C. Chiles. 2007. Cutting edge: IL-4-mediated protection of primary B lymphocytes from apoptosis via Stat6-dependent regulation of glycolytic metabolism. *J Immunol* 179: 4953-4957.
227. King, I. L., and M. Mohrs. 2009. IL-4-producing CD4+ T cells in reactive lymph nodes during helminth infection are T follicular helper cells. *J Exp Med* 206: 1001-1007.
228. Reinhardt, R. L., H. E. Liang, and R. M. Locksley. 2009. Cytokine-secreting follicular T cells shape the antibody repertoire. *Nat Immunol* 10: 385-393.
229. Deng, Y., Z. Wang, C. Chang, L. Lu, C. S. Lau, and Q. Lu. 2017. Th9 cells and IL-9 in autoimmune disorders: Pathogenesis and therapeutic potentials. *Hum Immunol* 78: 120-128.
230. Schmetterer, K. G., and W. F. Pickl. 2017. The IL-10/STAT3 axis: Contributions to immune tolerance by thymus and peripherally derived regulatory T-cells. *Eur J Immunol* 47: 1256-1265.
231. Yoon, S. O., X. Zhang, P. Berner, and Y. S. Choi. 2009. IL-21 and IL-10 have redundant roles but differential capacities at different stages of Plasma Cell generation from human Germinal Center B cells. *J Leukoc Biol* 86: 1311-1318.
232. Wu, Y., N. M. van Besouw, Y. Shi, M. J. Hoogduijn, L. Wang, and C. C. Baan. 2016. The Biological Effects of IL-21 Signaling on B-Cell-Mediated Responses in Organ Transplantation. *Front Immunol* 7: 319.
233. Linterman, M. A., L. Beaton, D. Yu, R. R. Ramiscal, M. Srivastava, J. J. Hogan, N. K. Verma, M. J. Smyth, R. J. Rigby, and C. G. Vinuesa. 2010. IL-21 acts directly on B cells to regulate Bcl-6 expression and germinal center responses. *J Exp Med* 207: 353-363.

234. Zotos, D., J. M. Coquet, Y. Zhang, A. Light, K. D'Costa, A. Kallies, L. M. Corcoran, D. I. Godfrey, K. M. Toellner, M. J. Smyth, S. L. Nutt, and D. M. Tarlinton. 2010. IL-21 regulates germinal center B cell differentiation and proliferation through a B cell-intrinsic mechanism. *J Exp Med* 207: 365-378.
235. Cannons, J. L., H. Qi, K. T. Lu, M. Dutta, J. Gomez-Rodriguez, J. Cheng, E. K. Wakeland, R. N. Germain, and P. L. Schwartzberg. 2010. Optimal germinal center responses require a multistage T cell:B cell adhesion process involving integrins, SLAM-associated protein, and CD84. *Immunity* 32: 253-265.
236. Cannons, J. L., L. J. Yu, B. Hill, L. A. Mijares, D. Dombroski, K. E. Nichols, A. Antonellis, G. A. Koretzky, K. Gardner, and P. L. Schwartzberg. 2004. SAP regulates T(H)2 differentiation and PKC-theta-mediated activation of NF-kappaB1. *Immunity* 21: 693-706.
237. Yusuf, I., R. Kageyama, L. Monticelli, R. J. Johnston, D. Ditoro, K. Hansen, B. Barnett, and S. Crotty. 2010. Germinal center T follicular helper cell IL-4 production is dependent on signaling lymphocytic activation molecule receptor (CD150). *J Immunol* 185: 190-202.
238. Hu, J., C. Havenar-Daughton, and S. Crotty. 2013. Modulation of SAP dependent T:B cell interactions as a strategy to improve vaccination. *Curr Opin Virol* 3: 363-370.
239. Kageyama, R., J. L. Cannons, F. Zhao, I. Yusuf, C. Lao, M. Locci, P. L. Schwartzberg, and S. Crotty. 2012. The receptor Ly108 functions as a SAP adaptor-dependent on-off switch for T cell help to B cells and NKT cell development. *Immunity* 36: 986-1002.
240. Dang, A. K., R. W. Jain, H. C. Craig, and S. M. Kerfoot. 2015. B cell recognition of myelin oligodendrocyte glycoprotein autoantigen depends on immunization with protein rather than short peptide, while B cell invasion of the CNS in autoimmunity does not. *J Neuroimmunol* 278: 73-84.
241. Compston, A., and A. Coles. 2008. Multiple sclerosis. *Lancet* 372: 1502-1517.
242. Bittner, S., A. M. Afzali, H. Wiendl, and S. G. Meuth. 2014. Myelin oligodendrocyte glycoprotein (MOG35-55) induced experimental autoimmune encephalomyelitis (EAE) in C57BL/6 mice. *J Vis Exp*.
243. Shetty, A., S. G. Gupta, M. Varrin-Doyer, M. S. Weber, T. Prod'homme, N. Molnarfi, N. Ji, P. A. Nelson, J. C. Patarroyo, U. Schulze-Topphoff, S. E. Fogal, T. Forsthuber, R. A. Sobel, C. C. Bernard, A. J. Slavin, and S. S. Zamvil. 2014. Immunodominant T-cell epitopes of MOG reside in its transmembrane and cytoplasmic domains in EAE. *Neurol Neuroimmunol Neuroinflamm* 1: e22.
244. Barun, B., and A. Bar-Or. 2012. Treatment of multiple sclerosis with anti-CD20 antibodies. *Clin Immunol* 142: 31-37.

245. Bettadapura, J., K. K. Menon, S. Moritz, J. Liu, and C. C. Bernard. 1998. Expression, purification, and encephalitogenicity of recombinant human myelin oligodendrocyte glycoprotein. *J Neurochem* 70: 1593-1599.
246. Oliver, A. R., G. M. Lyon, and N. H. Ruddle. 2003. Rat and human myelin oligodendrocyte glycoproteins induce experimental autoimmune encephalomyelitis by different mechanisms in C57BL/6 mice. *J Immunol* 171: 462-468.
247. Bansal, P., T. Khan, U. Bussmeyer, D. K. Challa, R. Swiercz, R. Velmurugan, R. J. Ober, and E. S. Ward. 2013. The encephalitogenic, human myelin oligodendrocyte glycoprotein-induced antibody repertoire is directed toward multiple epitopes in C57BL/6-immunized mice. *J Immunol* 191: 1091-1101.
248. Paus, D., T. G. Phan, T. D. Chan, S. Gardam, A. Basten, and R. Brink. 2006. Antigen recognition strength regulates the choice between extrafollicular plasma cell and germinal center B cell differentiation. *J Exp Med* 203: 1081-1091.
249. Petersen, T. R., E. Bettelli, J. Sidney, A. Sette, V. Kuchroo, and B. T. Backstrom. 2004. Characterization of MHC- and TCR-binding residues of the myelin oligodendrocyte glycoprotein 38-51 peptide. *Eur J Immunol* 34: 165-173.
250. Robertson, J. M., P. E. Jensen, and B. D. Evavold. 2000. DO11.10 and OT-II T cells recognize a C-terminal ovalbumin 323-339 epitope. *J Immunol* 164: 4706-4712.
251. Sinai, P., I. M. Dozmorov, R. Song, P. L. Schwartzberg, E. K. Wakeland, and C. Wulfig. 2014. T/B-cell interactions are more transient in response to weak stimuli in SLE-prone mice. *Eur J Immunol* 44: 3522-3531.
252. Breithaupt, C., A. Schubart, H. Zander, A. Skerra, R. Huber, C. Linington, and U. Jacob. 2003. Structural insights into the antigenicity of myelin oligodendrocyte glycoprotein. *Proc Natl Acad Sci U S A* 100: 9446-9451.
253. LaVallie, E. R., E. A. DiBlasio, S. Kovacic, K. L. Grant, P. F. Schendel, and J. M. McCoy. 1993. A thioredoxin gene fusion expression system that circumvents inclusion body formation in the E. coli cytoplasm. *Biotechnology (N Y)* 11: 187-193.
254. Katz, S. 1968. Partial molar volume and conformational changes produced by the denaturation of albumin by guanidine hydrochloride. *Biochim Biophys Acta* 154: 468-477.
255. Amor, S., N. Groome, C. Linington, M. M. Morris, K. Dornmair, M. V. Gardinier, J. M. Matthieu, and D. Baker. 1994. Identification of epitopes of myelin oligodendrocyte glycoprotein for the induction of experimental allergic encephalomyelitis in SJL and Biozzi AB/H mice. *J Immunol* 153: 4349-4356.

256. Litzenburger, T., R. Fassler, J. Bauer, H. Lassmann, C. Linington, H. Wekerle, and A. Iglesias. 1998. B lymphocytes producing demyelinating autoantibodies: development and function in gene-targeted transgenic mice. *J Exp Med* 188: 169-180.
257. Raines, R. T., M. McCormick, T. R. Van Oosbree, and R. C. Mierendorf. 2000. The S.Tag fusion system for protein purification. *Methods Enzymol* 326: 362-376.
258. Kostallas, G., P. A. Lofdahl, and P. Samuelson. 2011. Substrate profiling of tobacco etch virus protease using a novel fluorescence-assisted whole-cell assay. *PLoS One* 6: e16136.
259. Birnbaum, M. E., J. L. Mendoza, D. K. Sethi, S. Dong, J. Glanville, J. Dobbins, E. Ozkan, M. M. Davis, K. W. Wucherpfennig, and K. C. Garcia. 2014. Deconstructing the peptide-MHC specificity of T cell recognition. *Cell* 157: 1073-1087.
260. Liblau, R. S., H. Wekerle, and R. M. Tisch. 2011. Cumulative autoimmunity: T cell clones recognizing several self-epitopes exhibit enhanced pathogenicity. *Front Immunol* 2: 47.
261. Rosenthal, K. M., L. J. Edwards, J. J. Sabatino, Jr., J. D. Hood, H. A. Wasserman, C. Zhu, and B. D. Evavold. 2012. Low 2-dimensional CD4 T cell receptor affinity for myelin sets in motion delayed response kinetics. *PLoS One* 7: e32562.
262. Krishnamoorthy, G., A. Saxena, L. T. Mars, H. S. Domingues, R. Mentele, A. Ben-Nun, H. Lassmann, K. Dornmair, F. C. Kurschus, R. S. Liblau, and H. Wekerle. 2009. Myelin-specific T cells also recognize neuronal autoantigen in a transgenic mouse model of multiple sclerosis. *Nat Med* 15: 626-632.
263. Lucca, L. E., S. Desbois, A. Ramadan, A. Ben-Nun, M. Eisenstein, N. Carrie, J. C. Guery, A. Sette, P. Nguyen, T. L. Geiger, L. T. Mars, and R. S. Liblau. 2014. Bispecificity for myelin and neuronal self-antigens is a common feature of CD4 T cells in C57BL/6 mice. *J Immunol* 193: 3267-3277.
264. Bettelli, E., M. Pagany, H. L. Weiner, C. Linington, R. A. Sobel, and V. K. Kuchroo. 2003. Myelin oligodendrocyte glycoprotein-specific T cell receptor transgenic mice develop spontaneous autoimmune optic neuritis. *J Exp Med* 197: 1073-1081.
265. Barnden, M. J., J. Allison, W. R. Heath, and F. R. Carbone. 1998. Defective TCR expression in transgenic mice constructed using cDNA-based alpha- and beta-chain genes under the control of heterologous regulatory elements. *Immunol Cell Biol* 76: 34-40.
266. Ronchi, F., C. Basso, S. Preite, A. Reboldi, D. Baumjohann, L. Perlini, A. Lanzavecchia, and F. Sallusto. 2016. Experimental priming of encephalitogenic

- Th1/Th17 cells requires pertussis toxin-driven IL-1beta production by myeloid cells. *Nat Commun* 7: 11541.
267. Okuda, Y., C. C. Bernard, H. Fujimura, T. Yanagihara, and S. Sakoda. 1998. Fas has a crucial role in the progression of experimental autoimmune encephalomyelitis. *Mol Immunol* 35: 317-326.
268. Whittaker Hawkins, R. F., A. Patenaude, A. Dumas, R. Jain, Y. Tesfagiorgis, S. Kerfoot, T. Matsui, M. Gunzer, P. E. Poubelle, C. Larochelle, M. Pelletier, and L. Vallieres. 2017. ICAM1+ neutrophils promote chronic inflammation via ASPRV1 in B cell-dependent autoimmune encephalomyelitis. *JCI Insight* 2.
269. Marta, C. B., A. R. Oliver, R. A. Sweet, S. E. Pfeiffer, and N. H. Ruddle. 2005. Pathogenic myelin oligodendrocyte glycoprotein antibodies recognize glycosylated epitopes and perturb oligodendrocyte physiology. *Proc Natl Acad Sci U S A* 102: 13992-13997.
270. Kawakami, N., S. Lassmann, Z. Li, F. Odoardi, T. Ritter, T. Ziemssen, W. E. Klinkert, J. W. Ellwart, M. Bradl, K. Krivacic, H. Lassmann, R. M. Ransohoff, H. D. Volk, H. Wekerle, C. Linington, and A. Flugel. 2004. The activation status of neuroantigen-specific T cells in the target organ determines the clinical outcome of autoimmune encephalomyelitis. *J Exp Med* 199: 185-197.
271. Akirav, E. M., C. M. Bergman, M. Hill, and N. H. Ruddle. 2009. Depletion of CD4(+)CD25(+) T cells exacerbates experimental autoimmune encephalomyelitis induced by mouse, but not rat, antigens. *J Neurosci Res* 87: 3511-3519.
272. Arellano, G., E. Acuna, L. I. Reyes, P. A. Ottum, P. De Sarno, L. Villarroel, E. Ciampi, R. Uribe-San Martin, C. Carcamo, and R. Naves. 2017. Th1 and Th17 Cells and Associated Cytokines Discriminate among Clinically Isolated Syndrome and Multiple Sclerosis Phenotypes. *Front Immunol* 8: 753.
273. Ebrahimimonfared, M., A. Ganji, S. Zahedi, P. Nourbakhsh, K. Ghasami, and G. Mosayebi. 2018. Characterization of Regulatory T-Cells in Multiple Sclerosis Patients Treated with Interferon Beta-1a. *CNS Neurol Disord Drug Targets* 17: 113-118.
274. Li, X., A. Gadzinsky, L. Gong, H. Tong, V. Calderon, Y. Li, D. Kitamura, U. Klein, W. Y. Langdon, F. Hou, Y. R. Zou, and H. Gu. 2018. Cbl Ubiquitin Ligases Control B Cell Exit from the Germinal-Center Reaction. *Immunity* 48: 530-541 e536.
275. Dale, J. W., and P. J. Greenaway. 1985. Bacterial transformation (kushner method). *Methods Mol Biol* 2: 241-244.
276. Jain, R. W., A. K. Dang, and S. M. Kerfoot. 2016. Simple and Efficient Production and Purification of Mouse Myelin Oligodendrocyte Glycoprotein for Experimental Autoimmune Encephalomyelitis Studies. *J Vis Exp*.

277. Miller, S. D., and W. J. Karpus. 2007. Experimental autoimmune encephalomyelitis in the mouse. *Curr Protoc Immunol* Chapter 15: Unit 15 11.
278. Quah, B. J., and C. R. Parish. 2010. The use of carboxyfluorescein diacetate succinimidyl ester (CFSE) to monitor lymphocyte proliferation. *J Vis Exp*.
279. Shlomchik, M. J., and F. Weisel. 2012. Germinal centers. *Immunol Rev* 247: 5-10.
280. Victora, G. D., and M. C. Nussenzweig. 2012. Germinal centers. *Annu Rev Immunol* 30: 429-457.
281. Corcoran, L. M., and D. M. Tarlinton. 2016. Regulation of germinal center responses, memory B cells and plasma cell formation-an update. *Curr Opin Immunol* 39: 59-67.
282. von Budingen, H. C., T. C. Kuo, M. Sirota, C. J. van Belle, L. Apeltsin, J. Glanville, B. A. Cree, P. A. Gourraud, A. Schwartzburg, G. Huerta, D. Telman, P. D. Sundar, T. Casey, D. R. Cox, and S. L. Hauser. 2012. B cell exchange across the blood-brain barrier in multiple sclerosis. *J Clin Invest* 122: 4533-4543.
283. Tesfagiorgis, Y., S. L. Zhu, R. Jain, and S. M. Kerfoot. 2017. Activated B Cells Participating in the Anti-Myelin Response Are Excluded from the Inflamed Central Nervous System in a Model of Autoimmunity that Allows for B Cell Recognition of Autoantigen. *J Immunol* 199: 449-457.
284. Chen, J., M. Trounstein, F. W. Alt, F. Young, C. Kurahara, J. F. Loring, and D. Huszar. 1993. Immunoglobulin gene rearrangement in B cell deficient mice generated by targeted deletion of the JH locus. *Int Immunol* 5: 647-656.
285. Maruyama, M., K. P. Lam, and K. Rajewsky. 2000. Memory B-cell persistence is independent of persisting immunizing antigen. *Nature* 407: 636-642.
286. Leonardo, S. M., J. L. De Santis, L. P. Malherbe, and S. B. Gauld. 2012. Cutting edge: in the absence of regulatory T cells, a unique Th cell population expands and leads to a loss of B cell anergy. *J Immunol* 188: 5223-5226.
287. Chen, X., R. T. Winkler-Pickett, N. H. Carbonetti, J. R. Ortaldo, J. J. Oppenheim, and O. M. Howard. 2006. Pertussis toxin as an adjuvant suppresses the number and function of CD4+CD25+ T regulatory cells. *Eur J Immunol* 36: 671-680.
288. Deng, L., and R. A. Mariuzza. 2007. Recognition of self-peptide-MHC complexes by autoimmune T-cell receptors. *Trends Biochem Sci* 32: 500-508.
289. Ramadan, A., L. E. Lucca, N. Carrie, S. Desbois, P. P. Axisa, M. Hayder, J. Bauer, R. S. Liblau, and L. T. Mars. 2016. In situ expansion of T cells that recognize distinct self-antigens sustains autoimmunity in the CNS. *Brain* 139: 1433-1446.

290. Tomayko, M. M., N. C. Steinel, S. M. Anderson, and M. J. Shlomchik. 2010. Cutting edge: Hierarchy of maturity of murine memory B cell subsets. *J Immunol* 185: 7146-7150.
291. Shlomchik, M. J., and F. Weisel. 2012. Germinal center selection and the development of memory B and plasma cells. *Immunol Rev* 247: 52-63.
292. Suan, D., C. Sundling, and R. Brink. 2017. Plasma cell and memory B cell differentiation from the germinal center. *Curr Opin Immunol* 45: 97-102.
293. Baumjohann, D., T. Okada, and K. M. Ansel. 2011. Cutting Edge: Distinct waves of BCL6 expression during T follicular helper cell development. *J Immunol* 187: 2089-2092.
294. Shih, T. A., M. Roederer, and M. C. Nussenzweig. 2002. Role of antigen receptor affinity in T cell-independent antibody responses in vivo. *Nat Immunol* 3: 399-406.
295. Ma, C. S., E. K. Deenick, M. Batten, and S. G. Tangye. 2012. The origins, function, and regulation of T follicular helper cells. *J Exp Med* 209: 1241-1253.
296. Barnett, B. E., M. L. Ciocca, R. Goenka, L. G. Barnett, J. Wu, T. M. Laufer, J. K. Burkhardt, M. P. Cancro, and S. L. Reiner. 2012. Asymmetric B cell division in the germinal center reaction. *Science* 335: 342-344.
297. Schiessl, I. M., and H. Castrop. 2016. Deep insights: intravital imaging with two-photon microscopy. *Pflugers Arch* 468: 1505-1516.
298. Magness, S. T., H. Jijon, N. Van Houten Fisher, N. E. Sharpless, D. A. Brenner, and C. Jobin. 2004. In vivo pattern of lipopolysaccharide and anti-CD3-induced NF-kappa B activation using a novel gene-targeted enhanced GFP reporter gene mouse. *J Immunol* 173: 1561-1570.
299. Morancho, B., J. Minguillon, J. D. Molkenin, C. Lopez-Rodriguez, and J. Aramburu. 2008. Analysis of the transcriptional activity of endogenous NFAT5 in primary cells using transgenic NFAT-luciferase reporter mice. *BMC Mol Biol* 9: 13.
300. Gee, K. R., K. A. Brown, W. N. Chen, J. Bishop-Stewart, D. Gray, and I. Johnson. 2000. Chemical and physiological characterization of fluo-4 Ca(2+)-indicator dyes. *Cell Calcium* 27: 97-106.
301. Stosiek, C., O. Garaschuk, K. Holthoff, and A. Konnerth. 2003. In vivo two-photon calcium imaging of neuronal networks. *Proc Natl Acad Sci U S A* 100: 7319-7324.
302. Paredes, R. M., J. C. Etzler, L. T. Watts, W. Zheng, and J. D. Lechleiter. 2008. Chemical calcium indicators. *Methods* 46: 143-151.

303. Oh-hora, M. 2009. Calcium signaling in the development and function of T-lineage cells. *Immunol Rev* 231: 210-224.
304. Oeckinghaus, A., and S. Ghosh. 2009. The NF-kappaB family of transcription factors and its regulation. *Cold Spring Harb Perspect Biol* 1: a000034.
305. Heng, T. S., M. W. Painter, and C. Immunological Genome Project. 2008. The Immunological Genome Project: networks of gene expression in immune cells. *Nat Immunol* 9: 1091-1094.
306. Alrefai, H., K. Muhammad, R. Rudolf, D. A. Pham, S. Klein-Hessling, A. K. Patra, A. Avots, V. Bukur, U. Sahin, S. Tenzer, M. Goebeler, A. Kerstan, and E. Serfling. 2016. NFATc1 supports imiquimod-induced skin inflammation by suppressing IL-10 synthesis in B cells. *Nat Commun* 7: 11724.
307. Dietz, L., F. Frommer, A. L. Vogel, M. Vaeth, E. Serfling, A. Waisman, M. Buttman, and F. Berberich-Siebelt. 2015. NFAT1 deficit and NFAT2 deficit attenuate EAE via different mechanisms. *Eur J Immunol* 45: 1377-1389.
308. Reppert, S., E. Zinser, C. Holzinger, L. Sandrock, S. Koch, and S. Finotto. 2015. NFATc1 deficiency in T cells protects mice from experimental autoimmune encephalomyelitis. *Eur J Immunol* 45: 1426-1440.
309. Peng, S. L., A. J. Gerth, A. M. Ranger, and L. H. Glimcher. 2001. NFATc1 and NFATc2 together control both T and B cell activation and differentiation. *Immunity* 14: 13-20.
310. Lodygin, D., F. Odoardi, C. Schlager, H. Korner, A. Kitz, M. Nosov, J. van den Brandt, H. M. Reichardt, M. Haberl, and A. Flugel. 2013. A combination of fluorescent NFAT and H2B sensors uncovers dynamics of T cell activation in real time during CNS autoimmunity. *Nat Med* 19: 784-790.
311. Zhang, T. T., D. G. Gonzalez, C. M. Cote, S. M. Kerfoot, S. Deng, Y. Cheng, M. Magari, and A. M. Haberman. 2017. Germinal center B cell development has distinctly regulated stages completed by disengagement from T cell help. *Elife* 6.
312. Heise, N., N. S. De Silva, K. Silva, A. Carette, G. Simonetti, M. Pasparakis, and U. Klein. 2014. Germinal center B cell maintenance and differentiation are controlled by distinct NF-kappaB transcription factor subunits. *J Exp Med* 211: 2103-2118.
313. De Lorenzi, R., R. Gareus, S. Fengler, and M. Pasparakis. 2009. GFP-p65 knock-in mice as a tool to study NF-kappaB dynamics in vivo. *Genesis* 47: 323-329.
314. de Felipe, P., G. A. Luke, L. E. Hughes, D. Gani, C. Halpin, and M. D. Ryan. 2006. E unum pluribus: multiple proteins from a self-processing polyprotein. *Trends Biotechnol* 24: 68-75.

315. Bhattacharyya, S., A. Borthakur, P. K. Dudeja, and J. K. Tobacman. 2010. Lipopolysaccharide-induced activation of NF-kappaB non-canonical pathway requires BCL10 serine 138 and NIK phosphorylations. *Exp Cell Res* 316: 3317-3327.
316. Higai, K., M. Tsukada, Y. Moriya, Y. Azuma, and K. Matsumoto. 2009. Prolonged high glucose suppresses phorbol 12-myristate 13-acetate and ionomycin-induced interleukin-2 mRNA expression in Jurkat cells. *Biochim Biophys Acta* 1790: 8-15.
317. Hadjantonakis, A. K., and V. E. Papaioannou. 2004. Dynamic in vivo imaging and cell tracking using a histone fluorescent protein fusion in mice. *BMC Biotechnol* 4: 33.
318. Sheehy, A. M., and M. S. Schlissel. 1999. Overexpression of RelA causes G1 arrest and apoptosis in a pro-B cell line. *J Biol Chem* 274: 8708-8716.
319. Tang, T., J. Zhang, J. Yin, J. Staszkiwicz, B. Gawronska-Kozak, D. Y. Jung, H. J. Ko, H. Ong, J. K. Kim, R. Mynatt, R. J. Martin, M. Keenan, Z. Gao, and J. Ye. 2010. Uncoupling of inflammation and insulin resistance by NF-kappaB in transgenic mice through elevated energy expenditure. *J Biol Chem* 285: 4637-4644.
320. Roebroek, A. J., P. L. Gordts, and S. Reekmans. 2011. Knock-in approaches. *Methods Mol Biol* 693: 257-275.
321. Bak, R. O., N. Gomez-Ospina, and M. H. Porteus. 2018. Gene Editing on Center Stage. *Trends Genet* 34: 600-611.
322. Porteus, M. H., and D. Baltimore. 2003. Chimeric nucleases stimulate gene targeting in human cells. *Science* 300: 763.
323. Hsu, P. D., D. A. Scott, J. A. Weinstein, F. A. Ran, S. Konermann, V. Agarwala, Y. Li, E. J. Fine, X. Wu, O. Shalem, T. J. Cradick, L. A. Marraffini, G. Bao, and F. Zhang. 2013. DNA targeting specificity of RNA-guided Cas9 nucleases. *Nat Biotechnol* 31: 827-832.
324. Sander, J. D., and J. K. Joung. 2014. CRISPR-Cas systems for editing, regulating and targeting genomes. *Nat Biotechnol* 32: 347-355.
325. Muller, M. R., and A. Rao. 2010. NFAT, immunity and cancer: a transcription factor comes of age. *Nat Rev Immunol* 10: 645-656.
326. Casola, S. 2010. Mouse models for miRNA expression: the ROSA26 locus. *Methods Mol Biol* 667: 145-163.
327. Springer, P. S. 2000. Gene traps: tools for plant development and genomics. *Plant Cell* 12: 1007-1020.

328. Orban, P. C., D. Chui, and J. D. Marth. 1992. Tissue- and site-specific DNA recombination in transgenic mice. *Proc Natl Acad Sci U S A* 89: 6861-6865.
329. Chu, V. T., T. Weber, R. Graf, T. Sommermann, K. Petsch, U. Sack, P. Volchkov, K. Rajewsky, and R. Kuhn. 2016. Efficient generation of Rosa26 knock-in mice using CRISPR/Cas9 in C57BL/6 zygotes. *BMC Biotechnol* 16: 4.
330. Marangoni, F., T. T. Murooka, T. Manzo, E. Y. Kim, E. Carrizosa, N. M. Elpek, and T. R. Mempel. 2013. The transcription factor NFAT exhibits signal memory during serial T cell interactions with antigen-presenting cells. *Immunity* 38: 237-249.
331. Suter, S. E., T. A. Gouthro, P. A. McSweeney, R. A. Nash, M. E. Haskins, P. J. Felsburg, and P. S. Henthorn. 2006. Optimized transduction of canine paediatric CD34(+) cells using an MSCV-based bicistronic vector. *Vet Res Commun* 30: 881-901.
332. Lino, A. C., V. D. Dang, V. Lampropoulou, A. Welle, J. Joedicke, J. Pohar, Q. Simon, J. Thalmensi, A. Baures, V. Fluhler, I. Sakwa, U. Stervbo, S. Ries, L. Jouneau, P. Boudinot, T. Tsubata, T. Adachi, A. Hutloff, T. Dorner, U. Zimmer-Strobl, A. F. de Vos, K. Dahlke, G. Loh, S. Korniotis, C. Goosmann, J. C. Weill, C. A. Reynaud, S. H. E. Kaufmann, J. Walter, and S. Fillatreau. 2018. LAG-3 Inhibitory Receptor Expression Identifies Immunosuppressive Natural Regulatory Plasma Cells. *Immunity* 49: 120-133 e129.
333. Liu, Z., M. Y. Gerner, N. Van Panhuys, A. G. Levine, A. Y. Rudensky, and R. N. Germain. 2015. Immune homeostasis enforced by co-localized effector and regulatory T cells. *Nature* 528: 225-230.
334. Fazekas de St Groth, B., A. L. Smith, and C. A. Higgins. 2004. T cell activation: in vivo veritas. *Immunol Cell Biol* 82: 260-268.
335. Nojima, T., K. Haniuda, T. Moutai, M. Matsudaira, S. Mizokawa, I. Shiratori, T. Azuma, and D. Kitamura. 2011. In-vitro derived germinal centre B cells differentially generate memory B or plasma cells in vivo. *Nat Commun* 2: 465.
336. Kumar, T. R., M. Larson, H. Wang, J. McDermott, and I. Bronshteyn. 2009. Transgenic mouse technology: principles and methods. *Methods Mol Biol* 590: 335-362.
337. Zhu, J., and W. E. Paul. 2010. Peripheral CD4+ T-cell differentiation regulated by networks of cytokines and transcription factors. *Immunol Rev* 238: 247-262.
338. Ghosh, S., and J. F. Dass. 2016. Study of pathway cross-talk interactions with NF-kappaB leading to its activation via ubiquitination or phosphorylation: A brief review. *Gene* 584: 97-109.

339. Ramos Pittol, J. M., A. Oruba, G. Mittler, S. Saccani, and D. van Essen. 2018. *Zbtb7a* is a transducer for the control of promoter accessibility by NF-kappa B and multiple other transcription factors. *PLoS Biol* 16: e2004526.
340. Rudensky, A. Y., M. Gavin, and Y. Zheng. 2006. FOXP3 and NFAT: partners in tolerance. *Cell* 126: 253-256.
341. Macian, F. 2005. NFAT proteins: key regulators of T-cell development and function. *Nat Rev Immunol* 5: 472-484.
342. Martinez, G. J., R. M. Pereira, T. Aijo, E. Y. Kim, F. Marangoni, M. E. Pipkin, S. Togher, V. Heissmeyer, Y. C. Zhang, S. Crotty, E. D. Lamperti, K. M. Ansel, T. R. Mempel, H. Lahdesmaki, P. G. Hogan, and A. Rao. 2015. The transcription factor NFAT promotes exhaustion of activated CD8(+) T cells. *Immunity* 42: 265-278.
343. Fagerlund, R., K. Melen, X. Cao, and I. Julkunen. 2008. NF-kappaB p52, RelB and c-Rel are transported into the nucleus via a subset of importin alpha molecules. *Cell Signal* 20: 1442-1451.
344. Chen, F. E., D. B. Huang, Y. Q. Chen, and G. Ghosh. 1998. Crystal structure of p50/p65 heterodimer of transcription factor NF-kappaB bound to DNA. *Nature* 391: 410-413.
345. Codner, G. F., J. Mianne, A. Caulder, J. Loeffler, R. Fell, R. King, A. J. Allan, M. Mackenzie, F. J. Pike, C. V. McCabe, S. Christou, S. Joynson, M. Hutchison, M. E. Stewart, S. Kumar, M. M. Simon, L. Agius, Q. M. Anstee, K. E. Volynski, D. M. Kullmann, S. Wells, and L. Teboul. 2018. Application of long single-stranded DNA donors in genome editing: generation and validation of mouse mutants. *BMC Biol* 16: 70.
346. Hendel, A., R. O. Bak, J. T. Clark, A. B. Kennedy, D. E. Ryan, S. Roy, I. Steinfeld, B. D. Lunstad, R. J. Kaiser, A. B. Wilkens, R. Bacchetta, A. Tsalenko, D. Dellinger, L. Bruhn, and M. H. Porteus. 2015. Chemically modified guide RNAs enhance CRISPR-Cas genome editing in human primary cells. *Nat Biotechnol* 33: 985-989.
347. Maruyama, T., S. K. Dougan, M. C. Truttmann, A. M. Bilate, J. R. Ingram, and H. L. Ploegh. 2015. Increasing the efficiency of precise genome editing with CRISPR-Cas9 by inhibition of nonhomologous end joining. *Nat Biotechnol* 33: 538-542.
348. Yu, C., Y. Liu, T. Ma, K. Liu, S. Xu, Y. Zhang, H. Liu, M. La Russa, M. Xie, S. Ding, and L. S. Qi. 2015. Small molecules enhance CRISPR genome editing in pluripotent stem cells. *Cell Stem Cell* 16: 142-147.
349. Yang, H., H. Wang, and R. Jaenisch. 2014. Generating genetically modified mice using CRISPR/Cas-mediated genome engineering. *Nat Protoc* 9: 1956-1968.

350. Blanchfield, J. L., S. K. Shorter, and B. D. Evavold. 2013. Monitoring the Dynamics of T Cell Clonal Diversity Using Recombinant Peptide:MHC Technology. *Front Immunol* 4: 170.
351. Lucca, L. E., P. P. Axisa, M. Aloulou, C. Peral, A. Ramadan, P. Rufas, B. Kyewski, J. Derbinski, N. Fazilleau, L. T. Mars, and R. S. Liblau. 2016. Myelin oligodendrocyte glycoprotein induces incomplete tolerance of CD4(+) T cells specific for both a myelin and a neuronal self-antigen in mice. *Eur J Immunol* 46: 2247-2259.
352. Yusuf, I., J. Stern, T. M. McCaughy, S. Gallagher, H. Sun, C. Gao, T. Tedder, G. Carlesso, L. Carter, R. Herbst, and Y. Wang. 2014. Germinal center B cell depletion diminishes CD4+ follicular T helper cells in autoimmune mice. *PLoS One* 9: e102791.
353. DiToro, D., C. J. Winstead, D. Pham, S. Witte, R. Andargachew, J. R. Singer, C. G. Wilson, C. L. Zindl, R. J. Luther, D. J. Silberger, B. T. Weaver, E. M. Kolawole, R. J. Martinez, H. Turner, R. D. Hatton, J. J. Moon, S. S. Way, B. D. Evavold, and C. T. Weaver. 2018. Differential IL-2 expression defines developmental fates of follicular versus nonfollicular helper T cells. *Science* 361.
354. Fazilleau, N., L. J. McHeyzer-Williams, H. Rosen, and M. G. McHeyzer-Williams. 2009. The function of follicular helper T cells is regulated by the strength of T cell antigen receptor binding. *Nat Immunol* 10: 375-384.
355. Allen, D., T. Simon, F. Sablitzky, K. Rajewsky, and A. Cumano. 1988. Antibody engineering for the analysis of affinity maturation of an anti-hapten response. *EMBO J* 7: 1995-2001.
356. Preite, S., D. Baumjohann, M. Foglierini, C. Basso, F. Ronchi, B. M. Fernandez Rodriguez, D. Corti, A. Lanzavecchia, and F. Sallusto. 2015. Somatic mutations and affinity maturation are impaired by excessive numbers of T follicular helper cells and restored by Treg cells or memory T cells. *Eur J Immunol* 45: 3010-3021.
357. Brink, R., and T. G. Phan. 2018. Self-Reactive B Cells in the Germinal Center Reaction. *Annu Rev Immunol* 36: 339-357.
358. Reed, J. H., J. Jackson, D. Christ, and C. C. Goodnow. 2016. Clonal redemption of autoantibodies by somatic hypermutation away from self-reactivity during human immunization. *J Exp Med* 213: 1255-1265.
359. Sabouri, Z., P. Schofield, K. Horikawa, E. Spierings, D. Kipling, K. L. Randall, D. Langley, B. Roome, R. Vazquez-Lombardi, R. Rouet, J. Hermes, T. D. Chan, R. Brink, D. K. Dunn-Walters, D. Christ, and C. C. Goodnow. 2014. Redemption of autoantibodies on anergic B cells by variable-region glycosylation and mutation away from self-reactivity. *Proc Natl Acad Sci U S A* 111: E2567-2575.

360. Makela, O. 1967. Cellular heterogeneity in the production of an anti-hapten antibody. *J Exp Med* 126: 159-170.
361. Jelcic, I., F. Al Nimer, J. Wang, V. Lentsch, R. Planas, I. Jelcic, A. Madjovski, S. Ruhrmann, W. Faigle, K. Frauenknecht, C. Pinilla, R. Santos, C. Hammer, Y. Ortiz, L. Opitz, H. Gronlund, G. Rogler, O. Boyman, R. Reynolds, A. Lutterotti, M. Khademi, T. Olsson, F. Piehl, M. Sospedra, and R. Martin. 2018. Memory B Cells Activate Brain-Homing, Autoreactive CD4(+) T Cells in Multiple Sclerosis. *Cell* 175: 85-100 e123.
362. Fan, X., T. Jin, S. Zhao, C. Liu, J. Han, X. Jiang, and Y. Jiang. 2015. Circulating CCR7+ICOS+ Memory T Follicular Helper Cells in Patients with Multiple Sclerosis. *PLoS One* 10: e0134523.
363. Romme Christensen, J., L. Bornsen, R. Ratzner, F. Piehl, M. Khademi, T. Olsson, P. S. Sorensen, and F. Sellebjerg. 2013. Systemic inflammation in progressive multiple sclerosis involves follicular T-helper, Th17- and activated B-cells and correlates with progression. *PLoS One* 8: e57820.
364. Peters, A., L. A. Pitcher, J. M. Sullivan, M. Mitsdoerffer, S. E. Acton, B. Franz, K. Wucherpfennig, S. Turley, M. C. Carroll, R. A. Sobel, E. Bettelli, and V. K. Kuchroo. 2011. Th17 cells induce ectopic lymphoid follicles in central nervous system tissue inflammation. *Immunity* 35: 986-996.
365. Pikor, N. B., J. L. Astarita, L. Summers-Deluca, G. Galicia, J. Qu, L. A. Ward, S. Armstrong, C. X. Dominguez, D. Malhotra, B. Heiden, R. Kay, V. Castanov, H. Touil, L. Boon, P. O'Connor, A. Bar-Or, A. Prat, V. Ramaglia, S. Ludwin, S. J. Turley, and J. L. Gommerman. 2015. Integration of Th17- and Lymphotoxin-Derived Signals Initiates Meningeal-Resident Stromal Cell Remodeling to Propagate Neuroinflammation. *Immunity* 43: 1160-1173.
366. Quinn, J. L., G. Kumar, A. Agasing, R. M. Ko, and R. C. Axtell. 2018. Role of TFH Cells in Promoting T Helper 17-Induced Neuroinflammation. *Front Immunol* 9: 382.
367. Rostami, A., and B. Ciric. 2013. Role of Th17 cells in the pathogenesis of CNS inflammatory demyelination. *J Neurol Sci* 333: 76-87.
368. Hartung, H. P., and B. C. Kieseier. 2010. Atacicept: targeting B cells in multiple sclerosis. *Ther Adv Neurol Disord* 3: 205-216.

Curriculum Vitae

RAJIV WILLIAM JAIN

EDUCATION

- 01/05/2014 –
26/10/2018 Doctor of Philosophy
Thesis title: *B and T cell interactions in CNS autoimmunity*
Supervisors: Dr. Steven Kerfoot
Department of Microbiology and Immunology, Western
University, London, ON, Canada
- 01/05/2013 -
30/04/2014 Masters of Science (Conferred June 2014)
Thesis title: *Generating instantaneous reporters to monitor the
activity of the NFκB and NFAT transcription factors*
Supervisor: Dr. Steven Kerfoot
Department of Microbiology and Immunology, Western
University, London, ON, Canada
- 01/09/2009 -
30/04/2013 Bachelor of Medical Science (Conferred June 2013)
Thesis title: *Bimolecular fluorescence complementation
imaging of B and T-cell interactions*
Supervisors: Dr. Bryan Heit and Dr. Steven Kerfoot
Department of Microbiology and Immunology, Western
University, London, ON, Canada
-

SCHOLARSHIPS

- 01/07/2015 -
30/06/2018 endMS PhD studentship – Competitive, national, top 15% of
applicants were funded, \$22,000/yr
- 01/05/2013 -
30/04/2018 Western Graduate Research Scholarship – Internal, \$4,500/yr
- 13/06/2016 -
16/06/2017 endMS SPRINT program – Competitive, national, 9 of 50+
applicants are chosen per year, \$2,500/yr.
*This program involved completing an interdisciplinary project
focusing on Multiple Sclerosis along with two additional
applicants and one mentor.*
- 01/09/2009 -
30/04/2010 Queen Elizabeth II aiming for the top scholarship –
Competitive, national, \$660.
- 01/09/2009 Sir George Williamson Young Memorial Admission scholarship
– Entrance award based upon high school average, \$1,000.
- 01/09/2009 The Western Scholarship of Distinction – Entrance award
based upon high school average, \$500.

01/09/2009 Merlin Scientific Award – Awarded to the student with highest high school science average, \$500.

AWARDS AND PRIZES

01/09/2009 - Deans Honor list – Awarded for maintaining an average above
30/04/2013 80%.

TEACHING

01/09/2017 - Supervision of a 4th year honors thesis student, Western
30/04/2018 University

01/01/2015 - Teaching Assistant – Introductory Immunology, Western
30/04/2018 University

01/01/2015 - Supervision of a 4th year honors thesis student, Western
30/04/2015 University

01/09/2014 - Supervision of a 2nd and 3rd year scholars elective student,
30/04/2016 Western University

PUBLICATION RECORD

7. **Jain RW**, Parham KA, Tesfagiorgis Y, Craig HC, Romanchik E, and Kerfoot SM *Autoreactive, low-affinity T cells preferentially drive differentiation of short-lived memory B cells at the expense of germinal center maintenance*. **Cell Reports – Accepted** doi: <https://doi.org/10.1101/287789>
6. De Somma E*, **Jain RW***, Poon KWC*, Tresidder KA, Segal JP, and Ghasemlou N *Chronobiological regulation of psychosocial and physiological outcomes in multiple sclerosis*. **Neuroscience and Biobehavioral Reviews** [88, 73-83, 2018](#)
*These authors contributed equally
I contributed approximately one third of the written text to this review article.
5. Whittaker Hawkins RF, Patenaude A, Dumas A, **Jain R**, Tesfagiorgis Y, Kerfoot S, Matsui T, Gunzer M, Poubelle PE, Larochelle C, Pelletier M, and Vallières L *ICAM1+ neutrophils promote chronic inflammation via ASPRV1 in B cell-dependent autoimmune encephalomyelitis*. **Journal of Clinical Investigation Insight** [2\(23\): e96882. 2017](#)
I contributed to this work by cloning, expressing, purifying, and testing the bMOG_{tag} Ag. Additionally, I performed an EAE experiment along with Y Tesfagiorgis.
4. Tesfagiorgis Y, Zhu SL, **Jain R**, and Kerfoot S *Activated B Cells Participating in the Anti-Myelin Response Are Excluded from the Inflamed Central Nervous System in a Model of Autoimmunity that Allows for B Cell Recognition of Autoantigen*. **Journal of Immunology** [199\(2\), 449-57, 2017](#)
I contributed to this work by setting up a histology experiment, contributing to several flow cytometry experiments, and intellectual contributions.

3. **Jain RW, Dang AK, and Kerfoot S**
Simple and Efficient Production and Purification of Mouse Myelin Oligodendrocyte Glycoprotein for Experimental Autoimmune Encephalomyelitis Studies. *Journal of Visualized Experiments* [116](#), doi: [10.3791/54727](#), 2016
2. Dang AK, Tesfagiorgis Y, **Jain RW**, Craig HC, and Kerfoot S
Meningeal infiltration of the spinal cord by non-classically activated B cells is associated with chronic disease course in a spontaneous B cell-dependent model of CNS autoimmune disease. Frontiers in Immunology [470\(6\)](#), doi: [10.3389/fimmu.2015.00470](#), 2015
I contributed to this work by contributing to several flow cytometry experiments.
1. Dang AK, **Jain RW**, Craig HC, and Kerfoot S
B cell recognition of myelin oligodendrocyte glycoprotein autoantigen depends on immunization with protein rather than short peptide, while B cell invasion of the CNS in autoimmunity does not. Journal of Neuroimmunology [278](#), 73-84, 2015
I contributed to this work by contributing to the mMOG_{tag} purification protocol and several flow cytometry experiments.

CONFERENCE PRESENTATIONS (ORAL)

NATIONAL

Jain RW, Poon KWC, De Somma E, and Ghasemlou N.

Contribution of circadian rhythms to psychosocial and physiological outcomes in Multiple Sclerosis.

endMS summer school, June 14th 2017, Memorial University, St. Johns, NL, Canada

Jain RW, Craig HC and Kerfoot S.

MOG-Specific B Cells Preferentially Differentiate into Memory B Cells during Germinal Center Responses.

endMS Conference 2016, December 8th 2016, Marriot Downtown Eaton Centre, Toronto, ON, Canada

LOCAL

Jain RW, Craig HC, Parham AK, Tesfagiorgis Y, Romanchik E, and Kerfoot SM.

Autoreactive B cells preferentially differentiate into unresponsive memory B cells during germinal center responses

London Health Research Day, May 10th 2018, London Convention Center, London, ON, Canada

CONFERENCE PRESENTATIONS (POSTERS)

NATIONAL

Jain RW, Parham AK, Craig HC, Tesfagiorgis Y, Romanchik E, and Kerfoot SM.

Autoreactive T cells preferentially drive differentiation of non-responsive memory B cells at the expense of germinal center maintenance.

Keystone Symposia - B cells: Mechanisms in Immunity and Autoimmunity, July 17th 2018, International Congress Center, Dresden, Germany

Jain RW, Parham AK, Craig HC, Tesfagiorgis Y, Romanchik E, and Kerfoot SM.
Autoreactive T cells preferentially drive differentiation of non-responsive memory B cells at the expense of germinal center maintenance.
Canadian Society of Immunology 2018, June 1st 2018, London, ON, Canada

Jain RW, Drysdale L, Pin CL, Dick F, and Kerfoot SM.
Reporters for in vivo and in vitro monitoring of NFκB and NFAT signalling
Cellular and Molecular Imaging Symposium 2018, May 1st 2018, London, ON, Canada

Jain RW, Craig HC, Romanchik E, and Kerfoot S.
T cells direct B cell fate choices during germinal center responses.
Canadian Society of Immunology 2016, April 2nd 2016, The Westin Ottawa, Ottawa, ON, Canada

Jain RW, Craig HC, Romanchik E, and Kerfoot S.
Germinal center collapse and differential fate choices of cells in the anti-myelin autoimmune response.
Neuroinflammation Symposium 2015, May 1st 2015, Toronto, ON, Canada

LOCAL

Jain RW, Craig HC, Tesfagiorgis Y, Romanchik E, and Kerfoot S.
Autoreactive B Cells Preferentially Differentiate Into Memory B Cells During Germinal Center Responses.
London Health Research Day 2017, March 28th 2017, London Convention Center, London, ON, Canada

Jain RW, Craig HC, Romanchik E, and Kerfoot S.
T cells direct B cell fate choices during germinal center responses.
Infection and Immunity Research Forum 2016, September 1st 2016, London Convention Center, London, ON, Canada

Jain RW, Craig HC, Romanchik E, and Kerfoot S.
T cells direct B cell fate choices during germinal center responses.
London Health Research Day 2016, March 29th 2016, London Convention Center, London, ON, Canada

Jain RW, Craig HC, Romanchik E, and Kerfoot S.
Germinal center collapse and differential fate choices of cells in the anti-myelin autoimmune response.
London Health Research Day 2015, April 1st 2015, London Convention Center, London, ON, Canada

Jain RW, Craig HC, Romanchik E, and Kerfoot S.
Germinal center collapse and differential fate choices of cells in the anti-myelin autoimmune response.

*Infection and Immunity Research Forum 2014, November 1st 2014, Brescia College,
London, ON, Canada*

Jain RW, Heit B, and Kerfoot S.

Determining the activation state of B and T cells during their interactions at the beginning of immune responses.

*London Health Research Day 2014, March 31st 2014, London Convention Center,
London, ON, Canada*

Jain RW, Heit B, and Kerfoot S.

Determining the activation state of B and T cells during their interactions at the beginning of immune responses.

*Infection and Immunity Research Forum 2013, November 1st 2013, Brescia College,
London, ON, Canada*